Characterization of pectin remodelling enzymes from Arabidopsis thaliana and Verticillium dahliae : from protein structure to processivity

Josip Safran

Thèse de Doctorat

Mention – Biologie
Spécialité – Biochimie

Présentée à ***l'Ecole Doctorale en Sciences, Technologie, Santé (ED 585)***

de l'Université de Picardie Jules Verne

par

Josip Šafran

pour obtenir le grade de Docteur de l'Université de Picardie Jules Verne

Characterisation of pectin remodelling enzymes from Arabidopsis thaliana and Verticillium dahliae: from protein structure to processivity.
Caractérisation des enzymes de remodelage des pectines d'Arabidopsis thaliana et de Verticillium dahliae : de la structure protéique à la processivité.

Soutenue le 4 juin 2021, après avis des rapporteurs, devant le jury d'examen :

M^me^ M. CZJZEK, Directrice de recherche CNRS, Roscoff	**Rapportrice**
M. P. LEROUGE, Professeur, Université de Rouen	**Rapporteur**
M^me^ E. BONNIN, Ingénieure de recherche INRAe, Nantes	**Examinatrice**
M^me^ J. BOUCKAERT, Chargée de recherche CNRS, Lille	**Examinatrice**
M. F. GUERINEAU, Professeur, Université de Picardie, Amiens	**Président**
M. J. PELLOUX, Professeur, Université de Picardie, Amiens	**Directeur de thèse**
M. F. SENECHAL, Maître de Conférences, Université de Picardie, Amiens	**Co-encadrant**

ACKNOWLEDGEMENTS

*I wish to thank to the members of the jury for reading this manuscript. Thank you **Mirjam CZJZEK** and **Patrice LEROUGE** for being the external reviewers together with **Estelle BONNIN**, **Julie BOUCKAERT** and **François GUÉRINEAU** for being part of my jury. Equally, I wish to thank the Conseil Régional Hauts-de-France and the FEDER (Fonds Européen de Développement Régional) for their financial support through a PhD fellowship that allowed funding of my thesis.*

*I wish to say huge thank you to my thesis director **Jérôme PELLOUX** that guided me during this thesis. I thank you for the opportunity that you gave me and thank you for introducing me to the world of research. Thank you for being a constant moral support, source of inspiration and motivation. Thank you for being optimist during hard times and simply thank you for being a kind person.*

*I am extremely thankful to **Fabien SÉNÉCHAL** for being my co-supervisor during this thesis. Thank you for your enormous help, your nice ideas and daily advices. Thank you for being a moral support and thoughtful person. Most importantly thank you for your jokes that made my day.*

*I wish to thank **Julie BOUCKAERT** for showing me the magic of protein crystallisation, for her help in solving the protein structures and for her support during the sleepless nights at Synchrotron Soleil.*

*There are no words to express my gratitude to the **BIOPI team**, however I wish to thank **Corinne PAU-ROBLOT** for accepting me for my M2 internship and beginning my journey in Amiens. Huge thanks to **Valérie LEFEBVRE** for her kindness and willingness to help. Your smiles and advices were always there when I needed them. Thank you **Solène BASSARD** for your help in the lab but also for teaching me nice things about the French culture and especially music. I will always remember all the interesting "lab stories" that you shared with us. Equally, thank you, **Roland MOLINIÉ** and **Jean-Xavier FONTAINE** for your help and for all the long hours looking at the LC-MS/MS spectra.*

*An especially warm thank you goes to the rest of the **BIOPI team** for great working atmosphere and nice times we spent together.*

*I wish to thank **Serge PILARD** from the Analytical platform of UPJV for the advices and taking the time to look at all the LC-MS/MS samples. Huge thank you to **Clarisse BRIDOT** for her help with crystallisation experiments and **Martin SAVKO** and **Pierre LEGRAND** from Synchrotron Soleil for deciphering the crystal diffraction data. I sincerely thank **Davide MERCADANTE** for his computational analyses.*

*I wish to thank all the people from **GEC laboratory**, for supporting me and all my unannounced visits. Equally, I need to say huge thank you to all the staff from the **CROUS restaurant** without your food I cannot image finishing this thesis. Thank you **Biogym** friends for keeping my body in good shape despite sitting the long hours. Thank you, **Dolores** for checking on me every night during the writing of my thesis**.** I wish to thank responsible from the HUB building for preparing everything for my defence. Thank you, **Nicolas DELANCHY**, for all the delicious cakes you brought us. Thank you, **Gustavo CABALLERO**, **Akcan ISTIF**, **Zakaria BOUCHOUIREB**, **Mariama NDOUR, Catalina QUESADA**, and **Morgane ADÉLAÏDE**, for nice time spent together.*

*Thanks, all the interns that have helped me with my experiments, and especially my Croatian friends; **Paula PONGRAC**, **Irin STOŠIĆ**, **Maša BORAS**, **Maja GREDELJ**, **Antonia PAIĆ**, **Nicol KOLAR**, **Tea MARTINIĆ CEZAR** and **Klara CIK** thank you for the good times spent together.*

*I am extremely thankful to "**The Best Office**" for all the cakes, all the pranks, all the jokes, but principally the nice time I have spent with you. **Wafae TABI** you support me for the long time and I know that sometimes I have been hard. However, I will remember only your smiles, your witty responses and long talks after the work. **Adrien LEMAIRE** you are a perfect college and friend. You always had time to help (even when you had your own work) and working with you is a pleasure. **Pauline TREZEL**, the almost "living goddess" of board games. I appreciate your sincerity, kindness and your willingness to help. Thank you for teaching me how to avoid to be a "Crocodile". **Camille CARTON**, fashion icon, Tik-Tok legend and proud owner of 208. Thank you for the jokes, pranks and your willingness to turn me into a Tik-Tok star. Your good mode and your energy are contagious, thank you for sharing them with me.*

*Special thanks to **Olivier HABRYLO**. Thank you for being my mentor inside and friend outside of the lab. Thank you for sharing the good food and bad jokes with me. Thank you for showing me the good side of Amiens and Picardie. The moments together were unforgettable. I am grateful for correcting and improving my French.*

*It is my privilege to say thank you to my best friends **Nely RODRÍGUEZ MORAGA**, **Francisco "Pacho" RAMOS MARTÍN**, **Gaël HUET**, **Claudia HERRERA-LEÓN** and **Maria Emilia "Chili" CANO**. I will never forget the time we have spent together, all the nice moments, trips, good food and jokes we shared. I will always cherish **Nely's** encouragements and initiatives. Thanks to you I have tried dancing, climbing and slack line for the first time. Thank you for all the CrossFit sessions with me and thank you for "teaching" me Spanish. Thank you for your support during the thesis writing. Time spent with you in the house was precious. Thank you **Pacho** for your stories. Thanks to you I know everything about the Pelotos lab and people in Madrid. Your mental energy, your observations and your capacities for making people laugh are incredible. Thank you for including me. I hope one day I will be in one of Pachos stories. **Gaël**, the moments with you were always good. Our little competition, either on CrosFit, either when running or playing board games are unforgettable. **Claudia** the brave Lion, that come to rainy Amiens with a contagious smile. Thank you for the nice food and experiences that you brought to us from Mexico. I will always remember our trips together. **Chili** your calmness is incredible. One day I would like to be like you, even in the hardest situations you manage to keep a smile on your face. Thank you all for being the perfect friends. You made my stay in Amiens unforgettable.*
😊😊😊😊😊😊😊😊😊😊😊😊😊😊😊😊😊😊😊😊😊😊😊😊😊😊😊

My deepest and sincerest gratitude goes to my family. Thank you, your unconditional love and unlimited support, through every step of my journey. Thank you!

I love you.

*Želio bih zahvaliti mojoj **mami Vlasti**, **tati Darku**, **braći Marku i Luki** te njihovima curama **Mihaeli i Patriciji**, **baki Ani** i **djedu Josipu** za njihovu bezuvjetna ljubav i beskompromisnu potporu kroz svaki korak mog putovanja. Bez vaše potpore ne bih bio ovdje. Znam da rijetko kada vam to govorim ali vi ste najbolja obitelj koju netko moze zaželjeti. Veselim se daljnjem druženju sa vama i mojim malim nečacima **Hanom** i **Janom**.*

Hvala!

Volim vas!

TABLE OF CONTENT

ABBREVIATIONS

AT	*Arabidopsis thaliana*
AA	Amino acid
ADPG	Arabidopsis dehiscence zone polygalacturonase
AGA	Apiogalacturonan
AnPGC	*Aspergillus niger* PGC
AnPGI	*Aspergillus niger* PGI
AnPGII	*Aspergillus niger* PGII
BnPGIP	*Brassica napus* PGIP
C	Carbon
CESA	Cellulose synthase
Col	Columbia
CW	Cell Wall
DA	Degree of acetylation
DAMPs	Danger associated molecular patterns
DcPelC	*Dickeya chrysanthemi* PelC
DcPME	*Daucus carrota* PME
DdPME	*Dickeya dadanti* PME
DM	Degree of methylesterification
EDTA	Ethylenediaminetetraacetic acid
Endo-PGs	Endo-polygalacturonases
Endo-PLs	Endo pectate lyases
Endo-PNLs	Endo-pectin lyases
EtOH	Ethanol
Exo-PGs	Exo-polygalacturonases
Exo-PLs	Exo-pectate lyases
FN3	Fibronectin-type III
FpPG1	*Fusarium phyllophilum* PG1
GalA	Galacturonic acid
GATL	GAUT-like
GAUT	Galacturonosyltransferase
GH	Glycoside hydrolase
GH28	Glycoside hydrolase 28
HG	Homogalacturonan
HG-AT	HG-acetyltransferase
HGME	Homogalacturonan Modifying Enzymes
HMM	Hidden Markov Models
JA	Jasmonic acid
LRR	Leucine-rich repeat
MAN	Mannose

MAPK	Mitogen activated protein kinases
Mbp	Mega base pair
Me	Methyl
MeOH	Methanol
MST	Micro Scale Thermophoresis
n	Number
NAG	N-acetylglucosamine
O	Oxygen
OD	Optical density
OGs	Oligogalacturonides
ORF	Open reading frame
PAE	Pectin acetylesterase
PCR	Polymerase chain reaction
PCW	Primary Cell Wall
PGA	Polygalacturonic acid
PGIP	PG-inhibiting protein
PGLR	Polygalacturonase lateral root
PGX1	Polygalacturonase involved in expansion1
PLLs	Pectate lyase-like
PME	Pectin methylesterase
PMEI	PME Inhibitor
PvPGIP	*Phaseolus vulgaris* PGIP
QRT	QUARTET
RCPG	Root cap polygalacturonase
RE	Restriction enzyme
RG-I	Rhamnogalacturonan I
RG-II	Rhamnogalacturonan II
RGase	Rhamnogalacturonase
Rha	Rhamnose
ROS	Reactive oxygen species
rpm	Rotation per minute
RT	Room temperature
SA	Salicylic acid
SAXS	Small Angle X-ray Scattering
SCW	Secondary Cell Wall
SW	Sub well
WAK1	Wall associated kinase 1
WT	Wild-type
XGA	Xylogalacturonan
XyG	Xyloglucan

LIST OF FIGURES

SUPPLEMENTARY FIGURES

LIST OF TABLES

SUPPLEMENTARY TABLES

RESUME EN FRANÇAIS DE LA THESE

1. Introduction générale

Comprendre les mécanismes qui gouvernent le développement et les réactions de défenses des plantes est crucial pour améliorer nos connaissances fondamentales et plus largement pour mieux produire et exploiter la biomasse végétale. La paroi, qui entoure chacune des cellules végétales, représente la majorité de la biomasse végétale. La paroi est constamment remaniée, par l'activité d'enzymes, pour permettre de réguler le développement et les réactions de défense. Une meilleure compréhension de la structure et de l'activité de ces enzymes est donc nécessaire afin de mieux comprendre leurs rôles dans la modulation fine de la chimie des polysaccharides et de leurs propriétés mécaniques.

1.1. La paroi primaire et les pectines

Chez les plantes dicotylédones telles que la plante modèle *Arabidopsis thaliana* et le lin cultivé *Linum usitatissimum*, la paroi primaire est composée de deux polymères majeures, exploités par différentes industries : la cellulose pour, ses propriétés mécaniques, et les pectines pour leur propriétés gélifiantes. Structurellement, la paroi primaire est constituée de microfibrilles de cellulose enchevêtrée dans une matrice complexe composée de xyloglucanes (les principales hémicelluloses) et de pectines. L'arrangement de ces différents polysaccharides, associés à des protéines structurales, en un réseau organisé et dynamique, confère à la paroi une complexité structurale qui est à l'origine de ses diverses fonctions: résistance aux contraintes environnementales, détermination de la forme des cellules, port érigé de la plante et régulation des processus d'élongation et de différenciation cellulaire. Pour permettre à la fois le contrôle de la rigidité de la paroi, nécessaire au port érigé des plantes, et le relâchement pariétal indispensable à l'élongation cellulaire, de nombreuses familles de protéines vont intervenir dans le remodelage de celle-ci.

En particulier, les enzymes de remodelage des pectines ont pour rôle de moduler la structure fine des pectines, qui est le polysaccharide le plus complexe et le plus abondant dans la paroi primaire. De par leurs propriétés gélifiantes, les pectines ont en effet une fonction importante dans l'architecture pariétale et le contrôle de ses propriétés mécaniques. Les pectines sont constituées de

quatre principaux domaines riches en acide galacturonique (GalA) : les homogalacturonanes (HG), les rhamnogalacturonanes de type I, et en quantité mineure les rhamnogalacturonanes de type II et les xylogalacturonanes. Les HG, qui correspondent au polymère pectique le plus simple d'un point de vue structural (enchainement linéaire de GalA) sont néanmoins majoritaires puisqu'ils représentent 60 à 65% des pectines de la paroi primaire. Ils sont synthétisés au niveau de l'appareil de Golgi puis secrétés sous forme hautement méthylestérifiée (jusqu'à 80%) et faiblement acétylée (~5-10%) vers la paroi où ils peuvent être sélectivement déméthylestérifiés par les pectine méthylestérases (PME, 66 isoformes chez Arabidopsis) et déacétylés par les pectine acétylestérases (PAE, 12 isoformes chez Arabidopsis).

Ces dernières années, il a été montré que les pectines pouvaient jouer un rôle central dans la régulation du développement et dans la réponse au stress. En particulier la modulation du degré de méthylestérification (DM) apparaît de première importance. En effet, les HG partiellement déméthylestérifiés par les PME pourraient se lier entre eux grâce à des liaisons avec le Ca^{2+} et former des structures rigides de type « boîte à œufs ». Les HG partiellement déméthylestérifiés peuvent également être la cible d'enzymes de dégradation telles que les polygalacturonases (PG, 68 isoformes chez Arabidopsis) et les pectate lyases-like (PLL, 26 isoformes chez Arabidopsis). Au travers de l'action de ces différentes enzymes, le remodelage de la structure des HG affecte les propriétés gélifiantes des pectines et peut avoir d'importantes conséquences sur les propriétés mécaniques de la paroi.

Ces différentes enzymes sont, chez les plantes, des acteurs majeurs permettant de moduler de manière contrôlée les propriétés chimiques et mécaniques des pectines au cours du développement et en réponse aux stress. Cependant, de nombreux pathogènes de plantes tels que des champignons, des bactéries mais également des herbivores possèdent aussi dans leur arsenal enzymatique des enzymes de remodelage des pectines. A première vue, celles-ci apparaissent relativement similaires à celles de plantes, incluant notamment des PME, PG et PLL. Chez les pathogènes elles vont permettre la dégradation des pectines qui, associée à la dégradation d'autres domaines pariétaux, va faciliter l'infection au sein des cellules. Compte tenu de ces rôles distincts, des différences de structure protéique, de spécificités de substrats mais également de mode d'action doivent exister entre les enzymes de plantes et de pathogènes. Comprendre ces différences est un des objectifs de ce travail de thèse.

1.2. Les enzymes de modification des pectines

A l'heure actuelle de nombreux gènes codant des enzymes de modification des pectines ont été identifiés chez les plantes ainsi que chez de nombreux phytopathogènes. Dans la majorité des cas, ces enzymes appartiennent à des familles multigéniques. Cela est d'autant plus vrai chez les plantes et en particulier les plantes à fleurs apparues plus récemment au cours de l'évolution. De façon intéressante, l'augmentation du nombre d'isoformes concorde avec un accroissement de la complexité de la paroi et des pectines, ce qui suggère une régulation plus fine de la modification des pectines par ces familles d'enzymes. Même si tous ces gènes ne sont pas exprimés de manière identique, le rôle d'une telle diversité d'isoformes potentielles dans le remodelage des pectines peut poser question. Cela pourrait en effet suggérer des spécificités particulières, nécessaire au contrôle de la structure des pectines dans des contextes de microdomaines pariétaux (pH, ion, structure des pectines…).

1.2.1. Les pectine méthylestérases (PME)

De par leur activité de déméthylestérification, les PME vont libérer du méthanol ainsi que des protons H^+, participant ainsi à l'acidification de la paroi. Qu'elles soient d'origine végétale ou de pathogènes, il a été montré que l'activité des PME est dépendante du pH mais également de leur environnement ionique. Cela conditionne notamment l'interaction avec leurs substrats. En effet les HG sont d'autant plus chargés négativement qu'ils sont déméthylestérifiés. Ceci s'expliquant par le fait que chaque groupement méthyle libéré conduit à la formation d'un groupement carboxylique libre sur le GalA. Au-delà d'une régulation directe de l'activité PME qui passe par les ions et le pH environnant, des inhibiteurs protéiques ont été identifiés. Ils sont appelés PMEI pour PME Inhibitor et vont former un complexe stœchiométrique 1:1 avec les PME. Cette interaction bloque alors l'accès du site actif de l'enzyme à son substrat, empêchant ainsi la déméthylestérification. Fait intéressant, les PMEI n'existent que chez les plantes et ne peuvent inhiber que les PME endogènes. Cela implique donc un rôle des PMEI dans la régulation fine des PME endogènes lors du développement mais pas dans l'inhibition des enzymes de phytopathogènes lors des réactions de défense.

D'un point de vue structural, les PME peuvent être sous divisées en 2 groupes selon les domaines présents dans leurs séquences protéiques. Dans le premier groupe (groupe 1), les protéines sont constituées d'une partie mature et active, généralement précédée par des motifs

d'adressage vers la paroi (peptide signal notamment). Le second groupe (groupe 2 ou proPME) est composé d'isoformes, qui présentent une extension du coté N-terminal, appelée partie PRO. Cette partie PRO présente des similarités avec les PMEI et pourrait avoir une activité auto-inhibitrice. La majorité des proPME présentent des motifs dibasiques conservés (RRLL ou RKLL), situés entre la partie PRO et la partie mature, qui pourraient constituer un site de clivage protéolytique. Ces motifs de clivage pourraient être ciblés par les protéases de type subtilisine au cours de la maturation des PME dans le trans-Golgi. Le clivage de la partie PRO semble être un prérequis pour la sécrétion de PME actives dans la paroi, et il est probable que la partie PRO inactive les proPME au cours de leur transit dans l'appareil de Golgi, afin d'éviter une déméthylestérification précoce des HG avant leur sécrétion. Cette hypothèse est en adéquation avec le fait que seul les PME de groupe 1 ont été identifiées chez les pathogènes qui ne présentent par ailleurs pas de transit de l'enzyme avec leur substrat cible. Au contraire de ces différences de domaines, toutes les PME dont la structure tridimensionnelle a été résolue présentent au niveau du domaine mature un site actif conservé avec deux résidus aspartiques, deux résidus glutamines et une arginine, aussi bien pour des PME de plantes que de pathogènes.

Malgré un site actif conservé, les PME ne catalysent pas toute la déméthylestérification de façon similaire. Certaines PME peuvent effet déméthylestérifier les HG de façon processive. Cela implique la libération d'HG déméthylestérifiés en blocs, lesquels étant chargés négativement pourraient interagir avec des ions Ca^{2+} et former ainsi les structures de type « boite à œufs » mentionnées précédemment. *In vitro*, une telle interaction a été montrée comme favorisant la formation de gels pectiques et une rigidification de la paroi *in planta*. Cependant d'autres PMEs pourraient avoir un mode d'action plus aléatoire, c'est-à-dire une déméthylestérification discontinue, ne conduisant pas à la libération de blocs déméthylestérifiés. Cela aurait comme conséquence de favoriser la création de sites multiples d'hydrolyse pour les PG et PLL, lesquelles peuvent hydrolyser les HG et produire des oligogalacturonides (OGs). Cette hydrolyse permettrait à la fois un relâchement de la paroi et les OG libérés pourraient avoir un rôle dans la signalisation cellulaire. Cependant, des régions pectiques déméthylestérifiées en bloc pourraient aussi, dans certains cas, être des substrats pour des PG et PLL conduisant à la libération d'OGs de structures distinctes.

1.2.2. Les polygalacturonases (PG)

Les PG dégradent les HG par une hydrolyse des liaisons α1-4 des GalA, conduisant à la libération d'OGs. Selon le DM du substrat hydrolysé, les OG libérés vont différer dans leur degré de polymérisation (DP), leur degré de méthylesterification (DM) mais également leur degré d'acétylation (DA). Au sein de cette famille d'hydrolase, deux types d'activités ont été identifiées : les endo-PG et les exo-PG, qui vont hydrolyser de façon aléatoire en interne à la chaîne d'HG, ou spécifiquement au niveau des extrémités non réductrices. La première activité conduit à la production d'OGs de tailles variables tandis que la seconde permet la libération d'OGs de DP2 et 3. Quel que soit le type de PG, leur activité est généralement optimale à pH acide sur des HG présentant de faible DM. Une action préalable des PME est par conséquent un prérequis à l'activité des PG. Chez les plantes, les PGs sont sécrétées dans la paroi, *via* l'appareil de Golgi, où elles vont pouvoir dépolymériser les HG afin de réguler leurs propriétés gélifiantes et la production d'OG signalisant. A l'heure actuelle les PG végétales qui ont été caractérisées à partir d'extraits de paroi sont principalement de type endo tandis que chez les pathogènes, les deux types d'activités PG sont fréquemment identifiés. De telles différences pourraient s'expliquer par des différences structurales. Cependant les PG dont la structure est caractérisée présentent toute un site actif hautement conservé impliquant notamment des résidus aspartiques. Mais peu d'éléments permettent actuellement d'expliquer la différence entre activités endo et exo-PG, ou de comprendre les différences de liaison au substrat ou de processivité. Une compréhension plus approfondie de ces aspects nécessite de pouvoir déterminer la structure de PG de plantes, ce qui n'a pas encore été réalisé à l'heure actuelle.

Comme pour les PME, des inhibiteurs de PG appelé PGIP ont été identifiés chez les plantes. Ils seraient cette fois majoritairement impliqués dans l'inhibition des PG sécrétées par les pathogènes puisque c'est essentiellement contre ce type de PG que leur inhibition a été démontrée. Cependant contrairement au PMEI où l'absence d'inhibition sur les PME exogènes est claire, et parfaitement documenté, les déterminants structuraux des interactions, ou absence d'interaction, entre PGIP et PG de plantes restent à démontrer. Pour cela, il est de nouveau nécessaire de résoudre la structure tridimensionnelle de PG végétales.

La compréhension des déterminants structuraux et des propriétés biochimiques des PG d'origine végétale et pathogène pourrait également permettre d'identifier des OG pouvant être

libérés *in planta* lors de processus développementaux ou en réponse au stress. Ces molécules étant historiquement connues pour leur action élicitrice dans les mécanismes de défenses des plantes, elles pourraient également jouer un rôle essentiel dans la régulation du développement. Les caractériser plus finement permettrait aussi à long terme de développer de nouvelles stratégies de lutte contre les ravageurs de cultures.

1.2.3. Les pectate lyases (PLL)

Les PLL vont cliver les HG par β-élimination, ce qui conduit à la création d'une liaison insaturée. Au sein des PLL, deux sous-familles sont distinguées : les pectate lyases (PL) et les pectine lyases (PNL). Les PL présentent une affinité forte pour des HG faiblement méthylestérifiés voire complétement déméthylestérifiés, tandis que les PNL ont une préférence pour des substrats hautement méthyléstérifiés. Une autre différence réside dans leur dépendance au pH et aux ions Ca^{2+}. En effet les PL sont particulièrement actives à pH alcalin et en présence de calcium tandis que les PNL ont une activité optimale à pH acide et en absence d'ions Ca^{2+}. Des activités endo et exo pour les PL et les PNL ont été mises en évidence. Ces deux sous-familles ont été identifiées chez les plantes et les pathogènes, même si les activités PL sont majoritairement retrouvées chez les plantes. Au contraire chez les phyto-pathogène de nombreuses PNL ont été caractérisées, notamment chez les champignons tandis que des PL sont fréquemment observées chez les bactéries.

Ici encore une telle diversité rend difficile la compréhension des mécanismes qui régulent ces enzymes, et nécessite des caractérisations fines de leur structures et leurs propriétés biochimiques. Cela permettrait également de mieux caractériser les OG que ces enzymes pourraient libérer au sein de la paroi.

2. Chapitre 1 – PGLR et ADPG2 : deux PG d'Arabidopsis qui différent dans leur structure et leur processivité

Dans ce premier chapitre, le principal objectif était de produire des PG végétales en système hétérologue afin de les purifier pour les caractériser biochimiquement, mais aussi pour en déterminer la structure tridimensionnelle par diffraction des cristaux aux R-X. Cela a été réalisé avec succès pour deux PG d'Arabidopsis : ADPG2 (Arabidopsis Dehiscence zone PolyGalacturonase 2) et PGLR (PG Lateral Roots). Ces deux PG présentent un patron d'expression recouvrant dans la zone d'émergence des racines latérales chez Arabidopsis. Le choix de ces deux protéines doit permettre de déterminer en quoi deux PG exprimées de manière similaire au niveau

spatio-temporel peuvent différer dans leurs structures, spécificités de substrat et leurs modes d'action.

Après production de ces deux PG chez la levure *Pichia pastoris*, les enzymes ont été purifiées et leurs propriétés biochimiques ont été déterminées. ADPG2 et PGLR présentent une affinité pour des pectines de faibles DM et une activité optimale à pH acide. Indépendamment du substrat, ADPG2 présente une plus forte activité catalytique que PGLR. Par une approche de LC-MS/MS récemment développée au laboratoire, et qui permet d'analyser le profil des OG libérés après digestion d'un substrat pectique par une PG, nous avons pu caractériser ce profil pour les deux enzymes. Ainsi, PGLR et ADPG2 produisent des pools d'OGs distincts du point de vue de leur DP et DM et de leur DA : A partir de paroi de racines, ADPG2 produit des OG de plus faible DP (DP2-4) par rapport à PGLR, qui libère par ailleurs des OGs acétylés. Cela suggère une différence de processivité qui pourrait être reliée à une différence de liaison entre l'enzyme et le substrat.

En parallèle des expériences de cristallographie ont été menées et des cristaux ont été obtenus pour ces deux PG. La diffraction aux R-X a permis de résoudre la structure de ces deux PG avec des résolutions de 1,3 Å (PGLR) et 2,03 Å (ADPG2). Ces deux structures ont été comparées, montrant une conservation du site actif avec trois résidus aspartiques, deux histidines, une lysine, une arginine et une asparagine hautement conservés. Mais l'analyse a aussi mis en lumière des différences d'acides aminés au niveau des sous-sites avoisinant le site actif. Cela a permis d'établir que PGLR pouvait avoir une activité processive comparée à ADPG2, dont l'activité non processive conduit à la libération d'OG de plus petit DP, comme révélé par les approches de LC-MS/MS. Une analyse approfondie des potentiels électrostatiques de ces sous-sites a permis d'associer ces différences de mode d'action à la spécificité vis-à-vis du pH. En outre, l'analyse des structures et des comparaisons avec d'autres structures de PG fongiques a aussi permis de montrer les déterminants structuraux de l'interaction PG-PGIP. En effet les acides aminés essentiels à l'interaction (principalement une Asparagine et une Leucine) se trouvent être absents dans les PG végétales, expliquant ainsi l'absence d'inhibition des activités PG de plantes par des PGIP endogènes.

Cette étude a donc permis de démontrer que deux PG exprimées au même endroit, et à première vue similaires dans leurs propriétés biochimiques et au niveau de leur site actif, différent dans leur processivité ce qui peut expliquer la libération d'une d'un panel d'OGs distincts. *In planta* ces deux

PG pourraient moduler de manière différentielle l'hydrolyse des pectines, entraînant la production d'OG ayant des potentiels de signalisation différents ; Les travaux issus de cette étude feront prochainement l'objet d'une soumission au journal PNAS. Les structures ont quant à elles déjà été déposées sur PDB sous les identifiants 7B7A et 7B8B, respectivement pour PGLR et ADPG2.

3. Chapitre 2 – Caractérisation de VdPME1 et VdPG2 : deux enzymes de modification des pectines d'origine fongique

Dans ce second chapitre, l'objectif principal était d'étudier deux enzymes de modification des pectines, qui interviennent dans l'infection de plante par un pathogène. Ceci doit permettre de comprendre en quoi leurs caractéristiques biochimiques et structurales peuvent influencer la façon dont elles dégradent les HG au cours de l'infection. Pour cette étude nous avons donc choisi de travailler sur VdPME1 et VdPG2, deux enzymes sécrétées par le champignon *Verticillium dahliae*, connu pour sa pathogénicité sur le lin cultivé. Le choix d'une PME et d'une PG permet d'avoir une idée des changements séquentiels, opérés par les PME, qui sont nécessaire à l'action des PG.

Comme pour les deux PG végétales étudiées précédemment, ces deux enzymes ont été produites en système hétérologue, *Pichia pastoris*. Après purification, leurs caractéristiques biochimiques ont été déterminées. Nous avons ainsi démontré que VdPME1 avait une activité optimale à pH6 pour des substrats modérément méthylestérifiés, tandis que VdPG2 était particulièrement active à pH5 sur des HG faiblement ou non-méthylestérifiés. Ces résultats sont en adéquation avec les données publiées pour d'autres enzymes du même type ayant une origine fongique. De plus, grâce à l'utilisation de profilage par LC-MS/MS mentionnée précédemment, les OG libérés suite à l'action de VdPG2 sur des pectines commerciales ont été identifiés. Cela a permis de mettre en évidence une activité endo-PG libérant des OG à la fois non méthylestérifiés et méthylestérifiés. Cette même digestion réalisée après l'action de VdPME1, conduit à la libération d'OG non méthylestérifiés de faible DP, suggérant une action processive de cette PME qui conduit à une déméthylestérification complète du substrat.

La modélisation de la structure tridimensionnelle de ces deux enzymes a permis de confirmer les observations expérimentales. En effet VdPG2 présente une structure similaire à celles des endo-PG actuellement caractérisées. VdPME1 présente quant à elle une structure typique de PME fongique et l'analyse des potentiels électrostatiques de surface a permis d'émettre des hypothèses quant à la processivité de cette enzyme.

Enfin l'action de ces enzymes pouvant être déterminante dans la pathogénicité de *Verticilium*, des pectines de parois de lin ont été digérées avec VdPG2. Pour cela deux variétés ont été utilisées : Evéa (partiellement résistant) et Violin (partiellement sensible). Si le profil des OG libérés par VdPG2 à partir des parois de ces deux variétés est relativement similaire, un OG (GalA3Me) n'a été identifié que pour Evéa. Cet OG, s'il est libéré de façon endogène suite à l'infection par le champignon, pourrait avoir un rôle d'éliciteur de défenses, pouvant expliquer en partie la tolérance partielle de ce génotype.

Ces travaux ont fait l'objet d'une publication dans la revue International Journal of Biological Macromolecules en 2021.

4. Chapitre 3 – Caractérisation biochimique et structurale de VdPelB : une enzyme de dégradation des pectines ayant une activité pectin-pectate lyase

Ce troisième et dernier chapitre présente une étude réalisée sur une PLL de *Verticillium dahliae*, VdPelB. Cette enzyme a été étudiée en regard de VdPME1 et VdPG2 afin de pouvoir caractériser une enzyme de chaque famille chez le champignon pathogène du lin. Cependant, les résultats obtenus sur VdPelB ont rapidement justifié une étude spécifique : l'enzyme présente des propriétés biochimiques de PL mais aussi de PNL, ce qui est inhabituel. L'activité de VdPelB est dépendante du calcium et optimale à pH neutre/alcalin, ce qui est assez caractéristique des PL. Par contre elle présente une spécificité de substrat particulière puisqu'elle a une activité optimale sur des substrats hautement méthyléstérifiés, caractéristiques des PNLs. Afin d'approfondir d'analyser plus finement ces caractéristiques inhabituelles, l'approche de LC-MS/MS précédemment décrite a été utilisée et les OG libérés par cette enzyme ont été identifiés et comparés avec ceux libérés par une PL d'Aspergillus. L'analyse des OG libérés par VdPelB après digestion de différents substrats pectiques de DM variables, a révélé des différences notables avec ceux de la PL d'Aspergillus. Les résultats obtenus ont également confirmé une forte affinité de VdPelB pour des pectines hautement méthylestérifiées.

Pour identifier les déterminants structuraux pouvant expliquer une telle activité, la structure tridimensionnelle de VdPelB a été déterminée à une résolution de 1,2 Å. La structure a permis de révéler un site actif similaire à celui de nombreuses PLL caractérisées à ce jour, et d'une triade de résidus aspartiques permettant l'interaction avec les ions Ca^{2+}. Les différences ne semblant pas résider au niveau du site actif, les sous-sites on t été analysés. Cela a permis de montrer que, si la

majorité des acides-aminés présents au niveau des sous-sites étaient caractéristiques des PL, deux acides aminés, une Thréonine et une Glycine, sont distincts. Ces deux acides aminés remplacent des Arginines, Glutamines et Lysines habituellement localisés dans cette région des PLs. Les charges positives de ces acides-aminés pourraient ainsi expliquer l'interaction des PL avec des substrats faiblement méthylestérifiés, dont les charges négatives sont importantes. Au contraire, Glycine et Thréonine ne présentent pas les mêmes charges ce qui peut expliquer une moins bonne affinité pour de faibles DM. Par ailleurs, considérant la taille de ces deux acides aminés, l'encombrement stérique serait différent de celui d'une PL typique et permettrait une meilleure accommodation de substrat hautement méthylestérifiés.

Enfin, les pectines de parois de lin d'Evéa et de Violin ont été digérées par VdPelB et le profil des OG libérés a été analysé. Des différences au niveau de la diversité des OG libérés ont été identifiées, suggérant des changements au niveau de la structure des pectines entre ces deux variétés. Ceci pourrait conduire à la libération d'OG distincts lors de l'infection par *Verticillium*. Comme pour VdPG2 ceci pourrait en partie expliquer le fait qu'Evéa soit partiellement tolérant à *Verticilium* contrairement à Violin.

Cette étude fera prochainement l'objet d'une soumission dans un journal international à comité de lecture. La structure a quant à elle déjà été déposée sur PDB sous l'identifiant 7BBV.

5. Conclusion Générale et Perspectives

Les objectifs de la thèse étaient multiples et ont visé à identifier i) les spécificités biochimiques pouvant exister entre deux PG de plantes dont les patrons d'expression sont recouvrant, ii) les déterminants structuraux de ces mêmes PG expliquant les différences de processivité dans l'hydrolyse des pectines, iii) les spécificités de mode d'action d'une PME et d'une PG d'origine fongique impliquées dans la dégradation des pectines lors de l'infection et iv) les corrélations entre la structure et le mode d'action d'une PLL de ce même champignon phytopathogène.

En lien avec les deux premiers objectifs de la thèse, la production en levure et la purification de deux PG de plantes (PGLR et ADPG2) a permis de mettre en évidence des similarités biochimiques, telles que le pH et le substrat optimal. Mais cela a aussi mis en lumière des différences dans la diversité des OG produit par ces deux PG, suggérant des différences de processivité. La résolution de la structure tridimensionnelle de ces deux PG, une première pour des

PG de plantes, a mis en évidence une structure globalement similaire en particulier au niveau du site actif. Cependant des différences ont été observées au niveau des sous-sites et peuvent expliquer des différences de liaison de ces deux PG à des substrats de différents DM, et une activité plus processive pour PGLR comparée à ADPG2. Nous avons identifié des acides aminés clés chez PGLR qui pourraient faire l'objet de mutations chez ADPG2 afin de modifier sa processivité ou encore sa liaison vis-à-vis de substrats méthylestérifiés. La compréhension des déterminants structuraux permettant l'interaction enzymes-substrats étant essentiel, l'accent pourrait également être mis sur l'obtention de co-cristaux entre ces deux PG de plante et des OG en parallèle d'approches de dynamique moléculaire et de « docking ».

La comparaison structurale de ces deux PG avec d'autres PG d'origine fongique a aussi mis en évidence l'absence d'acides aminés déterminants dans l'interaction avec les PGIP. Or les PG de plantes apparaissent comme très rarement inhibées par les PGIP dont l'action est plutôt ciblée contre les PG de pathogènes. La mutation de ces acides aminés dans les PG de plantes pourrait permettre de valider le rôle clé de ceux-ci dans l'interaction PG-PGIP.

En lien avec le troisième objectif, une PME (VdPME1) et une PG (VdPG2) du pathogène de plante *V. dahliae* ont été produites en levure et purifiées. Ceci a permis de montrer un mode d'action processif de la PME directement lié au potentiel électrostatique de surface de la protéine. Cette processivité pourrait être étudiée en fonction du pH, afin de déterminer la dépendance de cette PME vis-à-vis de celui-ci. La PG présente quant à elle un mode d'action assez classique par rapport à d'autres PG d'origine fongique. Néanmoins de façon intéressante, son action sur des pectines de paroi de lin pour des cultivars sensibles et partiellement tolérants à *V. dahliae* a mis en lumière la production de certains OG qui pourraient avoir une action élicitrice de défense chez le cultivar partiellement tolérant.

Concernant le dernier objectif de la thèse, une PLL de *V. dahliae*, VdPelB, a été produite en levure et purifiée afin de déterminer ses propriétés biochimiques et notamment définir si celle-ci était plutôt de type PL ou PNL. Nos analyses ont révélé que VdPelB possédait des caractéristiques de PL et de PNL, en faisant une enzyme atypique. Ces propriétés mixtes s'expliquent grâce à l'analyse de la structure de cette PLL que nous avons pu obtenir. En particulier deux acides aminés pourraient expliquer une meilleure liaison à des substrats méthylestérifiés alors que cette enzyme

présente des caractéristiques essentiellement de type PL. La production de mutants affectés pour ces acides aminés pourrait permettre de valider ces hypothèses. Comme pour VdPG2, la digestion des pectines de lin pour les cultivars sensible et partiellement résistant a de nouveau mis en évidence des différences dans les OG produits, lesquels pourraient avoir un potentiel éliciteur lors des réponses de défense de la plante à l'attaque du pathogène.

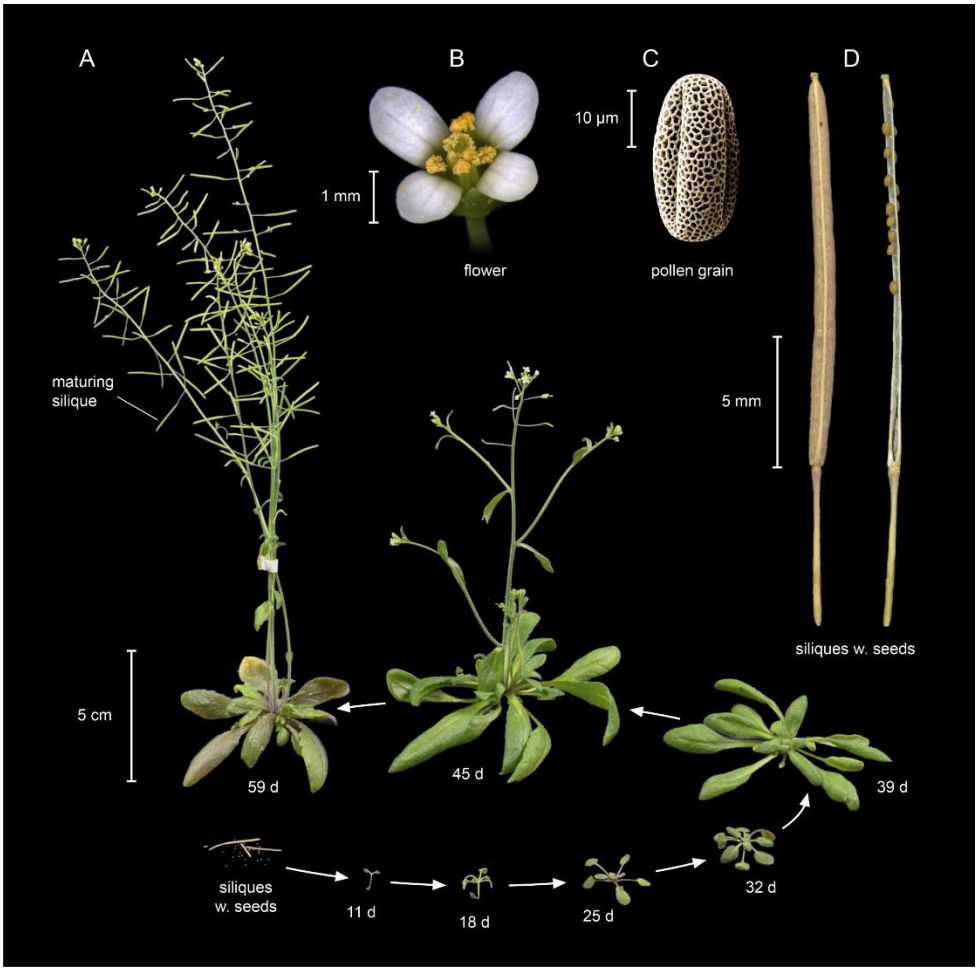

Figure 1. Life cycle of *Arabidopsis thaliana*
A) *Arabidopsis thaliana* accession Columbia (Col) at different stages of the life cycle, from seeds to seedlings (11 days), vegetative growth (39 days) and reproductive growth (45 days). B) Flowers, C) Pollen grain, D) Mature silique. Adapted from Krämer, 2015.

GENERAL INTRODUCTION

1. Chapter – Model organisms

1.1. *Arabidopsis thaliana* – a powerful model system for plant cell wall research

Arabidopsis thaliana (L.) Heynh. is a model plant for molecular biology, genetics and biochemistry researches. Arabidopsis, mouse ear cress or thale cress, is a flowering plant native from Eurasia and Africa, which belongs to the taxonomic family of the Brassicaceae in the eudicotyledonous group of angiosperms (Krämer, 2015). It has a short life cycle of six weeks where after three-weeks, the central stem produces flowers that self-pollinate. The plant usually grows up to 20-25 cm tall with leaves that form a rosette at the base of the plant (**Figure 1**). Roots are simple with a single primary root that grows vertically producing smaller lateral roots.

The popularity of *A. thaliana* as a model organism notably originated from its genome sequencing by the Arabidopsis Genome Initiative (Kaul et al., 2000), being the first published nuclear genome among flowering plants. Genome of a diploid *A. thaliana* comprises two sets of n = 5 chromosomes with a genome size of 157 Mbp making it a one of the smallest known flowering plants' genomes (Bennett et al., 2003). The most up-to-date version of the *A. thaliana* genome is curated by the Arabidopsis Information Resource (TAIR). About 10% of *A. thaliana* genes are coding protein or enzymes involved in cell wall metabolism: This includes cell wall polymers biosynthesis, transport, deposition, remodelling, turnover and regulation (McCann and Carpita, 2008; Liepman et al., 2010).

1.2. *Linum usitatissimum* – an important industrial plant

Fiber flax (*Linum usitatissimum L.*) is a flowering plant that belongs to the Linaceae family (**Figure 2**). Cultivated flax plants grow up to 1.2 m with slim stems. The leaves are glaucous green while flowers are pure pale blue. Flax is an important source of fiber used for textile manufacture,

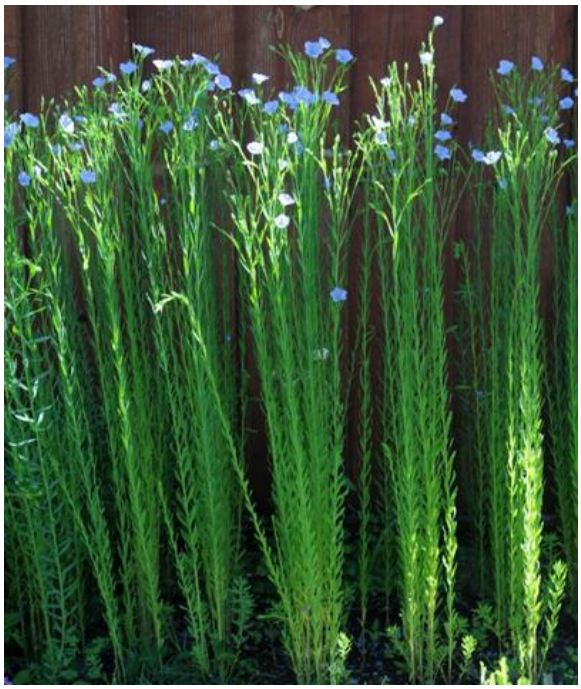

Figure 2. Morphology characterisation of flax
Photo of a flax plant, belonging to the Linacaeae family, with height of up to 1.2 m and blue flowers. Adapted from One Inch World.

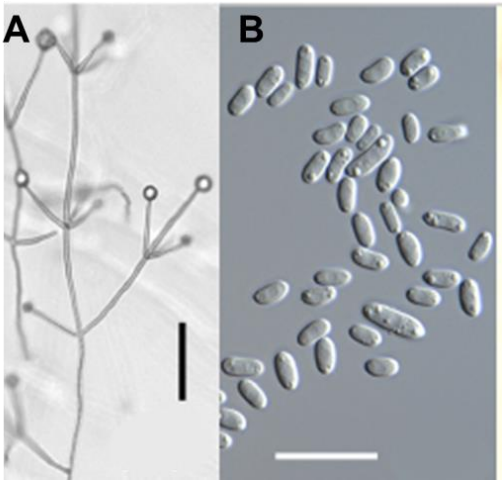

Figure 3. Morphological features of *Verticillium dahliae*
A) *V. dahliae* branched conidiophore 12 days post inoculation on water agar. Scale bar = 50 µm. B) Conidia growth after 9 days on potato dextrose agar. Scale bar = 20 µm. Adapted from Inderbitzin et al., 2011.

as well as more recently for materials, as biofibers that can replace glass fibers. In addition, flax is widely used for its nutritional value as seeds can be used for the production of linseed oil (Yan et al., 2012; Mohamed Zakriya and Ramakrishnan, 2020). France, Belgium and the Netherlands are some of the biggest flax producers, as the conditions in these regions are perfect for growing and retting flax, however the production is facing a new challenge (Yan et al., 2014). Flax is increasingly affected by fungi, such as *Fusarium oxysporum*, *Mycosphaerella linicola* and *Verticillium dahliae* contributing to lowering the yields, as well as seeds and fiber qualities (Wojtasik et al., 2016; Blum et al., 2018; Paumier et al., 2021). This makes flax an interesting model to assess the role of cell wall polymers in mediating tolerance to fungal infection, and to find potential determinants of flax's resistance to pathogens.

1.3. *Verticillium dahliae* – potent plant pathogen

Verticillium dahliae Kleb. is a soil-borne fungal plant pathogen that belongs to the Ascomycota phylogenetic group (**Figure 3**). It causes verticillium wilt in over 300 plant species including many economically important food crops (potato, tomato, cabbage, eggplant, lettuce, broccoli, cucumbers, pepper, pumpkin, spinach), ornamental flowers, trees and shrubs as well as *Arabidopsis thaliana*. *V. dahliae* is becoming prevalent among fiber flax (Fradin and Thomma, 2006; Klosterman et al., 2009; Duressa et al., 2013; Blum et al., 2018). *V. dahliae* infection starts form the root, later invading xylem vessels and progressing in an acropetal direction (Fitzell et al., 1980), leading to water transport disruption and causing the characteristic symptoms of wilting, a vascular discoloration and death of aerial tissues (Fradin and Thomma, 2006; Klosterman et al., 2009). Upon plant death *V.dahliae* survives in the form of microsclerotia, long-term resting spores, which are distributed in the soil or embedded within plant debris, and that have the ability to survive for up to 14 years (Ashworth, 1974; DeVay et al., 1974; Klosterman et al., 2009). Given this, it is interesting to study *V.dahliae* exoproteome, including secreted proteins, that are likely be involved in the infection process (Rep, 2005; Chen et al., 2016).

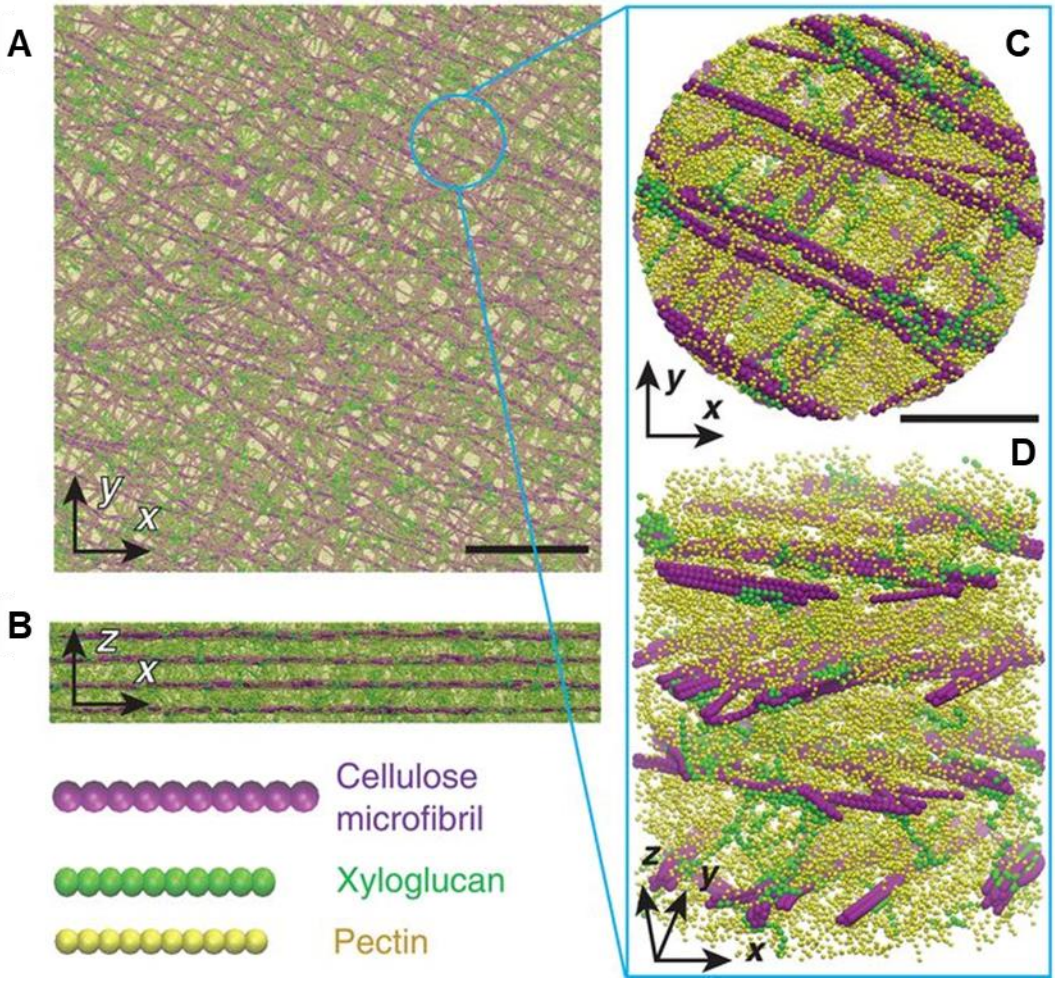

Figure 4. Assembly of the Coarse-Grained Molecular Dynamic model of a plant primary cell wall

Top (A) and side (B) views of the four-lamella wall, shown at the same scale. Close-ups of top (C) and side views (D). Scale bars, 200 nm (A and B), 25 nm (C and D). Adapted from Zhang et al., 2021.

2. Chapter – Primary cell wall

2.1. Structure and composition of the primary cell wall

Plant cell wall (CW) is a complex structure that surrounds, protects and determines the size and shape of the plant cells. Changes in CW structure plays a key role in controlling growth and differentiation processes, cell to cell adhesion, cell signalling and defence. Plant CW is composed of polysaccharides, proteins, aromatic and aliphatic components (**Figure 4**) that enable plants to grow in different environments and conditions (Cosgrove, 1997; Vogel, 2008; Cosgrove, 2016a). The plant CW is also involved in plant defences by acting as a physical barrier against pathogens (Underwood, 2012). The primary (PCW) is composed of 10% of proteins, and 90% of polysaccharides: cellulose, hemicelluloses and pectins in an approximately 30%, 30% and 30% ratio. This composition, while generally accepted, can vary among different species, cell type and location, developmental stage and in response to biotic and abiotic stresses (McNeil et al., 1984; Carpita, 1996; Cosgrove, 1997; Vogel, 2008; Doblin et al., 2010). Cellulose is the main structural polysaccharide of the primary and secondary CW, while pectins and hemicelluloses form a matrix in which cellulose microfibers are embedded (Fry, 2004; Caffall and Mohnen, 2009).

2.1.1. Cellulose

Cellulose is one of the most abundant polymers found in nature. It is a long homopolymer chain composed of β-D-glucopyranose linked by (1–4) glycosidic bonds forming protofibrils that are associated through hydrogen bonding into stiff microfibrils that can lead to a reduction of the extensibility of the CW (Cosgrove, 2016b; Dehors et al., 2019). Cellulose is synthesised by cellulose synthases (CESA). Minimum of three pairs of different CESA enzyme are needed to make a functional complex, rosettes, the different CESA units are used for synthesis of cellulose in primary and secondary CW differ (Cosgrove, 2005). Cellulose can be synthetized between few hundred up to several thousands of units making microfibers of 100 nm (Klemm et al., 2005; Salama, 2019). Its structure is a direct consequence of associations with other cellulose chains trough hydrogen bonding and Van der Waals forces (Caffall and Mohnen, 2009). In dicot such as Arabidopsis, cellulose makes up to 15% to 40% of PCW dry mass (Caffall and Mohnen, 2009). Cellulose can be in two forms, Type I and Type II, which differ in chain orientation but only Type

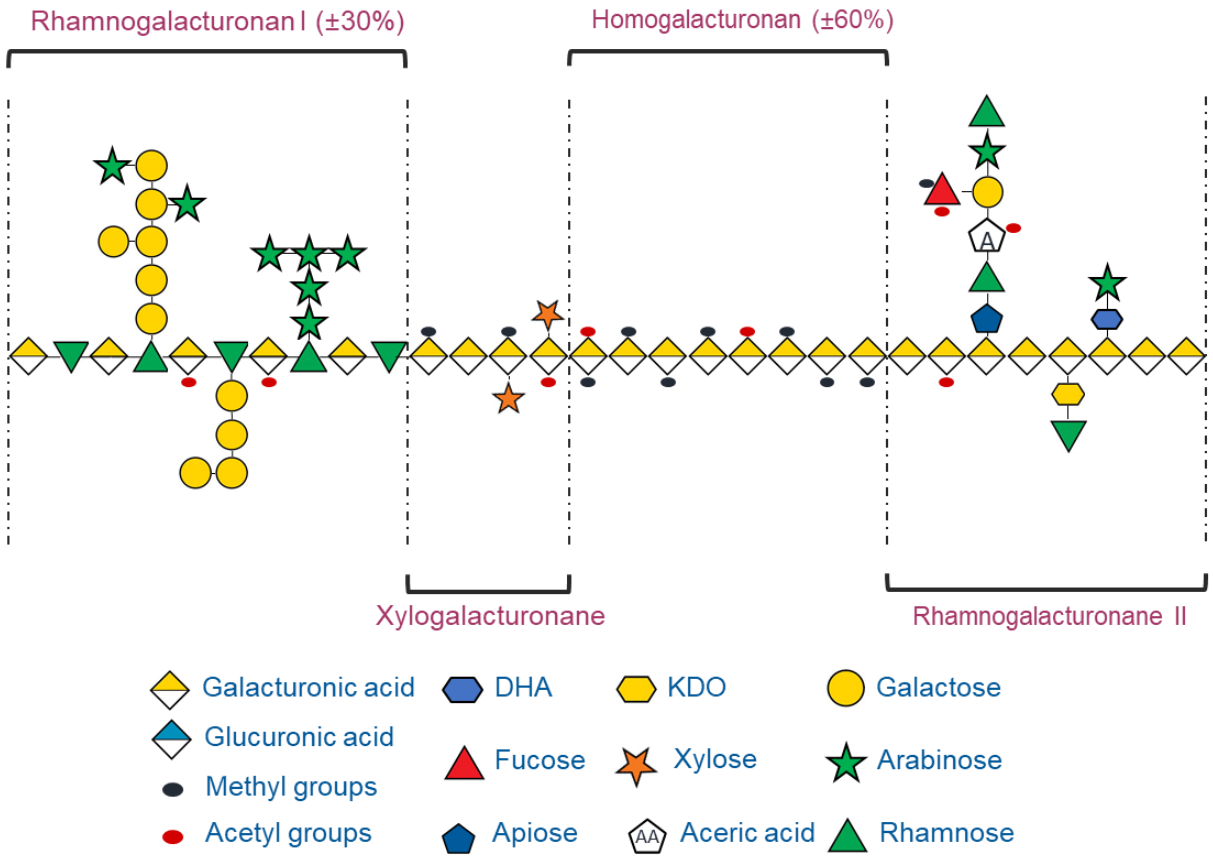

Figure 5. Schematic structure of pectic polysaccharides
Four different domains of pectins can be found. The relative abundance of the different types of pectins varies but rhamnogalacturonan I and homogalacturonan are the major components, whereas xylogalacturonan and rhamnogalacturonan II are minor components. KDO: 3-Deoxy D-manno-2-octulosonic acid; DHA: 3-deoxy-D-lyxo-2-heptulosaric acid. Adapted from Scheller et al., 2007.

I is naturally occurring. PCW cellulose fibers align parallel to cell elongation facilitating growth during primary cell growth (Kataoka and Kondo, 1999; Caffall and Mohnen, 2009).

2.1.2. Hemicelluloses

Hemicelluloses are a large family of CW polysaccharides that include xylans (β-1,4-linked xylose), mannans (β-1,4-linked mannose) and xyloglucans (XyG), linear chain of 1,4-β-glucose with 1-6-linked xylose. Xylose can be substituted by galactose, arabinose and fucose. Branching pattern is functionally and phylogenetically important. (Scheller and Ulvskov, 2010). Considering their structure, the physicochemical properties of the polysaccharides differ. In Arabidopsis, XyG is the most abundant hemicellulose polysaccharide in the PCW, accounting for 20-25% (w/w). XyG-cellulose network has been proposed to contribute to the load-bearing capacity of the PCW, preventing the self-association of cellulose microfibrils and thus regulating cell expansion. The XyG-cellulose network can be further crosslinked to pectins, adding structural and functional complexity to the CW (Carpita and Gibeaut, 1993; Nakamura et al., 2002; Somerville, 2004; Liepman et al., 2010).

2.2. Pectin structure and function

Pectins are complex polysaccharides and a major component of PCW composing up to 30% of cell wall dry mass in dicotyledons (Ridley et al., 2001; O'Neill and York, 2003). Pectins can be defined as polysaccharides rich in galacturonic acid (GalA) and are constituted of distinct domains: homogalacturonan (HG), rhamnogalacturonan I (RG-I) and in minor amounts rhamnogalacturonan II (RG-II) and xylogalacturonan (XGA, **Figure 5**). Due to its complex structure, about 67 glycosyltransferases, methyltransferases and acetyltransferases are required to synthesize pectins (Mohnen, 2008; Atmodjo et al., 2011; Anderson, 2016). Pectins were shown to regulate growth and development as well as cell to cell adhesion, defence responses, leaf abscission, fruit maturation, dehiscence and seed hydration (Ridley et al., 2001; Willats et al., 2001; Wolf et al., 2009; Altartouri and Geitmann, 2015; Altartouri et al., 2019; Haas et al., 2020).

2.2.1. Xylogalacturonan, rhamnogalacturonan II and rhamnogalacturonan I

Xylogalacturonans are composed by a linear chain of α-1,4-linked D-GalA, that can be substituted by β-1,3-xylose branches (Mohnen, 2008; Dehors et al., 2019). RG-II is composed

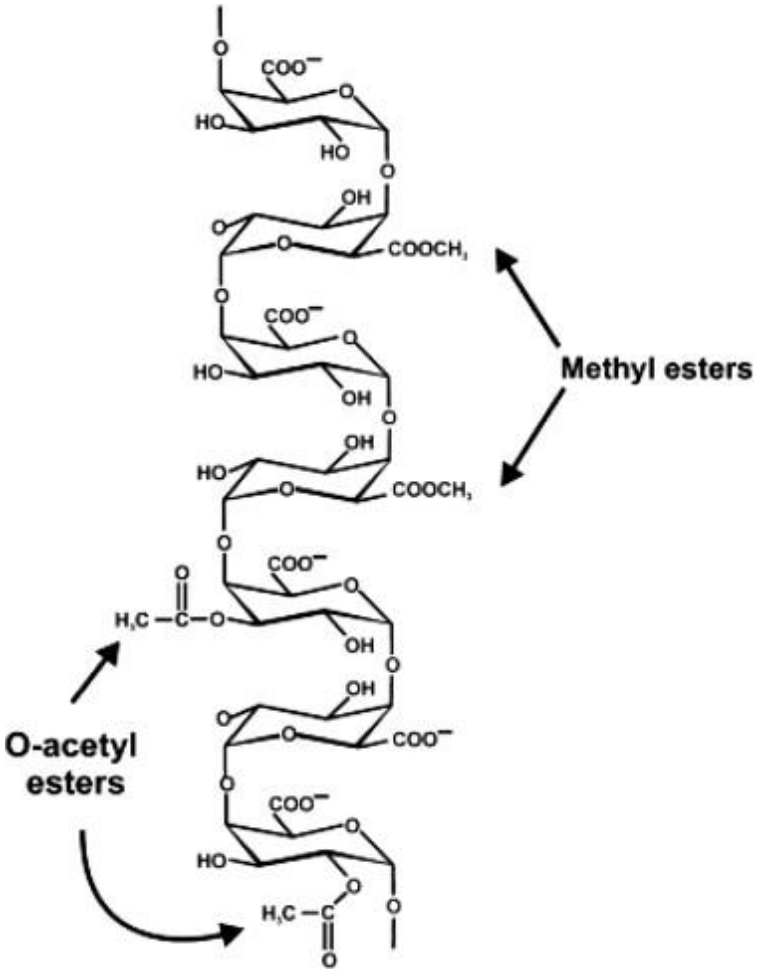

Figure 6. Homogalacturonan structure and modifications
The structure of HG can be methylesterified at carbon C-6 and/or acetylated at O-2 and/or O-3 positions. Adapted from Caffall and Mohnen, 2009.

by a α-1,4-linked D-GalA backbone that can be substituted with up to 12 different types of glycosyl residues including 2-O-methyl xylose, 2-O-methyl fucose, aceric acid, 2-keto-3-deoxy-D-lyxo heptulosaric acid (DHA) and 2-keto-3-deoxy-D-manno octulosonic acid (KDO, O'Neill et al., 2004; Caffall and Mohnen, 2009). RG-II is the most complex plant polysaccharide. RG-I structure consists of repeating units of GalA and rhamnose (Rha, α-D-GalA-1,2-α-L-Rha-1,4) that can be substituted with various side-chains, including galactans (β-1,4-linked D-galactan), arabinans (α-1,5-linked L-arabinan) and type-I arabinogalactan that may be additionally branched (Atmodjo et al., 2013) . RG-I, which can be found as arabinan, galactan, or arabinogalactan in the CW, may be crosslinked to other cell wall components such as xylans, XGA, proteins, and lignin. In a similar way, RG-II domains can interact together via borate ester linkages, which contributes to cell wall strengthening (O'Neill et al., 2004; Caffall and Mohnen, 2009; Dranca and Oroian, 2018).

2.2.2. Homogalacturonan

The most abundant pectin domain is HG, a linear chain of α-1,4-linked D-GalA that can be methylesterified and/or acetylated (**Figure 6**). In Arabidopsis, HG represents up to 60% of pectins dry mass.

HG backbone is synthesized in the *cis*-and *medial*-cisternae of the Golgi apparatus from nucleotide sugars, and is further methylesterified and acetylated by pectin methyltransferases and pectin acetyltransferases (Mohnen, 2008; Sénéchal et al., 2014). HG is synthetized by galacturonosyltransferases (GAUT) and GAUT-like (GATL), which catalyse the transfer of GalA from UDP-GalA to an oligo-GalA acceptor. As an example, HG can be composed of up to 70-100 GalA residues in apple, citrus and sugar beet (Thibault et al., 1993). The Arabidopsis genome contains 15 GAUTs, and 10 GATLs, but the exact function of each isoform in HG biosynthesis remains unclear (Sterling et al., 2001; Sterling et al., 2006; Atmodjo et al., 2013; Anderson, 2016; Lund et al., 2020). Nonetheless, GAUT13 and 14 were shown to be needed for pollen tube growth, as although Arabidopsis *gaut13* and *gaut14* single mutants did not shown any notable difference to the wild-type (WT), double mutants were defective in pollen tube growth (Wang et al., 2013). Furthermore, GAUT1 forms a complex with GAUT7 in the Golgi where they are responsible for synthetizing high-molecular-weight HG (Atmodjo et al., 2011; Amos et al., 2018).

HG can be methylesterified at carbon (C) -6 and/or acetylated at oxygen (O)-2 and/or O-3 (Sterling et al., 2001; Mohnen, 2008; Caffall and Mohnen, 2009; Dranca and Oroian, 2018). Methylesterification of GalA is achieved by putative methyltransferase, including QUASIMODO2, QUASIMODO3, COTTON GOLGI-RELATED2 and/or COTTON GOLGI-RELATED3 (Mouille et al., 2007; Held et al., 2011; Miao et al., 2011; Kim et al., 2015). This results in HG chains that have a degree of methylesterification (DM) typically 80% (Wolf et al., 2009). Homogalacturonans with high DM are unlikely to form a stiff gel making the CW flexible. On the other hand, poorly methylesterified HG (demethylesterified GalA) are negatively charged and can strengthen the PCW by forming complexes between distinct HG chains (so-called "egg-box" structures) thought interaction with calcium. This can affect the rheology of the PCW by promoting the formation of pectic gels (Willats et al., 2001; Cosgrove, 2005; Peaucelle et al., 2012; Dehors et al., 2019). HG-acetyltransferases are responsible for acetylation of HG in Golgi vesicles during HG exocytosis. The distribution and degree of acetylation (DA) depends on the species considered, but it is generally low. In Arabidopsis, the DA is 5-10% depending on the organs considered, while it is 30% in sugar beet (Ralet et al., 2008; Gou et al., 2012; Bonnin et al., 2014) .

The DM and DA can influence the mechanical properties of the CW (Mouille et al., 2007; Wolf et al., 2009; Dehors et al., 2019; Haas et al., 2020). Removal of methyl and acetyl groups is mediated through the activities of homogalacturonan modifying enzymes (HGME). HGs can notably be modified by pectin methylesterases (PMEs; EC 3.1.1.11), which control the DM (Pelloux et al., 2007; Wolf et al., 2009) and pectin acetylesterases (PAEs; EC 3.1.1.6) that hydrolyse the O-linked acetyls (Philippe et al., 2017). The action of PME and PAE creates substrate for polygalacturonases (endo-PGs, EC 3.2.1.15; and exo-PGs, EC 3.2.1.67) and pectate lyases-like enzymes (PLLs), the latter including pectate lyases (endo-PLs, EC 4.2.2.2 ; exo-PLs, EC 4.2.2.9) and pectin lyases (endo-PNLs, EC 4.2.2.10, Sénéchal et al., 2014).

Enzymatic hydrolysis of partially demethylesterified HG, by the action of plant and pathogen PGs and PLLs, can release oligogalacturonides (OGs). These OGs of various DP, DM and DA, can act as danger associated molecular patterns (DAMPs), triggering plant defences through jasmonic acid (JA) and salicylic acid (SA) signalling pathways (Norman et al., 1999; Denoux et al., 2008; Benedetti et al., 2015; Davidsson et al., 2017; Voxeur et al., 2019). Moreover, as pectin is fine-

Table 1. Inventory of PME, PAE, PG and PLL in plant and fungal genomes

Species	Pectin methylesterase (EC 3.1.1.11) CE8	Pectin acetylesterase (EC 3.1.1.6) CE13*	Endo-polygalacturonase (EC 3.2.1.15), exo-polygalacturonase (EC 3.2.1.67), exo-polygalacturonosidase (EC 3.2.1.82), rhamnogalacturonase (EC 3.2.1.171), endo-xylogalacturonan hydrolase (EC 3.2.1.–), rhamnogalacturonan α-l-rhamnopyranohydrolase (EC 3.2.1.40) GH28	Endo-pectate lyase (EC 4.2.2.2), exo-pectate lyase (EC 4.2.2.9), endo-pectin lyase (EC 4.2.2.10) PL1-4
Arabidopsis thaliana +	66	12	68	26
Verticillium dahliae # a	4	2	9	30
Aspergillus niger # b	3	2	20	6
Aspergillus acuelatus # c	7	1	19	35
Fusarium phyllophilum # d	9	3	11	50

[+]Full length Arabidopsis protein data were retrieved from Sénéchal et al., 2014.
[#]Full-length fungal protein data were retrieved from JGI MycoCosm fungal genomic resource.
[a] Klosterman et al., 2011, [b] Pel et al., 2007, [c] de Vries et al., 2017, [d] Ma et al., 2010.

tuned during plant growth and development, CW OGs can regulate gene expression by binding to membrane receptors, such Wall associated kinase 1-WAK, 1 triggering downstream signalling events (Brutus et al., 2010; Kohorn and Kohorn, 2012; Wolf et al., 2012; Ferrari et al., 2013; Sénéchal et al., 2014). For instance, OGs of DP3 were recently shown to act as signalling molecules during dark-grown hypocotyl elongation (Sinclair et al., 2017).

3. Chapter – Homogalacturonan modifying enzymes

3.1. HGMEs, large multigenic families

HGME, consisting of PMEs, PAEs, PGs, PLLs, form large multigenic families in several hundred different species inventoried in CAZy database (Lombard et al., 2010). Currently, there are 9316 entries for the glycoside hydrolase 28 (GH28) family (that includes PGs), 7044 entries for the CE8 family (that includes PMEs), 148 for the CE12 family (that includes PAEs) and 5609 entries for the PL1 family (that includes PLLs). In particular, when comparing Arabidopsis genome to fungal ones (limiting to species that are relevant in the context of the PhD thesis, *V. dahliae*, *Aspergillus niger*, *Aspergillus acuelatus* and *Fusarium phyllophilum*), the differences in numbers are high (**Table 1**). One of the possible explanations is that in Arabidopsis there have been at least 3 genome duplications, leading to a high level of gene redundancy or degeneracy, trough the accumulation of neutral to loss of function mutations (Park et al., 2008). Other possibility that arises from the high number of genes encoding HGME in plants, is the need to spatially and temporally fine-tune HG during development. It has been shown that PMEs, PAEs and PGs isoforms are indeed directly and indirectly involved in a number of physiological processes during vegetative and reproductive plant development (Pelloux et al., 2007; Gou et al., 2012; de Souza et al., 2014; Xiao et al., 2014; Rui et al., 2017).

3.2. PMEs structure and function

A high number of plant and microbial PMEs has been identified. In particular, in Arabidopsis 66 open reading frames (ORFs) encoding putative PMEs have been described. In contrast, despite larger genomes only 41 putative PME-encoding genes have been identified in grass species such

as *Brachypodium distachyon* and rice (*Oryza sativa*); which could be related to the lower amount of HG-type pectins present in the cell wall of Poaceae. As mentioned above, the number of PME isoforms is even lower in fungal species (Pelloux et al., 2007; Sénéchal et al., 2014). According to their sequence, plant PMEs have been divided in two groups: i) Group 1 PMEs have a mature PME domain (PFAM01095) but no PMEI domain. Similarly, no PMEI domain was not found in the proteins of bacteria and fungi; ii) Group 2 contains, in addition to the mature active part, a N-terminus extension, the PRO region (PFAM04043). This region shares similarities with PME inhibitors (PMEI). The processing of group 2 PMEs (removal of the PRO part) by specific subtilisin proteases is required for the export of an active protein to the CW (Camardella et al., 2000; Micheli, 2001; Markovič and Janeček, 2004; Pelloux et al., 2007; Wolf et al., 2009; Del Corpo et al., 2020).

3.2.1. Roles and regulation of PMEs in plants and pathogens

PMEs can be found in plants and microorganisms, where they play an important role in regulating HG structure with consequent effects on CW mechanical properties and development (**Table 2**, Pelloux et al., 2007; Wolf et al., 2009; Wu et al., 2018). As an example of the diversity of their roles, the contribution of PMEs in Arabidopsis is highlighted hereafter. It was for instance shown that *PME17*, a group 2 PME whose processing can be realized by SBT1.3, is involved in regulating root development (Sénéchal et al., 2015). It was further shown that the fine-tuning of the DM of pectins play a central role in primordia emergence: Auxin controls PME activity in the shoot apex and the overexpression of *PME5* can induce the formation of ectopic primordia. The expression of *PME5* is regulated through BELLRINGER, a transcription factor which mutation induce drastic defect on phyllotaxis (Peaucelle et al., 2011; Braybrook and Peaucelle, 2013). Recently, analysis of mutants for *PME2* showed the contribution of this isoform in meditating changes in the mechanical properties of the CW at the top of the dark-grown hypocotyl, with consequent effects on elongation (Hocq et al., 2021, BioRxiv). PME58, which is expressed in mucilage secretory cells was shown to play a role in mucilage structure and organization (Turbant et al., 2016). In addition, PME35 regulates the mechanical strength of the inflorescence stem, showing the relative contribution of pectin in mediating changes in the CW mechanical properties (Hongo et al., 2012). The regulation of PME expression by phytohormones appear of paramount importance: *PME41* was shown to be regulated through brassinosteroids, especially AtBZR1, in

Table 2. Roles of PME in Arabidopsis

Genes	AGI code	Involvement	Reference
PME2	At1g53830	Involved in lateral root emergence and hypocotyl elongation.	Hocq et al., 2021, BioRxiv
PME3	At3g14310	Cell elongation in hypocotyls. Involved in plant immune responses.	Hewezi et al., 2008
PME5	At5g47500	Involved in shoot apical meristem.	Peaucelle et al., 2011
PME6	At1g23200	Embryo development. Stomata function.	Levesque-Tremblay et al., 2015; Amsbury et al., 2016
PME7	At1g02810	Might be involved in basal thermotolerance.	Huang et al., 2017
PME17	At2g45220	Involved in root development and in response to various biotic and abiotic stresses.	Sénéchal et al., 2015
PME21	At3g05610	Expressed in dry and imbibed pollen grains.	Mollet et al., 2013; Leroux et al., 2015
PME23	At3g06830	Expressed in dry and imbibed pollen grains.	Mollet et al., 2013
PME31	At3g29090	Involved in salt tolerance.	Yan et al., 2018
PME34	At3g49220	Involved in thermotolerance.	Huang et al., 2017
PME35	At3g59010	Provides mechanical support to the Arabidopsis stem.	Hongo et al., 2012
PME37	At3g62170	Expressed in dry and imbibed pollen grains.	Mollet et al., 2013; Leroux et al., 2015
PME41	At4g02330	It may serve BR-mediated chilling tolerance in plants.	Qu et al., 2011
PME48	At5g07410	Involved in pollen grain germination.	Mollet et al., 2013; Leroux et al., 2015
PME50	At5g07430	Expressed in dry and imbibed pollen grains.	Mollet et al., 2013; Leroux et al., 2015

Genes	AGI code	Involvement	Reference
PME58	At5g49180	Involved in seed mucilage extrusion.	Turbant et al., 2016
PPME1	At1g69940	Promote pollen tube growth. Involved in plant immune responses.	Tian et al., 2006
QUARTET1 (QRT1)	At5g55590	Separation of pollen grains from tetrads.	Francis et al., 2006
VANGUARD1	At2g47040	Promote pollen tube growth.	Jiang et al., 2005
VGDH1	At2g47030	VGD1 homolog. Expressed in dry pollen grains.	Jiang et al., 2005; Mollet et al., 2013; Leroux et al., 2015

Adapted from Wu et al., 2018.

response to cold-stress (Hewezi et al., 2008; Sun et al., 2010). Furthermore, gibberellic acid regulates the activities of PMEs during hypocotyl growth and rosette expansion (Derbyshire et al., 2007; Ribeiro et al., 2012). It is therefore likely that phytohormones directly or indirectly control the expression, not only of PMEs, but also of all HGMEs (Sénéchal et al., 2014).

PMEs were further shown to play a key role in regulating pectin structure during reproductive development: for instance, and despite high gene redundancy in pollen, VANGUARD1 (VGD1) and PPME1 (PME9) were shown to be key actors of the regulation of pollen tube growth while QUARTET1 (QRT1) facilitate separation of pollen grains from tetrads (Jiang et al., 2005; Francis et al., 2006; Tian et al., 2006). Therefore, plant PMEs appear of major importance to control spatially and temporally the structure of HG to modulate a number of developmental processes. The fine-tuning of PME activity by the specific 1:1 interaction with PMEI is a key element in the regulation of the enzymes in the context of the cell wall microenvironment. In particular, the pH was shown to affect PME-PMEI interactions, with both pH-dependent and pH-independent isoforms (Hocq et al., 2017b; Sénéchal et al., 2017).

In contrast, bacterial and fungal PMEs, secreted during pathogen invasion, appear as key determinants of pathogenicity. During the early stages of pathogen attack, fungi, bacteria and insects express pectolytic enzymes, including PMEs which can create substrates for the subsequent action of pathogens PGs and PLLs causing a synergistic break down of the CW (Kars et al., 2005b; Pelloux et al., 2007; Jolie et al., 2010). Bacterial and fungal PMEs cannot be inhibited by plant PMEIs, in part due the differences in the depth of the substrate binding site of pathogen PMEs (Matteo et al., 2005).

3.2.2. Biochemical properties of plant and fungal PMEs

PME catalyses the hydrolysis of methyl ester bond at C-6 of GalA in pectins releasing methanol (MeOH). If all PMEs can catalyse the same reaction, their activities and processivities differ with regards to substrate, pH and temperature optimum as well as ions concentrations. PME activity was indeed shown to be affected by a number of factors. Regarding substrate, it was shown that most PME are active on 65-75% DM pectin as it is believed that a free carboxyl group next to the methoxy group is necessary for the activity (Jayani et al., 2005). Slight changes in pH, which can be related to pI of each of the isoforms, and the concentration of the cations can have an effect on the activity. Optimal pH is in general acidic to neutral for fungal PMEs and neutral to alkaline

for bacterial and plant PMEs. The activities of a number of neutral to alkaline PMEs have been described: *Dickeya dadanti*, *Daucus carrota* (carrot), *Citrus sinensis* (orange) *Carica papaya* (Lee et al., 2008; Kent et al., 2016; Kotnala et al., 2018), and, more recently, an atypical fungal PME from *V. dahliae* with optimal pH 7 was characterized (Safran et al., 2021). Well- characterized acidic to neutral PMEs are from the fungus genus *Aspergillus* and *Botryotinia* (Christgau et al., 1996; Kars et al., 2005b; Kent et al., 2016). PME activity is regulated by different cation concentrations. Cations can compete with positively charged proteins, for interactions with free carboxyl group created after hydrolysis, facilitating enzyme liberation from the complex (Jolie et al., 2010). PME activity increases with increasing cation concentrations, up to a certain optimum, followed by the decrease in the activity (Jolie et al., 2010). Some plant and fungal PMEs lose their activity in absence of cations making them salt dependant PMEs (Cameron et al., 2003; Kent et al., 2016; Kotnala et al., 2018). However, some salt-independent PME isoforms have been as well described (Savary et al., 2002; Luzio and Cameron, 2008; Safran et al., 2021). Optimal temperature of the majority of PMEs is between 40-50°C (Jayani et al., 2005). Plant PME from orange and papaya have a temperature optima at 55-60°C (Savary et al., 2002; Kotnala et al., 2018) while that characterized for Aspergillus is 45°C (Christgau et al., 1996), even some PMEs keep a high residual activity at low temperatures (Pan et al., 2014).

3.2.3. Mode of action of plants and pathogens PMEs

Different modes of action have been proposed for the activity of PMEs. Single chain and multiple-attack mechanisms are characterised by contiguous demethylesterification of HG before dissociation of the enzyme from the substrate, creating block-wise demethylesterification (processive mode of action). Such demethylesterification leads to large stretches of negatively-charged demethylesterified GalA which can bind Ca^{2+} and promote formation of egg box structures that could regulate the stiffness of the CW (Hocq et al., 2017a; Dehors et al., 2019). These mechanisms correspond to processive PMEs from plant and bacteria. In contrast, multiple chains mechanism is characterized by the hydrolysis of only one methylester before dissociation of PME from HG chain. PMEs from fungi act in this non-processive way (Johansson et al., 2002; Jolie et al., 2010; Hocq et al., 2017a). Furthermore, PME's mode of action is regulated by pH. It has indeed been reported that processive PMEs (most plant and bacterial PME) have a neutral to alkaline

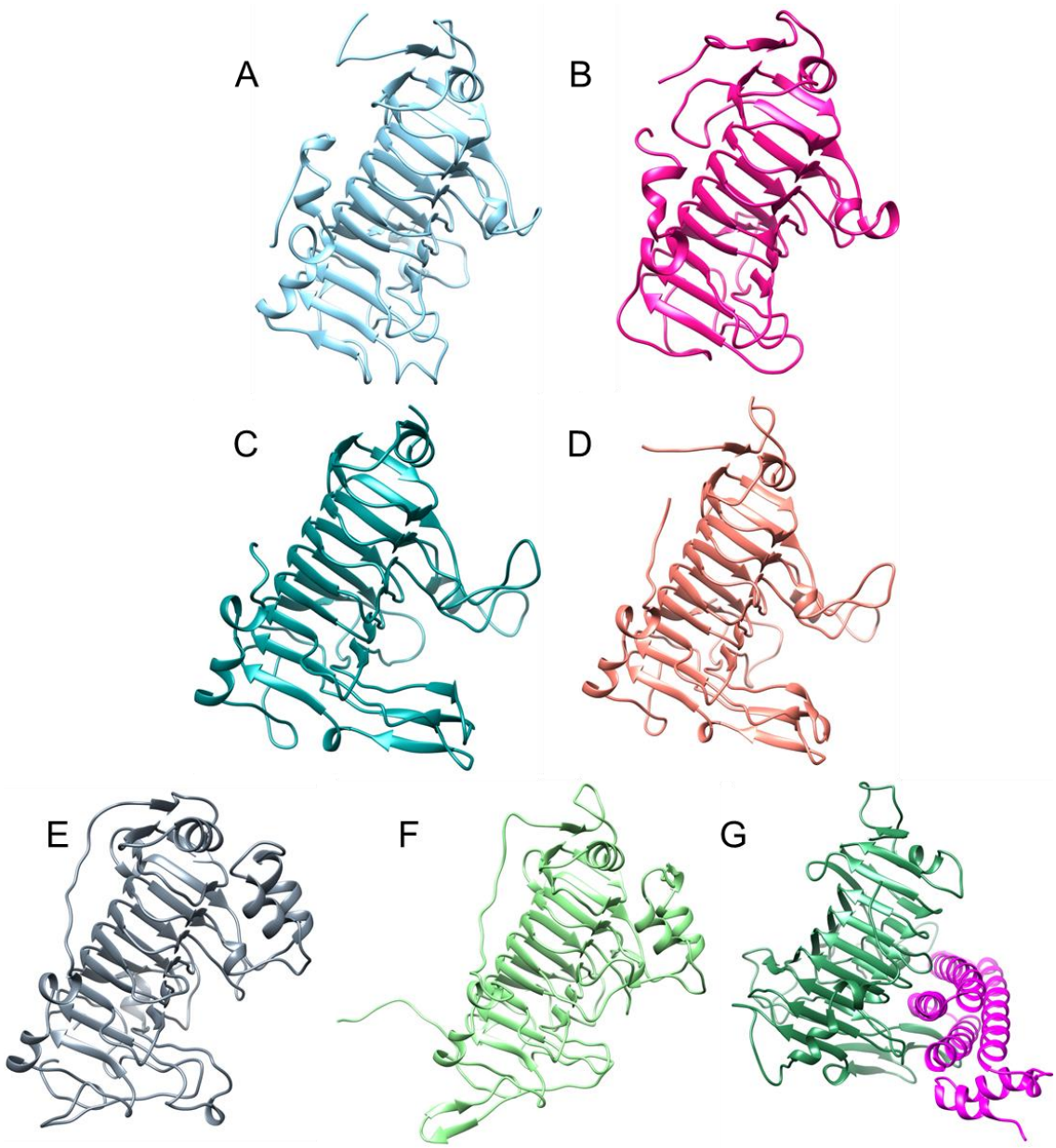

Figure 7. Structures of plant and pathogen PMEs
A) *Daucus carota* PME (PDB: 1HQ8), Johansson et al., 2002. B) *A. niger* PMEII (PDB: 5C1C), Kent et al., 2016. C) *Yersinia enterocolitica* PME (PDB: 3UW0), Boraston and Abbott, 2012. D) *Dickeya dadanti* PEMA (PDB: 1QJV), Jenkins et al., 2001. E) *Sitophilus oryzae* PME (PDB: 4PMH), Teller et al., 2014. F) *Escherichia coli* PME (PDB: 3GRH), Eklöf et al., 2009. G) *Solanum lycopersicum* PME (green) in complex with *Actinidia chinensis* PMEI (pink), (PDB: 1XG2), Matteo et al., 2005.

optimal pH, while non-processive PMEs (most fungi) are active at acidic pH (Kent et al., 2016). In detail; fungal, A. *niger* PMEII, (AnPMEII) is non-processive at pH4 while orange (CsPME), Carrot (DcPME) and *Dickeya dadanti* (DdPME, formerly known as *Erwinia chrysanthemi*) PMEs were shown to be processive at pH 7.5 (Lee et al., 2008; Kent et al., 2016). Moreover, the electrostatic properties of the proteins were shown to play a key role in determining PME processivity (Mercadante et al., 2014; Kent et al., 2016). However, this appears far more complex as it was recently shown that PME from the fungus *V. dahliae* (VdPME1) is processive at pH 7 (Safran et al., 2021). In addition, Arabidopsis PME2's processivity was shown to be pH-dependent, switching from high processivity at pH 8 to low processivity at pH 5 (Hocq et al., 2021, BioRxiv).

These two studies highlight the role of pH and electrostatic potentials, rather than the phylogenetic origin of PMEs, in the control of activity.

3.2.4. 3D structures of PMEs

The presence of 66 different PME isoforms in Arabidopsis questions the rationale for such abundance and the potential differences in their structure and mode of action. Up to date there are no structures reported for Arabidopsis PMEs. However, 3D structures have been resolved for carrot (*Daucus carota*) and tomato (*Solanum lycopersicum*) PMEs (Johansson et al., 2002; Matteo et al., 2005). Also, PME structure have been solved for bacteria, fungi and insects (**Figure 7**, Jenkins et al., 2001; Boraston and Abbott, 2012; Teller et al., 2014; Kent et al., 2016). Analysis of the structure of crystallised PMEs shows that they belong to family of right-handed parallel β-helix proteins consisting of three parallel β-sheets (PB1, PB2 and PB3) with interconnecting loops (T1, T2 and T3) protruding from the enzyme core. This fold is commonly found for all pectinases (Jenkins and Pickersgill, 2001). Superimposition of crystallised PMEs shows the similarity in the fold, even if the structure of the loops around the active site can differ.

3.2.5. PME active site architecture

From the structure of Carrot (DcPME) and *Dickeya dadanti* (DdPME) PMEs, the active site and subsites were determined. Pectin binding site is a long shallow cleft opened at both sides, formed by one loop on each side with the active site in the middle of it. The active site is well conserved in all PMEs consisting of two aspartic acid residues (Asp136, Asp157 in DcPME), two glutamines (Gln113, Gln135) and one arginine residue (Arg225, Johansson et al., 2002, **Figure 8**).

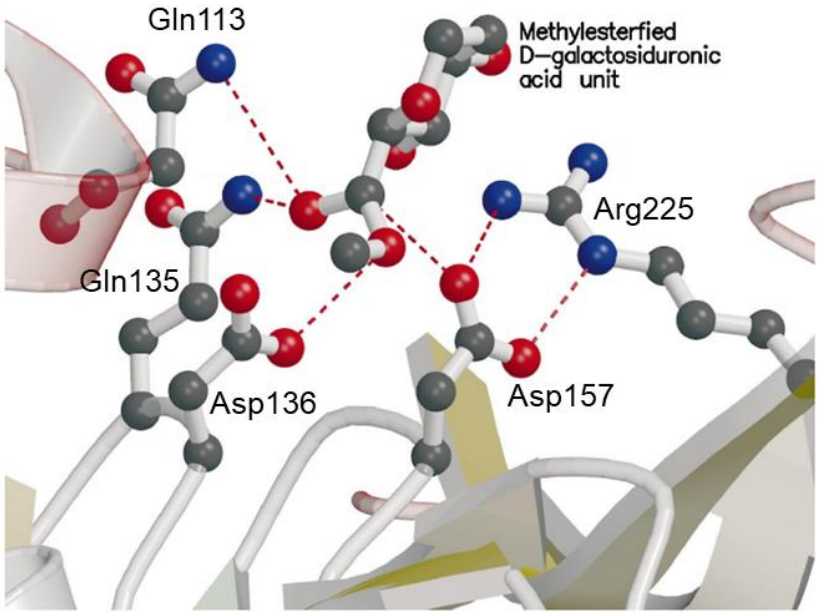

Figure 8. Carrot PME active site AA in interaction with the substrate
DcPME active site consists of three aspartic acids (Asp136, Asp157), two glutamines (Gln113, Gln135) and one arginine residue (Arg225). Adapted from Johansson et al., 2002.

A reaction mechanism has been proposed, in which Asp157 stabilized by a hydrogen bond to Arg225, performs a nucleophilic attack on the ester bond of the carboxymethyl group of pectins. A tetrahedral, negatively charged intermediate is formed, that is stabilised by an oxyanion hole created by one or two conserved Gln side chains. Consequently, a second Asp residues acts as a proton donor in the cleavage step and methanol (MeOH) is released. Water molecule is used to restore carboxylate group of the second Asp by cleaving the covalent bond between the substrate and the first Asp (Johansson et al., 2002; Fries et al., 2007).

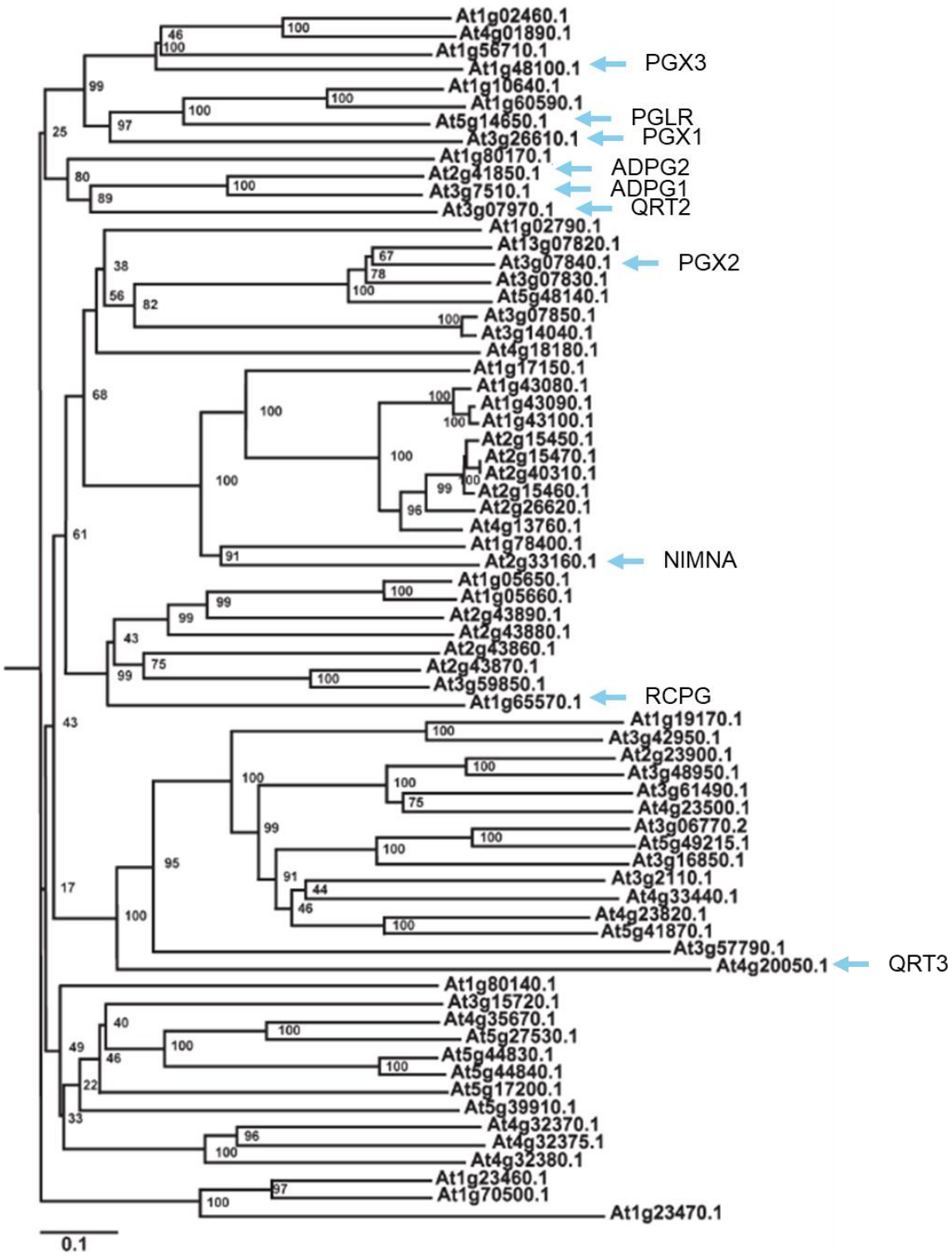

Figure 9. Phylogenetic tree generated from protein sequences alignment of Arabidopsis putative PGs

Phylogenetic tree was constructed using putative PGs amino acid (AA) sequences using ClustalW. Bootstrap values are indicated. Scale indicates 0.1 distance from the root of the tree. PG described in the PhD manuscript are labelled. Adapted from González-Carranza et al., 2007.

3.3. Structures and functions of PGs

PGs are essential as endogenously-produced plant proteins to fine-tune pectin structure during development (Xiao et al., 2014)**.** They are also secreted from plant pathogens notably, bacteria, fungi (Pickersgill et al., 1998; André-Leroux et al., 2005; Jayani et al., 2005; Kars et al., 2005a; Niture, 2008), and herbivorous insects (Shen et al., 2003; Habrylo et al., 2018; Xu et al., 2019) allowing pectin, and more widely, CW degradation, to facilitate infection. PGs belong to the GH28 family (Henrissat, 1991; Markovič and Janeček, 2001; Mahmood et al., 2021). Both plant and pathogen PGs consist of two types: endo-PGs (EC 3.2.1.15) and exo-PGs (EC 3.2.1.67). They can act on HG that were previously demethylesterified by PMEs, although they might as well hydrolyse pectins with high DM (Verlent et al., 2005; Sénéchal et al., 2014). In Arabidopsis 68 genes were annotated as a part of GH28 family (**Figure 9**), and some isoforms were shown to have different expression patterns and different roles during vegetative and reproductive developmental processes. This high number of isoforms suggest that they might have different structures and/or biochemical specificities.

3.3.1. PG roles in development

Over the last few years, a number of reports have shown that PGs play key roles in vegetative and reproductive development. They appear to play a major role in abscission and dehiscence, development of floral organs and pollen, as well as during growth of organs such as hypocotyls and roots (Rhee et al., 2003; González-Carranza et al., 2007; Swarup et al., 2008; Ogawa et al., 2009; Kumpf et al., 2013; Babu and Bayer, 2014; Xiao et al., 2014; Kamiya et al., 2016; Xiao et al., 2017; Yang et al., 2018). In Arabidopsis, the role of a number of PGs that are expressed in several different organs and during specific development processes are highlighted (²

Table 3). For instance, *POLYGALACTURONASE INVOLVED IN EXPANSION1* (*PGX1*) can determine floral organs patterning, as well as elongation of dark-grown hypocotyls (Xiao et al., 2014). *PGX2* regulates stem lignification, hypocotyl length and rosette leaf area (Xiao et al., 2017) while *PGX3* can determine rosette expansion, stomatal aperture and root elongation (Rui et al., 2017). Despite having somehow similar roles in development processes (see PGX1 and PGX2 for hypocotyl elongation), these PGs are not closely related phylogenetically in Arabidopsis (McCarthy et al., 2014), which could suggests distinct biochemical specificities.

2

Table 3. Roles of PG in Arabidopsis

Genes	AGI code	Involvement	Reference
ADPG1	At3g57510	Anther and silique dehiscence; pollen separation.	Ogawa et al., 2009
ADPG2	At2g41850	Flower abscission; anther and silique dehiscence; pollen separation.	González-Carranza et al., 2007; Ogawa et al., 2009
NIMNA	At2g33160	Suspensor elongation.	Babu and Bayer, 2014
PGLR	At5g14650	Involved in lateral root emergence.	Kumpf et al., 2013;Swarup et al., 2008
PGX1	At3g26610	Flower organ patterning, hypocotyl elongation, leaf expansion.	Xiao et al., 2014
PGX2	At1g78400	Hypocotyl elongation, leaf expansion, stem lignification, mechanical stiffening.	Xiao et al., 2017
PGX3	At1g48100	Root and hypocotyl elongation, rosette expansion, shape and size of stomata size.	Rui et al., 2017
QRT2	At3g07970	Flower organs abscission; anther dehiscence; pollen separation.	Ogawa et al., 2009
QRT3	At4g20050	Degrading pollen mother cell wall to allow microspore separation.	Rhee et al., 2003
RCPG	At1g65570	Cell separation in root cap.	Kamiya et al., 2016

Adapted from Yang et al., 2018.

Figure 10. Expression of ADPG2 during Arabidopsis developmental processes as revealed by GUS staining
Tissular location of the *GUS* expression, under the control of the promoter of ADPG2, viewed under light field. A) until C) Lateral roots, arrow indicates site of emergence. Bars represent 50 µm. Adapted from González-Carranza et al., 2007.

Figure 11. Localization of PGLR promoter activity during lateral root initiation
7 day-old transgenic roots expressing *proPGLR:GUS* were stained at different stages of lateral root emergence. Scale bars: 100 µm. Adapted from Hocq et al., 2020

PGs also play a role in pollen maturation as QUARTET3 (*QRT3*), which is specifically expressed in tapetum cells, acts on CW of pollen's tetrad, separating the micropores (Francis et al., 2006). Interestingly, NIMNA which encodes a putative exo-PG, has roles in early embryo cells and suspensor elongation (Babu and Bayer, 2014). ROOT CAP POLYGALACTURONASE (*RCPG*), is specifically expressed in root cap cells where it acts to hydrolyse pectins, allowing detachment of root cap cells. *RCPG* is directly controlled by BEARSKIN1 transcription factor, a master regulator of genes involved in the regulation of root cap turnover (Kamiya et al., 2016).

Mutations in ARABIDOPSIS DEHISCENCE ZONE POLYGALACTURONASE1 (*ADPGI*) and *ADPG2* form non-dehiscent siliques while *ADPGI*, *ADPG2* and *QRT2* loss-of-function mutants are delayed in anther dehiscence (Ogawa et al., 2009). *ADPGI*, *ADPG2* and *QRT2* genes are upregulated by JA treatment (Mandaokar et al., 2006) whereas in Arabidopsis JA-defective mutants PG activity is decreased (Ogawa et al., 2009). Also, FOR DNA BINDING WITH ONE FINGER4.7 (DOF4.7) transcription factor regulates *ADPG2* in abscission zone by directly binding to its promotor (Wei et al., 2010) while CCCH zinc-finger C3H14 activates the transcription of *ADPG1* during cell expansion (Kim et al., 2014). ADPG2 is also expressed in flower buds and mature siliques as well as in roots (Ogawa et al., 2009). In roots, ADPG2 in expressed during lateral root emergence (**Figure 10A-C**) and, as reported for PGLR, its expression is regulated by auxin. Interestingly, the expression of *ADPG2* in basal cells of trichomes suggests that these organs can as well abscise (González-Carranza et al., 2007).

POLYGALACTURONASE LATERAL ROOTS (PGLR) has been identified as predominantly expressed in roots albeit some expression was detected in reproductive organs, including floral buds, siliques and mature seeds (**Figure 11**, Hocq et al., 2020). Regarding its expression pattern, PGLR is likely to be involved in lateral root initiation by separating cortical and epidermal layers contributing to the elongation of the primordium (Swarup et al., 2008; Kumpf et al., 2013). *PGLR* expression is increased by auxin through the transcription factors LIKE-AUXIN3 and LATERAL ORGAN BOUNDARIES DOMAIN18 (Lee et al., 2015; Yang et al., 2018). Arabidopsis *pglr* mutants did not show any drastic phenotypes during the root development, but the exogenous application of purified enzyme on pollen tube triggers pollen tube burst (Hocq et al., 2020).

3.3.2. Roles of PGs and their products in response to stress

Additionally, to their roles in the control of pectin structure during plant development, it has been shown that plant PGs are also involved in plant resistance to biotic stress, including viruses, bacteria, fungi, oomycetes, nematodes and insects, (Cantu et al., 2008; Sénéchal et al., 2014**),** and abiotic stress (Le Gall et al., 2015**).** In response to stress, expression of HGMEs is modified depending on the type of stress and plant species considered (Sénéchal et al., 2014).

As a response to stress, but also during the growth and development, endogenous PMEs can have two kinds of activities on HGs. Firstly, through a processive demethylesterification, they can create blocks of free carboxyl groups that can form egg box structures through interaction with Ca^{2+} leading to CW strengthening that could increase basal defence. These blocks of free carboxyl groups can also be targeted by PGs (and PLLs) to be degraded. This can generate non-substituted OGs, with putative function in the signalling of plant defences. Secondly, PME-mediated random demethylesterification of HG, can generate multiple patterns of methylesterification that can be targeted by the activity of specific PGs (also PLLs). This can increase CW porosity and lead to the production of methylesterified OGs of distinct patterns, which could elicit specific plant defence responses (Ehwald et al., 1992; Sénéchal et al., 2014). Moreover, PGs can release OGs of similar or distinct structure depending on the mode of action of the enzymes. Indeed, most of phytopathogens release an arsenal of CW degrading enzymes which can generate CW fragments, including OGs, which can act as a damage-associated molecular patterns (DAMPs) to activate plant immune response (Ferrari et al., 2013).

OGs are probably the best characterised DAMPs in plants (Ferrari et al., 2013). Structurally, most of characterized active OGs have a DP between 10 and 15, which is the optimal size for Ca^{2+} mediated egg-box structure that is thought to be necessary for OGs activity (Cabrera et al., 2008; Ferrari et al., 2013). While most DAMP OGs investigated in the past were of relatively high DP, there is recent emphasis on short OGs of DP 2 to 6, which exhibit the same function (Davidsson et al., 2017; Voxeur et al., 2019). Short and long OGs have a similar way of activating plant defences. Indeed, this response is independent of signalling pathways that include hormones such as ethylene, JA and SA (Ferrari et al., 2007; Ferrari et al., 2013; Bacete et al., 2020), but requires mitogen activated protein kinases (MAPKs, Denoux et al., 2008). However, when comparing small- and high-DP OGs, there are some differences in the activation pathways. Large OGs and flagellin 22

(flg22), a strong bacterial elicitor, used as control, trigger reactive oxygen species (ROS) burst, while small OGs do not induce similar burst, but only a short-term, transient increase of ROSs. This shows that OG of distinct DPs differ in their ability to trigger ROS burst, which can be related to distinct ROS signatures (Ferrari et al., 2013; Davidsson et al., 2017). Moreover, OGs of small DPs initiate strong expression of PG-inhibiting proteins (PGIPs). During infection, OGs of short DPs appear in the early stages of infection shifting the plant response to PGIP production and ultimately inhibiting pathogen PGs to restrict infection. Additionally, as a consequence, short DP OGs can downregulate some genes involved in the control of plant development and growth (Ferrari et al., 2013; Davidsson et al., 2017).

3.3.3. Biochemical properties of PGs

PGs, while belonging to large multigenic families in different species, overall share similar biochemical properties. Up to now, there are 14512 annotated sequences with 216 different enzymes biochemically characterized from the GH28 family (CAZy and PFAM sources). It appears of prime importance to determine the biochemical properties of plant PGs to better understand how the fine-tuning of HG structure can regulate growth. In parallel, as fungal PGs are used in different biotechnological processes, understanding the differences in the specificities of isoforms is essential. The majority of fungal, insect, as well as some tomato, banana and Arabidopsis PGs have an optimum pH comprised between 3 and 6 (**Table 4**, Benen et al., 1999; Pathak et al., 2000; Kars et al., 2005a; Verlent et al., 2005; Niture, 2008; Sénéchal et al., 2014; Habrylo et al., 2018; Hocq et al., 2020). However, optimum pH can vary for plant PGs as it was reported that tomato PG shifts its optimum pH from 4-4.5 in the presence of NaCl, to pH 5-6 with KCl ions (Chun and Huber, 1998). While not so important in the context of the CW environment, temperature optimum is important in biotechnology processes. As PGs are widely used for fruit juice clarification, where temperature plays an important role (Nighojkar et al., 2019)**.** Most PGs have a temperature optimum between 40-60°C (Niture, 2008), but thermotolerant PGs have been reported from thermophilic bacteria (Kluskens et al., 2005).

Moreover, PGs strikingly differ in their specific activity. Five PGs from *Botryotinia fuckeliana* have different K_m values, that ranged from 0.16 to 0.6 $mg.mL^{-1}$ (Kars et al., 2005a). Other PGs from *Aspergillus niger* (AnPGI, AnPGII and AnPGC) have $K_m < 0.15$ $mg.mL^{-1}$ (Benen et al., 1999). The Km of *Fusarium moniliforme* PG1 is 0.16 $mg.mL^{-1}$ (Bonnin et al., 2001) while that of

Table 4. Biochemical properties of some PGs from plants and pathogens

Organism	PG form	Uniprot ID:	Mw (kDa)	Optimum pH	Reference
Arabidopsis thaliana	PGLR	Q9LYJ5	55	4	Hocq et al., 2020
Aspergillus aculeatus	PG1	O74213	43	4.2-4.6	Kauppinen et al. 1998, not published; Cho et al., 2001
Aspergillus niger	PG1	P26213	58	5	Bussink et al., 1991
Aspergillus niger	PGII	P26214	38	3.8–4.3	Bussink et al., 1990; Singh and Appu Rao, 2002
Aspergillus niger	PGC	A2QL39	61	4.2	Benen et al., 1999
Aspergillus niger	EPG*	-	124	4	Anand et al., 2017
Aspergillus tubingensis	PGX*	Q00293	78	4.2	Kester et al., 1996
Botryotinia fuckeliana	PG1	Q4G496	36	4.2	Kars et al., 2005a
Botryotinia fuckeliana	PG2	Q4G495	38	4.5	Kars et al., 2005a
Botryotinia fuckeliana	PG3	Q9Y7V9	60	3.2-4.5	Kars et al., 2005a
Botryotinia fuckeliana	PG4	Q9Y7W0	50	4.9	Kars et al., 2005a
Botryotinia fuckeliana	PG5	Q9Y7W1	60	4.5	Kars et al., 2005a
Botryotinia fuckeliana	EPG1*	-	65	5	Cabanne and Donèche, 2002
Caldicellulosiruptor bescii	PG1	B9MNB8	50	5.2	Chen et al., 2014
Chondrostereum purpureum	PG1	P79074	39	4.9	Miyairi et al., 1997

* Exo-PGs

Organism	PG form	Uniprot ID:	Mw (kDa)	Optimum pH	Reference
Colletotrichum lupini	PG1	A1E266	31	5	Bonivento et al., 2008
Fusarium moniliforme	PG1	Q07181	39	4	Caprari et al., 1993
Musa acuminata	PG3	-	29	4.3	Pathak et al., 2000
Saccharomyces cerevisiae	PGU1	P47180	39	5.5	Blanco et al., 1994
Solanum lycopersicum	PG2	P05117	47	4.4	Verlent et al., 2004
Sphenophorus levis	EPG	V9Q5P3	50	4-5	Habrylo et al., 2018
Thermotoga maritima	PELB*	Q9WYR8	50	6.4	Kluskens et al., 2005
Verticillium dahliae	PG2	G2X495	38	5	Safran et al., 2021
Yersinia enterocolitica	EPG1*	O68975	66	5.3	Liao et al., 1999

* Exo-PGs

Aspergillus tubingensis exo-PG is 3.2 mg.mL^{-1} (Kester et al., 1996). Insect PG shows a K_m of 2.4 ± 0.2 mg.mL^{-1} (Habrylo et al., 2018). Overall, most of the fungal endo-PGs have Km values between 0.15 - 20 mg.mL^{-1} while exo-PGs show lower specific activities on homogalacturonan (Niture, 2008). Interestingly, the Km determined for an Arabidopsis PG, PGLR, was 51.8 mg. mL^{-1} (Hocq et al., 2020), which is higher than most of that measured for pathogens' enzymes.

3.3.4. PGs mode of action

Depending on how PG hydrolyse the HG chain, they can be divided into two groups: endo-PGs and exo-PGs. Indeed, endo-PGs hydrolyse HG polymer inside the chain, releasing OGs of different DPs, while exo-PGs cleave only one or two GalA from the non-reducing end (Pagès et al., 2000; Abbott and Boraston, 2007; Sénéchal et al., 2014)., leading to OG of DP 1-2. Generally, PG activity increases with decreasing DM of the HG chain, which emphasize the need for an action of PME prior to PG (Bonnin et al., 2002; Verlent et al., 2005). This type of sequential activity is observed for multiple fungal PGs from different species (Benen et al., 1999; Bonnin et al., 2001; Kars et al., 2005a). However, the PME-mediated pattern of demethylesterification also plays a role in determining PG activity. Indeed, purified PG from tomato showed a better activity following tomato PME-mediated block-wise demethylesterification of HG, compared to random demethylesterification by PME from *A. acuelatus* (Verlent et al., 2005). In the same way, some PGs, such as PGI, PGII, PGC from *A. niger*, are more active on non-methylesterified substrates, with PGII being the most sensitive to the presence of methyl's (Benen et al., 1999).

Two different mode of actions have been proposed for endo-PG: i) single chain multiple attack, a processive mode of action that creates mostly di-GalA and tri-GalA as end products of the hydrolysis, and ii) multi chain attack, where the first products of the hydrolysis are subsequently hydrolysed into OGs of shorter DPs. When comparing the three *A. niger* PGs, PGI, PGII and PGC, it was shown that analysis of digestion products confirmed their endo activity. However their mode of action differ on OGs of specific DP (from 5 to 6, Benen et al., 1999). PGI and PGC were described as processive enzymes based on their bond cleavage frequencies, while PGII, and *F. monoliforme* PG1, had a multi chain attack mode of action (Benen et al., 1999; Bonnin et al., 2001).

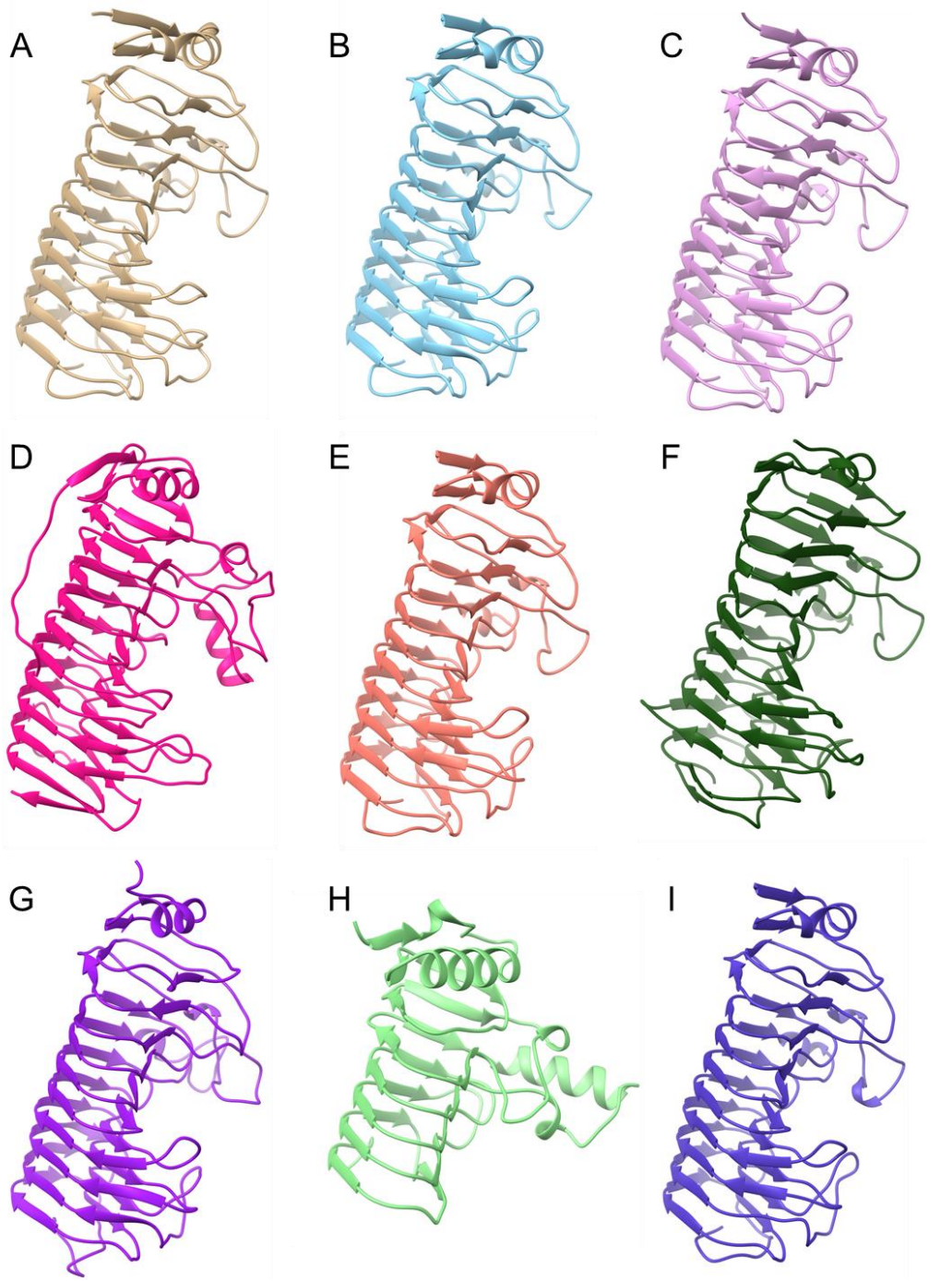

Figure 12. Endo-PG structures published in PDB
A) *Aspergillus aculeatus* PG (PDB: 1IA5), Cho et al., 2001. B) *Aspergillus niger* PGII (PDB: 1IA5), van Santen et al., 1999. C) *Aspergillus niger* PGI (PDB: 1NHC), Van Pouderoyen et al., 2003. D) *Pectobacterium parmentieri* PG (PDB: 1BHE), Pickersgill et al., 1998. E) *Colletotrichum lupini* PG (PDB: 2IQ7), Bonivento et al., 2008. F) *Chondrostereum purpureum* PG (PDB: 1K5C), Shimizu et al., 2002;G) *Fusarium phyllophilum* PG (PDB: 1HG8), Federici et al., 2001. H) *Parabacteroides merdae* PG (PDB: 4MXN), not published; I) *Komagataella phaffii* PG (PDB: 6KVE), Tao et al. not published

3.3.5. Structures of PGs

Plant and fungal PGs are usually expressed as monomeric enzymes with an average molecular weight comprised between 25 and 82 kDa, depending on the quantification method. However, PGs of high molecular weight have been characterized, including *B. paralicheniformis* PN32 and *A. niger* EPG, with masses of 110 and 124 kDa, respectively (Niture, 2008; Anand et al., 2017; Rahman et al., 2019).

As PGs have an important role during plant development and in mediating pathogenicity, numerous studies have investigated their structure. The first structure was that of an endo-PG from the bacteria *Pectobacterium carotovorum* (formerly known as *Erwinia carotovora,* PDB: 1BHE; Pickersgill et al., 1998). Other structures were subsequently characterized : *Aspergillus niger* PGII (PDB: 1IA5, van Santen et al., 1999), *Aspergillus aculeatus* PG (PDB: 1IA5, Cho et al., 2001), *Fusarium phyllophilum* PG (PDB: 1HG8, Federici et al., 2001), *Chondrostereum purpureum* PG (formerly known as *Stereum purpureum* PDB: 1K5C, Shimizu et al., 2002), *Aspergillus niger* PGI (PDB: 1NHC, Van Pouderoyen et al., 2003) and *Colletotrichum lupini* PG (PDB: 2IQ7, **Figure 12A-G** Bonivento et al., 2008) . Structures of exo-PGs have been also described with the first one being from the bacteria *Yersinia enterocolitica* PG (PDB: 2UVE, Abbott and Boraston, 2007). This first structure was followed by that of *Thermotoga maritima* PG (PDB: 3JUR, Pijning et al., 2009) and *Bacteroides thetaiotaomicron* PGI (PDB: 5OLP). In the PDB, two other PG structures were deposited without the corresponding publication but are included in this manuscript: *Parabacteroides merdae* PG (PDB: 4MXN) and *Komagataella phaffii* PG (PDB: 6KVE, **Figure 12H-I**). Up to now, and despite the high number of putative isoforms present, no structure for plant PGs were reported. Independently of their origin, PGs' structure folds into right handed parallel β-sheets that is characteristic, not only for PGs, but also for all pectinases, including PMEs (Johansson et al., 2002), PL/PNL (Yoder and Jurnak, 1995; Lietzke et al., 1996; Vitali et al., 1998) as well as rhamnogalacturonases (RGases, Petersen et al., 1997). Endo-PGs consist of 10 complete turns with 2 uncomplete ones (**Figure 12**). The number of AA per turn varies between 22 to 39 for AnPGII, to 22 to 29 for *A. acuelatus* PG (van Santen et al., 1999; Cho et al., 2001). The average rise per turn is 4.8 Å, characteristic for β-sheets. (Yoder and Jurnak, 1995). The β-helix is composed of parallel β-sheets, consisting of β-strands named PB1, PB2a, PB2b, and PB3. The naming was adapted from the pectate lyase, the first ever crystallised pectinase (Yoder et al., 1993a). Nonetheless, in pectate lyases only PB1, PB2 and PB3 exist while most PGs have one extra β-sheet, called PB2a, consisting

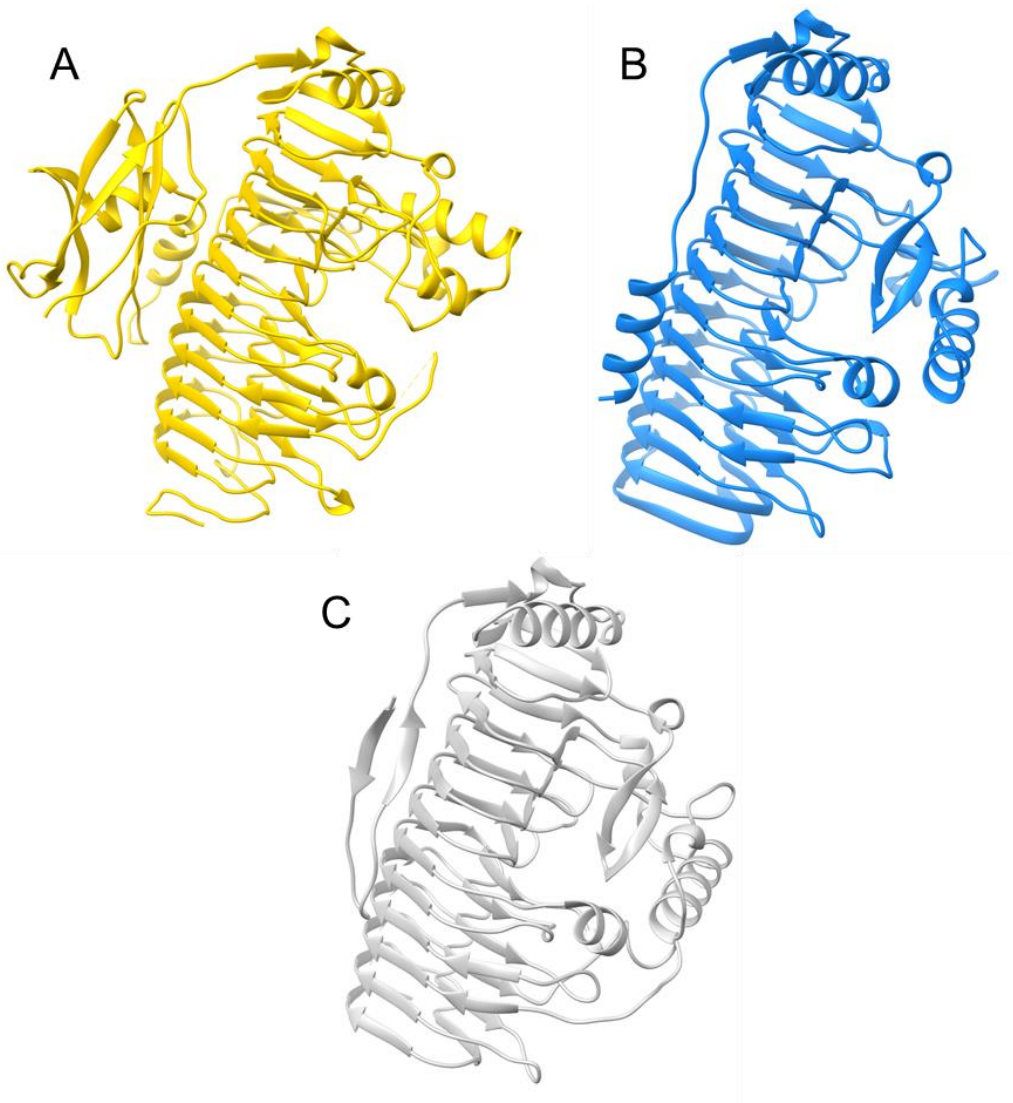

Figure 13. Exo-PG structures from PDB
A) *Yersinia enterocolitica* PG (PDB: 2UVE), Abbott and Boraston, 2007. B) *Thermotoga maritima* PG (PDB: 3JUR), Pijning et al., 2009; C) *Bacteroides thetaiotaomicron* PGI (PDB: 5OLP), Luis et al., 2018.

in three to five β-strands but maintaining the same overall shape (van Santen et al., 1999). Apart from β-sheets, one extra characteristic of PG is the α-helix on the N-terminus part of the protein, that is connected by a disulphide bridge to the first β-strand of PB1 β-sheet. Its function is maintaining the hydrophobic core (Jenkins et al., 1998; van Santen et al., 1999). The same type of capping exists on the C-terminus side of PGs. Turns connecting the PB1-PB2a, PB2a-PB2b, PB2b-PB3 and PB3-PB1 β-sheets are named T1-turns, T1a-turns, T2-turns and T3-turns, respectively. T2 turns are the shorter ones (one or two AA long) while T1, T1a and T3 turns have more variable length, and also contain the loops around the open-ended active site. T3 turns are longer, near the N-terminus while T1 turn near C-terminus end of PGs.

Exo-PGs structures have the same general fold and features as endo-PGs but some differences exist (**Figure 13A-C**). The first difference was revealed by the structure of *Yersinia enterocolitica* PG (PDB: 2UVE) that harbor a fibronectin-type III (FN3) domain (Abbott and Boraston, 2007; Wu et al., 2020). This domain is common in bacterial carbohydrate active enzymes and shares high structure similarity with human fibronectin-binding proteins. While its exact function remains unknown, it could act in carbohydrate recognition, or in mediating interactions with other proteins (Abbott and Boraston, 2007). The second major difference is the loops around the active site, as exo-PG, in contrast to endo-PGs, have a closed-end (pocket) active site. This closure comes from the N-terminus T3 loop, which is extended, through additional helix and coils. This opens the cleft only from C-terminus side of β-helix, generating the exo activity (Pijning et al., 2009). Additionally, it was proposed that loop regions help to guide substrate to the active site (Abbott and Boraston, 2007). Furthermore, PGs appear to be glycosylated, with N-glycosylation sites on consensus Asn-X-Thr/Ser sequences and O- glycosylation on Ser or Thr residues. About 5-10% of the fungal PGs carry either O- linked mannose (MAN) or N-acetylglucosamine (NAG, Niture, 2008). Arabidopsis PGLR was shown to be N-glycosylated following its expression in *Pichia pastoris*, suggesting that it is likely to be glycosylated also *in planta* (Hocq et al., 2020). The exact function of glycosylation is unknown for PGs, but it has been shown that it could, in *F. oxysporum*, promote secretion of PGs during infection (Di Pietro, 1996). Moreover, glycosylation is probably essential for activity, since some PGs lack activity when they were deglycosylated (Stratilová et al., 1998). Overall, glycosylation was reported to play a role in maintaining protein structure, function and stability as well as in the protein-protein interactions (Haltiwanger and Lowe, 2004; Shental-Bechor and Levy, 2008).

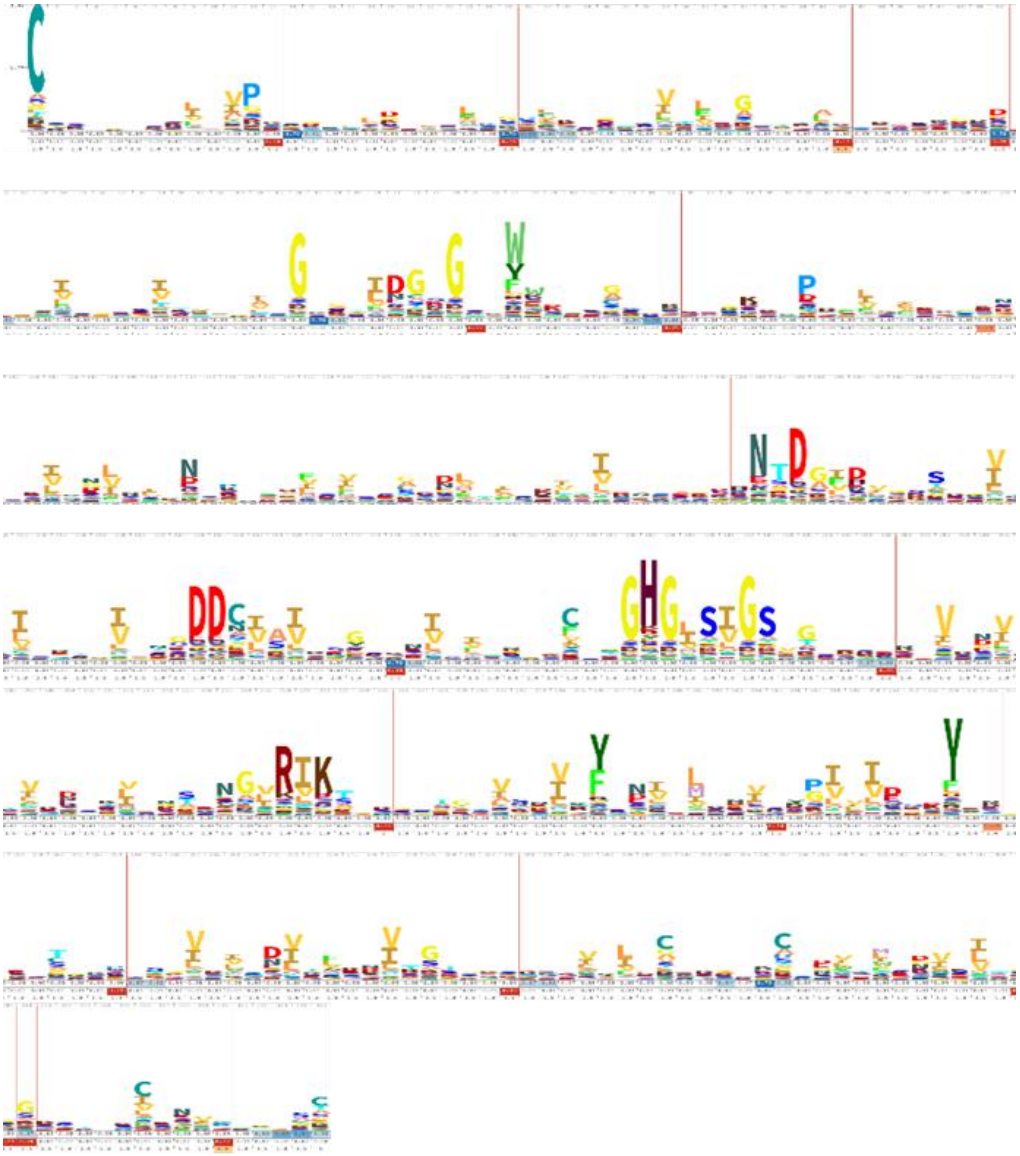

Figure 14. Hidden Markov Models (HMM) logo highliting conserved AA in GH28 family
HMM logo was generated from the alignment of 14512 AA sequences from the GH28 family. Larger letter size indicates higher frequencies of apparition in GH28 family. One letter code is used for AA, N-Asn, T-Thr, D-Asp, G-Gly, H-His, R-Arg, I-Ile, K-Lys, Y-Tyr. Adapted from PFAM (https://pfam.xfam.org/family/Glyco_hydro_28#tabview=tab4).

3.3.6. PG active site architecture

As previously mentioned, the PGs active site is positioned on the PB1 β-sheet and is surrounded by either the two loops in the endo-acting enzymes, or by and additional third loop closing the active site from one side in exo acting enzymes. Sequences alignment of PG sequences from fungus, insect and plants confirmed that there are four strictly conserved sequences motifs: Asn-Thr-Asp, Asp-Asp, Gly-His-Gly and Arg-Ile-Lys (**Figure 14,** Markovič and Janeček, 2001; Schuster-Böckler et al., 2004). In addition to these AA one His and one Tyr were found to be conserved in all PGs (Stratilová et al., 1996). These conserved AA are positioned on subsites -1/+1 of the active site, in the PG structures, where they act in the intricate hydrogen bonding network to ligands. Mutation of any of these residues causes significant decrease in PG activity (Armand et al., 2000; Shimizu et al., 2002; André-Leroux et al., 2005).

In PG structures three Asp, from Asn-Thr-Asp^1 and Asp^2-Asp^3 motifs, are directly involved in hydrolysis, with PGs showing an inverting-type catalytic mechanism (**Figure 15**). In this mechanism Asp^1 with Asp^3 acts as a base to activate the bound water molecule, while Asp^2 acts as a general acid. These three residues are separated by a distance of approximately 5 Å which is not common for the inverting mechanism, where a 10 Å distance is normally required to accommodate both water and substrate (Davies and Henrissat, 1995). On the position -1/+1, Arg and Lys, from the Arg-Ile-Lys motif, were described as involved in interaction with the substrate (Armand et al., 2000). On the other hand, their role is to maintain proper ionization state of a carboxylate (most probably Asp^2) involved in catalysis by sharing a proton (Armand et al., 2000).

3.3.7. Structure of subsites in PGs

While having conserved AA in the position -1/+1, PGs differ in the AA present throughout the binding groove with fungal PG sequences showing only 8.9% identity and 17.4% similarity (Markovič and Janeček, 2001). These differences could account for the specific activity of PGs, and in particular to substrate preference with regards to methyesterified and acetylated HG. In order to elucidate these differences, site directed mutagenesis coupled with kinetic of hydrolysis have revealed the roles of AA at specific subsites (Benen et al., 1999; Armand et al., 2000; Pagès et al., 2000; Bonnin et al., 2001; Pagès et al., 2001; Shimizu et al., 2002; André-Leroux et al., 2005). Bond cleavage frequencies showed that AnPGI, AnPGII, AnPGC and *Fusarium moniliforme*

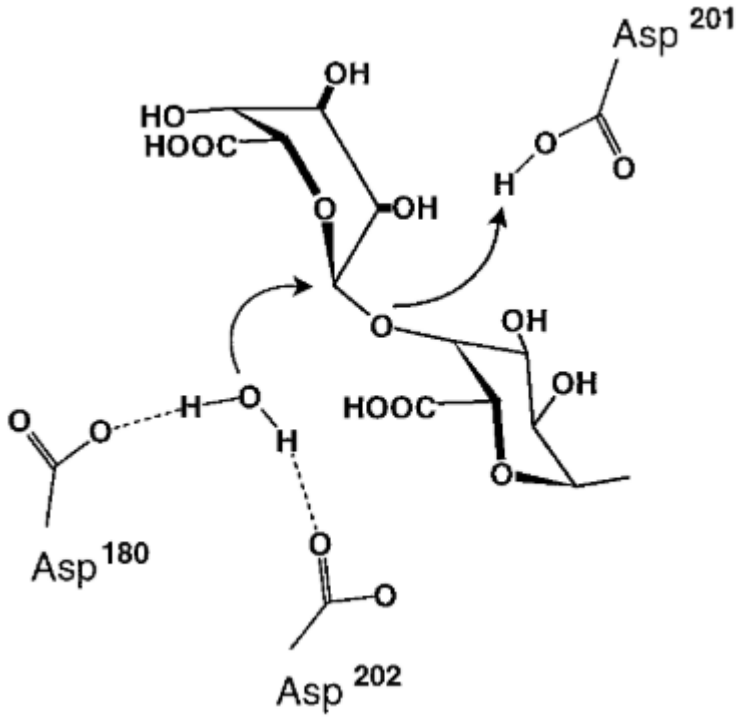

Figure 15. Schematic representation of the catalytic mechanism proposed for PGs
The conserved Asp201 (in AnPGII) acts as the proton donor, while Asp180 and Asp202 activate the hydrolytic water molecule. Adapted from van Santen et al., 1999.

(FmPG) have seven subsites ranging from -5 to +2 (Benen et al., 1999; Armand et al., 2000; Bonnin et al., 2001; André-Leroux et al., 2009).These studies also showed that AnPGII was the least tolerant for methylesterified substrates (Benen et al., 1999). In details, subsite mapping by site directed mutagenesis in AnPGII showed that on subsite -4 Asn186 is important for binding at reducing end. -2, Asp183/Asn and Met150/Gln, +2, Asp282/Lys mutations reduced the specific activity, while +1, Tyr291/Leu/Phe mutation decreased the specific activity and increased the K_m suggesting a role in substrate binding. Two mutations affected the substrate preference: +2 Glu252/Ala increased, while -3 Asn186/Glu decreased, the affinity for methylesterified substrate (Pagès et al., 2000).

The comparison of AnPGI, AnPGII and FmPG, from *A. niger* and *F. monoliforme*, that are differentially tolerant to methylesterified and acetylated substrates allowed to determine the structural basis of such differences (André-Leroux et al., 2009). AnPGI was shown to be the most active compared to AnPGII and FmPG, and more tolerant for acetylation but displayed low activity on methylesterified pectins. In contrast, FmPG was the most tolerant for methylesterified pectin. -5 and -4 subsites in AnPGII and FmPG are polar, consisting of Asn, Ser, Thr and Gln, which could facilitate the binding to substrates of higher DM compared to AnPGI. Regarding the acetylation tolerance, two subsites have been shown to be crucial in AnPGI: Ser191 and Asp240 on subsites -3 and -4. Asp240 is responsible for positioning the substrate, while the hydrogen of Ser191 binds it. One important AA in AnPGI subsite -5, Arg96, was identified as responsible for the processivity of this enzyme (Pagès et al., 2001).

3.3.8. Chemical inhibitors of PGs

Most of fungal PGs are involved in plant pathogenesis as virulent factors. Thus, knowing the ways of inhibiting their activity is of first importance for preventing plant diseases. Fungal PGs can be inhibited by their substrates, OGs and metal ions both *in vivo* and *in vitro*. For example, FmPG is inhibited by pectin and glucuronic acid D-lactone (Niture, 2008) while different fungal PGs are inhibited by various ions such as Co^{2+}, Zn^{2+}, Ba^{2+}, Ca^{2+}, Mn^{2+} and Hg^{2+} (Cabanne and Donèche, 2002; Mohamed et al., 2006; Martins et al., 2007). The only Arabidopsis PG that was characterized, PGLR, was inhibited by green tea catechin, EGCG, and by PP60, which were previously reported to inhibit PMEs (Hocq et al., 2020). Polyphenols and tannic acid could inhibit as well *Verticillium*

sp. and *Cryphonectria parasitica* PG (Patil and Dimond, 1967; Gao and Shain, 1995; Hocq et al., 2020).

3.3.9. PG inhibiting proteins (PGIP)

3.3.9.1. PGIP genes and roles in plant resistance

PG activity can also be inhibited by proteinaceous compounds (Protsenko et al., 2008). Up to now, there are more than 9900 sequences annotated in PFAM that carry the leucine-rich repeat (LRR, PF12799) motif characteristic of PGIP. Only few of the PGIP from different plant species were characterized (Kalunke et al., 2015). Depending on species, the number of genes encoding PGIP genes is highly variable: Two genes have been identified in Arabidopsis, sixteen in *Brassica napus* and only one in wheat (Ferrari et al., 2003; Di Giovanni et al., 2008; Hegedus et al., 2008). Although some of the PGIPs were expressed in bacteria, *Pichia pastoris* and in plants, some did not show any PG-inhibiting activity *in vitro* (D'Ovidio et al., 2006). Whereas plants PGIP can specifically interact with fungal PGs, forming a stoichiometric complex leading to inhibition, the interaction differ, with a certain specificity depending on the pathosystem considered (Kalunke et al., 2015). In CW, it was further shown that PGIPs are bound to demethylesterified HG through positive residues, indicating that PGIP use overlapping, although not identical, regions to interact with both HG and PGs. It appears that DM and the pattern of methylesterification of HG are responsible for the formation of a complex (Di Matteo et al., 2006; Protsenko et al., 2008).

The important role of PGIP in defence was demonstrated by overexpressing *PGIP* isoforms in plants. Indeed, Arabidopsis plants overexpressing *AtPGIP1* and *AtPGIP2* showed a reduction of disease symptoms in response to *B. fuckeliana* (Ferrari et al., 2003) and an enhanced resistance to *F. graminearum* (Ferrari et al., 2012). Furthermore, Arabidopsis expressing *Phaseolus vulgaris* PGIP2 (*PvPGIP2*) and *Brassica napus* PGIPs (*BnPGIP1* or *BnPGIP*2) showed reduction of disease symptoms (Ten Have et al., 1998; Bashi et al., 2013). In contrast, the silencing of *AtPGIP* genes in Arabidopsis leads to enhanced susceptibility against *B. fuckeliana* (Ferrari et al., 2006). In distinct species, such as Tobacco, plants expressing PvPGIP2, *V. vinifera* PGIP1, *Capsicum annum* PGIP1 and *B. rapa* PGIP2 showed enhanced resistance to *B. fuckeliana* infection (Manfredini et al., 2005; Joubert et al., 2006). It appears that this enhanced resistance to pathogens is not the sole consequence of the direct inhibition of fungal PG by plant PGIP, but is also mediated by the

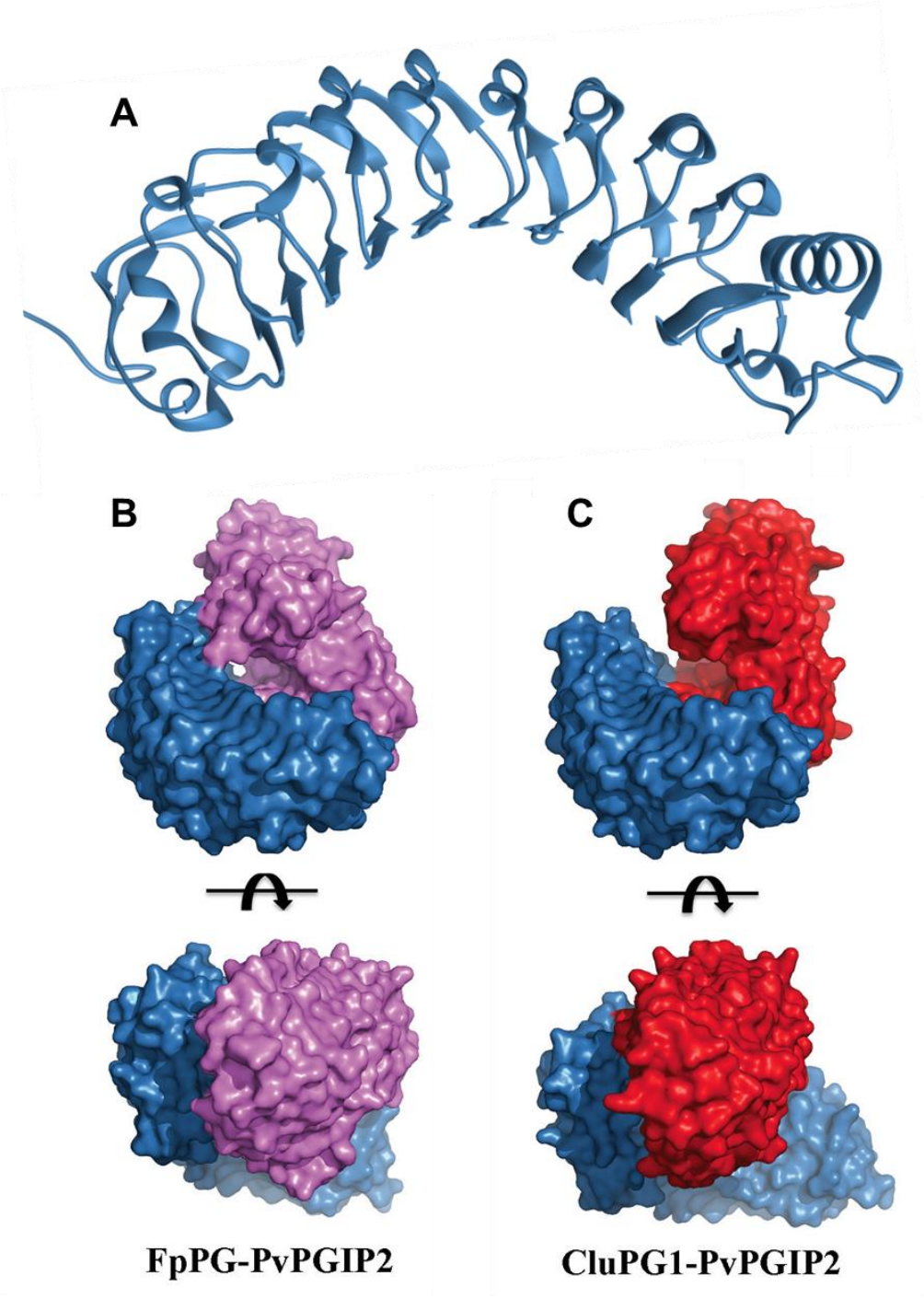

Figure 16. Structure of PvPGIP2 and comparative analysis between the CluPG1-PvPGIP2 and FpPG-PvPGIP2 complexes.
A) Ribbon representation of the PvPGIP2 solenoid (PDB: 1OGQ). B) Surface representation of the complex formed by FpPG (in magenta) and PvPGIP2 (in blue). PvPGIP2 contacts both edges of the active site cleft in FpPG while only one edge is in contact in CluPG1. C) Surface representation of the complex formed by CluPG1 (in red) and PvPGIP2 (in blue). Contacts are visible only on C-terminus side of FpPG. Adapted from Benedetti et al., 2013.

changes in the expression of genes involved in metabolic pathways and CW remodelling (Alexandersson et al., 2011; Nguema-Ona et al., 2013; Hou et al., 2020; Weiller et al., 2020). However, if tomato overexpressing PvPGIP did not show any resistance against *B. fuckeliana*, it did when a pear PGIP was used. These results lead to the conclusions that not all PGIPs are able to inhibit all PGs, but the interaction is enzyme-specific (Powell et al., 2000; Kalunke et al., 2015). Plant PGIPs also show protection against the bacterial pathogen *Xylella fastidiosa*, through the inhibition of a PG that is an important virulence factor (Agüero et al., 2005).

3.3.9.2. Structural determinants of PGIP-PG interaction

The inhibition of pathogens' PG by plant PGIP was extensively studied across several plants and different organisms. To understand the structural determinants of the interaction – or absence of interaction, the structure of PvPGIP2 (PDB: 1OGQ, Di Matteo et al., 2006) was resolved. PvPGIP2 belong to a leucine-rich repeat (LRR) family characterized by the tandem repetition of a consensus motif rich in leucines (Mattei et al., 2001). The fold consists of 10 coils of the consensus sequence X-X-Leu-X-Leu-X-X-Asn-X-Leu-t/s-Gly-X-Ile-Pro-X-X-Leu-X-X-Leu-X-X-Leu* flanked by N- and C-terminus cysteine-rich regions. On the concave surface of the protein solenoid resides the AA responsible for determining the affinity and the specificity of FvPGIP2 towards specific PGs (**Figure 16A**, Di Matteo et al., 2006).

Up to date, although there is no high-resolution structure of a PG-PGIP complex, Small Angle X-ray Scattering (SAXS), coupled with site directed mutagenesis revealed the AA required for the interaction (Benedetti et al., 2011; Kalunke et al., 2015). SAXS analysis was realised using PvPGIP2 and *Fusarium phyllophilum* PG (FpPG, previously known as *Fusarium moniliforme*) as the structures of both enzymes are known, and they were shown to interact (**Figure 16B**, Benedetti et al., 2011). It has been shown that two proteins interact in head to head orientation with PvPGIP2 concave surface interacting with the loops around the active site of FpPG (Benedetti et al., 2011). Specific binding occurs in the N-terminus T3 loop of FpPG and specifically with Asn121 and His110 of PvPGIP2. This Asn is part of the conserved region containing Ser-Asn-Ser-Asn and is subjected to diversification in other PGs (Mariotti et al., 2009; Benedetti et al., 2011). On the C-terminus of FpPG, Ala274 was the main AA identified for the interaction. While *F. verticillioides PG* has high degree of sequence identity with FpPG, but a Thr in this position, it was not inhibited by PvPGIP2 (Benedetti et al., 2013). This kind of interaction between FpPG and PvPGIP2, where

*X represents any AA

the active site is completely covered, with both N- and C-terminus loops engaged in the interaction impairing accessibility of PG to the substrate is referred as a competitive mechanism of interaction (Federici et al., 2001; Benedetti et al., 2013). Two additional modes of inhibition were reported for plant PGIP: a non-competitive and an intermediate between the two. Non-competitive mode of inhibition was demonstrated for the interaction between *Colletotrichum lupini* (CluPG1) and PvPGIP2. In this case the PG active site is still partially accessible to the substrate as CluPG1 and PvPGIP2 only interact at the C-terminus loop (**Figure 16C**). CluPG1 N-terminus loop is characterised by Gly-Gly-Lys-Thr, which explain the absence of recognition by PvPGIP2. On the other hand, C-terminus Glu290 in CluPG1 was shown to play an important role in hydrogen bonding with PvPGIP2 (Benedetti et al., 2013), and AnPGII was as well shown to interact with PvPGIP2 at the C-terminus (Benedetti et al., 2011). Overall, the interaction area on C-terminus seem to be more conserved and is likely to play a major role in PG-PGIP interactions (Benedetti et al., 2013).

It is generally accepted that plant PG do not interact with plant PGIPs. However, up to now there has been only one report of direct inhibition test. PGLR expressed in *P. pastoris* was indeed not inhibited by PvPGIP2 while *A. acuelatus* PG showed over 90% of inhibition in the same conditions (Hocq et al., 2020). Several structural differences are likely to explain this lack of inhibition of plant PGs, but, in absence of 3D structures of plant enzymes, it remains highly hypothetical. For instance, the mutation of FpPG His188 into Pro, that is conserved in all plant PGs and situated in the entrance to the active site, decreased PvPGIP2 affinity for FpPG (Federici et al., 2001).

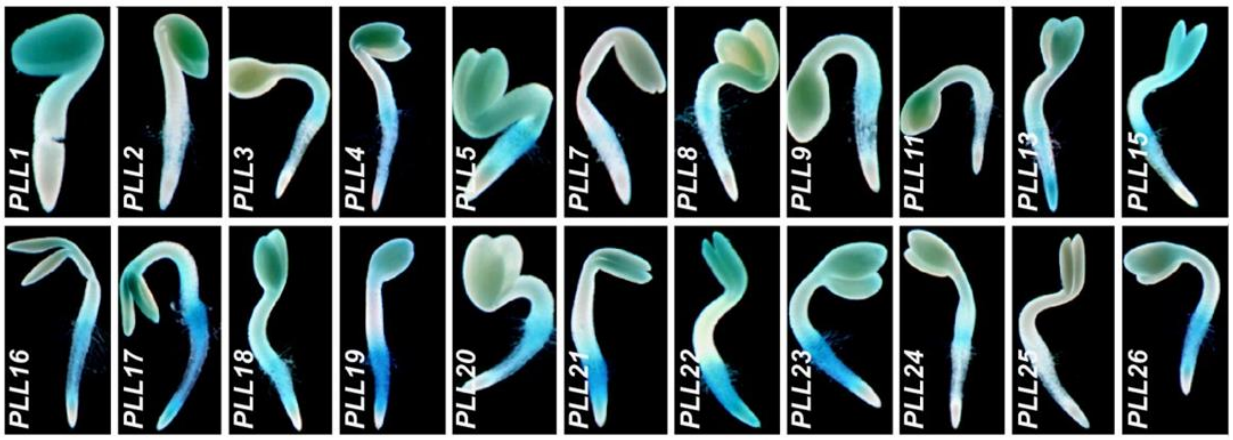

Figure 17. PLL expression in Arabidopsis determined by the activity of their promoters
PLLpro:GUS constructs stained after 1 day of growth. Adapted from Nocker and Sun, 2010.

3.4. Pectate Lyase-Like

Pectate lyase-like (PLLs) the third large family of pectinolytic enzymes. More than 6000 sequences from bacteria, fungi, nematodes and plants are annotated as putative PL/PNLs in CAZY database (Dominguez-Puigjaner et al., 1997; Doyle and Lambert, 2002; Marin-Rodriguez, 2002; Jayani et al., 2005; Nocker and Sun, 2010; Sénéchal et al., 2014). PL/PNL belong to the polysaccharide lyase family 1-4 and 9 (PL1-4, PL9). PLs (Pectate Lyases) include endo-PLs (EC 4.2.2.2) and exo-PLs (EC 4.2.2.9) while PNLs (Pectin Lyases) include endo-PNLs (EC 4.2.2.10). While both PL and PNL act on HG chain by β-elimination, creating unsaturated bonds, PNLs show high activity on methylesterified pectins while PLs are more active on demethylesterified substrates (Zeuner et al., 2020). Microbial PL/PNL enzymes are widely used in food industry in pectinolytic cocktails, for instance for bio-degumming and cleaning of bast fibers, or for fruit juice clarification (Kohli and Gupta, 2019), while plant PL/PNL have important roles in controlling development (Marín-Rodríguez et al., 2003; Nocker and Sun, 2010).

3.4.1. PLL functions in plant vegetative and reproductive development

Like other pectin remodelling enzymes, PLLs are encoded by large multigenic families in plants. In Arabidopsis there are 26 genes that show distinct expression patterns in different organs and development stages. The majority of Arabidopsis PLLs have overlapping expression patterns in stems, leaves and roots, even if the intensity of expression can vary. In seedlings, PLLs are expressed in cotyledons, hypocotyl, root/hypocotyl junction, and/or root tips (**Figure 17**, Nocker and Sun, 2010). In the sepals, petals, and stamens 18 PLLs showed high expression, with 14 PLLs being expressed in pollen, during pollen germination and pollen tube growth (Pina et al., 2005; Palusa et al., 2007). Six PLLs (PLL16, PLL19, PLL21-23, PLL26) showed strong promoter activity during lateral root initiation, which is likely to be related to the required cell wall loosening allowing primordia emergence (Malamy and Benfey, 1997). Their promoter activities partially correspond to that reported for PGLR and ADPG2, suggesting similar functions for these enzymes in this peculiar developmental process (González-Carranza et al., 2007; Nocker and Sun, 2010; Hocq et al., 2020).

In other plants species, PLLs were shown to be expressed during fruit ripening. Ripening alters the flavour of the fruit and influences its quality by modulating its firmness. This notably involves

drastic changes in the structure of pectins, and major contributions for PLLs were shown. For instance, in mango, *Pel1* gene was upregulated during fruit ripening, and in response to ethylene. Moreover, a low induction of the expression of 4 *PLL* genes increased fruit ripening time in mango, showing a positive correlation between PLL-mediated changes in pectin structure and fruit ripening (Deshpande et al., 2017; Uluisik and Seymour, 2020). In addition, in strawberry, the silencing of *Apel* 14, *Apel* 23, and *Apel* 39 genes led to smaller intercellular spaces and firmer fruits. The same effect was shown for banana and grape fruit (Nunan et al., 2001; Jiménez-Bermúdez et al., 2002; Marin-Rodriguez, 2002; Santiago-Domenech et al., 2008). Similarly, in tomato, *SlPL* (Solyc03g111690) was responsible for degrading pectins in the middle lamella leading to decreased resistance to grey mould (Yang et al., 2017). In cotton a PLL, GhPEL plays a role in cotton fibre elongation as the silencing of this gene affected fiber elongation and the degradation of de-esterified pectin in PCW (Wang et al., 2010). In *Zinnia elegans*, PL gene expression was upregulated by auxin and *ZePel* was shown to control vegetative growth, in particular treachery elements differentiation, with consequences on cell elongation and differentiation (Domingo et al., 1998). In similar way, in rice, a pectate lyase (*DEL1)* was shown to play a central role in leaf growth and senescence (Leng et al., 2017).

3.4.2. Biochemical properties of PLL

PLLs from various sources, mostly from bacteria and fungus, were biochemically characterized (**Table 5**). In contrast, data related to plant enzymes is scarce. The enzymes' characterization showed that they differ in their pH-dependence and requirement for cations, substrate specificity and 3D-structure (Jayani et al., 2005). PL are mostly produced in bacteria, while fungi from the genus *Aspergillus*, *Penicillium*, and *Fusarium* predominantly produce PNLs (Yadav et al., 2009; Cao, 2012). PL/PNL cleave HG by β-elimination leading to the formation of an unsaturated C4-C5 bond at the non-reducing end of the substrate (Mayans et al., 1997). PL have more affinity for non-methylesterified or low methylesterified pectins, and optimal pH near 8.5 and they require Ca^{2+} ions for their activity. The latter was further demonstrated by the addition of ethylenediaminetetraacetic acid (EDTA), which drastically reduced PL activity (Mayans et al., 1997).

Table 5. Biochemical properties of selected PLL and PNLs

Organism	PL /PNL	Uniprot ID:	Mw (kDa)	Optimum pH	Ca^{2+}	Reference
Aspergillu luchuensis	PNL/PelB	G7Y0I4	37.9	6.8	-	Zeuner et al., 2020
Aspergillus luchuensis	PNL/PelC	G7XAF0	37.4	-	-	Zeuner et al., 2020
Aspergillus luchuensis	PNL/PelD	G7Y107	37.2	4.9	-	Zeuner et al., 2020
Aspergillus luchuensis	PNL/PelF	G7XZ48	47.3	-	-	Zeuner et al., 2020
Aspergillus niger	PNL/PelB	Q00205	38	-	-	Kusters-van Someren et al., 1992
Aspergillus niger	PNL/PelA	Q01172	40	6.5	-	Kusters-van Someren et al., 1991
Aspergillus parasiticus	PNL	A0A0F0IB20	41	4	+	Yang et al., 2020
Aspergillus tubingensis	PNL/PelA	A0A100IK89	37.9	4.9	-	Zeuner et al., 2020
Bacillus clausii	PL	A0A0P0J4R7	35	10.5	+	Zhou et al., 2017
Bacillus pumilus	PL/ Pel-22[#]	D8X181	34	7.5	Fe^{2+}	Ouattara et al., 2010
Bacillus pumilus	PL/ Pel-66[#]	D8X180	42	8	+	Ouattara et al., 2010
Bacillus pumilus	PL/ Pel-90[#]	D8X179	42	8	+	Ouattara et al., 2010
Bacillus sp.	PL/PL47	-	50	8	+	Takao et al., 2000
Bacillus sp. RN1	PL	B1B6T1	33	10	+	Sukhumsiirchart et al., 2009
Bacillus subtilis	PL	JQ655773*	46	9.5	+	Zhang et al., 2013
Botryotinia fuckeliana	PNL/PNL1	G2Y8C5	40	8	-	Voxeur et al., 2019
Dickeya dadanti	PL/PelE	P11073	37.9	9	+	Lietzke et al., 1996

* GenBank ID, [#] PLLs that showed high activity on both pectate and pectin substrates

Organism	PL /PNL	Uniprot ID:	Mw (kDa)	Optimum pH	Ca^{2+}	Reference
Dickeya dadanti	PL/PelN	D2BWX2	43	7.4	Fe^{2+}	Hassan et al., 2013
Fusarium lateritum	PL	-	16	10	+	Yadav et al., 2017
Hevea brasiliensis	PL	B3SXR0	43.9	10	+	Chotigeat et al., 2009
Humicola insolens	PL	A0A5C0BBP1	27	10	+	Wang et al., 2020
Mangifera indica	PL	Q52PJ2	48	8	+	Chourasia et al., 2006
Massilia eurypsychrophila	PL	A0A5A4LL78	34.7	10	+	Tang et al., 2019
Musa acuminata	PL	Q43783	44	8.5	+	Marín-Rodríguez et al., 2003
Paenibacillus barcinonensis.	PL/PNL[#]	Q9X6Z2	23	10	+	Soriano et al., 2000
Penicillium canescens	PNL	-	38	5	-	Sinitsyna et al., 2007
Talaromyces purpureogenus	PNL	R9XVW6	45	6	-	Pérez-Fuentes et al., 2014
Xanthomonas campestris	PL/PlD	K7PRH9	38	9	+	Yuan et al., 2012
Zinnia elegans	PL	O24554	44	7	+	Domingo et al., 1998

* GenBank ID, [#] PLLs that showed high activity on both pectate and pectin substrates

The most bacterial PLs, that are characterised, are from the genus *Dickeya* and *Bacillus* and they share similar biochemical properties (Jayani et al., 2005). If for most PL, Ca^{2+} is the preferred cation, *Bacillus pumilus*/ Pel-22 and *D. dadanti* showed the highest activity with Fe^{2+} (Ouattara et al., 2010; Hassan et al., 2013). Most PLs are active on pectate, polygalacturonic acid (PGA), but they can tolerate pectins of low degree of methylesterification. Their molecular weight range between 30 and 40 kDa with pH optimum between 7.5–10.0 (Jayani et al., 2005; Yadav et al., 2009). Only a few PL have been characterised from plants: PL from *H. brasiliensis*, *Z. elegans* and mango fruit show optimal pH 7, 10 and 8, respectively (Domingo et al., 1998; Chourasia et al., 2006; Chotigeat et al., 2009).

In contrast to PL, PNL are most active on high DM pectins and acidic pHs (5.5), without any requirement for Ca^{2+} (Mayans et al., 1997; Sénéchal et al., 2014). Fungal PNL, notably from *Aspergillus niger* and *A. aculeatus*, are present in the majority of pectinase cocktails used in industry and their biochemical activities are the best characterized (Zeuner et al., 2020) . Their optimum pH is acidic to neutral, ranging from pH 4 to 7.5. Apart from the DM, the DA of pectins appear of importance as PNL activity was impaired when using sugar beet pectin (with high degree of acetylation) or RG-I that are as well acetylated. (Zeuner et al., 2020).

A number of reports described enzymes with potential dual PL/PNL activities. For instance, *D. dadanti* PelN, while being most active on PGA (PL-like) showed high residual activity on pectins DM 91% (PNL-like, Hassan et al., 2013). Similar observations were described for *Humicola insolens* and *Bacillus sp.* enzymes, that were most active at pH 10 on both PGA, apple (DM 70-75%) and citrus (DM 89%) pectins (Soriano et al., 2000; Wang et al., 2020). On the other hand, a PLL from *Fusarium lateritum* showed alkaline optimal pH (10), was only active on low DM (6.7%) pectins and required Ca^{2+} , was named a PNL and not a PL (Yadav et al., 2017) suggesting bias use of term PL and PNL.

For PLs two modes of action have been described, endo and exo, while only endo PNLs have been characterised so far (Sénéchal et al., 2014). For instance, *Aspergillus* sp. PNL showed different rates of OGs release when acting on pectin of distinct DM. OGs of high DP (5–7) are first released, and further degraded into shorter ones, DP3 and DP4, that are the final products (Van Alebeek et al., 2002; Zeuner et al., 2020). Similar observations were reported for *B. fuckeliana* PNL on Arabidopsis leaves, where only accumulation of OGs > DP4 were shown (Voxeur et al., 2019).

These differences in the release of OGs of various DP/DM suggest differences in the 3D structures of PNL, that can be as well envisaged for PLs.

3.4.3. 3D structure of PLL

PL and PNL being, together with PG and PMEs, part of pathogens virulence factors, it is of prime interest to characterize them both biochemically and structurally. The first structure, pectate lyase C from *Dickeya chrysanthemi* was reported in 1993 (Yoder et al., 1993a) while the last one, VexL from *Achromobacter denitrificans* was published in 2018 (Liston et al., 2018). Up to now, there is a large number of published structure for PL/PNL from bacteria (Yoder et al., 1993a; Pickersgill et al., 1994; Lietzke et al., 1996; Akita et al., 2001; Thomas et al., 2002; Creze et al., 2008; Alahuhta et al., 2011; Zheng et al., 2012; Tang et al., 2013; Zhang et al., 2013; Liston et al., 2018) and fungus (Mayans et al., 1997; Vitali et al., 1998). In addition, one plant enzyme, Jun a 1, from *Juniperus ashei* was crystallised, suggesting that it has a PLL activity and that it is a major cedar pollen allergen (Czerwinski et al., 2005). Besides, four PLL structures, from *Bacillus* sp. TS-47, *Xanthomonas campestris*, *Thermotoga maritima*, *Pectobacterium carotovorum* have been deposited to PDB without corresponding publications (**Figure 18 and Figure 19**).

PLL structures resembles to that of other pectinases including PMEs (Johansson et al., 2002), endo-PGs (van Santen et al., 1999; Cho et al., 2001; Shimizu et al., 2002), exo-PGs (Abbott and Boraston, 2007) and RGases (Petersen et al., 1997). The structures are composed of right handed parallel β-helix. The first PNL structure, correspond to *Aspergillus niger* PelA (AnPelA, Mayans et al., 1997) that, apart from having β-helix topology, is characterised by three sheet topologies called PB1, PB2 and PB3. In AnPelA all three β-sheets consisted of nine strands containing between three and five AA. N- and C-terminus ends are capped by short α-helix and extended AA chains. Turns between the sheets are called T1, T2 and T3 (Mayans et al., 1997). T3 loop differentiates in PLLs however there are two major conformations. Complex T3 conformation is present in PNLs from *Aspergillus* and *Bacillus* (Mayans et al., 1997; Vitali et al., 1998) while simpler T3 loops are found in PLs from *Achromobacter denitrificans* and *Juniperus ashei*, (Czerwinski et al., 2005; Liston et al., 2018). PLs from genus *Bacillus* and *Dickeya*, having most of crystallised enzymes, exhibited both configuration (Pickersgill et al., 1994; Lietzke et al., 1996; Akita et al., 2001; Creze et al., 2008). Another key feature of PLLs is Asn ladder. Firstly, discovered

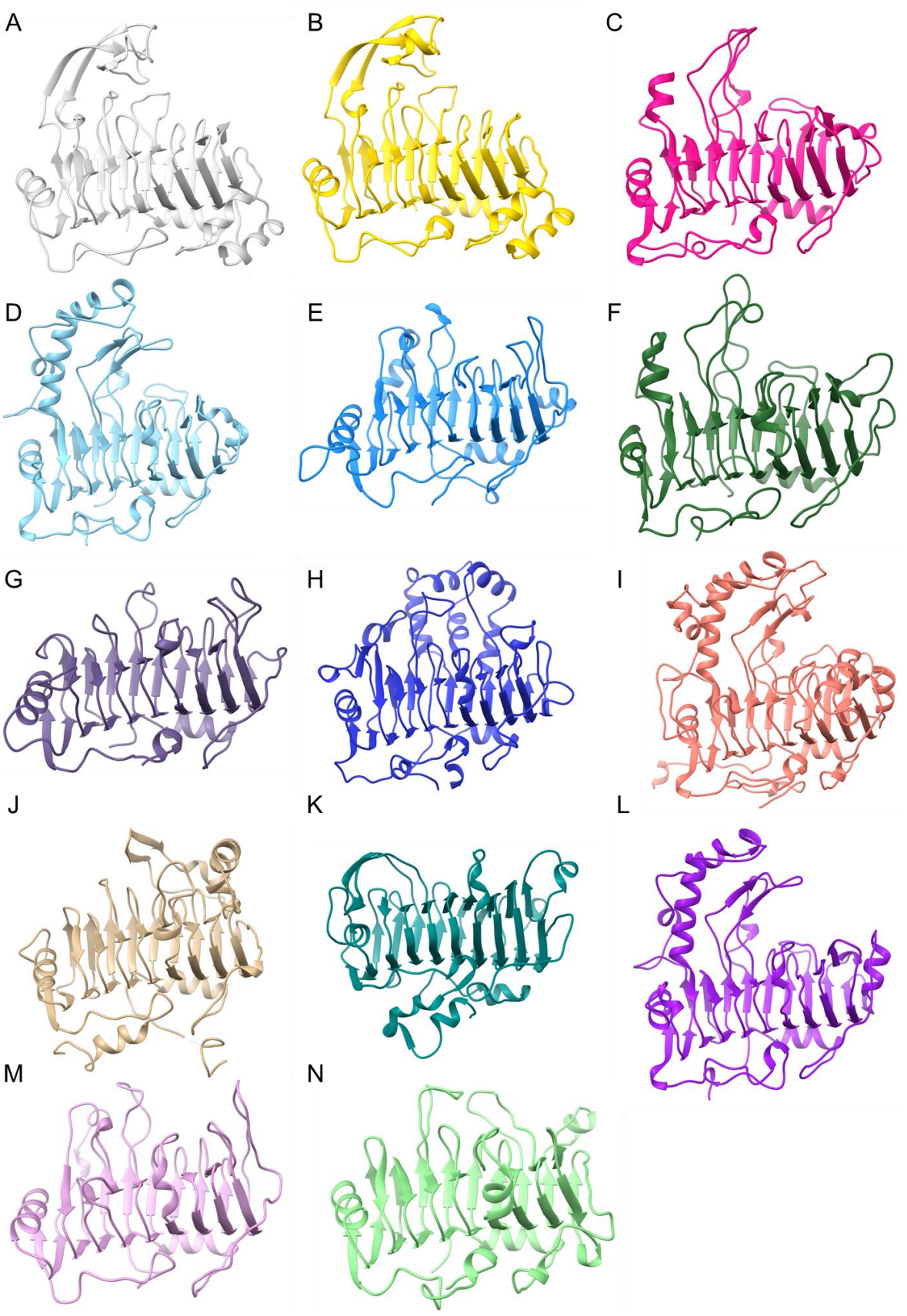
A
B
C
D
E
F
G
H
I
J
K
L
M
N

Figure 18. PNL and PL structures corresponding to PL1 family published in PDB
A) *Aspergillus niger* PelA (PDB: 1IDJ), Mayans et al., 1997. B) *Aspergillus niger* PelB (PDB: 1QCX), Vitali et al., 1998. C) *Dickeya chrysanthemi* PelA (PDB: 1JRG), Thomas et al., 2002. D) *Bacillus subtilis* Pel (PDB: 1BN8), Pickersgill et al., 1994. E) *Dickeya chrysanthemi* PelC (PDB: 1AIR), Lietzke et al., 1996. F) *Dickeya chrysanthemi* PelE (PDB: 1PCL), Yoder et al., 1993b. G) Bacillus sp. N16-5 Pel (PDB: 3VMV), Zheng et al., 2012. H) *Paenibacillus* sp. 0602 PelN (PDB: 5GTG), Zhou et al., 2017b. I) *Acidovorax citrulli* Pel (PDB: 4HWV), Tang et al., 2013. J) *Achromobacter denitrificans* VexL (PDB: 6FI2), Liston et al., 2018. K) *Juniperus ashei* Pel (PDB: 1PZX), Czerwinski et al., 2005. L) *Bacillus* sp. TS-47 PelC (PDB: 1VBL)*. M) *Xanthomonas campestris* Pel (PDB: 2QX3)*. N) *Thermotoga maritima* Pel (PDB: 3ZSC)*. *Structures published in PDB without the corresponding publication.

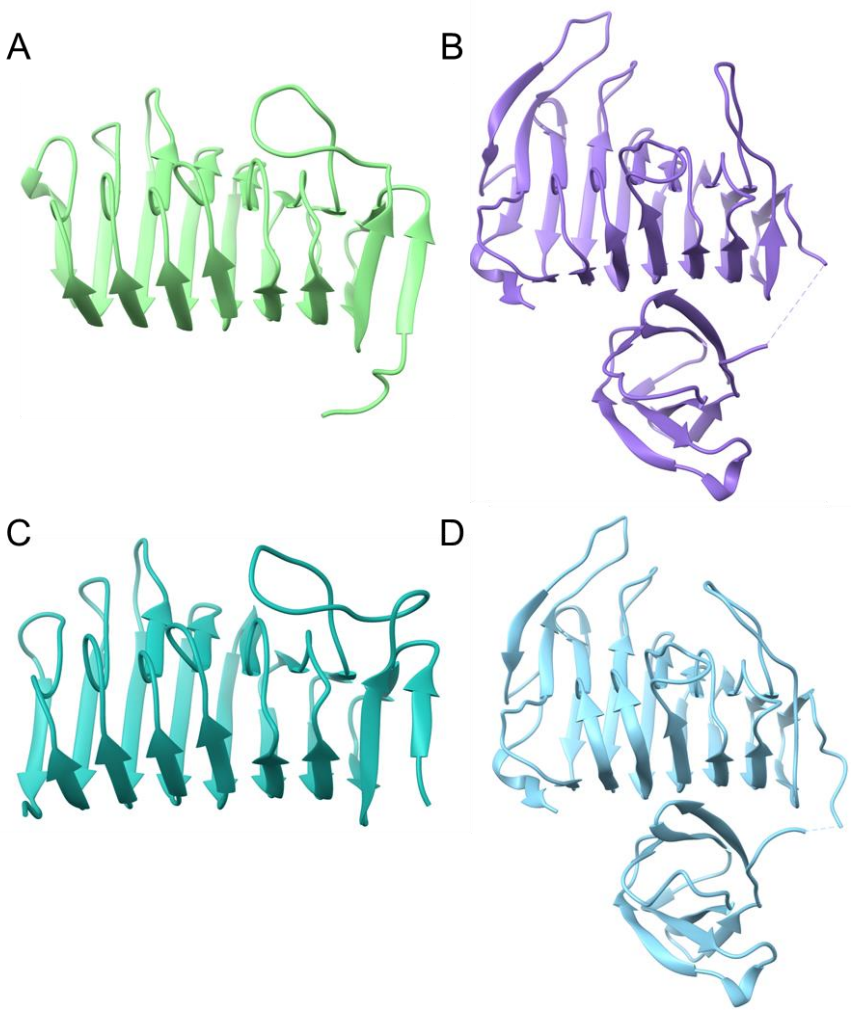

Figure 19. PL structures corresponding to PL3 family published in PDB
A) *Caldicellulosiruptor bescii* Pel (PDB: 3T9G), Alahuhta et al., 2011. B) *Dickeya chrysanthemi* PelI (PDB: 3B4N), Creze et al., 2008. C) *Bacillus* sp. KSM-P15 Pel (PDB: 1EE6), Akita et al., 2001. D) *Pectobacterium carotovorum* Pel (PDB: 4U49)*. *Structure published in PDB without the corresponding publication.

in *D. chrysanthemi* (Yoder et al., 1993a) it is present in both PL and PNL on T2 turn between PB2 and PB3. Asn side chain are orientated in a way to achieve maximum number of hydrogen bonds stabilizing the structure (Yoder et al., 1993a; Mayans et al., 1997; Vitali et al., 1998). Second conserved AA stack belongs to aromatic AA, mostly Phe, on the PB3 sheet (Thomas et al., 2002). However, these stacks were not detected in *Bacillus* sp. KSM-P15 Pel (Akita et al., 2001).

3.4.4. Differences in PL and PNL binding and active sites

Active site cleft is situated on PB1 β-sheet surrounded by T1 and T3 loops that can differ in size and shape between PNLs and PLs. PNL binding cleft is dominated by aromatic AA. In particular, in AnPelA this consist of four tryptophans (Trp66, Trp81, Trp151 and Trp212) and three tyrosine's (Tyr85, Tyr211 and Tyr215). These AA do not form stacks but are arranged in edge to face interactions (Mayans et al., 1997). These aromatic residues promote binding with non-charged, highly methylesterified substrates. This is consistent with the high activity of the enzyme on pectin of high DM. In contrast, PL have binding sites that are rich in charged acidic and basic residues. The binding groove of *D. chrysanthemi* PelC (DcPelC) notably includes Glu166, Lys190, Arg223, Arg224 Asn243, Tyr268, that facilitate binding the more negatively charged substrates (Scavetta et al., 1999).

In PL active site, Ca^{2+}, required for the activity, is localized in the binding groove and coordinated by three Asp. These three Asp are highly conserved and have a similar positions as, within the GH28 family, they are responsible for substrate cleavage (Creze et al., 2008; Ali et al., 2015). In DcPelC, Ca^{2+} ion is coordinated by seven ligands. Five of them consist of Asp131, both carboxyl O, and one carboxyl O from Asp129, Glu166 and Asp170 together with two water molecules (Scavetta et al., 1999). In PLs, Asp131 and Asp170 are absolutely conserved while on position 166 either Asp or Glu can be present (Mayans et al., 1997). In addition, Asp129 DcPelC can be replaced by Glu119 in Bsp165PelA (Zheng et al., 2012). Most of the published PL structures harbour only one Ca^{2+}, while four Ca^{2+} were reported in DcPelC crystallised in complex with GalA (DP5). These additional Ca^{2+} ions connect the carboxyl group of GalA to the AA inside the protein (Scavetta et al., 1999). *Bacillus* sp. KSM-P15 Pel, a PL from the PL3 family, does not share the same positioning of the Ca^{2+}. Ca^{2+} is indeed situated in a T3 loop where it is coordinated by Asp80, Val81, Lys103 and three water molecules. Calcium does not have a role in substrate cleavage but

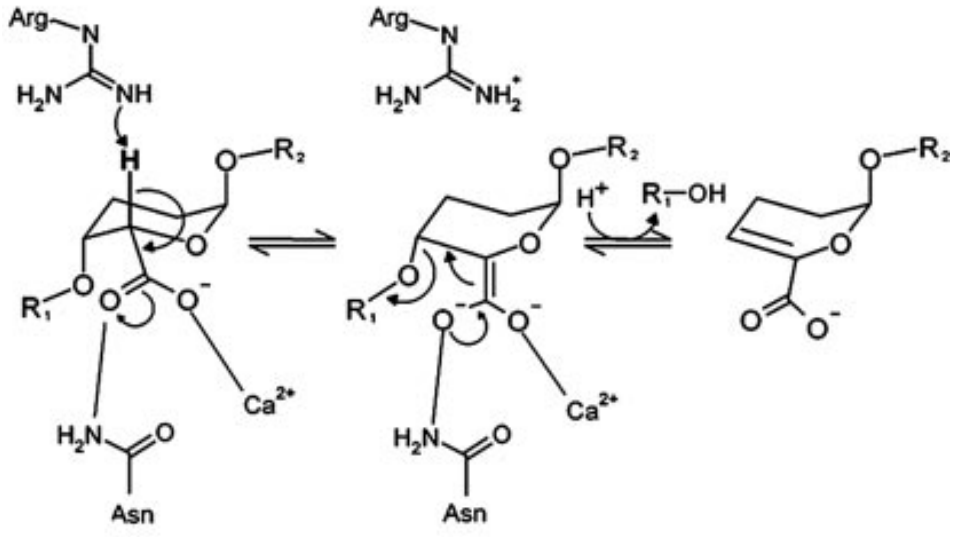

Figure 20. General Ca^{2+} assisted β-elimination mechanism used by pectate lyases
Adapted from Abbott and Boraston, 2007.

in stabilizing the T3 loop, making it necessary for stabilizing the structure, a unique feature for this PL (Akita et al., 2001). PNL active site is similar to that of PL except it does not harbour any Ca^{2+}. In PNLs, Arg176 corresponds to Glu166, Val180 to Asp170 and the only conserved AA is Asp154 which corresponds to Asp131 when comparing the AnPelA to DcPelC (Yoder et al., 1993b; Mayans et al., 1997; Scavetta et al., 1999). One additional AA that is conserved in the two enzymes is Arg236 (AnPelA) and Arg218 (DcPelC). This Arg together with Asp154 or Ca^{2+} (for PLs) play a role in the β-elimination mechanism (Yoder et al., 1993b; Mayans et al., 1997; Scavetta et al., 1999). The reaction mechanism (**Figure 20**) involves three processes: neutralization of the carboxyl group adjacent to the scissile glyosidic bond, abstraction of the C5 proton, and transfer of the proton to the glyosidic oxygen (Scavetta et al., 1999). The role of Ca^{2+} in PL, or Arg176 in PNL, is in the first and second step where they destabilise the C5 proton, binding it and being responsible for bringing the C5 proton within the vicinity of the catalytic Arg236 (AnPelA) or Arg218 (DcPelC, Mayans et al., 1997; Scavetta et al., 1999; Ali et al., 2015). The role of Arg236 was confirmed by its mutation to Lys, which abolished enzyme's activity (Scavetta et al., 1999).

THESIS OBJECTIVES

HG being one of the most abundant pectic domain in the PCW, its modification plays a central role during plant development but also during pathogen infection. To understand the differences between plant and pathogens' enzymes, we aim at characterizing HG modifying enzymes from three families, PMEs, PGs and PLLs, and from two organisms *Arabidopsis thaliana*, and *Verticillium dahliae*, a versatile plant pathogen. In both plants and pathogens, HG modifying enzymes are encoded by rather large multigenic families, which obviously questions the rationale for such abundance, and the specificity of each of the isoforms.

By combining different experimental approaches, including molecular biology, protein expression, enzymology and structural biology the objectives of the thesis are as follow:

1. ***Deciphering the differences among plant PGs.***

In Arabidopsis PGs are encoded by a family of 68 genes with potential overlapping expression patterns. How plant PGs are regulated (pH, temperature…) and how they act on pectins to release OGs of specific structure remains largely unknown. For this purpose, we will characterize PGLR and ADPG2, two Arabidopsis PG that are expressed during lateral root emergence.

2. ***Determining the structure of plant PGs.***

Although 3D structures were resolved for bacterial and fungal PGs, no structure for plant PGs is currently available. This is a clear gap in our understanding of the way plant and fungal enzymes differ, in particular with regards to the PGIP-mediated inhibition of activity. In addition, obtaining a structure for a plant PGs will help understanding the structural determinants of the production of specific OGs. Above-mentioned plant PGs (PGLR andADPG2) will be used for crystallization diffraction experiments.

3. ***Understanding the mode of action of fungal PMEs and PGs***

Fungal pathogens use an enzymatic arsenal to degrade plant cell wall, allowing plant colonization. How the sequential action of enzymes determines cell wall degradation is poorly documented. The characterization of the mode of action of one PME (VdPME1) and one

PG (VdPG2) from *V. dahliae* will serve as a case study. In addition, this will allow comparing the mode of action of fungal (VdPG2) and Arabidopsis (PGLR and ADPG2) PGs.

4. Relating the structure of a fungal PLL to its mode of action

Together with above-mentioned PMEs and PGs, PLLs are key actors of the enzymatic arsenal used by fungi for infection. PLLs, are divided into two subfamilies (PLs and PNLs), with distinct specificities related to substrate, pH and requirement for Ca^{2+} ions. *V.dahliae* secretes a number of PLLs during infection but their biochemical properties as well as structure is not known. Using VdPelB as an example, we will assess the structural determinants of the PLL-mediated production of OGs.

Overall, these objectives should contribute to a better understanding of the structure-function of pectin remodelling enzymes. The comparison of plant and fungal enzymes, should allow determining the digestions products, OGs, that are likely to be involved in either the regulation of plant development, or plant defence.

RESULTS AND DISCUSSION

1. Chapter – Structure and processivity of two plant polygalacturonases

In plants, polygalacturonases (PGs) play a key role in modulating HG structure with consequent effects on a number of diverse developmental processes. In Arabidopsis, PG are encoded by a large multigenic family which obviously questions the biochemical diversity among isoforms, and their specific role in controlling pectin structure. To determine how diverse PGs are, we focused on two PGs, PGLR (Hocq et al., 2020) and ADPG2 (Ogawa et al., 2009) which have overlapping expression patterns during lateral root emergence. The comparison of the two enzymes should reveal the potential biochemical structural and functional diversity among plant PGs. In addition, their characterization should allow deciphering the main differences between plant and fungal enzymes, in particular with regards to their regulation by PGIP.

We used multidisciplinary approaches, including heterologous expression, protein purification, enzymology, LC-MS/MS profiling of digestions products and structural biology to reveal the differences between PGLR and ADPG2. This showed that plant PG differ in their structure and processivity, paving the way for identifying their role *in planta*.

Results are formatted as a manuscript for submission to *Proceeding of the National Academy of Sciences.*

Additional data are reported in **Annex 1** to **Annex 6**.

Authors list

Josip Safran[1#], Wafae Tabi[1#], Olivier Habrylo[1], Julie Bouckaert[2], Paula Pongrac[1], Solène Bassard[1], Serge Pilard[3], Corinne Pau-Roblot[1], Estelle Bonnin[4], Davide Mercadante[5], Valérie Lefebvre[1], Fabien Sénéchal[1], Jérôme Pelloux[1]

[1] : UMRT INRAE 1158 BioEcoAgro – BIOPI Biologie des Plantes et Innovation, SFR Condorcet FR CNRS 3417, Université de Picardie, 33 Rue St Leu, 80039 Amiens, France. [2] : UMR 8576 Unité de Glycobiologie Structurale et Fonctionnelle (UGSF) IRI50, Avenue de Halley, 59658 Villeneuve d'Ascq, France. [3] : Plateforme Analytique, Université de Picardie, 33, Rue St Leu, 80039 Amiens, France.[4] : INRA, Paroi Végétale et Polysaccharides Pariétaux, CS 71627, 44316 Nantes Cedex 3, France. [5]: School of Chemical Sciences, The University of Auckland, Private Bag 92019, Auckland 1142, New Zealand.

#: Contributed equally as first authors

Corresponding author: Jérôme Pelloux (jerome.pelloux@u-picardie.fr)

1.1. Abstract

The fine-tuning of plant cell wall pectins by polygalacturonases (PG) plays a key role in mediating changes in polymer chemistry with consequent effects on cell wall mechanics and plant development. Plant PG are encoded by large multigenic families, which questions the rationale for such abundance. We report the biochemical and structural characterization of PGLR and ADPG2, two PGs from Arabidopsis whose expression overlap in roots. We determined the substrate specificity of both enzymes and showed that the oligogalacturonides (OGs) produced by PGLR and ADPG2 differed, suggesting distinct accommodation of the substrate and/or enzymes' processivities. To understand the structural determinants of such differences, PGLR and ADPG2 3D structure were resolved by X-Ray diffraction at 1.3 and 2.03 Å, respectively. If amino acids (AA) at the active site were strongly conserved, those in subsites differed, which could play a role in substrate recognition and/or binding. Some AA of PGLR active site were mutated and their contribution to activity and substrate binding determined. We finally showed that the key amino-acids identified for fungal PGs that enable interaction with plant PGIPs were absent in plant enzymes, which could explain the selective inhibition of pathogen PGs during attack. Our data help sampling the diversity of plant PGs' landscape, which will help determining their potential roles *in vivo*.

1.2. Significance statement

Plant polygalacturonases (PGs) control the degree of polymerization of cell wall pectins, releasing oligogalacturonides (OGs) with consequent effects on cell wall integrity, cell wall mechanics and plant development. The striking number of genes encoding PGs in plants questions the rationale for such diversity. We report the structure of two PGs from Arabidopsis and show that numerous discrete structural differences can explain distinct substrate binding abilities, and the release of peculiar OGs. Site-directed mutagenesis identified key AA involved in substrate binding and hydrolysis. Further analyses of the structures also revealed the determinants of the lack of inhibition of plant PGs by PolyGalacturonase Inhibiting Proteins (PGIP) as well as the key AA involved in the pH dependencies of the two PGs. This work provides insights into the functional diversity of plant cell wall remodelling enzymes.

1.3. Introduction

The plant primary cell wall, composed of an intricate network of polysaccharides and proteins, needs to be remodelled to mediate changes in its mechanical properties and determine the extent of cell growth or the response to environmental stress (Bidhendi and Geitmann, 2016). Pectins, the major polysaccharide of the primary cell wall of dicotyledonous species such as Arabidopsis, are notably composed of homogalacturonan (HG) domain, a homopolymer of α-1,4-linked-D-galacturonic acid (GalA) units, that can be methylesterified or acetylated (Mohnen, 2008). The fine-tuning of the degree of methylesterification (DM) and acetylation (DA) of HG was shown to control a wealth of developmental processes such as differentiation and growth of some vegetative and reproductive organs (Hewezi et al., 2008; Peaucelle et al., 2008; Pelletier et al., 2010; Raiola et al., 2011; Gou et al., 2012; de Souza et al., 2014; Leroux et al., 2015; Stranne et al., 2018). In parallel, the control of the degree of polymerization (DP) of HG by polygalacturonases (PGs) can regulate root/hypocotyl growth, stomata functioning and pollen formation in Arabidopsis (Rhee et al., 2003; Ogawa et al., 2009; Xiao et al., 2014; Rui et al., 2017; Xiao et al., 2017; Hocq et al., 2020). Phytopathogenic organisms, including microorganisms and parasitic plants, also produce PGs, thus contributing to host colonization by degrading the physical barrier of plant cell wall (Kirsch et al., 2016). Although all perform the same enzymatic reaction, which is hydrolysis of the α-(1–4) glycosidic bond between two adjacent non-methylesterified D-GalA units, PGs can differ in their mode of action and are referred as endo-PGs (EC 3. 2.1.15) or exo-PGs (EC 3.2.1.67). To determine how protein structure can mediate difference in enzyme's processivity, 3D structures for phytopathogens' endo and exo-PGs were resolved and compared (Pickersgill et al., 1998; van Santen et al., 1999; Cho et al., 2001; Shimizu et al., 2002; Van Pouderoyen et al., 2003; Abbott and Boraston, 2007; Pijning et al., 2009). Endo- and exo-PGs from microorganisms' fold into a right-handed parallel beta-helix and harbour four conserved AA stretches, NTD, DD, GHG and RIK, in their active site (Markovič and Janeček, 2001). The aspartic acid residues in the two first segments form the catalytic acids. In a typical endo-PG such as *Aspergillus aculeatus* PG1 (AaPG1) the active site is a tunnel-like binding cleft, allowing the enzyme to bind to the polysaccharide and produce oligogalacturonides (OGs) of various degrees of polymerization and substitution (Cho et al., 2001). The structure of exo-PGs differs, with the insertion of stretches of AA that turn the open-ended channel into a closed pocket, as highlighted for *Yersinia enterocolitica* PG (Abbott and Boraston, 2007). This restricts the attack to the non- reducing end of the substrate, thus releasing

non methylesterified GalA monomers or dimers. Pathogen's PGs can interact with PolyGalaturonase Inhibiting Proteins (PGIP) produced by plants upon infection, either through competitive or non-competitive interactions, and this appear as one of the main ways for plant to restrict pectin degradation and pathogen's invasion (Benedetti et al., 2011). In contrast, plant PGs are not inhibited by PGIP, which suggests structural differences among enzymes. The PG-mediated degradation of HG can have two distinct consequences: i) it impacts polysaccharide rheology, decreasing its stiffness and promoting cell growth (or infection by pathogens) and ii) it produces OGs which can act as signalling molecules (Ferrari et al., 2013; Davidsson et al., 2017). OGs were indeed shown to elicit defence response, through binding with cell wall integrity receptors, but were as well recently reported, in relation to auxin, to control plant development (Savatin et al., 2011). It is likely that the fine structure of OG can determine its interaction with receptors and can trigger distinct downstream signalling events. In plants, PGs are encoded by large multigenic families (68 genes in Arabidopsis), which obviously questions the rationale for such abundance in the context of the cell wall. Considering the number of genes encoding pectin degrading enzymes, and potential compensation mechanisms among the family, the use of mutants can only bring partial clues to sample the diversity of plant PGs' landscape. Here we report on the biochemical and structural characterization of two plant PGs, PGLR and ADPG2, whose expression overlap in Arabidopsis roots. PGLR and ADPG2 can produce distinct OGs, showing that plant PGs are not equal in their mode of action. We further report on the structural differences between plant PGs, and with regards to fungal enzymes, and on the identification of key AA that are required for substrate interaction and activity. Investigating the surface electrostatic potentials, we shed new light on the differences in the activity/processivity of the enzymes.

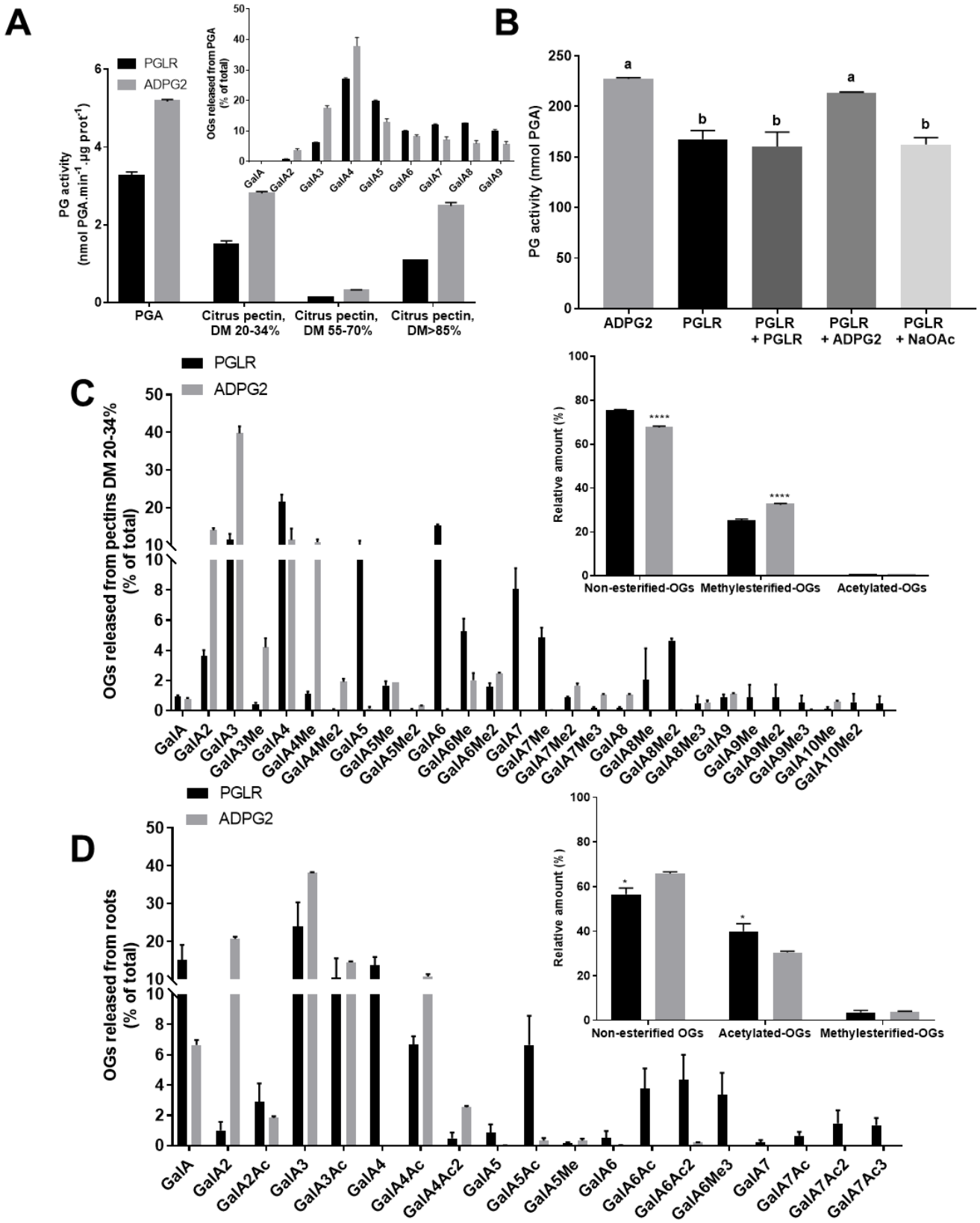
A
PGLR
ADPG2
PG activity (nmol PGA.min-1.µg prot-1)
OGs released from PGA (% of total)
GalA
GalA2
GalA3
GalA4
GalA5
GalA6
GalA7
GalA8
GalA9
PGA
Citrus pectin, DM 20-34%
Citrus pectin, DM 55-70%
Citrus pectin, DM>85%
B
PG activity (nmol PGA)
a
b
b
a
b
ADPG2
PGLR
PGLR + PGLR
PGLR + ADPG2
PGLR + NaOAc
C
PGLR
ADPG2
OGs released from pectins DM 20-34% (% of total)
Relative amount (%)
****
****
Non-esterified-OGs
Methylesterified-OGs
Acetylated-OGs
GalA
GalA2
GalA3
GalA3Me
GalA4
GalA4Me
GalA4Me2
GalA5
GalA5Me
GalA5Me2
GalA6
GalA6Me
GalA6Me2
GalA7
GalA7Me
GalA7Me2
GalA7Me3
GalA8
GalA8Me
GalA8Me2
GalA8Me3
GalA9
GalA9Me
GalA9Me2
GalA9Me3
GalA10Me
GalA10Me2
D
PGLR
ADPG2
OGs released from roots (% of total)
Relative amount (%)
*
*
Non-esterified OGs
Acetylated-OGs
Methylesterified-OGs
GalA
GalA2
GalA2Ac
GalA3
GalA3Ac
GalA4
GalA4Ac
GalA4Ac2
GalA5
GalA5Ac
GalA5Me
GalA6
GalA6Ac
GalA6Ac2
GalA6Me3
GalA7
GalA7Ac
GalA7Ac2
GalA7Ac3

Figure 21. Substrate specificity of PGLR and ADPG2 and oligogalacturonides production
A) Substrate specificity of PGLR and ADPG2. Activity was measured at 50°C and pH 5.2 during 1 hour using substrates of increasing degrees of methylesterification (DM, Inset: Oligoprofiling of OGs released by PGLR and ADPG2 after 1 hour of digestion on polygalacturonic acid (PGA, DM 0) at 40°C, pH 5.2), B) Activity test by adding PGLR or ADPG2 for 1 hour after a first digestion of PGA by PGLR (NaOAc: negative control). C) Oligoprofiling of OGs after overnight digestion of DM 20-34% pectins by PGLR and ADPG2 at 40°C, pH 5.2 after (Inset: Cumulative OGs released by PGLR and ADPG2 after over-night digestion on DM 20-34% pectins at 40°C, pH 5.2), Two-way ANOVA with Sidask's multiple comparison test, P value ****<0.0001, n=3. D) Oligoprofiling of OGs after digestion of roots cell wall by PGLR and ADPG2 at 40°C, pH 5.2 after over-night digestion, (Inset: Cumulative OGs released by PGLR and ADPG2 after over-night digestion of roots cell walls at 40°C, pH 5.2). Two-way ANOVA with Sidask's multiple comparison test, P value *0.0290, n=3.

1.4. Results

1.4.1. PGLR and ADPG2 produce distinct OGs

PGLR and ADPG2 were produced as recombinant proteins in *Pichia pastoris* and purified (**Figure S1A**, Hocq et al., 2020). They both show optimal activity at acidic pHs (pH 4 PGLR and pH 5 ADPG2). ADPG2 has optimal temperature activity from 25 to 50°C while PGLR shows maximum activity at 50°C (**Figure S1B** and **C**). Their activity was tested on a range of pectic substrates of various DMs, showing that, for both enzymes, the maximum activity was for non-methylesterified pectins – PGA **(Figure 21A**). Although the activity decreased with increasing DM, a residual activity was measured on pectins with DM>85%. We next demonstrated that ADPG2 had an overall better affinity for PGA compared to PGLR, with Km values of 8.6 and 51.8 $mg.mL^{-1}$ respectively, as well as a higher maximal velocity (149 and 71.9 nmol of $GalA.min^{-1}.\mu g^{-1}$ for ADPG2 and PGLR), respectively (**Figure S1D**, Hocq et al., 2020). We next used a recently developed LC-MS/MS oligoprofiling approach (Voxeur et al., 2019) and, using PGA as a substrate, we showed that both enzymes have endo activities, with ADPG2 releasing higher proportion of short-sized OGs compared to PGLR (**Figure 21A, Inset**). To further confirm these differences in kinetic parameters (i.e. higher activity and shorter products generated by ADPG2 in comparison to PGLR), we tested their additive effects (**Figure 21B**). We showed that PGLR or ADPG2 maximum activities were reached after 1-hour digestion, generating products that cannot be re-cut. However,

the addition of ADPG2 for 1 hour following a first hour of incubation with PGLR, lead to increase of PG activity, reaching the level of 2 hours incubation with ADPG2. This confirmed that the end-products generated by either of the enzymes differ, and that ADPG2 is able to cut short-sized substrates (represented here by the end-products of PGLR). We next determined the fine structure of OGs generated by either PGLR or ADPG2 on more complex pectic substrates, that differ in their DMs. When using pectins of DM 20-34%, we showed that the pool of OGs produced by PGLR differed to that of ADPG2 (**Figure 21C, Inset**). In particular, PGLR released unsubstituted OG of DP5 to DP9, as well as specific methylesterified forms of more than 6 GalA units that were not or poorly produced by ADPG2. The main products of ADPG2 were unsubstituted OGs of DP2 to DP4 as well as GalA4Me (**Figure 21C**). On pectin DM>85% both enzymes released higher amounts of methylesterified OGs in accordance with the higher DM of the substrate (**Figure S2A**, **Inset**), however, the relative proportion of methylesterified OGs released from pectins DM>85% strikingly differed between PGLR (above DP6) and ADPG2 (for which the most abundant products were GalA2, GalA3, GalA3Me and GalA4Me, **Figure S2A**). We compared the OGs produced by PGLR, ADPG2 and AaPG1 from pectins DM 20-34% and showed, using principal component analysis (PCA) that the OGs generated by ADPG2 and AaPG1 were more closely related (Dim1 57.7%) with GalA2, GalA7Me3, GalA4Me being the loadings for Dim1 and GalA3, GalA6Me2, GalA9Me3 being, for instance, the loadings for Dim2 (**Figure S3A**).Finally, considering the localization of the expression of PGLR and ADPG2, we tested the activities of both enzymes on Arabidopsis root cell wall, whose pectins are known to be methylesterified and acetylated (Willats et al., 2001). We notably showed that PGLR released a higher proportion of acetylated OGs (GalA5Ac, GalA6Ac, GalA6Ac2) compared to ADPG2, in addition to the higher mean DP (**Figure 21D** and **Figure 21D**, **Inset**). Similarly, to what was observed on model pectins, the main OGs produced by ADPG2 were unsubstituted OGs, GalA2 and GalA3. This overall shows that two PGs that overlap in their expression patterns can differ in their biochemical specificities, which questions the structural determinants of the enzymes' activity.

1.4.2. Structure determination of PGLR and ADPG2

PGLR crystallised as single molecule in a P1 space group and three data sets were collected from the same crystal at 1.3 Å resolution (**Figure S4A**). For ADPG2, one data set was collected at 2.03 Å resolution and ADPG2 belongs to orthorhombic space group $P2_12_12_1$ with two molecules in asymmetric units: chains A and B, are highly similar with a Cα root mean square deviation

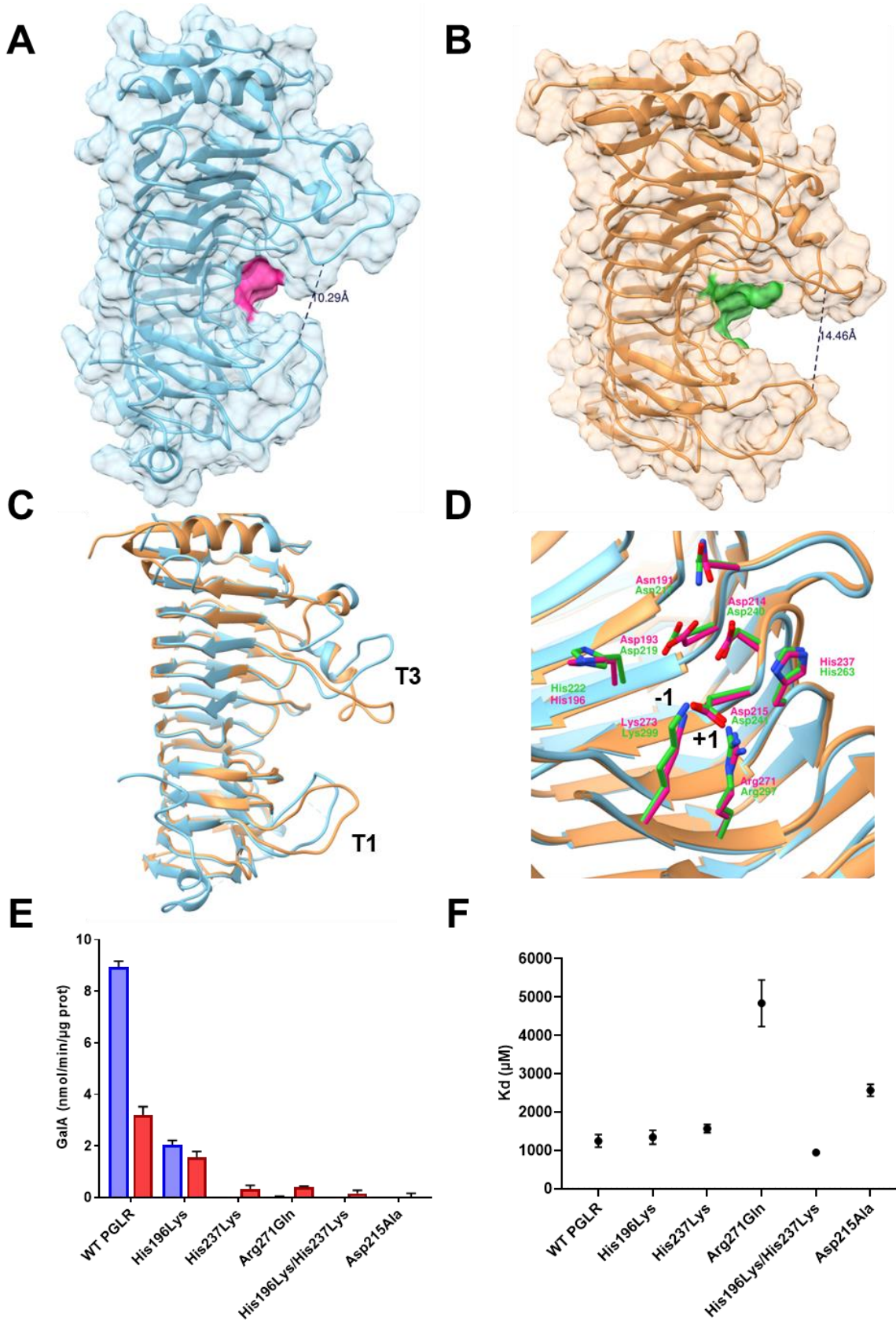
A
10.29Å
B
14.46Å
C
T3
T1
D
Asn191
Asp214
Asp240
Asp193
Asp219
His237
His263
His222
His196
-1
Lys273
Lys299
Asp215
Asp241
+1
Arg271
Arg297
E
GalA (nmol/min/µg prot)
10
8
6
4
2
0
WT PGLR
His196Lys
His237Lys
Arg271Gln
His196Lys/His237Lys
Asp215Ala
F
Kd (µM)
6000
5000
4000
3000
2000
1000
0
WT PGLR
His196Lys
His237Lys
Arg271Gln
His196Lys/His237Lys
Asp215Ala

Figure 22. Structure comparison of PGLR and ADPG2
A) Surface and ribbon diagram of PGLR. Amino-acids of the active site are pink-colored. B) Surface and ribbon diagram of ADPG2. Amino-acids of the active site are green-colored. C) Structural alignment of PGLR and ADPG2 displaying the active site and binding groove. D) Active site of the PGLR and ADPG2 highlighting amino-acids involved in hydrolysis. Black numbers indicate the subsites. E) Total PG activity of WT and mutated forms of PGLR. Assays were realized on PGA (blue bars) and pectins DM20-34% (red bars). F) MST analysis of the interaction between WT and mutated forms of PGLR with OG of DP12DM5.

(rmsd) value of 0.358 Å (**Figure S5A** and **B**). PGLR structure consists of 429 (AA) with 18 AA at the N-terminus and 20 AA at the C-terminus that were not modelled because of poor electron densities. ADPG2 consists of 420 AA with 41 AA at the N-terminus and 14 AA on C-terminus that were not modelled. Overall electron densities were well defined except for some loop area, as indicated by the high B-factors (**Figure S6**). While no site for glycosylation could be revealed on ADPG2 structure, PGLR harboured two N-glycosylation sites: Asn255 (glycosylation motifs: NAG–NAG) and Asn313 (glycosylation motifs: NAG–NAG–BMA–MAN–MAN–MAN, **Figure S4B and C**). The final models' geometry, processing and refinement statistics are summarized (**Table S1**). PGLR and ADPG2 structures have been deposited in the Protein Data Bank as entries 7B7A and 7B8B, respectively.

1.4.3. Structure comparison of PGLR and ADPG2

PGLR (**Figure 22A**) and ADPG2 (**Figure 22B**) harbour right-handed parallel β-helical structures which are common to pectinases (Cho et al., 2001). The β-helix is formed by three parallel β-sheets - PB1, PB2 and PB3 – which contain 11, 12, and 11 β-strands respectively, as well as a small β-sheet PB1a having only 3 β-strands (**Figure S7A** and **B**). Turns connecting the PB1-PB2, PB1a-PB2, PB2-PB3 and PB3-PB1 β-sheets are named T1-turns, T1a-turns, T2-turns and T3-turns according to Yoder and Jurnak (**Figure S7C** and **D**, Yoder and Jurnak, 1995). T2 turns are the shorter ones (one or two AA long) while T1, T1a and T3 turns have more variable length and also contain the loops around the active site. Both enzymes have a α-helix on N-terminus end that is connected to T1 turn by a disulfide bridge which shields the hydrophobic core of the enzyme (van Santen et al., 1999). While C–terminus end is also protected by tail-like structure with disulfide bridge shielding the C–terminus, PGLR has additional tail (Leu389 – Cys406) wrapping the PB1a β–sheet. Comparison of PGLR and ADPG2 structures indicate high structural

conservation (**Figure 22C**). Superimposition based on the secondary structure resulted in rmsd of 0.617 Å, predominantly due to the structural deviation in the region around the active site, in particular Asn130–Pro142 (T3 turn, PGLR numbering) and Tyr304-Val318 loop (T1 turn, PGLR numbering) that are important for the substrate preference and the absence of interaction with PGIPs. Between these loops, a large cleft is present, exposing PB1. This cleft, opened at both sides, is well suited for accommodating the substrate and identifying PGLR and ADPG2 as endo-PGs, in accordance with their biochemical characterization (**Figure 21A, Inset**, Hocq et al., 2020). PGLR shows narrower cleft of 10.29 Å compared to 14.46 Å for ADPG2, between Arg139 and Gly308 and Cys164 and Ser335 measured at Cα atoms for PGLR and ADPG2, respectively (**Figure 22A** and **B**). Furthermore, differences in the AA alongside the binding groove are likely to be crucial for substrate binding and processivity.

1.4.4. Structure of active site

Comparison of the PG sequences and structures from bacteria, fungi and plants, reveal that the active site is formed by only eight AA that are strictly conserved and responsible for the hydrolysis of the substrate (van Santen et al., 1999; Markovič and Janeček, 2001; Shimizu et al., 2002; Park et al., 2008). They correspond to Asn191–Asn217, Asp193–Asp219, His196–His222, Asp214–Asp240, Asp215–Asp241, His237–His263, Arg271–Arg297, Lys273–Lys299 for PGLR and ADPG2 (first AA referring to PGLR, second to ADPG2, **Figure 22A** and **B**). 7 of these AA (underlined hereafter) are included into four absolutely conserved structural motifs Asn-Thr-Asp, Asp-Asp, Gly-His-Gly, Arg-Ile-Lys and are positioned at subsites -1 and +1 of the active site (Pagès et al., 2000; Shimizu et al., 2002; André-Leroux et al., 2009). Three Asp residues are involved in hydrolysis where Asp214 act as a proton donor while Asp193 and Asp215 acts as a general base which activates the nucleophilic water that attack the anomeric carbon of the substrate (Shimizu et al., 2002).

To determine the importance of these residues for the activity and substrate interaction, five site-directed mutations were designed in the sequence of PGLR: in the active site (Asp215Ala), in the binding site (Arg271Gln), and in amino-acids that putatively modulate the pH-dependence of the enzyme (His196Lys, His237Lys and His196Lys/His237Lys). Wild-type (WT) and mutant recombinant proteins were purified by affinity chromatography (**Figure S8**). We measured their activity on PGA and pectins DM 20-34% (**Figure 22E**) and determined their binding affinity to the

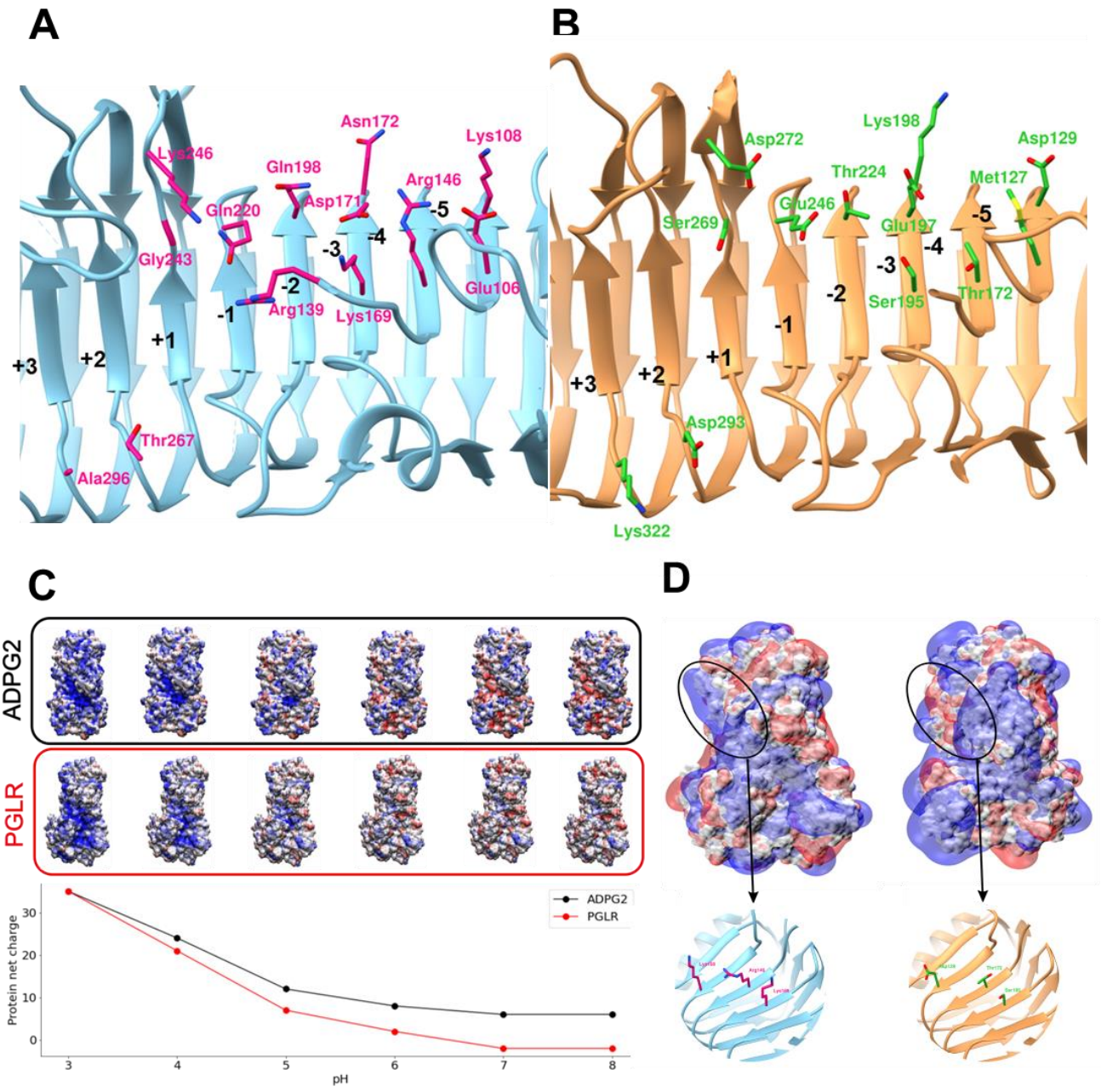

Figure 23. Structure of subsites and surface electrostatic potentials of PGLR and ADPG2
A) Structure of -5/+3 subsites of PGLR. B) Structure of -5/+3 subsites of ADPG2. AA corresponding to PGLR Arg139 is not shown. Black numbers indicate position of subsites. C) Surface electrostatic potential of PGLR and ADPG2 across a pH3-8 range. D) Surface electrostatic potential of PGLR (left) and ADPG2 (right) at pH5. Key amino-acids are represented in sticks.

substrate by assessing their dissociation constant (Kd) using Microscale thermophoresis (MST, **Figure 22F**). For that purpose, we used a mix of various DP and DM centred on a DP12 and DM5 (named hereafter DP12DM5) on which PGLR shows activity (**Figure S2B)**. All of the mutants appear to lose activity compared to WT PGLR. His196Lys showed 22% and 17% of residual activity on PGA and pectins DM 20-34%, respectively, highlighting a potential change in the dependence of activity with regards to DM. In contrast, no residual activity on either substrate was measured for His237Lys and His196Lys/His237Lys mutants. All of the three above-mentioned mutants showed similar Kd compared to WT. As expected considering the importance of Asp215 in binding a water molecule responsible for hydrolysis, Asp215Ala mutation resulted in a total loss of activity on both substrates (**Figure 22E**). However, the mutated protein was still able to interact with an OG of DP12DM5, albeit to a lesser extent compared to WT (Kd of 2567 µM versus 1246 µM, **Figure 22F**). Arg271Gln mutant showed also strong reduction in specific activity (only 3% of WT using pectins DM 20-34%), and an increase in Kd compared to WT (4840 µM versus 1246 µM, **Figure 22F**) showing the importance of this residue in carboxyl group recognition and binding at subsite +1 (Pagès et al., 2000; Shimizu et al., 2002).

1.4.5. Characterization of the subsites

While AA at the active site, as well as the β-helical structure, are conserved in PGs from different organisms, there are considerable differences in the surrounding loops, as well at specific subsites. Sequence analysis with bacterial and fungal enzymes show that PGLR and ADPG2 (**Figure S9**) share 40.92% sequence identity, and only 20.94%/21.24% with *A. acuelatus*, AaPG1 (Cho et al., 2001), 23.81%/25.60% with *A.niger*, AnPG1 (Van Pouderoyen et al., 2003), 19.06%/21.27% with *A.niger*, AnPGII (van Santen et al., 1999), 19.77%/21.78% with *F.phyllophilum*, FpPG1 (Federici et al., 2001), 23.67%/21.14% with *P. carotovorum*, PcPG1 (Pickersgill et al., 1998) and 20.30%/19.40% with *C. purpureum,* CpPG1 (Shimizu et al., 2002). Although having low sequence identity, plant PGs show high structural homology with previously described PGs. with a rmsd between 0.84 and 1.1 Å between equivalent Cα atoms. Despite conserved active site, thirteen AA on PGLR, positioned alongside the binding groove and at distant sites, previously shown to be of importance for substrate interaction and processivity (Pagès et al., 2000; Cho et al., 2001; André-Leroux et al., 2009), differ between PGLR and ADPG2 (**Figure 23A** and **B**). These AA were compared with that of AaPG1. At subsite -5, PGLR harbours Arg146 that is responsible for interaction with carboxyl group of GalA while ADPG2 and AaPG1 have Thr172

and Ala108, respectively (**Figure S10A**). Similarly, at subsite -4 Thr224 (ADPG2) or Gly164 (AaPG1) are mutated into Gln198 in PGLR. (**Figure S10A**, Pagès et al., 2000). At subsite -4, -3 and -2 a positively charged patch formed by Gln198, Gln220 and Lys246 (PGLR) is mutated into Thr224/Gly164 as well as acidic Glu246/Asn186 and Asp272/Gly210 in ADPG2/AaPG1. At subsite -1 Ser269 (ADPG2) or Ser208 (AaPG1), normally hydrogen-bonded to GalA is mutated in Gly243 in PGLR. Finally, at subsite +2 and +3 Asp293/Asp231 and Lys322/Lys261 in ADPG2/AaPG1 are replaced by Thr267 and Ala296 in PGLR.

1.4.6. PGLR and ADPG2 electrostatic potentials and dynamics

To understand how protein structure might determine enzymes' pH and substrate dependence as well as processivity, we calculated PGLR and ADPG2 electrostatic potentials across a pH 3-8 range (**Figure 23C**). The protein net charge decreases from pH 3 to pH 8, with both enzymes being positively charged at acidic pHs. At pH 5 PGLR shows a positively charged patch corresponding to Lys108, Arg146 and Lys169 on subsite -5, -4, -3, a highly positive charge at -1 subsite, corresponding to His196, and at +1 subsite, corresponding to His237. In contrast, ADPG2 shows high polar surface at subsite -3, -4 and -5 corresponding to Asp129, Thr172 and Ser195 and highly positive charge on -1 and +1 corresponding to His222 and His263, respectively (**Figure 23D**).

1.4.7. Structural determinants of the absence of PGIP-mediated inhibition of plant PGs

In order to complete the structural characterization of the 2 plant PGs in comparison with fungal ones, we investigated the structural determinants of pathogenic PG regulation/inhibition by interaction with plant PGIP that occurs during pathogen attacks (Kalunke et al., 2015). For that purpose, the structures of ADPG2 and PGLR were superimposed to the *F. phyllophilum* PG (FpPG1, reclassified from *Fusarium moniliforme* (Mariotti et al., 2009)) - *Phaseolus vulgaris* PGIP2 (PvPGIP2) complex to assess the structural determinants of the absence of inhibition of plant PGs by plant PGIPs (**Figure 24A**). It has been previously shown that PGLR is not inhibited by PvPGIP2 (Hocq et al., 2020). In FpPG1, the Ser120-Asn121-Ser122-Asn123 stretch plays a key role in the PG-PGIP interaction with Asn121 interacting with His110 of PvPGIP2 on N-terminus loop (**Figure 24B**, Benedetti et al., 2011). The T3 loop of PGLR and ADPG2 is different, not harbouring AA equivalent to Asn121: PGLR loop is rich in hydrophobic Met (132,133 and 137) buried inside the loop, while ADPG2 loop is rich in Lys (160, 162, 166) therefore lacking such interaction and facilitating potential clashes which could hinder the interactions. Similar

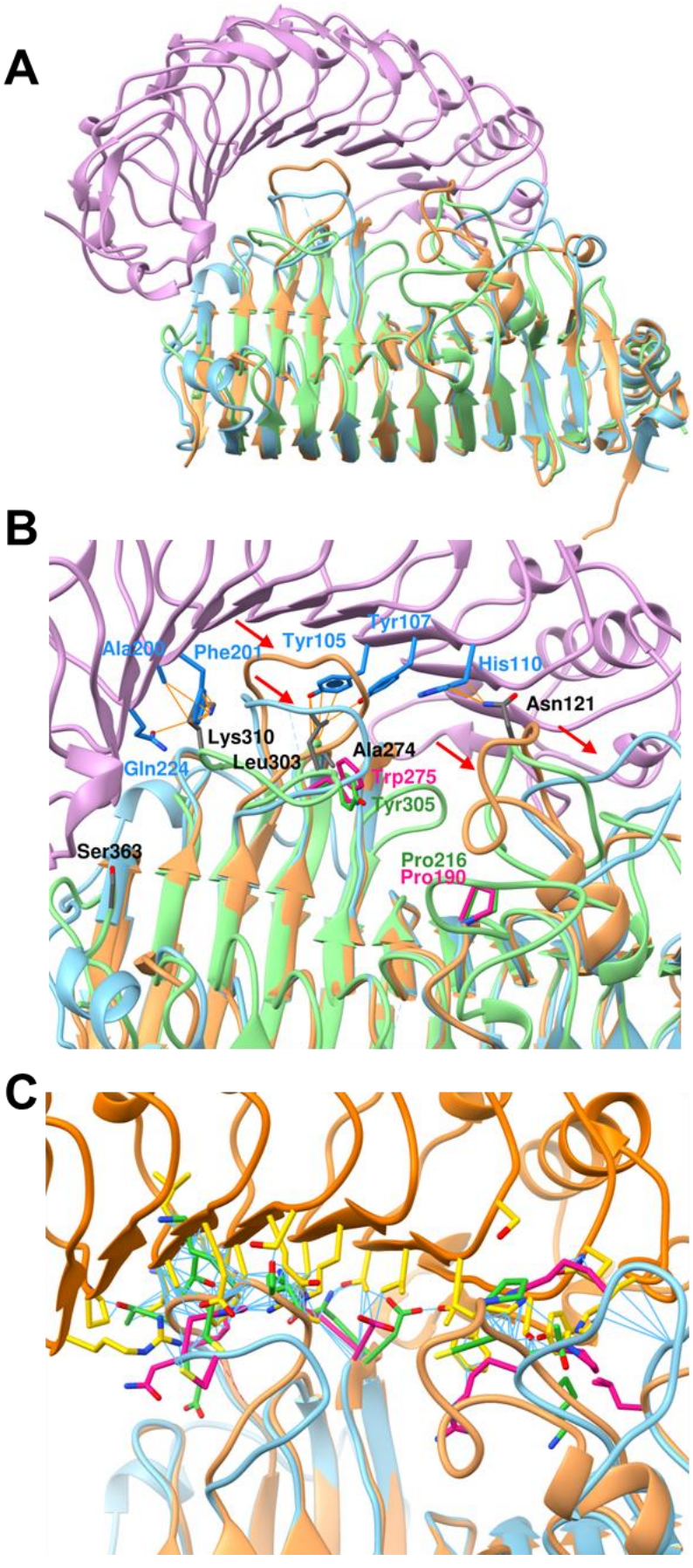
A
B
Ala200
Phe201
Tyr105
Tyr107
His110
Asn121
Lys310
Leu303
Ala274
Gln224
Trp275
Tyr305
Ser363
Pro216
Pro190
C

Figure 24. Structural determinants of the absence of plant PG-plant PGIP interaction
A) Ribbon representation of *Phaseolus vulgaris* PGIP2 (PvPGIP2, plum), PGLR (blue), ADPG2 (brown), *Fusarium phyllophilum* PG (PpPG1, green) interaction. B) Detailed representation of AA involved in PvPGIP2-FpPG1 interaction (PvPGIP2 amino-acids in blue and FpPG1 amino-acids in grey), with orange lines representing van der Waals contacts. Key AA (Asn121, Leu303) mediating the interaction in FpPG1 are absent in PGLR and ADPG2. PGLR and ADPG2 loop region indicated by red arrows. PvPGIP2 (plum), PGLR (blue), ADPG2 (brown), *Fusarium phyllophilum* PG (PpPG1, green) are represented. C) Interaction of AtPGIP1 with PGLR and ADPG2. The structure of AtPGIP1 was modelled onto PvPGIP and AA included in clashes closer than 0.6 Å are shown as blues lines. Amino acids of AtPGIP1 (yellow), PGLR (pink) and ADPG2 (green) are shown.

observation was made for AnPGII were no contact was observed in this loop (**Figure S11,** Benedetti et al., 2011). On C-terminus loop Ala274 is the AA that contributes most for the FpPG1-PGIP interaction while in PGLR/ADPG2 it is replaced by Gly278/Gly303 (Benedetti et al., 2013) that have no interacting abilities. Alignment of PGLR and ADPG2 with fungal PGs showed that Pro190/Pro216 are replaced by His in fungal PGs and Trp275/Tyr301 are inserted in plant PGs (**Figure S9**).

To compare the structures of Arabidopsis PGIP and their interactions with PGLR and ADPG2 we have modelled AtPGIP1 and AtPGIP2. Models were superimposed to PvPGIP2 and are highly similar with rmsd of 0.312 and 0.294 Å for AtPGIP1/AtPGIP2, respectively (**Figure S12A**). Furthermore, their interaction properties were studied in comparison to PvPGIP2. AtPGIP1 and 2 lack His110 and Gln224, that are replaced by Trp residues in both AtPGIPs, needed for interaction with FpPG1 and AnPGII (Ferrari et al., 2003). When looking at the PGLR/ADPG2-AtPGIP1/AtPGIP2 complexes several AA are involved in steric clashes (**Figure 24C** and **Figure S12B** and **C**) making the interaction highly unlikely.

1.5. Discussion

The fine-tuning of HG-type pectin structure by PGs play a central role in the control of the polysaccharide chemistry, contributing to changes in the cell wall mechanical properties. This has dramatic consequences on plant development (Ogawa et al., 2009; Xiao et al., 2014; Rui et al., 2017; Xiao et al., 2017). In Arabidopsis, PGs are encoded by 68 genes, which questions the rationale for such abundance in the context of the cell wall. Here we report on the biochemical and structural characterization of two plant PGs, PGLR and ADPG2, whose expression overlap in Arabidopsis roots. Both structures show common right handed β-parallel fold commonly found in pectinases, including fungal endo-PGs (van Santen et al., 1999; Cho et al., 2001; Shimizu et al., 2002), exo-PGs (Abbott and Boraston, 2007), pectin/pectate lyases (Yoder and Jurnak, 1995; Lietzke et al., 1996; Vitali et al., 1998) and rhamnogalacturonases (Petersen et al., 1997). There are three main β-sheets that are connected with loops containing between one and seventeen AA. Both enzymes are dominated by a large cleft, that can accommodate the substrate, which is opened from both sides, suggesting, based on the structure, that PGLR and ADPG2 are endo-PGs (van Santen et al., 1999). Amino-acids at the active site (Asn191–Asn217, Asp193–Asp219, His196–His222, Asp214–Asp240, Asp215–Asp241, His237–His263, Arg271–Arg297, Lys273–Lys299, first AA referring to PGLR, second to ADPG2) are structurally conserved when compared to that of previously reported structures (van Santen et al., 1999; Shimizu et al., 2002; Abbott and Boraston, 2007), even while some differences exist (i.e. Pro190, His196, Pro235 in PGLR are replaced by His, Asp and Gly in bacterial and fungal PGs). To further determine the role of some of these amino-acids in activity and/or substrate binding, we designed specific mutations for PGLR. Our results confirmed the importance of Asp215 in the hydrolysis, as well as Arg271 in binding and positioning the substrate at subsite +1, as previously reported for fungal PGs (van Santen et al., 1999; Pagès et al., 2000). Asp215 together with Asp193 binds a water molecule that is responsible for hydrolysis, while Asp214 acts as proton donor in the mechanism. Mutating any of these three AA leads to diminution of the total activity. Arg226 (CpPG1 numbering) was identified as one of the AA that is associated with the carboxyl group of the GalA through hydrogen bonding (Shimizu et al., 2002). This further confirms the role of Arg271 in the carboxyl group recognition in the subsite +1 in PGLR. Based on the position and of the physicochemical properties of His196 and His 237, we postulated that these residues could play a role in the pH-dependence of the enzyme. His196Lys, His237Lys and the double mutant were not affected in their binding with substrate, but

where His196Lys mutant showed residual activity, His237Lys and the double mutant did not. His237 is one of the strictly conserved AA in PGs and changing it to Lys could affect the positioning of the substrate in the active site, leading to enzyme's lack for hydrolysing the glyosidic bond. Unfortunately, the overall decrease of activity of these mutants did not enable us investigating pH-dependency since activity was low for all assessed pHs. Although some studies identified mutation that are responsible for pH shift (Kim et al., 2006), the success rate is low with high risk of losing the catalytic activity (Ma et al., 2016). The mutations, by modifying the charge and the size of the AA, could have an effect on the positioning of the substrate (Villar et al., 1997).

Although structurally conserved, the biochemical specificities (substrate, pH, temperature) of PGLR and ADP2 differ. If PGLR and ADPG2 were formally shown to be endo-PGs, as previously reported fungal PGs (van Santen et al., 1999; Cho et al., 2001; Van Pouderoyen et al., 2003), the OGs released by either of the enzymes from PGA, pectins of various DM or cell wall material were strikingly different. For instance, PGLR released OGs of higher DP and degree of acetylation compared to ADPG2. In addition, PCA showed that the digestion products of ADPG2 were more similar to that of AaPG1 (Dim1 57.7%), suggesting similarities in substrate binding and/or processivity of these enzymes. This was further demonstrated by the analysis of PGLR, ADPG2 and AaPG1 enzymes' structures which shows that they have unequal distribution of subsites. While having highly conserved active site on -1/+1, PGLR lacks the AA connected to the +3/+2 subsite. Asp293 and Lys322 in ADPG2 (Asp231 and Lys261 in AaPG1) are indeed replaced by Thr267 and Ala296 in PGLR, which could partly explain the lack of activity of PGLR on OGs of short DP. Docking studies on AaPG1 indeed showed that Asp231 and Lys261 can interact with substrate of DP = 8 (Cho et al., 2001) and therefore, at subsite +3 Asp293 and Lys 322 in ADPG2 could stabilise the interaction with the substrate. Compared to ADPG2, PGLR released specific non-methylesterified OGs of high DP and acetylated OGs from pectins DM >85% and root cell wall, respectively. With regards to methylesterification, these differences could be partly explained by the enzymes' structure as methyl substitutions supress the negative charge of the GalA. As ADPG2 subsites -3, -4 and -5 are more polar, composed of Ser195, Thr172 and Asp129, it would be more tolerant for interacting/releasing with methylesterified substrate. This might explain the higher activity of ADPG2 on DM>85%. In contrast, PGLRs, Arg146, Lys169 and Gln198 could interact more frequently with the negative charge of the GalA (André-Leroux et al., 2005). The release

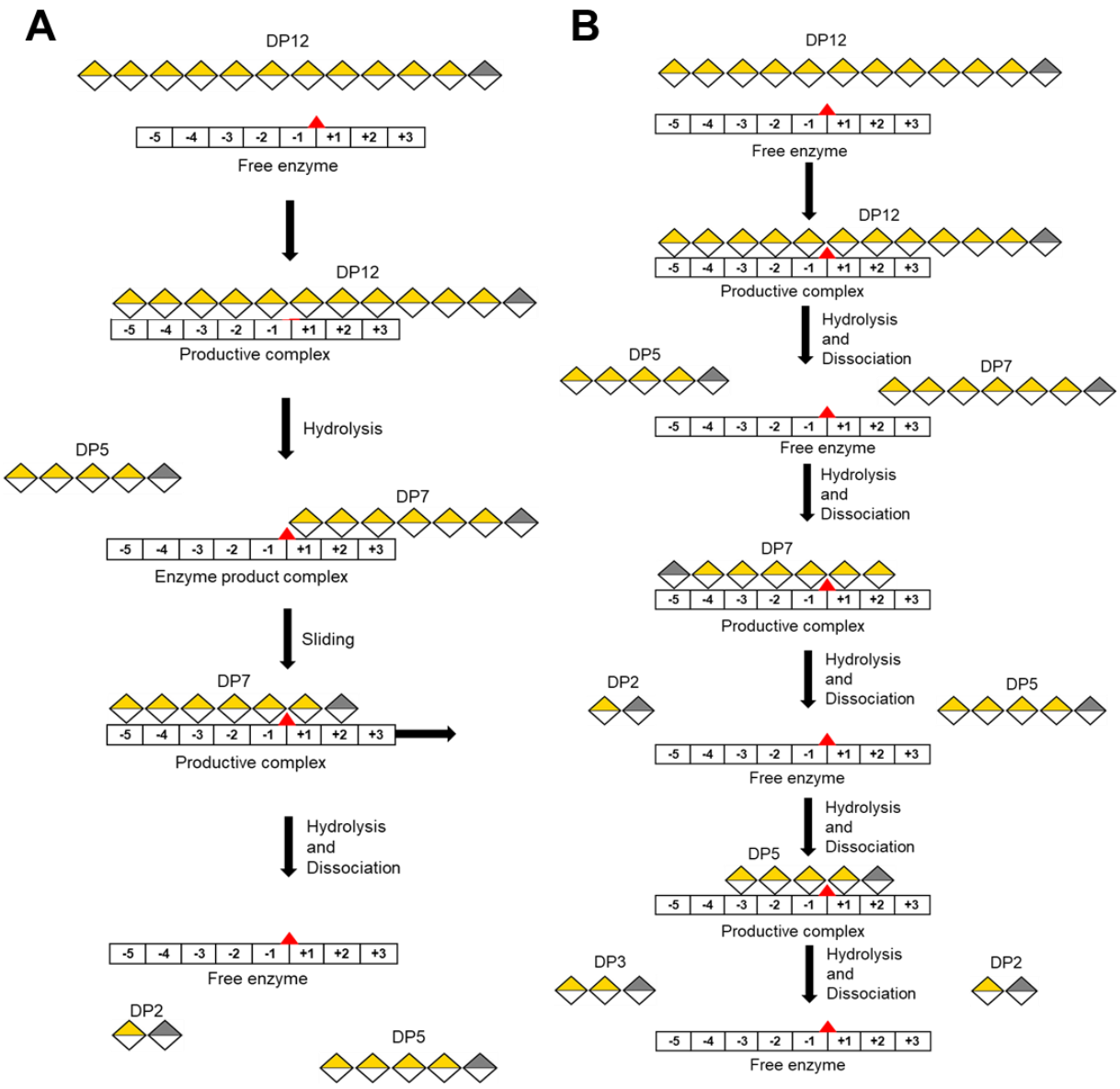

Figure 25. Model of the mode of action of PGLR and ADPG2
A) PGLR and B) ADPG2. Based on the differences in structure and OGs identified by LC-MS/MS analysis we propose a model by which PGLR has a processive mode of action where the enzyme slides onto the substrate and generates OGs of high DP. In contrast ADPG2 has a non-processive mode of action, where it interacts with the substrate, hydrolyses and dissociates, generating OGs of short DPs. Reducing end of the substrate is grey-coloured.

of acetylated OGs by PGLR could be related to the presence of Gln198 and Gln220 as the structurally conserved Ser191, Asn213 and Asp240 were shown to potentially modulate tolerance to acetylation in AnPG1 (Bonnin et al., 2002; André-Leroux et al., 2005). Unfortunately, these authors were unable to obtain a crystallised complex of PGs with substituted pectin in the active site to further confirm these predictions. Therefore, some additional AA could play a role in substrate preference.

The lower activity of PGLR, and the release of OG of higher DPs compared to ADPG2, could be related to differences in the processivity of the enzymes and in particular in the surface electrostatic potential of the protein. Three positively-charged AA, Lys108, Arg146, Lys169, that are perfectly placed in the binding groove of PGLR at subsites -3, -4 and -5, could modulate the interaction with the substrate and hereby the processivity. Processive or multi attack enzymes can act on the same polymer multiple times before dissociating, and this can be related to the degree of enclosure of the substrate (Benen et al., 1999; Breyer and Matthews, 2001). Processive enzymes indeed fully enclose their substrate and PGLR shows narrower cleft than ADPG2, 10.3 Å compared to 14.4 Å (between Arg139/Gly308 and Cys164/Ser335 measured at Cα atoms), a wider cleft facilitating dissociation from the substrate. Furthermore, Arg139 perfectly positioned at the entrance of PGLR's active site, possess positive charge and can bind strongly negatively charged pectin (Tu et al., 2015). Its position partially corresponds to Asn94 which was showed to play a role in substrate binding particularly in hydrogen bonding on subsites – 1/+1 in Achaetomium sp. Xz8 PG8fn (Tu et al., 2015). Moreover, in AnPG1 one important AA, Arg96 (**Figure S10C**) which is flexible enough to play a role in processivity is not present in PGLR/ADPG2 where is replaced with Glu106/Met127. However, Lys108 could play the same role in PGLR (Van Pouderoyen et al., 2003). Considering the above-mentioned structural and biochemical results, we can propose a model describing the mode of action of PGLR and ADPG2 (**Figure 25A** and **B**), where PGLR acts as a processive enzyme sliding onto the substrate and releasing mainly OG of DP>5 while ADPG2 acts randomly by hydrolysing and dissociating larger DP that can be re cut in a second hydrolysis, releasing OG of DP 2-4 (Benen et al., 1999).

While the regulation of plant pectin methylesterases (PMEs) is mediated through the 1:1 interaction with specific plant inhibitors (PMEIs), plant PG activity is not inhibited by plant PGIP (Federici et al., 2001). PGLR activity was indeed not inhibited by *Phaseolus vulgaris* PGIP

(PvPGIP2, Hocq et al., 2020). In addition, reports showed that the inhibition of fungal PGs by plant PGIP is highly variable, with, for instance, PvPGIP2 inhibiting *F. phyllophilum* PG but having non-competitive inhibition with *Aspergillus niger* PG (Ferrari et al., 2003; Sella et al., 2004; Di Matteo et al., 2006; Raiola et al., 2008; Benedetti et al., 2011). Our results shed new light on the structural basis for the absence of plant PG-plant PGIP interactions. Structurally, the key AA of FpPG1 needed for determining the interaction with PvPGIP2 are Ser120-Asn121-Ser122-Asn123, with Asn121 responsible for the interaction with His110 of PvPGIP2 (**Figure 24B**). The T3 loop in PGLR and ADPG2 are structurally different to that of FpPG1 and do not carry any equivalent AA. Instead PGLR loop is rich in hydrophobic Met (132,133 and 137), while ADPG2 loop is rich in Lys (160, 162, 166). In AnPGII, the equivalent Asn in the loop is absent, replaced by Gly127, causing the non-competitive inhibition mechanism described for PvPGIP2 (Benedetti et al., 2011). Furthermore, an important residue in FpPG1, His188, is replaced by Pro190/Pro216 in PGLR/ADPG2. His/Pro mutation was shown to cause considerable decrease in FpPG1-PvPGIP interaction (Federici et al., 2001). Additionally, in FpPG1, insertion of Trp after Ser270 causes the loss of FpPG1 inhibition by introducing favourable stacking interaction of Tyr302, and movement of Lys269 side chain. PGLR and ADPG2 both present similar insertion (Trp275/Tyr301, respectively), that could explain their absence of inhibition by PvPGIP2.

In contrast to the regulation of PMEs by PMEIs in plants, previous work demonstrated the absence of regulation of Arabidopsis PG activity by endogenous PGIPs (Cervone et al., 1990) Here we approached this question using the modelling of Arabidopsis PGIP1 and PGIP2 and highlighted the structural bases of the absence of PGIP-mediated regulation of PG activity in plants. If AtPGIP1 and AtPGIP2 showed highly conserved structure with that of PvPGIP2, they are lacking the His110 and Gln224 required for inhibition of FpPG1 (Ferrari et al., 2003). This, together with the above-mentioned structural features of PGLR and ADPG2, is likely to explain the absence of inhibition of Arabidopsis PG by endogenous PGIP in the context of the cell wall.

Among a multigenic family, our work highlights the potential role of each of the isoforms in the fine-tuning of pectin structure *in planta* showing that, despite PGLR and ADPG2 redundant expression, their structural and biochemical specificities differ. In addition, by the identification of the determinants of PG-PGIP interaction, we also bring novel pieces of information explaining the absence of endogenous regulation of plant PG activity.

1.6. Material and methods

1.6.1. Sequences retrieval and analysis

Arabidopsis thaliana PGLR (At5g14650) and ADPG2 (At2g48150) coding sequences were retrieved from publicly available genome database TAIR (https://www.arabidopsis.org/). The presence of putative signal peptide was predicted using SignalP-5.0 Server (http://www.cbs.dtu.dk/services/SignalP/). Glycosylation sites were predicted using NetNGlyc 1.0 Server (http://www.cbs.dtu.dk/services/NetNGlyc/). Sequence alignments were performed using MEGA multiple sequence alignment program (https://www.megasoftware.net/). For protein structure and function prediction we used I-TASSER prediction software (https://zhanglab.ccmb.med.umich.edu/I-TASSER/). UCSF Chimera (http://www.cgl.ucsf.edu/chimera/) was used for creation of graphics.

1.6.2. Cloning, heterologous expression and purification of AtPGLR and ADPG2

AtPGLR was previously expressed in *Pichia pastoris* and biochemically characterized (Hocq et al., 2020). AtPGLR mutants were created using cDNA and specific primers carrying mutations (**Table S2**)**.** At2g41850 (ADPG2) coding sequence was codon-optimized for *Pichia pastoris* expression. Cloning and protein expression was done as previously described Hocq et al., 2020 and Safran et al., 2021.

1.6.3. AtPGLR and ADPG2 enzyme analysis

Bradford method (Bradford, 1976) was used to determine the protein concentration, with Bovine Serum Albumin (A7906, Sigma) as a standard. Deglycosylation was performed using Peptide-N-Glycosidase F (PNGase F) at 37°C for one hour according to the supplier's protocol (New England Biolabs, Hitchin, UK). Enzyme purity and molecular weight were estimated by 12 % SDS-page electrophoresis using mini-PROTEAN 3 system (BioRad, Hercules, California, United States) Gels were stained using PageBlue Protein Staining Solution (Thermo Fisher Scientic) according to the manufacturer’s protocol.

1.6.4. AtPGLR and ADPG2 biochemical characterization

The substrate specificity of AtPGLR and ADPG2 were determined with the DNS method (Miller, 1959) as previously described (Hocq et al., 2020). Polygalacturonic acid (PGA, 81325, Sigma); Citrus pectin with degree of methylesterification (DM) 20-34% (P9311, Sigma), DM 55-70% (P9436, Sigma) or DM >85% (P9561, Sigma); apple pectin with DM 70-75% (76282, Sigma);

were used as substrates. Results were expressed as nmol of GalA.min^{-1}.μg^{-1} of proteins. The optimum temperature was determined by incubating the enzymatic reaction between 25 and 60°C during 60 min using PGA (0.4%, w/v) at pH5. The pH optimum was determined between pH 4 and 7 using sodium acetate buffer (pH 3 to 5) and phosphate citrate buffer (pH 6 to 8) and 0.4 % (w/v) PGA as a substrate. The ADPG2 kinetic parameters were calculated using GraFit7 software (Michaelis-Menten/Hill; Erithacus Software, Horley, Surrey, UK) using PGA as a substrate. The reactions were performed using 1 to 8 mg.mL^{-1} PGA concentrations during 10 min at 50°C in 50 mM sodium acetate (pH5). All experiments were realized in triplicate.

1.6.5. Digestion of cell wall pectins and released OGs profiling

OGs released after digestions by recombinant PGLR and ADPG2 were identified as described in Voxeur et al (Voxeur et al., 2019). Briefly, PGA (81325), citrus pectin with DM 24-30% (P9311, Sigma) or DM >85% (P9561, Sigma) were prepared at 0.4 % (w/v) final concentration dissolved in 100 mM ammonium acetate buffer (pH 5) and incubated with either PGLR and ADPG2 at 0.03 $\mu g.\mu L^{-1}$. After digestion, non-digested pectins were pelleted by centrifugation, and the supernatant was dried in speed vacuum concentrator (Concentrator plus, Eppendorf, Hamburg, Germany). The same procedure was applied for roots of Arabidopsis seedlings that were grown for 7 days at 21°C, 16 h/8 h light/dark photoperiod. Roots were cut, incubated in ethanol 100 % (w/v) for 24 h, washed two times 5 min with acetone 100 % (w/v) and left to dry 24 h. Thirty roots per replicate were rehydrated in 150 µL 100 mM ammonium acetate pH 5 during 2 h on room temperature (RT) and digested with PGLR and ADPG2 at 0.02 $\mu g.\mu L^{-1}$, using the above-mentioned protocol. Separation of OGs was as described previously Hocq et al., 2020, using an ACQUITY UPLC Protein BEH SEC column (125Å, 1.7 µm, 4.6 mm x 300 mm). and the analysis was done as described in Safran et al., 2021.

1.6.6. Molecular interaction assay

Molecular interactions between PGLRs (WT and mutants) and selected OG was done using Microscale thermophoresis (MST) approach as described in Sénéchal et al., 2017 with some modifications. Briefly, PGLRs were labelled with Monolith protein labelling kit blue NHS amine reactive (Lys, NanoTemper, catalog no. MO-L003) and conserved in MST buffer (50 mM Tris pH 7.4, 150 mM NaCl, 10 mM MgCl2, 0.05 % Tween-20). For all experiments, constant final

concentration of labelled PGLRs was 1650 µM. Mix of OGs centred on DP12DM5 was prepared at 14028 µM concentration in MST buffer/dH_2O in 1:1 ratio. For all experiments, a constant concentration of labelled PGLRs was titrated with decreasing concentrations of non-labelled DP12DM5 from 7014 to 0.214 µM. The resulting mixtures were loaded into a Monolith NT.115 series standard capillaries (NanoTemper, catalogue no. MO-K002). Thermophoresis experiments were performed with 40% of MST power and 20% of LED power for fluorescence acquisition.

1.6.7. Crystallization of proteins

PGLR and ADPG2 were concentrated at 10 mg ml^{-1}. Crystallization was performed using the sitting-drop vapour-diffusion method. Crystallisation conditions were screened using a Mosquito robot (TTP Labtech) and the PACT premier plate (Molecular Dimensions, Sheffield, UK). PGLR and ADPG2 (100 nL) were mixed with an equal volume of precipitant (1:1). The crystals that resulted in best diffraction data were obtained with 0.2 M Sodium fluoride, 0.1 M Bis-Tris propane pH 8.5, 20 % w/v PEG 3350 (H1 condition, PACT premier plate) for PGLR and 0.2 M Sodium malonate dibasic monohydrate, 20 % w/v PEG 3350 (E12 condition, PACT premier plate) for ADPG2. Crystals for PGLR and ADPG2 formed after 6 and 2 months, respectively. Scale-up of the best condition was realized by mixing 1 µL of the best precipitant condition with 1 µL of the enzyme in the hanging drop vapor-diffusion method. Crystals were mixed with precipitation solution and PEG 3350 (35% w/v) before mounting in a loop and flash cooling in liquid nitrogen.

1.6.8. X-ray data collection and processing

The diffraction data were collected at PROXIMA-1 beamline (Synchrotron Soleil, Saint Aubin, France), at a temperature of -173°C using a PILATUS 6M end EIGER 16M detector (Dectris). Data were collected using X-rays with wavelength 0. 978564 Å. For ADPG2 one data set was collected at 2.03 Å resolution while for PGLR three data sets were collected from the same crystal at 1.3 Å resolution. Data were merged, scaled and processed using XDS (Kabsch, 2010a) and XSCALE (Kabsch, 2010b). PGLR crystal belonged to triclinic space group P1 with one molecule in asymmetric unit, while ADPG2 belongs to orthorhombic space group $P2_12_12_1$ with two molecules in asymmetric units.

1.6.9. Structure solution and refinement

The structure of PGLR was solved by molecular replacement using *Phaser* (McCoy et al., 2007). The data were phased using rhamnogalacturonase A (PDB: 1RMG, Uniprot Q00001, Petersen et al., 1997) as a search model. Model was built using *Autobuild* and refined using *Refine* from PHENIX suite (Liebschner et al., 2019). The model was iteratively improved with *Coot* (Emsley et al., 2010) and *Refine*. ADPG2 structure was solved by molecular replacement using PGLR as a starting model and the above-mentioned iterative procedure. The final refinement statistics are summarized (**Table S1**)**.** The final structure for PGLR and ADPG2 have been deposited in the Protein Data Bank as entries 7B7A and 7B8B, respectively.

Acknowledgements

This work was supported by a grant from the Agence Nationale de la Recherche (ANR-17-CE20-0023) and by the Conseil Regional Hauts-de-France and the FEDER (Fonds Européen de Développement Régional) through a PhD studentship awarded for to J.S. We wish to thank Pierre Legrand and all the staff at Proxima1 beamline (Synchrotron SOLEIL, Gif sur Yvette, France) for X-ray diffraction data collection. The technical assistance of Maša Boras, a former master 2 student is gratefully acknowledged.

Author's contribution

J.P., F.S., V.L. and D.M. designed research; J.S., W.T., O.H.; J.B., S.B., P.P., D.M., S.P., C. P-R., and V.L. performed research; J.S., W.T., D.M., V.L. and J.P. analyzed data; and J.S., W.T., F.S., V.L. and J.P. wrote the paper.

Conflicts of interest

There are no conflicts of interest.

1.7. Supplemental data

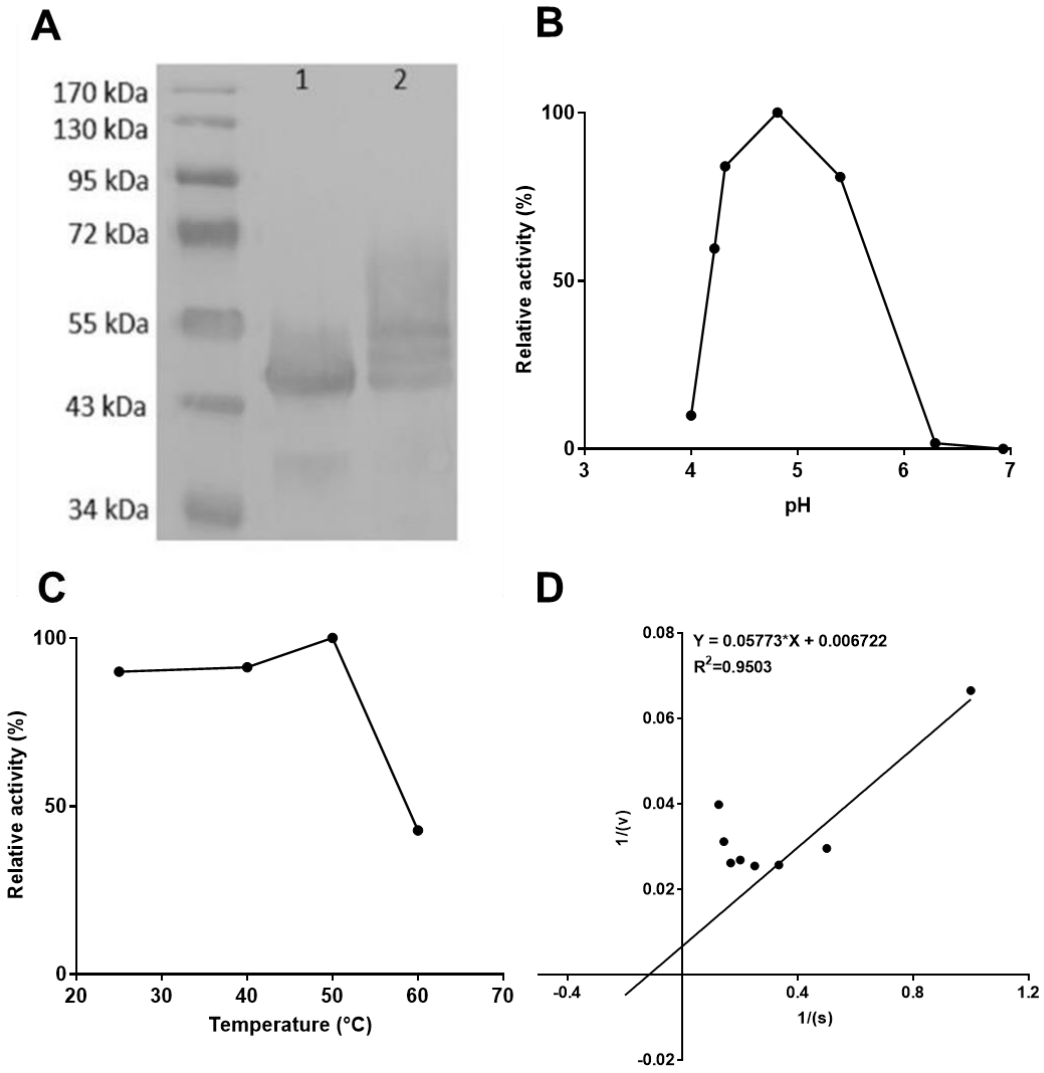

Figure S1. Purification and biochemical characterization of ADPG2
A) Western blot analysis of ADPG2 with anti-His antibodies on de-glycosylated form of ADPG2 obtained after digestion by PNGase F (1) and non-digested native sample (2). B) pH-dependence of ADPG2 activity. The activities were measured after 1 hour of incubation with PGA at 25°C at various pHs C) Temperature-dependence of ADPG2 activity. The activities were measured after 1 hour of incubation with PGA at pH 5.2 at various temperature D) Determination of Km and Vmax for ADPG2. Activity was assessed using various concentrations of polygalacturonic acid (PGA) at 25°C and pH 5.2 using the 3,5-dinitrosalicylic acid method. All experiments were performed in triplicate (n=3).

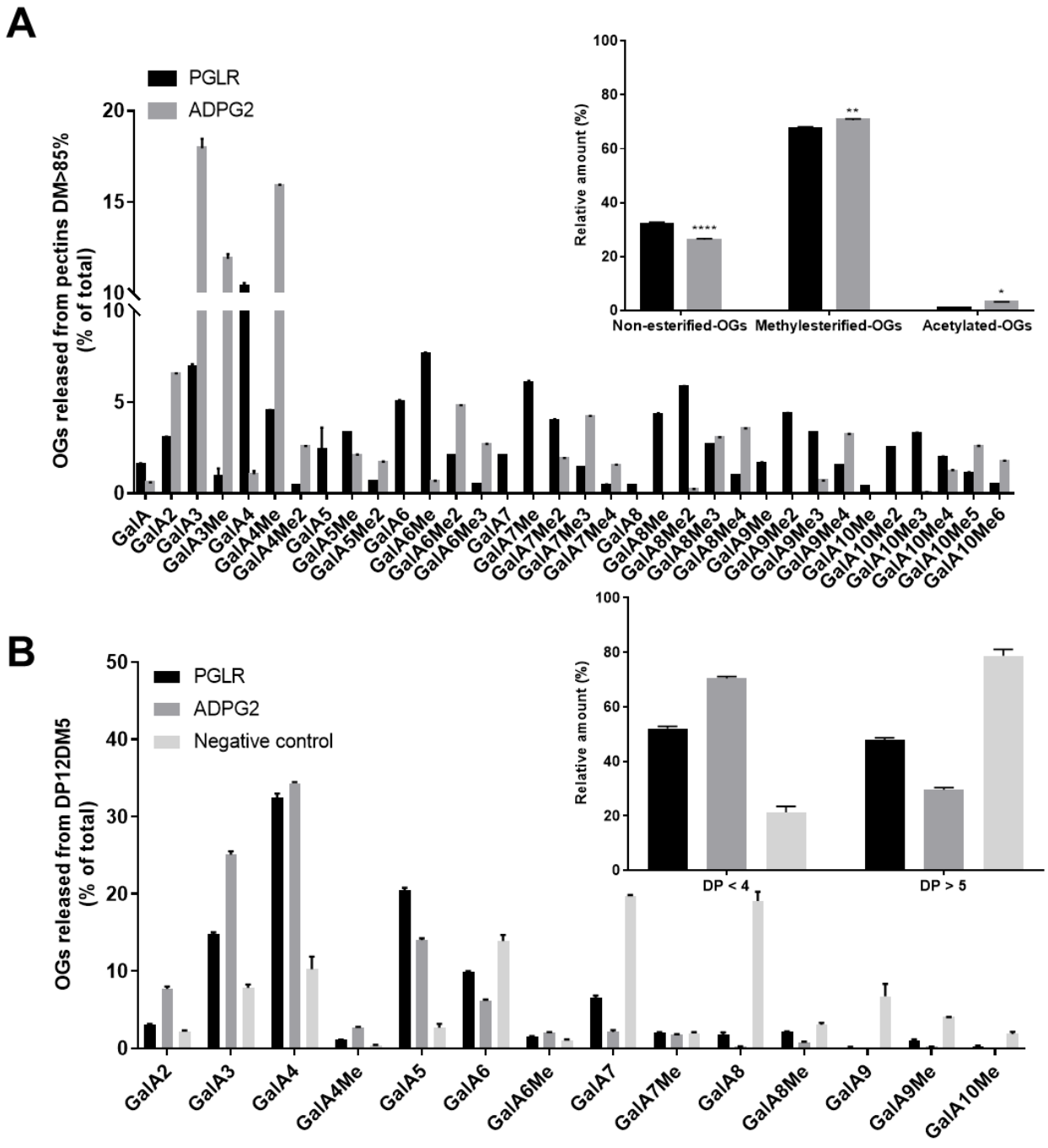

Figure S2. Oligogalacturonides produced by PGLR and ADPG2 from pectins of DP12DM5 and DM >85%

A) Oligoprofiling of OGs after overnight digestion of pectins of DM >85% by PGLR and ADPG2 at 40°C, pH 5 after (Inset: Cumulative OGs released by PGLR and ADPG2). Two-way ANOVA with Sidask's multiple comparison test, P value =0.0387; *=0.0038; ****<0.0001 B) Oligoprofiling of OGs after over-night digestion of DP12DM5 pectins by PGLR and ADPG2 at 40°C, pH 5 (Inset: Cumulative OGs released by PGLR and ADPG2). Negative control: undigested DP12DM5 pectins.

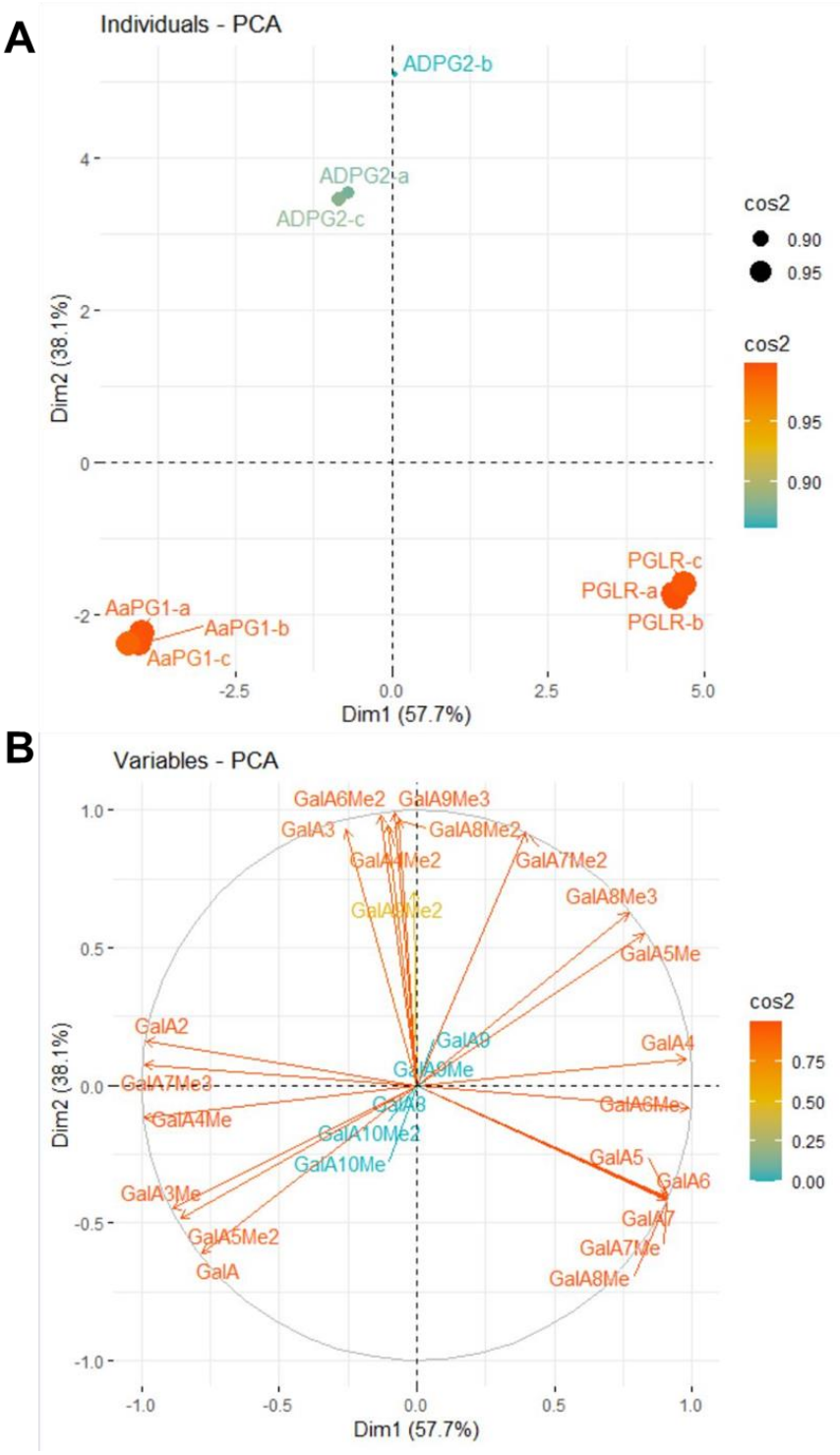

Figure S3. Principal Component Analysis (PCA)of oligogalacturonides released from pectins DM 20-34% by PGLR, ADPG2 and AaPG1

A) Score plot B) Loading plot. The oligogalacturonides released after overnight digestions of pectins DM 20-34% by PGLR, ADPG2 and AaPG1 were analysed by PCA using R-package (FactoMineR and Factoextra).

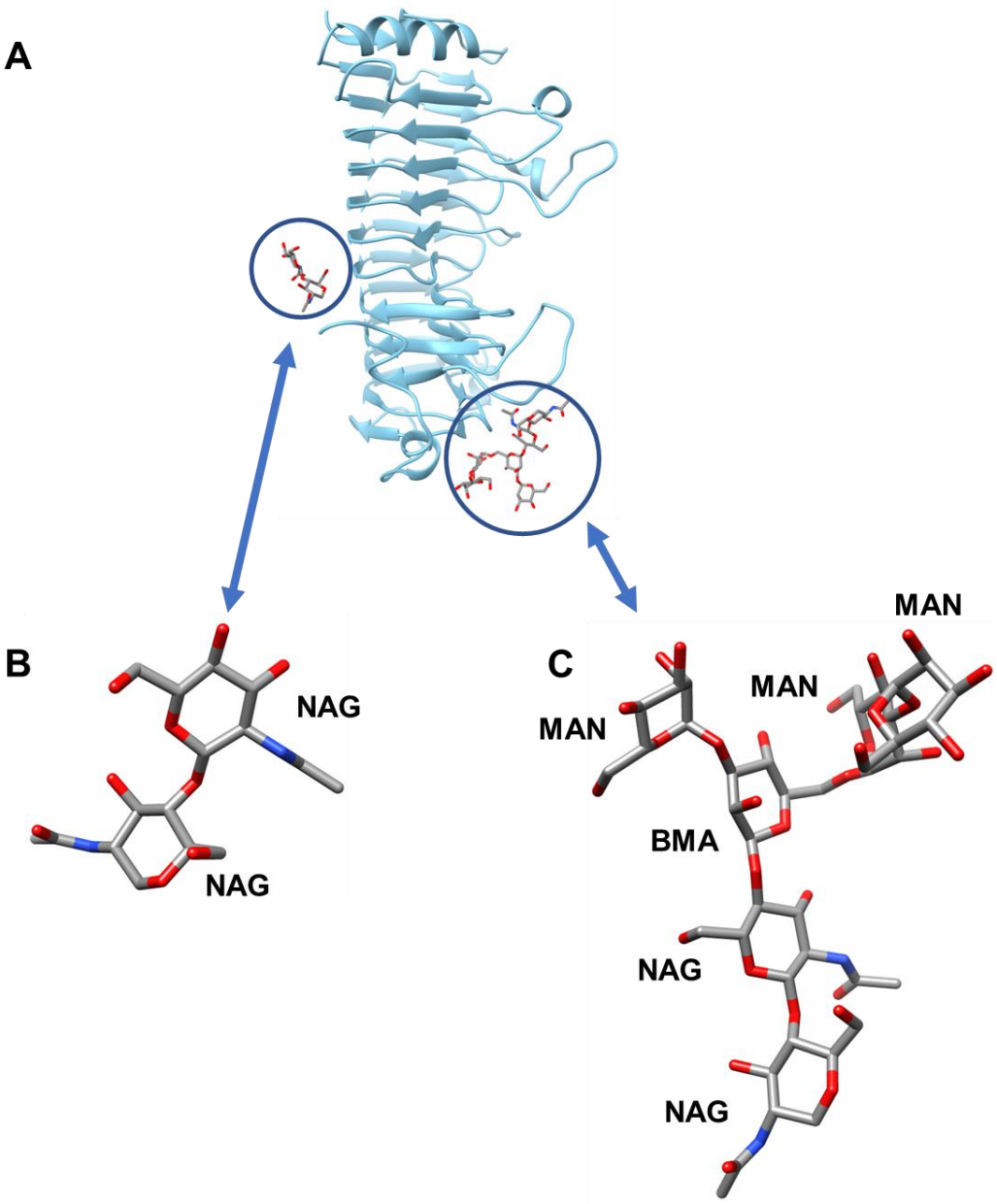

Figure S4. Crystallised PGLR in the P1 space group containing 2 N-glycosylated sugars
A) Ribbon diagram of the PGLR structure containing 1 molecule in the asymmetric unit. B) Asn255-linked NAG-NAG C) Asn313 linked NAG–NAG–BMA–MAN–MAN–MAN. NAG; N-acetylglucosamine, BMA; β-mannose, MAN α-mannose

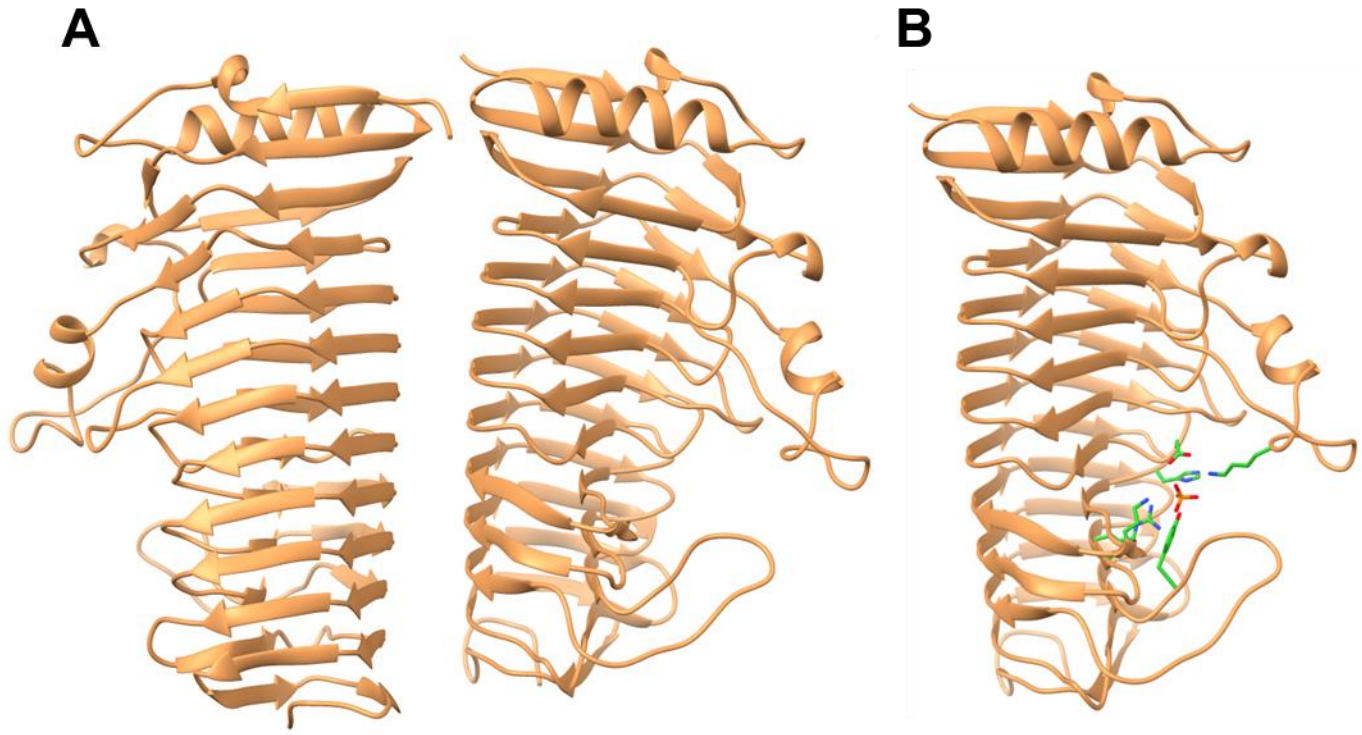

Figure S5. Crystallised ADPG2 in the P 2_1 2_1 2_1 space group
A) Ribbon diagram of the ADPG2 structure containing 2 molecules in the asymmetric unit. B) ADPG2 displaying the active site groove with crystallised PO_4^- and the AA stabilizing it.

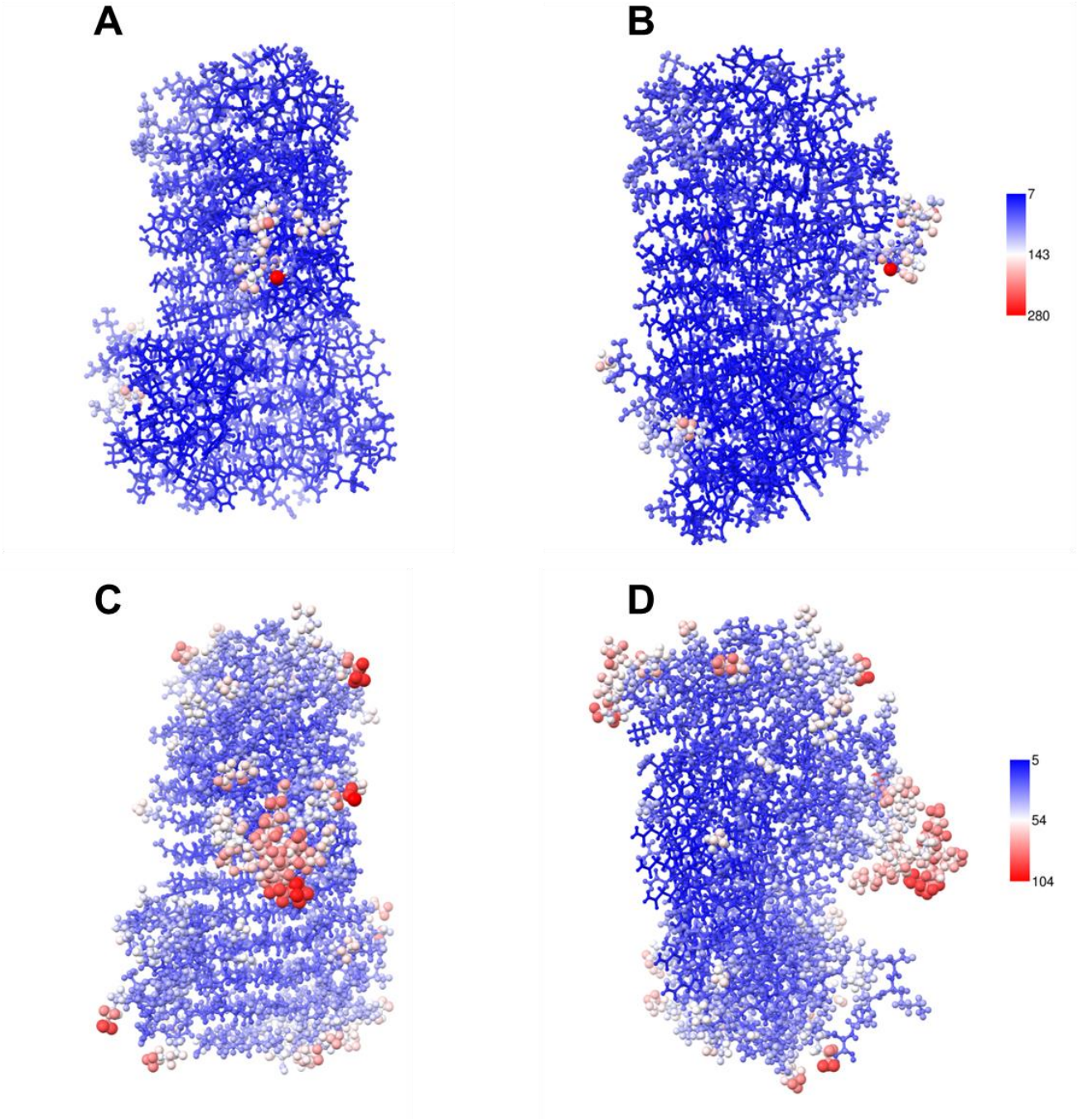

Figure S6. PGLR and ADPG2 B-factors
A) and B) Ball and stick representations of PGLR B-factors. PGLR. C) and D) ball and stick representations of ADPG2 B-factors.

Table S1. Data collection, processing and refinement for PGLR and ADPG2

Characteristics	PGLR	ADPG2
Data collection		
Diffraction source	PROXIMA1A	PROXIMA1A
Wavelength (Å)	0.978	0. 978
Temperature (°C)	100.15	100.15
Detector	PILATUS3 6M	EIGER X 16M
Crystal-to-detector distance (mm)	190.0	279.3
Rotation range per image (°)	0.1	0.1
Total rotation range (°)	360	360
Crystal data		
Space group	P1	P 21 21 21
a, b, c (Å)	38.97, 41.83, 63.33	71.78, 88.56, 113.87
α, β, γ, (°)	93.25, 99.86, 114.95	90.00, 90.00, 90.00
Subunits per asymmetric unit	1	2
Data statistics		
Resolution range (Å)	34.50 - 1.30	47.90 - 2.03
Total No. of reflection	761833	94647
No. of unique reflection	83670	47350
No. of reflections, test set	4184	2368
R_{merge} (%)	7.6 (77.7)	2.1 (32.3)
Completeness (%)	96.2 (92.1)	99.9 (99.3)
($I/\sigma(I)$)	16.2 (2.8)	16.9 (1.9)
Multiplicity	9.1(6.9)	2 (2)
$CC_{1/2}$ (%)	99 (86.4)	1 (89.3)
Refinement		
R_{crys} /R_{free} (%)	14. 2/17.7	18.8/23.0
Average B-factor (Å^2)	29.0	20.26
No. of non-H atoms		
Protein	3085	5563
Ion	-	5
Ligand	100	-
Water	609	999
Total	3794	6567
R.m.s. deviations		
Bonds (Å)	0.012	0.006
Angles (°)	1.531	0.899
Ramachandran plot		
Most favoured (%)	94.6	93.58
Allowed (%)	5.4	6.28
Outlier (%)	-	0.14

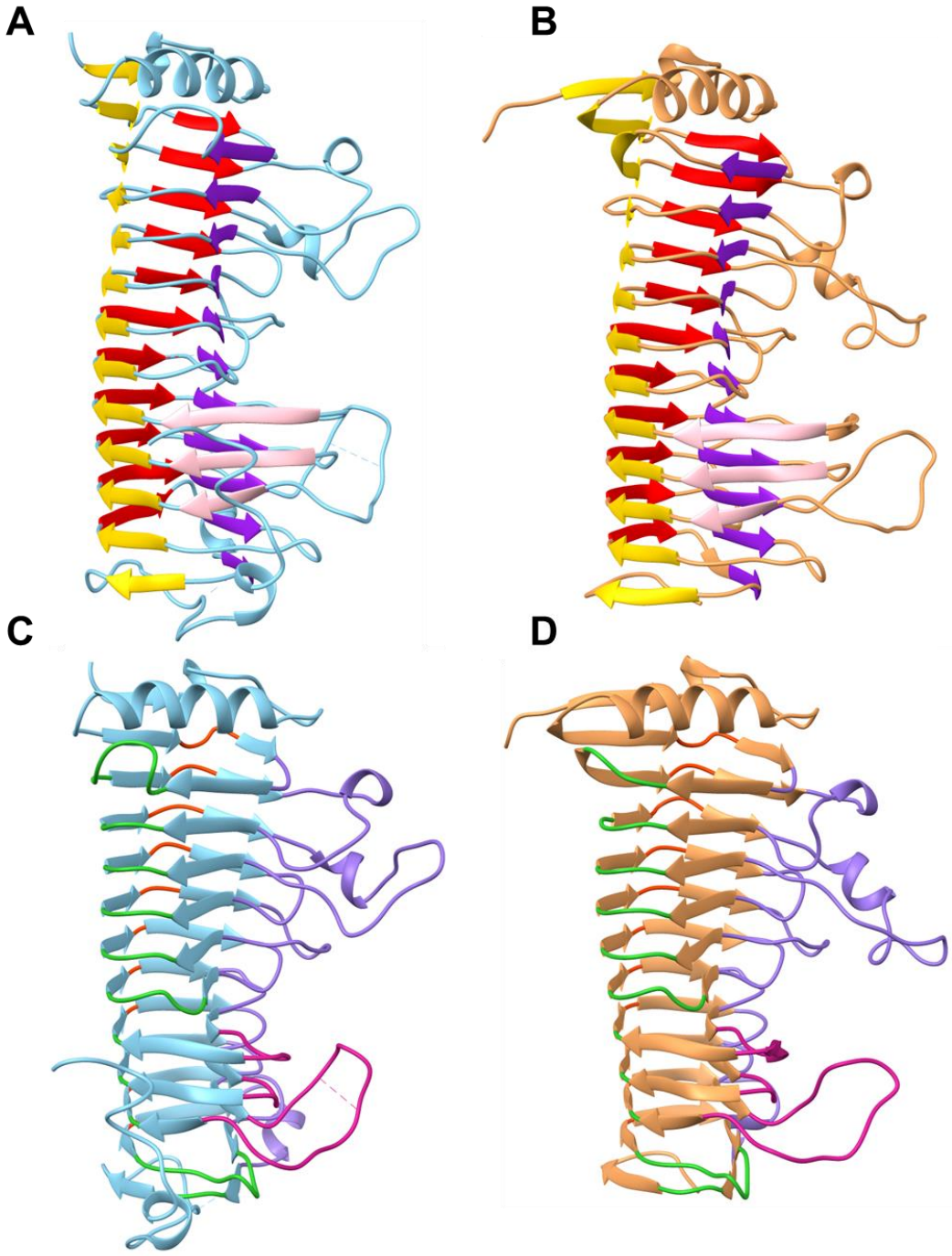

Figure S7. β-sheets and T-turns structures of PGLR and ADPG2
A) Ribbon structure representing β-sheets (PB1-purple, PB2a-pink, PB2b-yellow and PB3-red) for PGLR. B) Ribbon structure representing β-sheets (PB1-purple, PB2a-pink, PB2b-yellow and PB3-red) for ADPG2. C) Ribbon structure representing T-turns for PGLR (T1-lime green, T1a-violet red, T2- orange red, T3 medium purple). D) Ribbon structure representing T-turns for ADPG2 (T1-

lime green, T1a-violet red, T2- orange red, T3 medium purple). β-strands and T-turns are named accordingly to Petersen et al. 1997

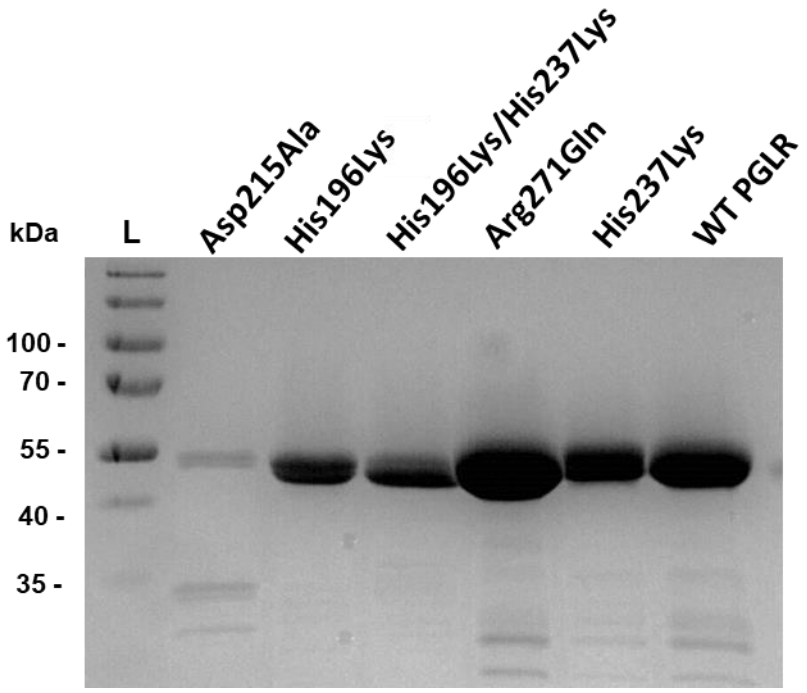

Figure S8. SDS-PAGE of native and mutated purified forms of PGLR
SDS-PAGE analysis of purified native and mutated forms of PGLR. Asp215Ala 0.58 µg, His196Lys 1.09 µg His196Lys/His237Lys 1.63 µg, Arg271Gln 4.51 µg, His237Lys 1.28 µg and WT PGLR 2.66 µg of proteins were resolved on a 12% polyacrylamide gel and were stained by Coomassie blue.

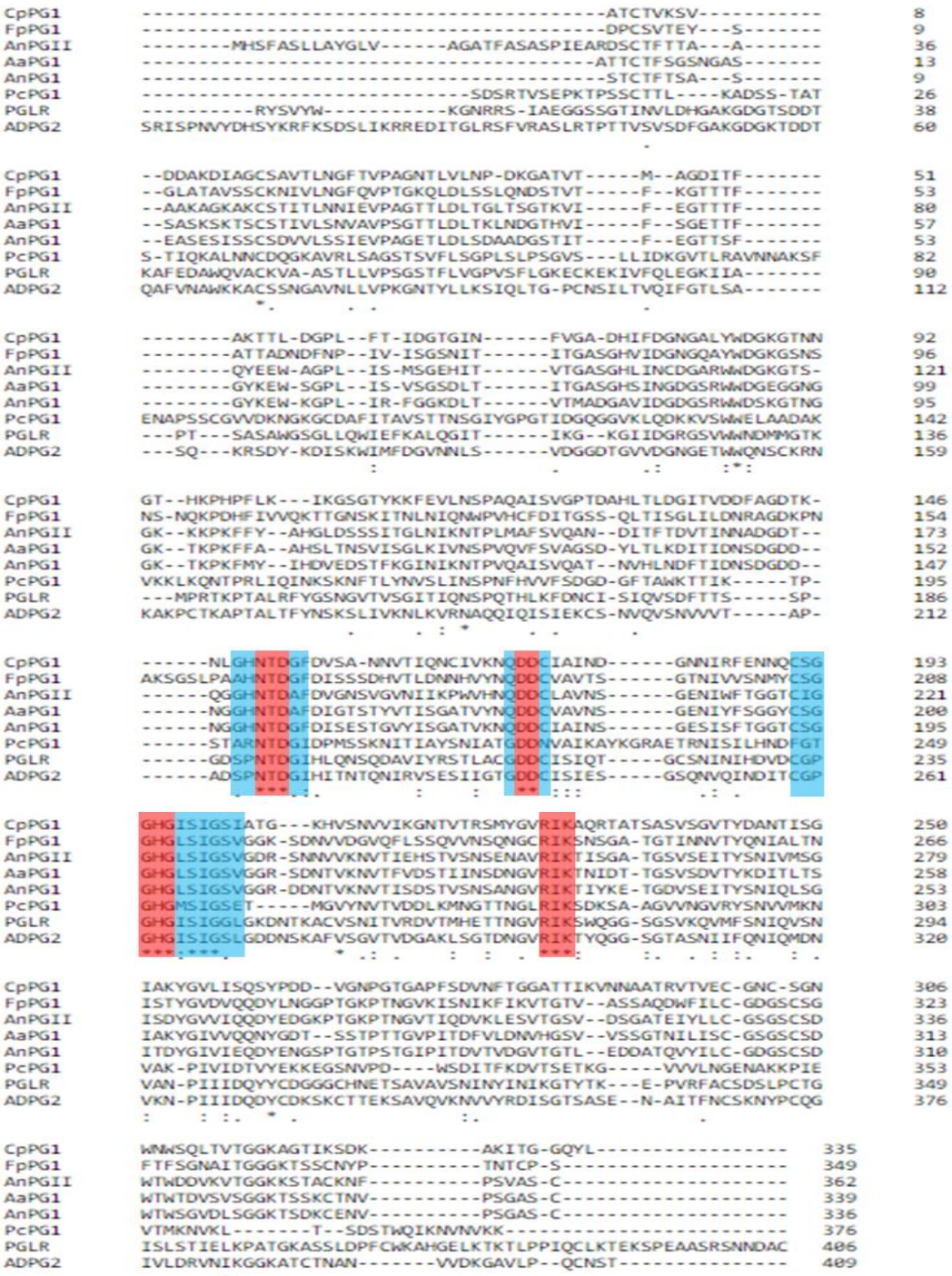

Figure S9. Sequence alignment of PGLR and ADPG2 with characterized and crystalized fungal PGs

Selected PGs; *Pectobacterium carotovorum* PG1 (PcPG1, PDB: 1BHE), *Aspergillus niger* PGI (AnPGI, PDB: 1NHC) and PGII (AnPGII PDB: 1CZF), *Fusarium phyllophilum* PG1 (FpPG1, 1HG8), Aspergillus aculeatus (AaPG1, PDB: 1IB4) and *Chondrostereum purpureum* (CpPG1, DB: 1KCD). The AA of the active are red-boxed while and the conserved AA are blue-boxed; The alignment was performed using ClustalW.

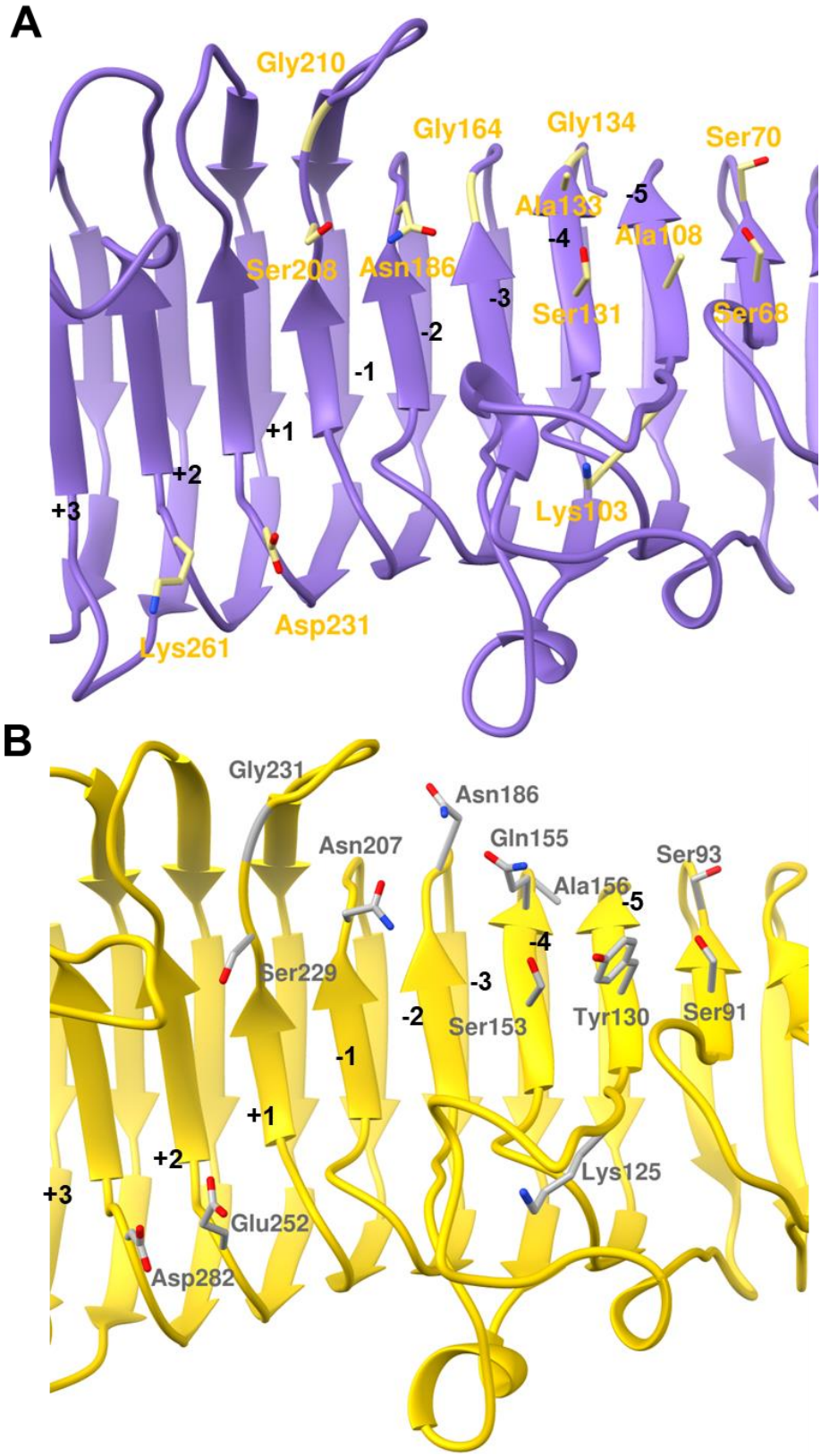
A
Gly210
Gly164
Gly134
Ser70
Ala133
-5
-4
Ala108
Ser208
Asn186
-3
Ser131
Ser68
-2
-1
+1
+2
+3
Lys103
Asp231
Lys261
B
Gly231
Asn186
Asn207
Gln155
Ser93
Ala156
-5
-4
Ser229
-3
-2
Ser153
Tyr130
Ser91
-1
+1
+2
Lys125
+3
Glu252
Asp282

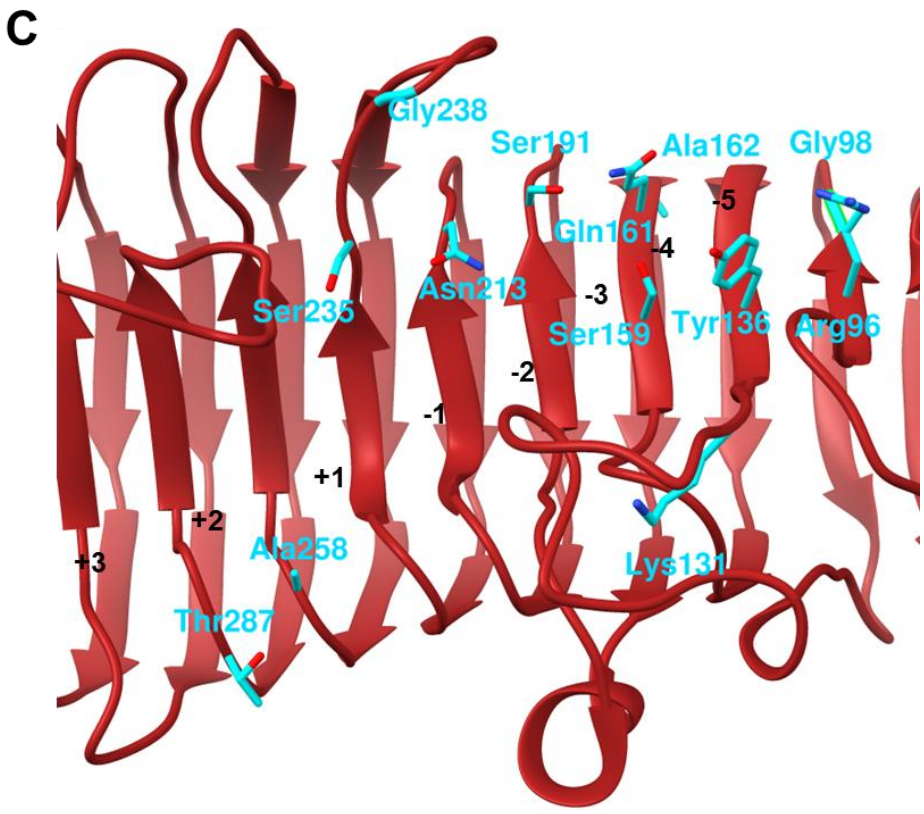

Figure S10.Structure of AaPG1, AnPG1 and AnPGII subsites
A) Structure of the -5/+3 subsites of AaPG1 (purple with khaki labelled AA). B) Structure of the -5/+3 subsites of AnPGII (yellow with grey labelled AA).C) Structure of the -5/+3 subsites of AnPGI (red with cyan labelled AA). AA important for determining substrate specificity are indicated. Black numbers indicate the subsites.

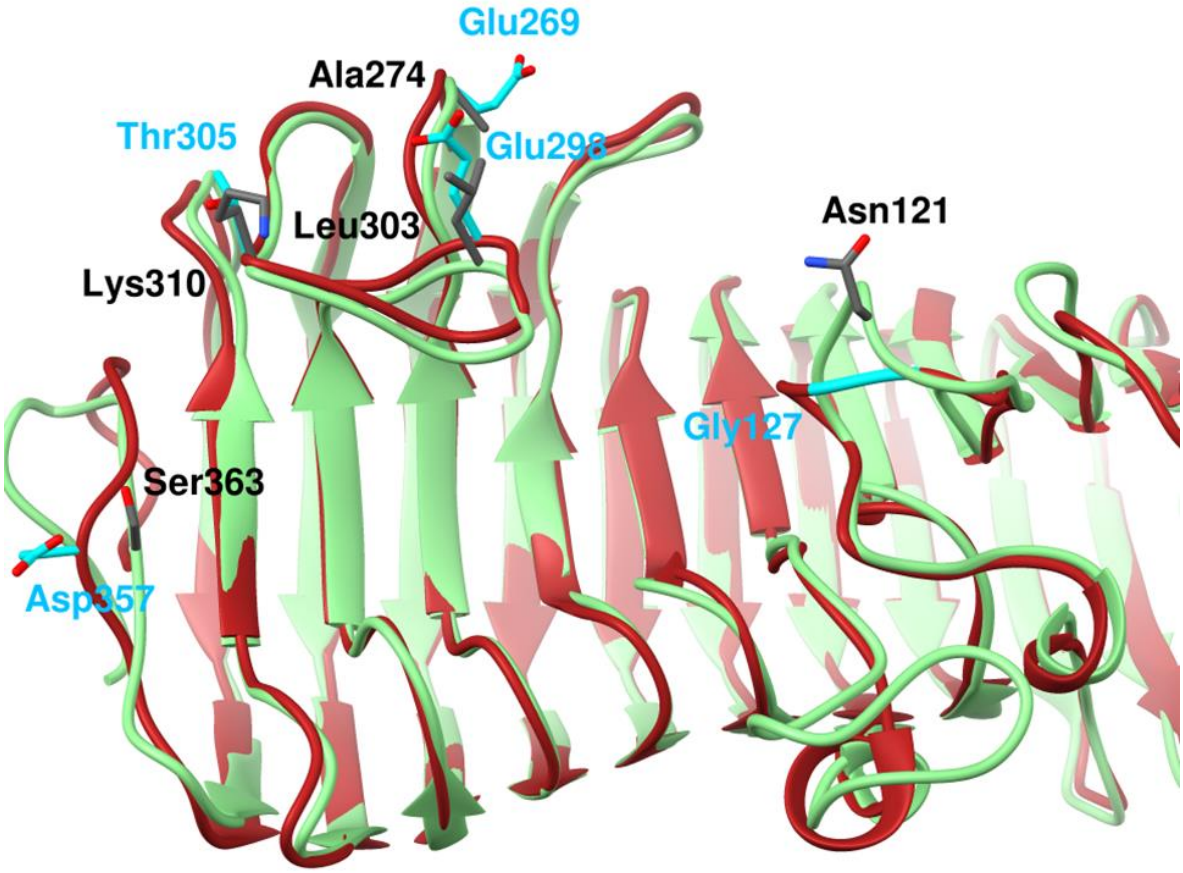

Figure S11. Structural determinants for the non-competitive inhibition of AnPG1 by PvPGIP
AnPGI structure (red with cyan-labelled AA) was superimposed to the structure of GfPG1 (green with black-labelled AA). The amino-acids (Asn121, Ala274, Leu303, Lys310 and Ser363) known to be of importance for the interaction between GfPG1 and PvPGIP2 (not shown here) are absent in AnPG1.

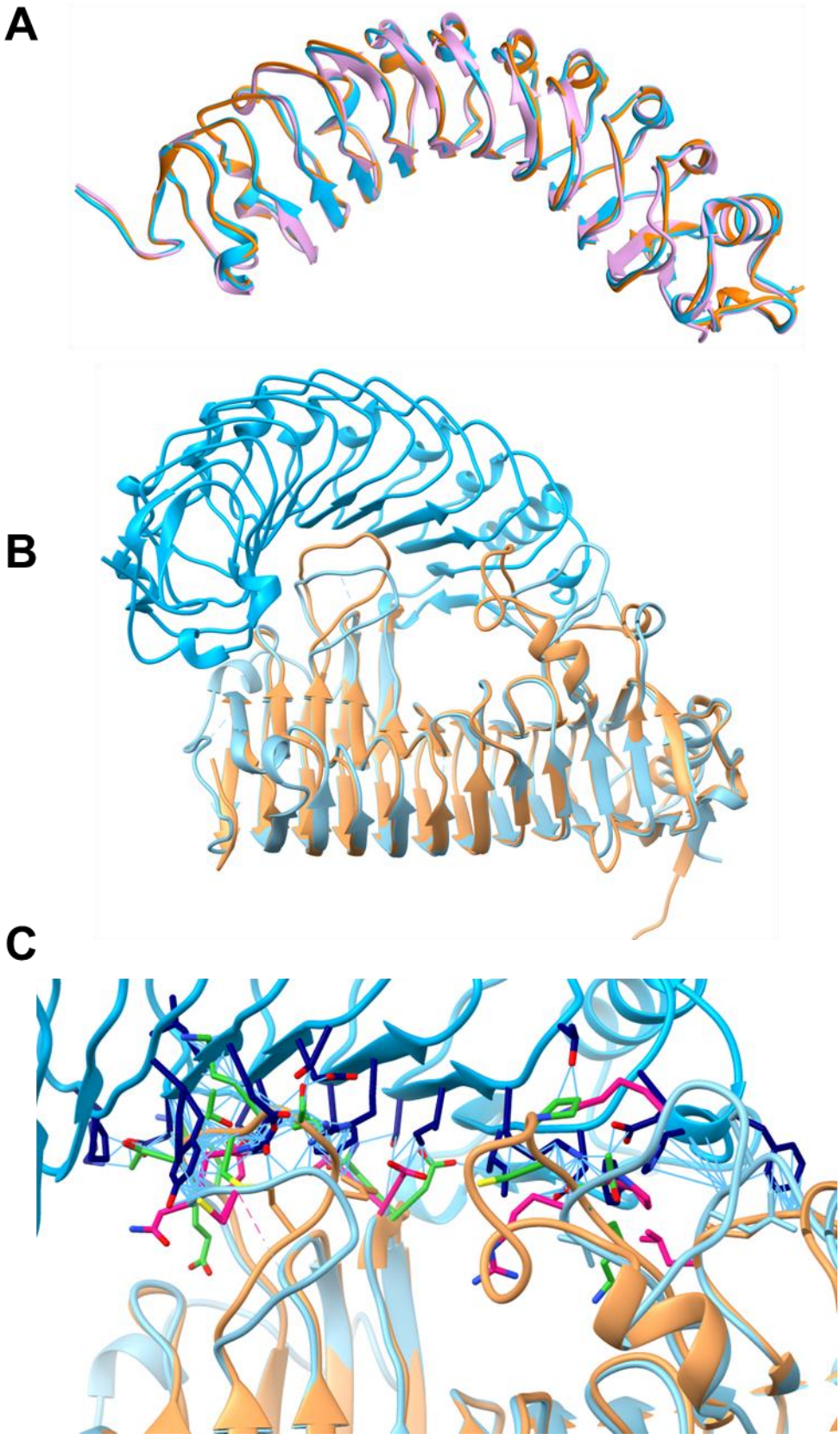
A
B
C

Figure S12. Structural determinant of the absence of interaction between AtPGIP2 and PGLR or ADPG2

A) Superimposition of AtPGIP1 (orange) and AtPGIP2 (dark blue) to PvPGIP2 (plum). B) Ribbon representation of AtPGIP2 (dark blue) in interaction with PGLR (blue) and ADPG2 (brown). C) Interaction of AtPGIP2 with PGLR and ADPG2. The structure of AtPGIP2 was modelled onto PvPGIP and AA included in clashes closer than 0.6 Å are shown as blues lines. Amino acids of AtPGIP2 (dark blue), PGLR (pink) and ADPG2 (green) are shown.

Table S2. Primers for cloning PGLR, ADPG2 and mutated forms of PGLR into pPICz*α*B expression vectors.

Table with primers used for the cloning of coding sequences into pPICzαB. Restriction enzymes sites for *Eco*RI, *Not*I are underlined, added bases are written in *italics*. Mutation bases are bolded.

Enzyme	Gene ID	Forward 5'- 3'	Reverse 3'- 5'
ADPG2	At2g41850	*TCTAA*GAATTC*A*CTCAAGAATCAGCCCTAATGTATATGACCA	*TGCAC*GCGGCCGC*A*AGTGGAGTTGCACTGAGGCA
PGLR D215A	At5g14650-D215A	GTTTGGATGGAAATGCA**AGC**GTCACCACAAGCC	GGCTTGTGGTGAC**GCT**TGCATTTCCATCCAAAC
PGLR H196K	At5g14650-H196K*	CCTGGGAGTTTTGCAA**CCT**AATACCGTCAGTG	CACTGACGGTATT**AAG**TTGCAAAACTCCCAGG
PGLR H237K	At5g14650-H237K*	CCAATGGAAATACC**CCT**ACCTGGACCACAATC	GATTGTGGTCCAGGT**AAG**GGTATTTCCATTGG
PGLR R271Q	At5g14650-R271Q	CTTGCCAAGACTTGAT**CTG**GACACCGTTTGTAG	CTACAAACGGTGTC**CAG**ATCAAGTCTTGGCAAG

* At5g14650 H196K-H237K single and double mutants were made using these primers.

1.8.Literature

Abbott DW, Boraston AB (2007) The Structural Basis for Exopolygalacturonase Activity in a Family 28 Glycoside Hydrolase. J Mol Biol **368**: 1215–1222

André-Leroux G, Tessier D, Bonnin E (2009) Endopolygalacturonases reveal molecular features for processivity pattern and tolerance towards acetylated pectin. Biochim Biophys Acta - Proteins Proteomics **1794**: 5–13

André-Leroux G, Tessier D, Bonnin E (2005) Action pattern of Fusarium moniliforme endopolygalacturonase towards pectin fragments: Comprehension and prediction. Biochim Biophys Acta - Proteins Proteomics **1749**: 53–64

Benedetti M, Andreani F, Leggio C, Galantini L, Di Matteo A, Pavel NV, De Lorenzo G, Cervone F, Federici L, Sicilia F (2013) A single amino-acid substitution allows endo-polygalacturonase of Fusarium verticillioides to acquire recognition by PGIP2 from Phaseolus vulgaris. PLoS One **8**: 1–11

Benedetti M, Leggio C, Federici L, de Lorenzo G, Pavel NV, Cervone F (2011) Structural resolution of the complex between a fungal polygalacturonase and a plant polygalacturonase-inhibiting protein by small-angle x-ray scattering. Plant Physiol **157**: 599–607

Benen JAE, Kester HCM, Visser J (1999) Kinetic characterization of Aspergillus niger N400 endopolygalacturonases I, II and C. Eur J Biochem **259**: 577–585

Bidhendi AJ, Geitmann A (2016) Relating the mechanics of the primary plant cell wall to morphogenesis. J Exp Bot **67**: 449–461

Bonnin E, Le Goff A, Körner R, Vigouroux J, Roepstorff P, Thibault JF (2002) Hydrolysis of pectins with different degrees and patterns of methylation by the endopolygalacturonase of Fusarium moniliforme. Biochim Biophys Acta - Protein Struct Mol Enzymol **1596**: 83–94

Bradford MM (1976) A rapid and sensitive method for the quantitation of microgram quantities of protein utilizing the principle of protein-dye binding. Anal Biochem **72**: 248–254

Breyer WA, Matthews BW (2001) A structural basis for processivity. Protein Sci **10**: 1699–1711

Cervone F, De Lorenzo G, Pressey R, Darvill AG, Albersheim P (1990) Can Phaseolus PGIP inhibit pectic enzymes from microbes and plants? Phytochemistry **29**: 447–449

Cho SW, Lee S, Shin W (2001) The X-ray structure of Aspergillus aculeatus Polygalacturonase and a Modeled structure of the Polygalacturonase-Octagalacturonate Complex. J Mol Biol **311**: 863–878

Davidsson P, Broberg M, Kariola T, Sipari N, Pirhonen M, Palva ET (2017) Short oligogalacturonides induce pathogen resistance-associated gene expression in Arabidopsis thaliana. BMC Plant Biol **17**: 1–17

Emsley P, Lohkamp B, Scott WG, Cowtan K (2010) Features and development of Coot. Acta Crystallogr Sect D Biol Crystallogr **66**: 486–501

Federici L, Caprari C, Mattei B, Savino C, Di Matteo A, De Lorenzo G, Cervone F, Tsernoglou D (2001) Structural requirements of endopolygalacturonase for the interaction with PGIP (polygalacturonase-inhibiting protein). Proc Natl Acad Sci U S A **98**: 13425–13430

Ferrari S, Savatin D V, Sicilia F, Gramegna G, Cervone F, Lorenzo G de (2013) Oligogalacturonides: plant damage-associated molecular patterns and regulators of growth and development. Front Plant Sci **4**: 1–9

Ferrari S, Vairo D, Ausubel FM, Cervone F, De Lorenzo G (2003) Tandemly duplicated Arabidopsis genes that encode polygalacturonase-inhibiting proteins are regulated coordinately by different signal transduction pathways in response to fungal infection. Plant Cell **15**: 93–106

Gou JY, Miller LM, Hou G, Yu XH, Chen XY, Liu CJ (2012) Acetylesterase-mediated deacetylation of pectin impairs cell elongation, pollen germination, and plant reproduction. Plant Cell **24**: 50–65

Hewezi T, Howe P, Maier TR, Hussey RS, Mitchum MG, Davis EL, Baum TJ (2008) Cellulose binding protein from the parasitic nematode heterodera Schachtii interacts with arabidopsis pectin methylesterase: Cooperative cell wall modification during parasitism. Plant Cell **20**: 3080–3093

Hocq L, Guinand S, Habrylo O, Voxeur A, Tabi W, Safran J, Fournet F, Domon J-M, Mollet J-C, Pilard S, et al (2020) The exogenous application of AtPGLR, an endo - polygalacturonase, triggers pollen tube burst and repair. Plant J **103**: 617–633

Kabsch W (2010a) Integration, scaling, space-group assignment and post-refinement. Acta Crystallogr Sect D Biol Crystallogr **66**: 133–144

Kabsch W (2010b) Xds. Acta Crystallogr D Biol Crystallogr **66**: 125–32

Kalunke RM, Tundo S, Benedetti M, Cervone F, De Lorenzo G, D'Ovidio R (2015) An update on polygalacturonase-inhibiting protein (PGIP), aleucine-rich repeat protein that protects crop plants against pathogens. Front Plant Sci **6**: 1–17

Kim T, Mullaney EJ, Porres JM, Roneker KR, Crowe S, Rice S, Ko T, Ullah AHJ, Daly CB, Welch R, et al (2006) Shifting the pH profile of Aspergillus niger PhyA phytase to match the stomach pH enhances its effectiveness as an animal feed additive. Appl Environ Microbiol **72**: 4397–4403

Kirsch R, Heckel DG, Pauchet Y (2016) How the rice weevil breaks down the pectin network: Enzymatic synergism and sub-functionalization. Insect Biochem Mol Biol **71**: 72–82

Leroux C, Bouton S, Kiefer-Meyer MC, Fabrice TN, Mareck A, Guénin S, Fournet F, Ringli C, Pelloux J, Driouich A, et al (2015) PECTIN METHYLESTERASE48 is involved in arabidopsis pollen grain germination. Plant Physiol **167**: 367–380

Liebschner D, Afonine P V., Baker ML, Bunkoczi G, Chen VB, Croll TI, Hintze B, Hung LW, Jain S, McCoy AJ, et al (2019) Macromolecular structure determination using X-rays, neutrons and electrons: Recent developments in Phenix. Acta Crystallogr Sect D Struct Biol **75**: 861–877

Lietzke SE, Scavetta RD, Yoder MD, Jurnak F (1996) The Refined Three-Dimensional Structure of Pectate Lyase E from Erwinia chrysanthemi at 2.2 A Resolution. Plant Physiol **111**: 73–92

Ma F, Xie Y, Luo M, Wang S, Hu Y, Liu Y, Feng Y, Yang GY (2016) Sequence homolog-based molecular engineering for shifting the enzymatic pH optimum. Synth Syst Biotechnol **1**: 195–206

Mariotti L, Casasoli M, Caprari C, De Lorenzo G (2009) A divergent polygalacturonase of Fusarium phyllophilum shows sequence and functional similarity to the enzyme of F. Verticillioides. J Plant Pathol **91**: 129–139

Markovič O, Janeček Š (2001) Pectin degrading glycoside hydrolases of family 28: sequence-structural features, specificities and evolution. Protein Eng Des Sel **14**: 615–631

Di Matteo A, Bonivento D, Tsernoglou D, Federici L, Cervone F (2006) Polygalacturonase-inhibiting protein (PGIP) in plant defence: A structural view. Phytochemistry **67**: 528–533

McCoy AJ, Grosse-Kunstleve RW, Adams PD, Winn MD, Storoni LC, Read RJ (2007) Phaser crystallographic software. J Appl Crystallogr **40**: 658–674

Miller GL (1959) Use of Dinitrosalicylic Acid Reagent for Determination of Reducing Sugar. Anal Chem **31**: 426–428

Mohnen D (2008) Pectin structure and biosynthesis. Curr Opin Plant Biol **11**: 266–277

Ogawa M, Kay P, Wilson S, Swain SM (2009) Arabidopsis Dehiscence Zone Polygalacturonase1 (ADPG1), ADPG2, and Quartet2 are polygalacturonases required for cell separation during reproductive development in Arabidopsis. Plant Cell **21**: 216–233

Pagès S, Heijne WHM, Kester HCM, Visser J, Benen JAE (2000) Subsite mapping of Aspergillus niger endopolygalacturonase II by site-directed mutagenesis. J Biol Chem **275**: 29348–29353

Park K-C, Kwon S-J, Kim P-H, Bureau T, Kim N-S (2008) Gene structure dynamics and divergence of the polygalacturonase gene family of plants and fungus. Genome **51**: 30–40

Peaucelle A, Louvet R, Johansen JN, Höfte H, Laufs P, Pelloux J, Mouille G (2008) Arabidopsis Phyllotaxis Is Controlled by the Methyl-Esterification Status of Cell-Wall Pectins. Curr Biol **18**: 1943–1948

Pelletier S, Van Orden J, Wolf S, Vissenberg K, Delacourt J, Ndong YA, Pelloux J, Bischoff V, Urbain A, Mouille G, et al (2010) A role for pectin de-methylesterification in a developmentally regulated growth acceleration in dark-grown Arabidopsis hypocotyls. New Phytol **188**: 726–739

Petersen TN, Kauppinen S, Larsen S (1997) The crystal structure of rhamnogalacturonase a from Aspergillus aculeatus: A right-handed parallel β helix. Structure **5**: 533–544

Pickersgill R, Smith D, Worboys K, Jenkins J (1998) Crystal Structure of Polygalacturonase from Erwinia carotovora ssp. carotovora. J Biol Chem **273**: 24660–24664

Pijning T, van Pouderoyen G, Kluskens L, van der Oost J, Dijkstra BW (2009) The crystal

structure of a hyperthermoactive exopolygalacturonase from Thermotoga maritima reveals a unique tetramer. FEBS Lett **583**: 3665–3670

Van Pouderoyen G, Snijder HJ, Benen JAE, Dijkstra BW (2003) Structural insights into the processivity of endopolygalacturonase I from Aspergillus niger. FEBS Lett **554**: 462–466

Raiola A, Lionetti V, Elmaghraby I, Immerzeel P, Mellerowicz EJ, Salvi G, Cervone F, Bellincampi D (2011) Pectin methylesterase is induced in Arabidopsis upon infection and is necessary for a successful colonization by necrotrophic pathogens. Mol Plant-Microbe Interact **24**: 432–440

Raiola A, Sella L, Castiglioni C, Balmas V, Favaron F (2008) A single amino acid substitution in highly similar endo-PGs from Fusarium verticillioides and related Fusarium species affects PGIP inhibition. Fungal Genet Biol **45**: 776–789

Rhee SY, Osborne E, Poindexter PD, Somerville CR (2003) Microspore Separation in the quartet 3 Mutants of Arabidopsis Is Impaired by a Defect in a Developmentally Regulated Polygalacturonase Required for Pollen Mother Cell Wall Degradation. Plant Physiol **133**: 1170–1180

Rui Y, Xiao C, Yi H, Kandemir B, Wang JZ, Puri VM, Anderson CT (2017) POLYGALACTURONASE INVOLVED IN EXPANSION3 functions in seedling development, rosette growth, and stomatal dynamics in Arabidopsis thaliana. Plant Cell **29**: 2413–2432

Safran J, Habrylo O, Cherkaoui M, Lecomte S, Voxeur A, Pilard S, Bassard S, Pau-Roblot C, Mercadante D, Pelloux J, et al (2021) New insights into the specificity and processivity of two novel pectinases from Verticillium dahliae. Int J Biol Macromol **176**: 165–176

van Santen Y, Benen JAE, Schroter KH, Kalk KH, Armand S, Visser J, Dijkstra BW (1999) 1.68-angstrom crystal structure of endopolygalacturonase II from Aspergillus niger and identification of active site residues by site-directed mutagenesis. J Biol Chem **274**: 30474–30480

Savatin D V., Ferrari S, Sicilia F, de Lorenzo G (2011) Oligogalacturonide-auxin antagonism does not require posttranscriptional gene silencing or stabilization of auxin response repressors in Arabidopsis. Plant Physiol **157**: 1163–1174

Sella L, Castiglioni C, Roberti S, D'Ovidio R, Favaron F (2004) An endo-polygalacturonase (PG) of Fusarium moniliforme escaping inhibition by plant polygalacturonase-inhibiting proteins (PGIPs) provides new insights into the PG-PGIP interaction. FEMS Microbiol Lett **240**: 117–124

Sénéchal F, Habrylo O, Hocq L, Domon JM, Marcelo P, Lefebvre V, Pelloux J, Mercadante D (2017) Structural and dynamical characterization of the pH-dependence of the pectin methylesterase-pectin methylesterase inhibitor complex. J Biol Chem **292**: 21538–21547

Shimizu T, Nakatsu T, Miyairi K, Okuno T, Kato H (2002) Active-site architecture of endopolygalacturonase I from Stereum purpureum revealed by crystal structures in native and ligand-bound forms at atomic resolution. Biochemistry **41**: 6651–6659

de Souza A, Hull PA, Gille S, Pauly M (2014) Identification and functional characterization of

the distinct plant pectin esterases PAE8 and PAE9 and their deletion mutants. Planta **240**: 1123–1138

Stranne M, Ren Y, Fimognari L, Birdseye D, Yan J, Bardor M, Mollet JC, Komatsu T, Kikuchi J, Scheller H V., et al (2018) TBL10 is required for O-acetylation of pectic rhamnogalacturonan-I in Arabidopsis thaliana. Plant J **96**: 772–785

Tu T, Meng K, Luo H, Turunen O, Zhang L, Cheng Y, Su X, Ma R, Shi P, Wang Y, et al (2015) New insights into the role of T3 loop in determining catalytic efficiency of GH28 endo-polygalacturonases. PLoS One **10**: 1–16

Villar K Del, Mitsuzawa H, Yang W, Sattler I, Tamanoi F (1997) Amino acid substitutions that convert the protein substrate specificity of farnesyltransferase to that of geranylgeranyltransferase type I. J Biol Chem **272**: 680–687

Vitali J, Schick B, Kester HCM, Visser J, Jurnak F (1998) The Three-Dimensional Structure of Aspergillus niger Pectin Lyase B at 1.7-Å Resolution. Plant Physiol **116**: 69–80

Voxeur A, Habrylo O, Guénin S, Miart F, Soulié MC, Rihouey C, Pau-Roblot C, Domon JM, Gutierrez L, Pelloux J, et al (2019) Oligogalacturonide production upon Arabidopsis thaliana-Botrytis cinerea interaction. Proc Natl Acad Sci U S A **116**: 19743–19752

Willats WGT, McCartney L, Mackie W, Knox JP (2001) Pectin: cell biology and prospects for functional analysis. Plant Mol Biol **47**: 9–27

Xiao C, Barnes WJ, Zamil MS, Yi H, Puri VM, Anderson CT (2017) Activation tagging of Arabidopsis POLYGALACTURONASE INVOLVED IN EXPANSION2 promotes hypocotyl elongation, leaf expansion, stem lignification, mechanical stiffening, and lodging. Plant J **89**: 1159–1173

Xiao C, Somerville C, Anderson CT (2014) POLYGALACTURONASE INVOLVED IN EXPANSION1 functions in cell elongation and flower development in Arabidopsis. Plant Cell **26**: 1018–1035

Yoder MD, Jurnak F (1995) The Refined Three-Dimensional Structure of Pectate Lyase C lmplications for an Enzymatic Mechanism. Plant Physiol **107**: 349–364

2. Chapter – New insights into the specificity and processivity of two novel pectinases from *Verticillium dahliae*

As highlighted in the first chapter, plant PG structurally differ from that of fungal pathogens. To determine the biochemical differences between plant and fungal enzymes, we characterized pectinases from *V. dahliae*, a soilborne pathogen, that can infect more than 300 different plant species, and which is becoming prevalent among fiber flax (Klosterman et al., 2009; Blum et al., 2018). During infection *V. dahliae* secretes PMEs, PGs and PLLs, and while these enzymes have been reported to play a role in determining pathogenicity, their biochemical characteristics are not known. In this chapter we are focusing on one PME (VdPME1) and one PG (VdPG2) from *V. dahliae* to further determine the potential sequential action of these enzymes. In addition to elucidating their biochemical specificities, we used LC-MS/MS profiling of digestions products on commercially available pectins and flax root pectins to determine their mode of action. For VdPME1, we linked proteins surface charge to its processivity.

This chapter is presented as a manuscript that was published in *International Journal of Biological Macromolecules* 176 (2021) 165–176.

Additional data are reported in **Annex 7** to **Annex 9**.

Authors list

Josip Safran[a], Olivier Habrylo[a], Mehdi Cherkaoui[a], Sylvain Lecomte[b], Aline Voxeur[c], Serge Pilard[d], Solène Bassard[a], Corinne Pau-Roblot[a], Davide Mercadante[e], Jérôme Pelloux[a], Fabien Sénéchal[a,*]

[a]: UMRT INRAE 1158 BioEcoAgro – BIOPI Biologie des Plantes et Innovation, SFR Condorcet FR CNRS 3417, Université de Picardie, 33 Rue St Leu, 80039 Amiens, France. [b]: Linéa Semences, 20 Avenue Saget, 60210 Grandvilliers, France. [c]: Institut Jean-Pierre Bourgin, INRAE, AgroParisTech, Université Paris-Saclay, 78000 Versailles, France. [d]: Plateforme Analytique, Université de Picardie, 33 Rue St Leu, 80039 Amiens, France. [e]: School of Chemical Sciences, The University of Auckland, Private Bag 92019, Auckland 1142, New Zealand.

Corresponding author: Fabien Sénéchal (fabien.senechal@u-picardie.fr)

2.1. Abstract

Pectin, the major non-cellulosic component of primary cell wall can be degraded by polygalacturonases (PGs) and pectin methylesterases (PMEs) during pathogen attack on plants. We characterized two novel enzymes, VdPG2 and VdPME1, from the fungal plant pathogen *Verticillium dahliae*. VdPME1 was most active on citrus methylesterified pectin (55-70%) at pH 6 and a temperature of 40°C, while VdPG2 was most active on polygalacturonic acid at pH 5 and a temperature of 50°C. Using LC-MS/MS oligoprofiling, and various pectins, the mode of action of VdPME1 and VdPG2 were determined. VdPME1 was shown to be processive, in accordance with the electrostatic potential of the enzyme. VdPG2 was identified as endo-PG releasing both methylesterified and non-methylesterified oligogalacturonides (OGs). Additionally, when flax roots were used as substrate, acetylated OGs were detected. The comparisons of OGs released from *Verticillium*-susceptible and partially resistant flax cultivars identified new possible elicitor of plant defence responses.

Keywords: Pectin**,** polygalacturonase, pectin methylesterase, flax, oligogalacturonides, *Verticillium dahliae*

2.2. Introduction

The plant cell wall is a complex and dynamic structure of proteins and polysaccharides, consisting of a hydrogen-bonded network of cellulose microfibrils and hemicelluloses embedded in a matrix of pectins (Carpita and Gibeaut, 1993). Pectins are the most complex combination of plant cell wall polysaccharides and are found in the middle lamella and primary cell walls of dicotyledonous plants, where they can contribute up to 30% of dry cell mass (Ridley et al., 2001). The composition of pectin differs depending on plant species and organs, but generally consist mainly of homogalacturonan (HG), rhamnogalacturonan I (RG-I) and rhamnogalacturonan II (RG-II) domains. HG, which is a linear homopolymer of α-1,4-linked galacturonic acids (GalA), is the most abundant pectic domain representing up to 65% of pectin (Mohnen, 2008). HG can be methylesterified at the C-6 carboxyl and can be O-acetylated at O-2 or O-3. HG chains can be modified by different enzyme families, including pectin acetylesterase (PAEs; EC 3.1.1.6), pectin methylesterases (PMEs; CE8, EC 3.1.1.11), polygalacturonases (PGs; GH28, EC 3.2.1.15, EC 3.2.1.67, EC 3.2.1.82), pectate lyases (PLs; EC 4.2.2.2) and pectin lyase (PNLs, EC 4.2.2.10). While these enzymes are endogenously produced by plants to fine-tune pectin structure during development, they are also secreted by some bacteria, fungi, insects and nematodes during plant infestation (Jayani et al., 2005; Lionetti et al., 2017; Habrylo et al., 2018; Yang et al., 2018; Vicente et al., 2019). PMEs act on methylesterified GalA chain where they hydrolyse the O6-ester linkage between methyl group and GalA. PAE play similar role by hydrolysing the O2-acetylated linkage. Demethylesterification makes HG more susceptible to degradation by pectin-degrading enzymes such as PLs, PNLs and PGs (Limberg et al., 2000). PMEs may differ with respect to their pH optimum, substrate specificity and salt requirements, and have an optimum activity between pH 4-6 for fungal PMEs and pH 6-8 for plant PMEs (Kars et al., 2005b). It has been shown that plant and bacterial PMEs remove long stretches of methyl groups in a processive manner before dissociating from the HG chain, whereas fungal enzymes act more randomly and are considered as non-processive PMEs (Cameron et al., 2003). PGs are a family of hydrolases that cut the HG chain releasing oligogalacturonides (OGs) of different degree of polymerisation (DP) and methylesterification/acetylation. Depending on their mode of action, PGs are subdivided into endo-PGs (EC 3.2.1.15), which randomly hydrolyse internal sites and exo- PGs (EC 3.2.1.67, EC 3.2.1.82) that hydrolyse HG from non-reducing end, creating monomers or dimers of GalA. These two types of PGs preferably act on partially demethylesterified HG chains and have been identified

in various fungal species where they can be a determinant of the pathogenicity (Niture, 2008). Indeed, various fungi secrete pectinases, including PGs, to degrade plant cell walls and invade cells. For instance, it has been shown that Botrytis PG1 and Verticillium PG1 are important virulence factors in tomato and cotton, respectively (Ten Have et al., 1998; Liu et al., 2017). *Verticillium dahlia*e Kleb. soil-borne vascular fungus, which attack a broad range plants and has increasing effects on flax species, also produces a number of pectinases for degrading cell wall. Infection of *V.dahliae* occurs at the root surface levels, later invading xylem vessels with progression in acropetal direction (Fradin and Thomma, 2006; Blum et al., 2018). To date, without effective chemical control, there is no flax cultivar totally resistant to Verticillium wilt (Blum et al., 2018), thus it appears of prime importance to understand the pathogenicity of this fungus by characterizing pectinases such as PGs and PMEs. Such a characterisation is indeed required to devise strategies useful to control or inhibit pathogenic activity and must occur on multiple levels: from the characterisation of the protein mechanism of action to the enzymatic structures and dynamics, which provide information on substrate specificity and processive tendencies of different PMEs and PGs. Considering the large number of protein isoforms and ubiquitous presence of PMEs and PGs across plants, bacterial and fungi, relating the functional behaviour and the structural features of PGs and PMEs is challenging. The lack of knowledge for these enzymes is aggravated by the relatively scarce number of resolved structures, compared to the whole number of PGs and PMEs isoforms. More recently the *in-silico* comparison of PMEs electrostatic potentials has underscored the relation between protein electrostatics and substrate specificity, highlighting the importance of balancing electrostatic vs. hydrophobic interactions within the binding groove of PMEs to promote fine-tuning of substrates specificity and different processivity profiles (Mercadante et al., 2014). Although the fold of PGs and PMEs is conserved, with a binding groove able to allocate approximately 10 saccharide units (Fries et al., 2007) in as many subsites, subtle differences exist between the chemical microenvironments of different subsites, which can either bind, with different affinities, negatively charged, carboxy-methylated or O-acetylated saccharide units. The structural and biochemical description of newly identified PGs and PMEs, with the combination of *in-vitro, ex-vivo* and *in-silico* methods, thus become powerful tools to characterize and contextualize the action of these enzymes within plant physiology and pathology.

The aims of this study are to characterize two novel enzymes from *V. dahliae*, VdPME1 (VDAG_05799) and VdPG2 (VDAG_04977) using biochemical and computational approaches.

In particular, their mode of action can be determined using a recently developed SEC-MS technique (Voxeur et al., 2019), which enables analysis of the OGs generated from commercial pectin as well from flax roots. Our hypothesis is that we can relate the structure of enzymes to their processivity and this can have impact on the OG produced during plant-pathogen interactions.

2.3. Material and Methods

2.3.1. Bioinformatical analysis

V. dahliae PGs and PMEs were identified using publicly available genome data (ftp.broadinstitute.org/). Sequences were checked for signal peptide using SignalP-5.0 Server (http://www.cbs.dtu.dk/services/SignalP/). Glycosylation sites were predicted using NetNGlyc 1.0 Server (http://www.cbs.dtu.dk/services/NetNGlyc/) and NetOGlyc 4.0 Server (http://www.cbs.dtu.dk/services/NetOGlyc/). The sequence alignments were performed using MEGA multiple sequence alignment program. UCSF Chimera (http://www.cgl.ucsf.edu/chimera/) was used for creation of graphics.

2.3.2. Modelling, calculations and comparison of protein electrostatic

VdPME1 and VdPG2 models were created using I-TASSER structure prediction software (https://zhanglab.ccmb.med.umich.edu/I-TASSER/). The linearized version of the Poisson-Boltzmann equation was used to solve the electrostatic potentials of the PMEs from *Verticillium dahliae*, *Dickeya chrysanthemi*, *Citrus sinensis* and *Daucus carota* after that radii and partial charges were assigned to each atom of the structures according to the parameters from the AMBER99 force field (Wang et al., 2000) by using PDB2PQR (version 2.1.1, Dolinsky et al., 2004).

The PMEs structures were superimposed to fairly compare the electrostatic potential differences across the calculated grids, and the electrostatic potentials were calculated using the APBS software version 3 (Baker et al., 2001). The potentials were computed at pH 7, which is the pH used for the activity tests of VdPME1, with protonation states of single residues assigned using the PROPKA software, version 3.3 (Søndergaard et al., 2011). Poisson-Boltzmann equation was solved by discretizing the molecule on a 19.3 nm^3 grid (grid spacing equal to $6x10^{-2}$ nm) centred on the C_α atom of one of the PMEs catalytic aspartic acid residues, conserved across PMEs. The computation of the electrostatic potential was carried out considering a dielectric term of 78.5 for

Table 6. Primers used for cloning *Verticillium dahliae* enzymes into pPICz*α*B expression vectors

VdPG2: Polygalacturonase; VdPME1: Pectin methylesterase. Restriction enzymes sites for *Eco*RI, *Pst*I, *Not*I are underlined, added bases are written in *italics*.

Enzyme	Gene ID	Forward 5'- 3'	Reverse 3'- 5'
VdPG2	20706440	*TCTAA*GAATTC*AC*AACCCTCT TCCCGCCAAG	*TGCAC*GCGGCCGCAGAGCAC GCGGCAGGG
VdPME1	20707262	*TCTAA*CTGCAG*GA*GCCACGAG GACCTCG	*TGCAC*GCGGCCGCCATGTACG AAGCGTCATAGTAG

the solvent, in order to account for an aqueous environment, with solute dielectric set to 4.0 and temperature set at 298.15 K. Electrostatic potentials were numerically compared by calculating electrostatic similarity indices (Blomberg et al., 1999; Wade et al., 2001). We calculated the cross-product between two electrostatic potentials calculated at each grid point as follows:

$$SI_{a,b}^{H} = \frac{2\phi_a(i,j,k)\phi_b(i,j,k)}{\left(\phi_a^2(i,j,k) + \phi_b^2(i,j,k)\right)}$$

Where $\phi_a^2(i,j,k)$ and $\phi_b^2(i,j,k)$ are the electrostatic potentials calculated at the grid points *i*,*j*,*k* for proteins *a* and *b* (Blomberg et al., 1999; Wade et al., 2001).

2.3.3. Fungal strain and growth

V.dahliae was isolated from CALIRA company flax test fields (Martainneville, France) and was kindly provided by Linéa-Semences company (Grandvilliers, France). Fungus was grown in flasks containing 50 mL M3 medium (Mitchell et al., 1997) enriched with different carbon source: polygalacturonic acid sodium salt (PGA, P3850, Sigma) and pectin esterified potassium salt from citrus fruit (55-70% methylesterified, P9436, Sigma) at 10 $g.L^{-1}$ in order to stimulate *PG* and *PME* expression and secretion. Flasks were kept 15 days in dark condition under 25°C, 80 rpm agitation, and mycelium was harvested by vacuum filtration using Buchner flask. Fresh mycelium was frozen in liquid nitrogen, lyophilized and ground using mortar and pestle. Total RNA isolation cDNA synthesis was as previously described in Lemaire et al. 2020.

2.3.4. Cloning and heterologous expression of VdPG2 and VdPME1

One PG, VDAG_04977 (hereafter named VdPG2, gene ID: 20706440) and one PME, VDAG_05799 (hereafter named VdPME1, gene ID: 20707262) were amplified using cDNA and gene-specific primers listed in **Table 6** excluding the signal peptide. Amplified genes were gel purified with gel extraction kit (Neo biotech, Nanterre, France), ligated to pPICZαB (Invitrogen, Carlsbad, California, United States) in frame with His-tag, previously digested with *Pst*1 and *Not*1 for VdPG2 and *Eco*R1 and *Not*1 for VdPME1, and used for transformation of *E. coli* TOP10 (Invitrogen). After sequencing, linearized vector was used to transform *Pichia pastoris* X33 strain as described in the instruction manual EasySelect Pichia Expression Kit manual (Invitrogen).

2.3.5. VdPG2 and VdPME1 expression, purification and enzyme analysis

VdPG2 and VdPME1 were produced in *Pichia pastoris* as described in the EasySelect Pichia Expression Kit manual (Invitrogen) and in Lemaire et al. (2020). After purification, enzyme buffer was changed to reaction buffer using PD Spintrap G-25 column (GE Healthcare). Determination of protein concentration, glycosylation patterns, enzyme purity and molecular weight were as described in Lemaire et al., 2020.

2.3.6. VdPG2 and VdPME1 biochemical characterization

The substrate specificity of VdPG2 was determined with the DNS method (Miller, 1959) using polygalacturonic acid (81325, Sigma); Citrus pectin with degree of methylesterification (DM) 20-34% (P9311, Sigma), DM 55-70% (P9436, Sigma) or DM >85% (P9561, Sigma); apple pectin with DM 70-75% (76282, Sigma); sugar beet pectin with DM 42% and degree of acetylation 31% (DA, CP Kelco, Atlanta, United States) using $2.45.10^{-3}$ $\mu g.\mu L^{-1}$ VdPG2 as described in Habrylo et al., 2018. Results were expressed as nmol of $GalA.min^{-1}.\mu g^{-1}$ of proteins.

The substrate specificity of VdPME1 was determined using above-mentioned substrates and the alcohol oxidase assay (Klavons and Bennett, 1986; Castaldo and Al., 1989) with modifications as described in L'Enfant et al., 2019. VdPME1 concentration was $2.3.10^{-3}$ $\mu g.\mu L^{-1}$. Results were expressed as nmol of $MeOH.min^{-1}.\mu g^{-1}$ of proteins.

2.3.7. VdPG2 and VdPME1 temperature, salt and pH dependency assay

The VdPG2 optimum temperature was determined by incubating the enzymatic reaction from 20 to 70°C during 60 min using polygalacturonic acid (0.4%, w/v) diluted in 50 mM ammonium acetate buffer (pH 5). The VdPG2 pH optimum was determined between pH 3 and 8 using sodium acetate buffer (pH 3 to 5) and Tris-HCl buffer (pH 6 to 8) and PGA as a substrate at 0.4% (w/v) final concentration. The VdPME1 pH optimum was determined by mixing citrus pectin DM 55-70% (P9436, Sigma) at 0.4% (w/v) final concentration using sodium acetate buffer (pH 3 to 5) and Tris-HCl buffer (pH 6 to 9). The VdPME1 optimum temperature was determined by incubating the enzymatic reaction from 10 to 60°C using citrus pectin DM 55-70% (P9436, Sigma) at 0.4% (w/v) diluted in 50 mM sodium phosphate buffer (pH 7) as mentioned above. VdPME1 activity was calculated using a standard curve between saponified and non-saponified samples as nmol of $MeOH.min^{-1}.\mu g^{-1}$ of proteins. All experiments were conducted in triplicate.

2.3.8. Determination of Km, Vmax, and specific activity

The VdPG2 kinetic parameters were calculated using GraFit7 software (Michaelis-Menten/Hill; Erithacus Software, Horley, Surrey, UK) using PGA as a substrate. The reactions were performed using 1 to 20 $mg.mL^{-1}$ PGA concentrations at 50 mM sodium acetate (pH 5) during 10 min at 50°C. The same procedure was used for VdPME1 with 1 to 20 $mg.mL^{-1}$ pectin DM 55-70% concentrations in 50 mM sodium phosphate buffer (pH 7) during 20 min at 30°C.

2.3.9. Oligoprofiling of digested commercial pectins

Oligogalacturonides (OGs) released after digestions by recombinant VdPG2 and VdPME1 were identified as described in Voxeur et al. 2019 (Voxeur et al., 2019). Briefly, citrus pectin of DM 24-30% (P9311, P9436, Sigma), DM 55-70% (P9436, Sigma) or DM >85% (P9561, Sigma) were prepared at 0.4% (w/v) final concentration in 50 mM ammonium acetate buffer (pH 5) and incubated with VdPG2 at $2.45.10^{-3}$ $\mu g.\mu L^{-1}$ concentration during 15 min, 45 min, 90 min, 180 min and overnight at 40°C. To analyse the processivity of VdPME1, citrus pectins DM 55-70% (P9436, Sigma) were digested with VdPG2 for 2 h (to obtain OG of various DP and DM) as mentioned above. Resulting OGs were lyophilised, and resuspended in 90 µL 50 mM Tris-HCl buffer (pH 7). 10 µL of VdPME1 at $2.3.10^{-3}$ $\mu g.\mu L^{-1}$ concentration was added and the reaction was incubated for 15 min and overnight at 40°C. The rest of the procedure was as previously described. Pellets were resuspended in 200 µL dH_2O.

2.3.10. Oligoprofiling of digested cell wall pectins from flax roots

Flax seeds from two different cultivars, Évéa (partially resistant to Verticillium wilt) and Violin (more susceptible to Verticillium wilt) were kindly provided by Linéa-Semences (Grandvilliers, France). Seeds were sterilized using Triton 0.01% (w/v, T8787, Sigma) diluted in ethanol 70% (w/v) and dried overnight. Seeds grew during three days on wet towel tissue at 21°C, 16 h/8 h light/dark. Forty roots were cut and placed into ethanol 100% (w/v) for 24 h. They were washed two times for 5 min with acetone 100% (w/v) and left to dry 24 h. Roots were rehydrated in 140 µL 50 mM ammonium acetate pH 5 during 2 h at RT and digested with VdPG2 at $2.45.10^{-3}$ $\mu g.\mu L^{-1}$ concentration, using the above-mentioned protocol.

2.3.11. Ultra-performance size-exclusion chromatography (UP-SEC) coupled with electrospray ionization high-resolution mass spectrometry (ESI-HRMS)

OGs produced from above-mentioned commercial pectins and flax roots after digestion were subjected to chromatographic separations and MS-detection as described in Hocq et al., 2020. We have determined, according to Voxeur et al., 2019, the relative amount of each oligogalacturonide (OG) comparing its peak area to the peak area of total OGs (sum of all areas) detected for each sample. Only the most abundant OGs, present as more than 1% of the total OGs, were plotted. With this method we cannot compare OGs between them, but we can emphasize the comparison, for a given OG, between different conditions such as substrates, cultivars as well as enzymes used for digestions.

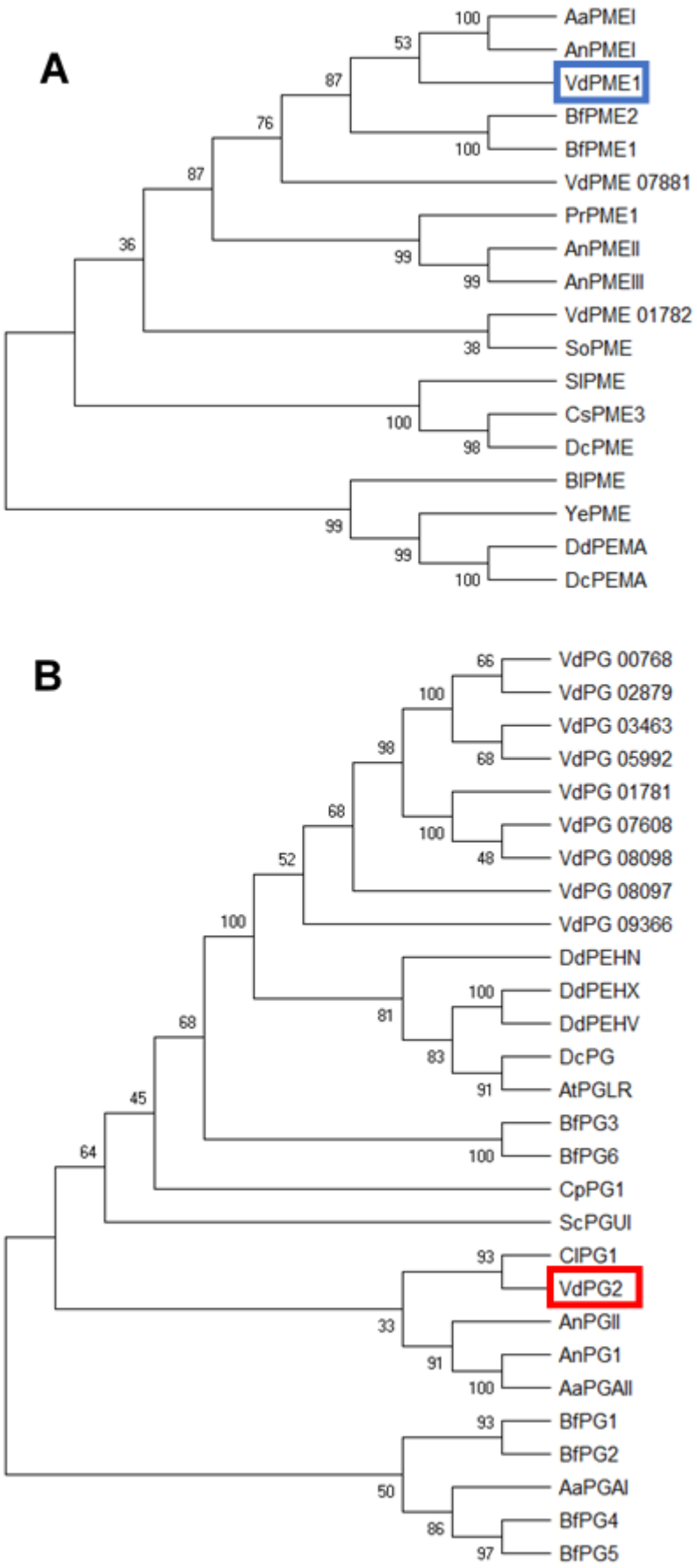
A
AaPMEI
AnPMEI
VdPME1
BfPME2
BfPME1
VdPME 07881
PrPME1
AnPMEII
AnPMEIII
VdPME 01782
SoPME
SlPME
CsPME3
DcPME
BlPME
YePME
DdPEMA
DcPEMA
B
VdPG 00768
VdPG 02879
VdPG 03463
VdPG 05992
VdPG 01781
VdPG 07608
VdPG 08098
VdPG 08097
VdPG 09366
DdPEHN
DdPEHX
DdPEHV
DcPG
AtPGLR
BfPG3
BfPG6
CpPG1
ScPGUI
ClPG1
VdPG2
AnPGII
AnPG1
AaPGAII
BfPG1
BfPG2
AaPGAI
BfPG4
BfPG5

Figure 26. Phylogenetic relationships of VdPME1 and VdPG2 with selected fungal and bacterial enzymes

Phylogenetic tree for PMEs (A) and PGs (B) *V. dahliae* PG2 (VdPG2, **VDAG_04977**) and PME1 (VdPME1, **VDAG_05799**) are red and blue-boxed, respectively. Amino acids sequences used are the following: *V. dahliae* PMEs (VDAG_07881, VDAG_1782) and *V. dahliae* PGs (VDAG_00768, VDAG_01781, VDAG_02879, VDAG_03463, VDAG_05992, VDAG_07608, VDAG_08097, VDAG_08098, VDAG_09366). *B. licheniformis* PME (Q65F39). *D. dadantii* PEHN (E0SDX9), PEHX (E0SKR4), PEHV (E0SKR2), PEMA (P0C1A9). *D. chrysanthemi* PEMA (P0C1A8). *Y. enterocolitica* PME (A1JJ76). *C. purpureum* PG1 (P79074) *B. fuckeliana* PGI (Q4G496), PG2 (Q4G495), PG3 (Q9Y7V9), PG4 (Q9Y7W0), PG5 (Q9Y7W1), PG6 (Q9Y7W2), PME1 (A0A384JQ57), PME2 (A0A384JCI5). *A. aculeatus* PGAI (O74213), PGAII (Q70HJ4), PMEI (Q12535). *A. niger* PGI (P26213), PGAII (P26214), PMEI (P17872), PMEII (G3YAL0), PMEIII (A0A345K402). *P. rubens* PME1 (B6HGX6). *C. lupini var. setosum* PG1 (A1E266). *S. cerevisiae* PGUI (P47180). *S. oryzae* PME (E7CIP7). *D. carota* PME (P83218), PG (Q75XT0). *S. lycopersicum* PME (P14280). *C. sinensis* PME3 (P83948). *A. thaliana* PGLR (Q9LYJ5). The maximum-likelihood tree was deduced from the genetic distances between aligned amino-acid sequences using MEGA. UniProt accession numbers were used.

2.4. Results and Discussion

2.4.1. Sequence analysis and phylogeny

V. dahliae encodes more than 40 putative pectinolytic enzymes. Among them, 30 PLs and PNLs (belonging to PL1, PL3 and PL9 families), 9 PGs (including putative endo and exo) and 4 PMEs. We first performed phylogenetic analysis and compared Verticillium PGs and PMEs protein sequences with selected bacterial, fungal, insect and plant enzymes. The 18 PMEs clustered into five clades with plant PMEs (carrot DcPME, orange CsPME3 and tomato SlPME) in a distinct clade, as well as insect rice weevil PME (SoPME, **Figure 26A**). VdPME1 appears to be closely related to the two other PMEs from Aspergillus species, which are recognized as non-processive PMEs in their mode of action. VdPME1 showed 51.23% and 51.08% sequence identity with AaPMEI (Christgau et al., 1996) and AnPMEI (Khanh et al., 1991), respectively. As shown on **Figure 26B** PGs, comprising 28 sequences, which clustered in seven clades allowing clear separation between putative endo and exo PGs from *V.dahliae* (VdPG 02879, VdPG 03463, VdPG 05992, VdPG 07608 VdPG 00768, VdPG 01781, VdPG G08089) with endo VdPG2 (04977). The plant PGs from *D. carota* (DcPG) and *A. thaliana* PGs (AtPGLR) clustered in a separated clade as well as PGs from yeast *S. cerevisiae* (ScPGUI) and fungal *C. purpureum* PG1 (CpPG1). VdPG2 forms an independent clade with fungal PGs from *C. lupini var. setosum* (ClPG1. 68.14% sequence

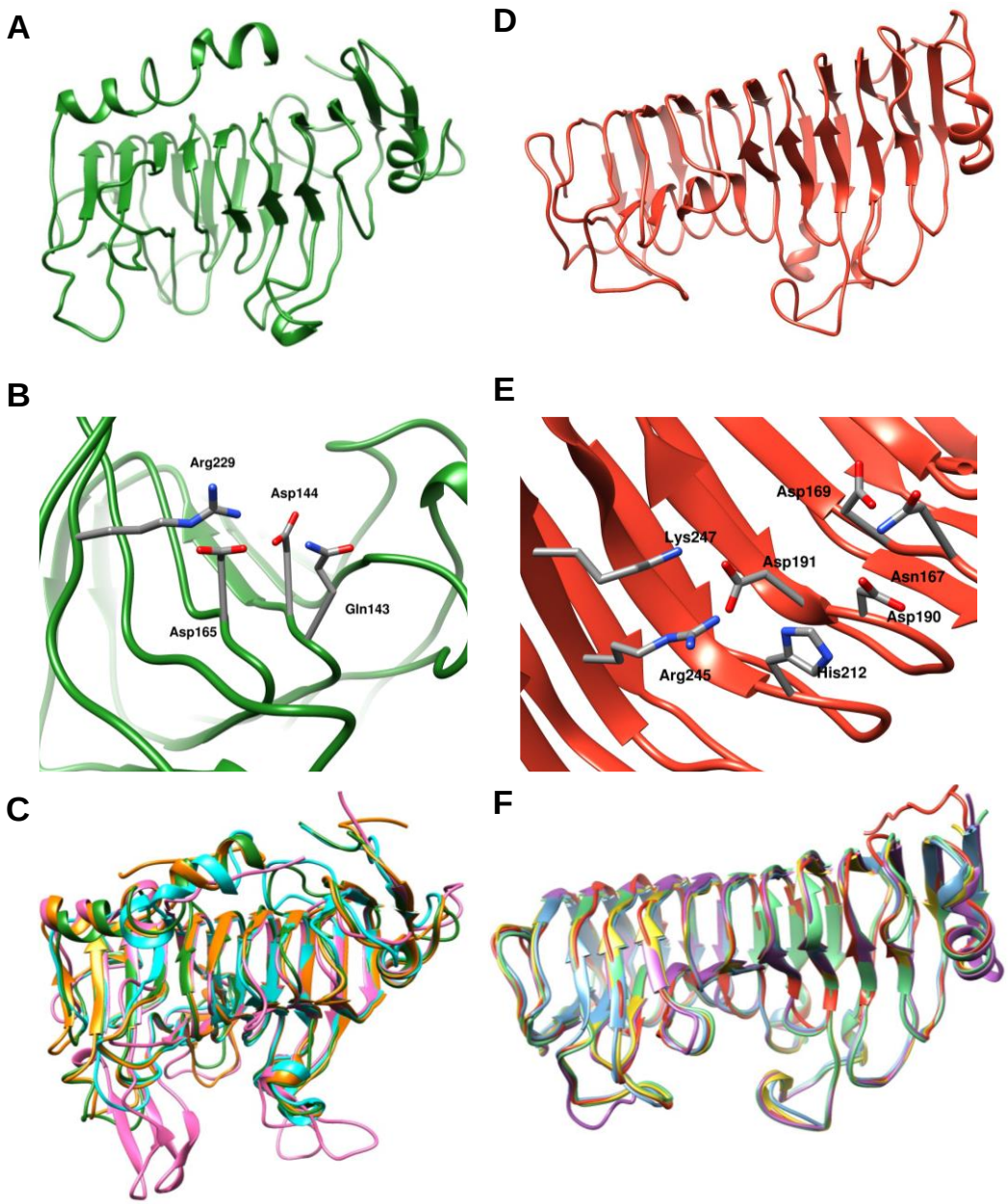

Figure 27. Homology modelling and structural comparison of VdPME1 and VdPG2
A) VdPME1 homology model created using I-TASSE. B) Structure of the active site of VdPME1. Gln-143, Asp-144, Aps-165 and Arg-229 (VdPME1 numbering) are coloured in grey. C) Structural alignment of VdPME1 with crystallised enzymes from *D. carota* (DcPME, orange, PDB: 1GQ8), *D. dadantii* (DdPME, pink, PDB: 2NT6) and *A. niger* (AnPME, cyan, PDB: 5C1C). D) VdPG2 homology model created using I-TASSER. E) Structure of the active site of VdPG2. Asn-167, Asp-169, Aps-190 and Aps-191, His-212, Arg-245, Lys-247 (VdPG2 numbering) are colored in grey. F) Structural alignment of VdPG2 PGs with crystallised enzymes from *A. niger* (AnPGII, bleu, PDB: 1CZF), *A. niger* (AnPGI, green, PDB: 1NHC), *A. acuelatus* (AaPG, purple, PDB: 1IA5) and *C. lupini* (ClPG1, yellow, PDB: 2IQ7, A1E266).

identity) which was shown to be endo-PGs (Bonivento et al., 2008).

2.4.2. Homology modelling and structure analysis

To fully understand the structural features of VdPG2 and VdPME1, their structures were modelled using the I-TASSER server for protein structure prediction. VdPME1 model was created using *D. carota PME* (P83218, PDB:1GQ8, (Johansson et al., 2002)) as the template, with 31.42% amino acid (AA) identity and 46.6% similarity. Although VdPME1 doesn't share a high degree of identity with its template, the modelling remarkably provided a structure with a root mean square deviation (RMSD) of only 4.1±2.8Å. The model consisted of 314 AA, without the 16 AA of the signal peptide. Modelling shows that the enzyme is a right handed β-helix (**Figure 27A**) structure that shares four highly conserved regions, as well as key active site residues characterized in other PMEs. These four regions comprise one N terminus region (Gly47, Ser48, Tyr49, Ala50 and Glu51), two internal regions (Tyr166-Phe166 (mutation in VdPME1) Gly167, Asp168, Thr169 and Asp165, Phe166, Ile167, Phe168 and Gly169) and one C-terminus region (Leu227, Gly228, Arg229, Pro300 and Trp301, Markovič and Jörnvall, 1992). The AA of the active site are Gln143, Asp144, Asp165 and Arg229 (**Figure 27B, Figure S13**) where the two Asp act as a general acid/base in the catalytic mechanism (Fries et al., 2007; Kent et al., 2016). The VdPME1 showed high structural superposition with *D. dadantii*, *A. niger* and *D. carota* PMEs (PDB: 2NT6, 5C1C, 1GQ8, **Figure 27C**).

The VdPG2 model was created using *A. acuelatus* PGAI (O74213, PDB:1IA5, (Cho et al., 2001) as a best template with an estimated RMSD of 5.6±3.5Å. VdPG2 exhibits lower sequence identity with AaPGAI (55.74%) compared to ClPG1 (68.14%) but higher structural homology. The final model consists of 352 AA without the 18 AA of the signal peptide. The structure is a right handed β-helix with 10 complete turns (**Figure 27D**). Members of GH28 family, including endo and exo PGs have conserved AA motifs, including Asn167, Thr168, Asp169 (NTD) Asp189, Asp190 (DD), Gly211, His212, Gly213 (GHG), Arg244, Ile245, Lys246 (RIK, **Figure 27E**, **Figure S14**, Markovič and Janeček, 2001; Park et al., 2008) in VdPG2. Structural alignment with published PGs structures (Cho et al., 2001; Van Pouderoyen et al., 2003; Bonivento et al., 2008) confirmed that VdPG2 is likely to be an endo-PG with a tunnel like active cleft (**Figure 27F**). Furthermore, while the catalytic AA are strongly conserved, tunnel like active cleft having the same shape differ

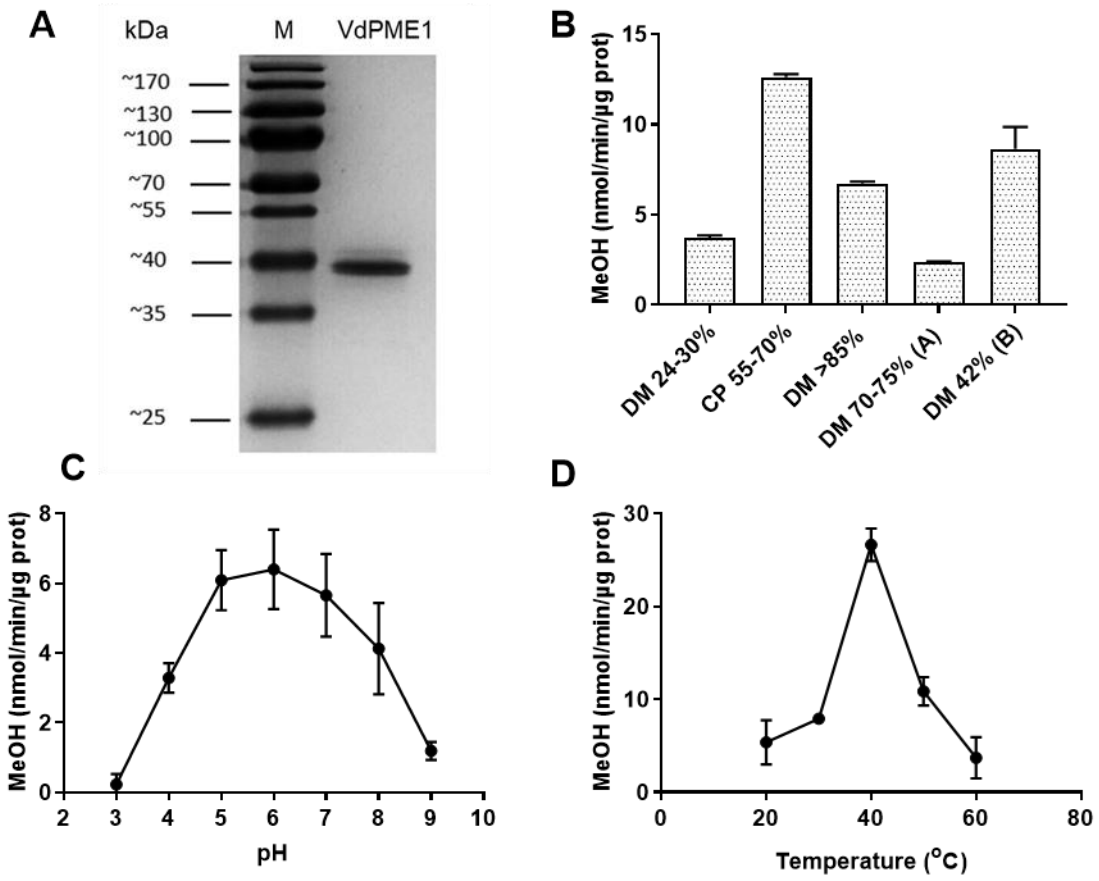

Figure 28. Biochemical characterization of VdPME1

A) SDS-PAGE analysis of VdPME1 following His-tag affinity purification. The gel was stained with Coomassie blue. The band at ± 40 kDa, corresponds to His-tagged and multiple bands corresponds to differently N-glycosylated forms of the purified enzyme. B) Substrate specificity of VdPME1: Activity of VdPME1 was measured on pectic substrates of distinct DM and DA. Activity was measured at pH 7.5 using the alcohol oxidase coupled assay. C) Influence of the pH on VdPME1 activity. Activity was measured using sodium acetate (pH 3-5) and Tris-HCl (pH 6-9) buffer. D) Influence of the temperature on VdPME1 activity. Activity was measured on pectins 55%-70% DM, pH 7.5 using the alcohol oxidase assay. The values are calculated as a MeOH released in as nmol of MeOH.min^{-1}.μg^{-1} of proteins. Data represent mean ± SD of three replicates.

in size, specifically regarding the size of the substrate which could be accepted (Van Pouderoyen et al., 2003).

2.4.3. Cloning, expression and purification of VdPG2 and VdPME1

The *VdPG2* (VDAG_04977) and *VdPME1* (VDAG_05799) genes consisting of 1113 and 993 bp, respectively; were amplified using gene specific primers without the signal peptide (**Table 6**), ligated in pPICZαB vector, expressed in *P. pastoris* and secreted in the culture media. The open reading frame consisted of 384 and 343 AA for VdPG2 and VdPME1, respectively, containing the poly-histidine tag for affinity chromatography purification. Following purification, VdPME1 and VdPG2 were resolved on SDS-PAGE, having an apparent molecular mass of ~ 39 and 50 kDa, respectively (**Figure 28A, Figure 29A**). The observed molecular mass is slightly higher compared to the predicted mass of 36.5 and 39.7 kDa, which could be related to the presence of two (Asn84, Asn201) and five (Asn122, Asn199, Asn220, Asn232, Asn331) potential N-glycosylation sites in VdPME1 and VdPG2, respectively. Additional O-glycosylation sites were predicted in VdPME1. The occurrence of glycosylation was confirmed through digestion with PNGase, leading to the expected shift in molecular mass for both enzymes (**Figure S15**).

2.4.4. Biochemical characterization of VdPME1

Although PMEs from different species catalyse the same reaction, they can differ in their pH and temperature optima, substrate specificities and processivity (Jolie et al., 2010). VdPME1 exhibited the highest activity on moderately methylesterified citrus pectin (DM 55-70%, **Figure 28B**), albeit an activity was also detected on a wide range of pectic substrates that varied in their DM. VdPME1 activity was 68% of the maximum on sugar beet pectin of DM 42%, 53% on citrus pectin of DM >85% and 29% on citrus pectin of DM 30%; suggesting that VdPME1 acts preferably on moderate DM. This is in accordance with the results described for PME from *A. niger* (Zhang et al., 2018) and *B. licheniformis* PME (Remoroza et al., 2015). Furthermore, while citrus (DM 55-70%) and apple (DM 70-75%) pectins have slightly different DM, the differences in activity could result from distinct patterns of methylesterification or xylose linkages (higher amount in apple pectin, Dheilly et al., 2016) which could reduce the accessibility to the substrate (de Vries et al., 1984). When using citrus pectin DM 55-70% as substrate, VdPME1 was active over a broad range of pH (**Figure 28C**). While the maximum relative activity is at pH 6, residual activities were 95% and 72% at pH 5 and 7, respectively. pH optimum contrasted with that of fungal PMEs, AaPMEI

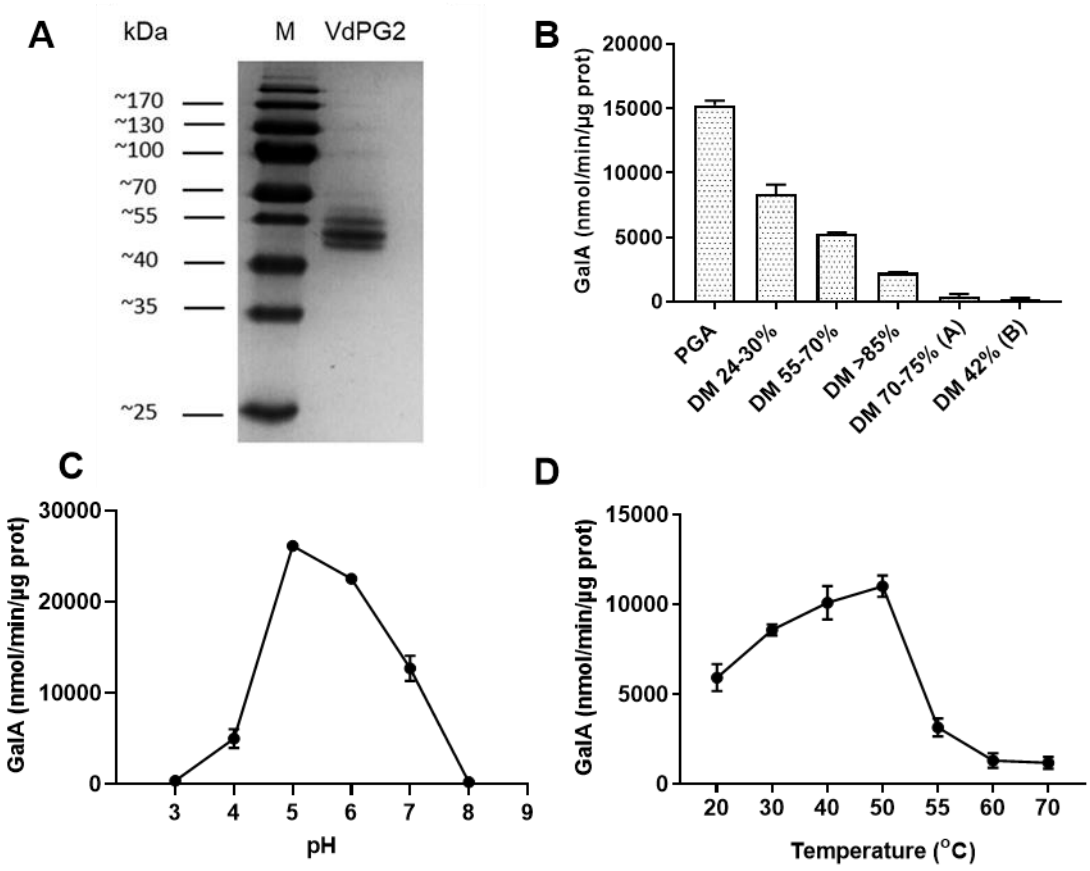

Figure 29. Biochemical characterization of VdPG2.
A) SDS-PAGE analysis of VdPG2 following His-tag affinity purification. The gel was stained with Coomassie blue and the bands at 38 kDa corresponds to His-tagged and multiple bands correspond to differently N-glycosylated forms of the purified enzyme. B) Substrate specificity of VdPG2. Activity of VdPG2 was measured on PGA and pectic substrates of distinct DM and DA. Activity was measured at pH 5 using the DNS method. C) Influence of the pH on VdPG2 activity. Activity was measured on PGA at 50°C using the DNS method. D) Influence of the temperature on VdPG2 activity. Activity was measured on PGA, pH 5 using the DNS method. The values are calculated as a nmol of GalA $min^{-1}.\mu g^{-1}$ of proteins. Data represent mean ± SD for three replicates.

(pH 4.5, Christgau et al., 1996), AnPMEII (pH 4.5, Kent et al., 2016), plant DcPME (pH 7.5, Markovič et al., 2002), and orange CsPME3 (pH 7, Christensen et al., 1998). Temperature optimum, assessed using citrus DM 55-70%, was 40°C (**Figure 28D**). The activity of VdPME1 drastically declined when not at optimal temperature with 40% and 30% of maximum activity at 50°C and 30°C, respectively. Similar values were reported for *P. chrysogenum* F46 PME (40°C, Pan et al., 2014), *A. niger* ZJ5 PME (45°C, Zhang et al., 2018) and CsPME3 at (50°C, Christensen et al., 1998). Salt dependency of VdPME1 activity was determined using 0 to 300 mM NaCl (**Figure S16**). Non-substantial effect was observed when using 0 to 50 mM concentration, while the residual activity was 50% and 24% at 100 mM and 300 mM NaCl, respectively. In that respect, as NaCl had no positive effect on activity, VdPME1 appears to be a salt-independent PME (Jolie et al., 2010), as opposed to previously reported fungal AaPMEI (Christgau et al., 1996) where salt increased the activity. Therefore, although of fungal origin, VdPME1 is more similar to Valencia orange peel PME where no salt is needed for the activity (Savary et al., 2002). The enzymatic parameters were determined using citrus pectin DM 55-70% as a substrate. K_m and V_{max} were 3.27 ± 0.16 mg.mL^{-1} and 89.91 ± 1.39 nmol of MeOH.min^{-1}. µg^{-1} of proteins respectively (**Table S3**). These K_m values show a high affinity for the substrate, and are comparable to that of *A.niger* ZJ5 (AnPMEIII, 3.27 mg.mL^{-1}, Zhang et al., 2018) with higher V_{max} values (5.63 nmol of MeOH.min^{-1}.µg^{-1}). In contrast, the V_{max} are much lower than AaPMEI (5500 nmol of MeOH.min^{-1}.µg^{-1}, Christgau et al., 1996).

2.4.5. Biochemical characterization of VdPG2

VdPG2 was most active on PGA (**Figure 29B**) and its activity was negatively correlated with increasing the DM of pectins. A number of fungal, bacterial and plant PG show similar trend (Benen et al., 1999; Kars et al., 2005a; Cheng et al., 2017). VdPG2 residual activity was 57% on citrus pectin DM 30%, and 34% on citrus pectin DM 55-70%. Similar biochemical characteristics were described for *A. luchuensis* PGA B (Tan et al., 2020) and *P. occitanis* PG2 (Sassi et al., 2016). The activity of VdPG2 was close to null on sugar beet pectin which could be explained by the overall structure and acetylation patterns of the substrate, which could impair PG activity (Habrylo et al., 2018). Using PGA as a substrate we showed that the optimal VdPG2 activity was at pH 5 (**Figure 29C**), while at pH 6 and pH 7 only 14% and 49% of the activity measured at pH 5 were detected, respectively. This is similar with the previously reported fungal acidic pectinase BfPG1 and BfPG2 (pH 4.2 and 4.5) that also showed high sequence similarity to VdPG2 (Kars et al.,

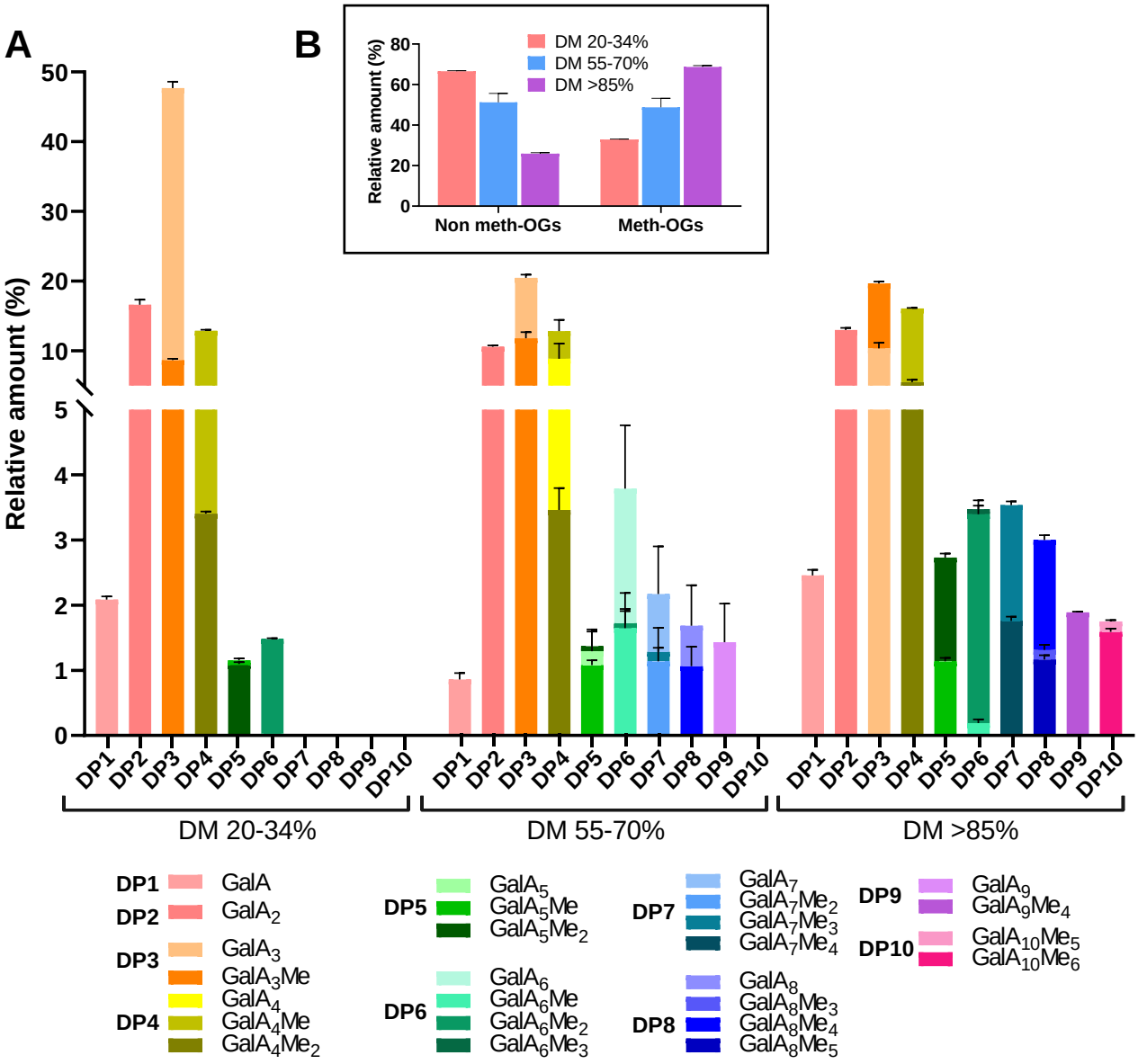

Figure 30. HP-SEC-MS analysis of OGs released by VdPG2 after over-night incubation with citrus pectins

A) OGs released by activity of VdPG2 on pectins of distinct DM (20-34%, 55-70% and >85%) were separated using SEC and analysed using MS/MS. OGs are represented according to their DP and DM. Figure shows 88.5% (DM 20-34%), 80% (DM 55-70%) and 82.6% (DM >85%) of total OGs detected. B) Total of the non-methylesterified and methylesterified OGs. Data are means ± SD; n = 3. Subscript numbers indicate the DP and DM.

2005a). In contrast, the optimal pH for VdPG2 was slightly higher to that of *C. pteridis* PG activity on (pH 4, Ladeira Ázar et al., 2019), *A. acuelatus* PG (pH 4.5, Silva et al., 2019) and *S. purpureum* PG (pH 4.5, Carli et al., 2019).

Temperature optimum was at 50°C (**Figure 29D**), with 90% and 78% residual activities at 40°C and 30°C, respectively. Above 50°C there was a sharp decline in activity. These temperatures optimums (40-50°C) were previously reported for a number of fungal, insect and plant PGs (Habrylo et al., 2018; Hocq et al., 2020; Tan et al., 2020). In contrast *F. palustris* and *S. purpureum* PGs were most active at 60°C (Carli et al., 2019; Tanaka et al., 2019). The enzymatic parameters were calculated using PGA as a substrate (**Table S3**). K_m and V_{max} were 8.34 ± 0.74 $mg.mL^{-1}$ and 40.28 ± 1.2 µmol of GalA min^{-1}. $µg^{-1}$ of proteins respectively. This is in the range of previously reported values for fungal PGs (Niture, 2008).

2.4.6. Identification of the VdPG2 released OGs

The analysis of the digestion products of PG is a key to understand the diversity of this family of enzymes and assess the potential role of the various isoforms. Using a recently developed LC-MS approach (Voxeur et al., 2019), OGs released by VdPG2 were identified after digestion of citrus pectin of various DM. When digesting citrus pectin of DM 20-34% (**Figure 30A, DM 20-34%**, **Figure S17A**) the majority of released OGs were non-methylesterified OGs, of DP 3 and 2 ($GalA_3$ 47.67% and $GalA_2$ 16.63% of total OGs detected). Moreover, $GalA_3$ and $GalA_2$ were not cleaved and accumulated during the reaction, as in order to hydrolyse them, the enzyme would have to fold into unfavourable conformation (Rexova-Benkova, 1973). Other OGs were methylesterified GalA of DP 3 and 4 ($GalA_4Me$ 12.88% and $GalA_3Me$ 8.70%). Altogether, these four OGs represented 85.89% of all detected OGs. $GalA_6Me_2$, was the OG with the highest DP detected. This shows that VdPG2 act as an endo enzyme, in contrast to exo-PGs which release mostly GalA products (Markovič and Janeček, 2001). When using a more methylesterified substrate (DM 55-70%), the $GalA_3$ was still the most abundant OG (20.49%) with a relative abundance of $GalA_4Me$ and $GalA_3Me$ of 12.82% and 11.82% (**Figure 30A, DM 55-70%, Figure S17B**), respectively. Furthermore, additional methylesterified OGs of DP7 and DP8 were detected ($GalA7Me_2$, $GalA7Me_3$, $GalA8Me_4$). Interestingly, when digesting the citrus pectin DM 55-70% increase of non-methylesterified OGs is observed, notably $GalA_4$ (8.88%) and $GalA_6$ (3.78%). This could be due to the random distribution of methyls in HG chain coupled with single-attack (non-

processive) nature of VdPG2 which cloud lead to increased release of non-methylesterified OGs. $GalA_3Me$, $GalA_4Me$ and $GalA_2$ were the most abundant OGs identified after digestion of citrus pectins of DM >85%, with 19.66%, 16.07% and 13%, respectively (**Figure 30A, DM >85%**, **Figure S17C)**. In contrast the relative amount of $GalA_3$ was drastically reduced to 10.37% (of total OGs detected), and 74.14% of all OGs were methylesterified. Overall VdPG2 released 66.56% of non-methylesterified OGs from citrus pectin DM 20-34% and 25.86% from pectins of DM >85% (**Figure 30B**). These OGs represent the final products after 24 h digestion and it can be assumed that they cannot be further hydrolysed due to unfavourable methyl substitutions. This was tested by analysing the OGs released following 15, 45, 90 and 180 min incubation, with DM 24-30%, where no differences between various incubation times were observed (**Figure S18**).

As a means of comparing the mode of action of VdPG2 with previously characterized PG, the digestion profile of AaPGM2, a commercial endo-PG M2 from *Aspergillus aculeatus,* was compared with that of VdPG2. Citrus pectin with DM 20-34% and DM 55-70% were digested during 2 hours with each of the enzymes and the released OGs were compared (**Figure S19**). Overall, both enzymes released the same OGs in different relative quantities. Differences came from the abundance of non-methylesterified $GalA_3$ (17% for AaPGM2 vs 47% VdPG2) and the absence of $GalA_4Me_2$ detected following AaPGM2 digestion of pectin DM 20-34% (**Figure S19A**). Higher differences were detected with pectin DM 55-70% (**Figure S19B**), where AaPGM2 releases OGs of higher DP with complex methyl substitutions. This further reinforce the previous statement that VdPG2 has less affinity for pectins with complex methylesterification patterns compared to AaPGM2. The mode of action of these two enzymes differ and probably these differences are likely to be dependent on the active site subsites, as reported for AnPGII, where the Glu252Ala mutation increased the activity of the enzyme on partially methylesterified substrate (Pagès et al., 2000). That specific AA is different for two enzymes (Asp259, VdPG2 numbering) which could explain this distinct behaviour, but AA at other subsites should be also considered when determining enzyme specificity.

2.4.7. VdPME1 has a processive mode of action

As a way to determine the mode of action of VdPME1, we first digested moderately methylesterified substrate citrus pectin DM 55-70% for 2 hours using VdPG2 (**Figure 31A**). This led to the release of methylesterified and non-methylesterified OGs. This pool of OGs was

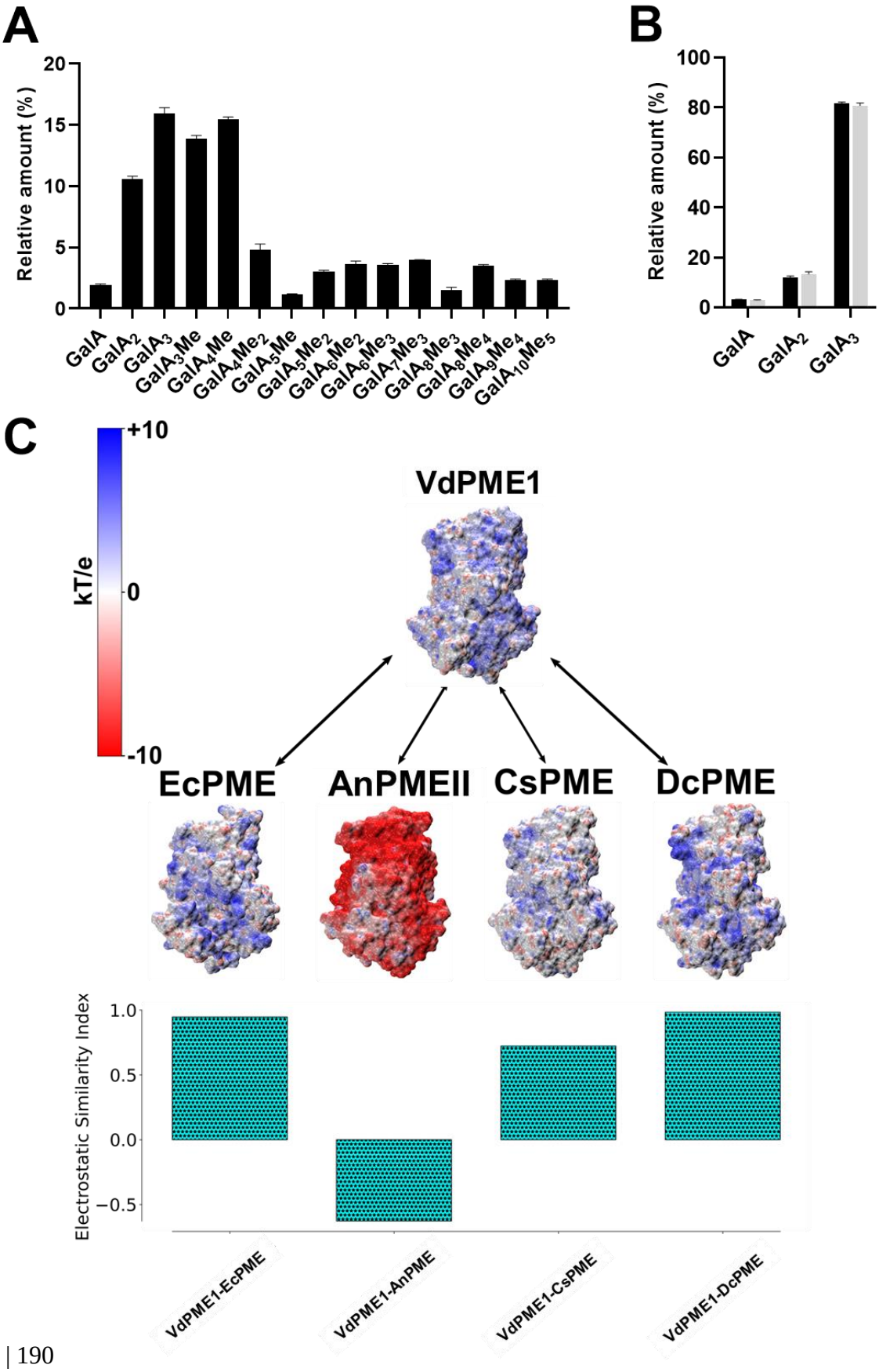
A
Relative amount (%)
20
15
10
5
0
GalA
GalA2
GalA3
GalA3Me
GalA4Me
GalA4Me2
GalA5Me
GalA5Me2
GalA6Me2
GalA6Me3
GalA7Me3
GalA8Me3
GalA8Me4
GalA9Me4
GalA10Me5
B
Relative amount (%)
100
80
60
40
20
0
GalA
GalA2
GalA3
C
+10
kT/e
0
-10
VdPME1
EcPME
AnPMEII
CsPME
DcPME
Electrostatic Similarity Index
1.0
0.5
0.0
−0.5
VdPME1-EcPME
VdPME1-AnPME
VdPME1-CsPME
VdPME1-DcPME

Figure 31. Mode of action and electrostatic potential of VdPME1
A) Population of OGs of various DP and DM generated by action of VdPG2 during 2 h at 37°C on pectin DM 55-70%. B) OG produced from the "VdPG2-population" after 15 min (black) and overnight incubation (grey) with VdPME1. Only mono-, di-, tri- galacturonic acids were identified. Data are means ± SD; n = 3. Subscript numbers indicate the DP and DM. C) Electrostatic potentials, projected on the enzyme surface, calculated for *V.dahliae* (VdPME1), *Dickeya dadantii* (DdPME), *Citrus sinensis* (CsPME) and *Daucus carota* (DcPME) PMEs at pH 7.0. Positive and negative regions of the potential are coloured from blue to red with a scale ranging between -10 and +10 kT/e. Pairwise similarity indices calculated to understand the resemblance of electrostatic potentials between the PME from *V. dahliae* (VdPME1) and the other PMEs are shown as bars in the lower panel. A similarity index of +1.0 shows correlated electrostatic potentials (high similarity – see methods for more details), whereas a value of -1.0 shows anti-correlated potentials. Any value in between shows different to no correction (similarity index = 0).

subsequently used as substrate for determining the mode of action of VdPME1 at pH 7 after 15 min and overnight digestion. LC-MS/MS oligoprofiling showed that for the two incubation times, only non-methylesterified GalA, $GalA_2$ and $GalA_3$ were detected (**Figure 31B**). Together, these data show that VdPME1 can produce long stretches of non-methylesterified GalA that have been, in the context of the experiment, further hydrolysed by the still-active VdPG2. Processive PMEs have been reported to have a neutral to alkaline optimal pH while non-processive PMEs are active at acidic pH (Kent et al., 2016). It has been shown that *A. niger* PMEII, (AnPMEII) that has an optimal pH at 4.5 is a non-processive, while orange (CsPME), carrot (DcPME) and *D. dadantii* (DdPME) PMEs were shown to be processive at pH 7.5 (Lee et al., 2008; Kent et al., 2016). Considering the importance of the electrostatic properties in defining substrate specificity and processivity (Mercadante et al., 2014), we have performed a quantitative analysis of the electrostatic properties of the modelled VdPME1 and compared those to what is known for other well-characterised PMEs. As shown on the **Figure 31C** the comparison highlights a clear difference with the acidophile AnPMEII with electrostatics characterising the binding grooves being of opposite signs (a strong negative electrostatic potential for AnPMEII, and a strongly positively charged group for VdPME1 at pH 7.0). The electrostatic potential of VdPME1 is similar to that of the CsPME and DcPME, known to be processive at neutral pH, with an overall positive charge and a similarity index close to 1.0. This contrasted with the negative electrostatic potential of AnPMEII which can facilitate the dissociation of the enzyme-substrate complex for highly de-methylesterified substrates, which have a strong negative charge and anticorrelated similarity index. The relation between the electrostatic

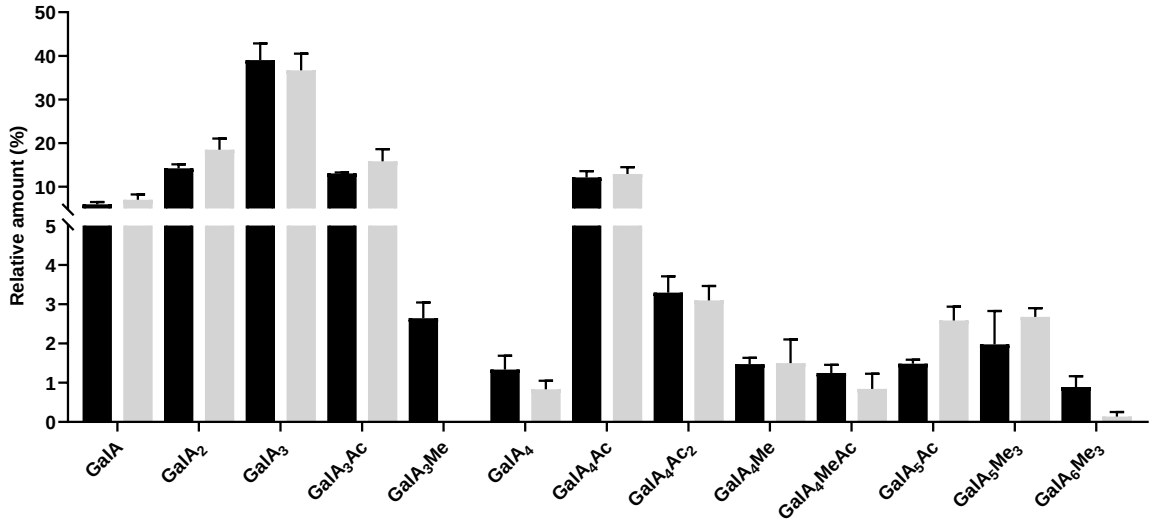

Figure 32. Analysis of OGs released by VdPG2 from flax roots
VdPG2 was incubated overnight with roots from Évéa (spring flax, partially resistant to Verticillium wilt, black) and Violin (winter flax, more susceptible to Verticillium wilt, grey). Data are means ± SD; n = 3. Subscript numbers indicate the DP and DM.

properties of the binding groove and processivity could be explained on the basis of simple electrostatics, with the repulsion between carboxylate groups of HGs and negatively charged residues in the binding groove being a determinant for low affinity. Nevertheless, residue-specific preferences for different methylesterification or acetylation states for the substrate in specific subsites along the binding groove are most likely important to quantitatively tune processivity among PMEs showing processive behaviour.

2.4.8. Two Verticillium-sensitive and tolerant cultivars differ in their root pectin structure

Phytopathogenic fungi use pectinolytic enzymes, including PGs, PMEs, PLLs during infection to degrade pectins (Mandelc and Javornik, 2015). *V. dahliae* as a soilborne pathogen attacks flax root to infect the plants. In order to determine the contribution of VdPG2 in degrading flax cell wall we digested roots cell wall of two flax cultivars Évéa (*Verticillium*-partially resistant), and Violin (*Verticillium*-susceptible) with VdPG2. VdPG2 showed activity on flax roots and OGs up to DP6 were detected (**Figure 32**). In particular, VdPG2 released non-methylesterified (GalA, $GalA_2$, $GalA_3$, $GalA_4$) and methylesterified ($GalA_3Me$ and $GalA_4Me$, in both cultivars, approx. 1.5%) OGs which have been previously identified from commercial pectic substrates. In addition, VdPG2 released acetylated substrates, $GalA_3Ac$, $GalA_4Ac$, $GalA_4Ac_2$, showing that the enzyme is able to hydrolyse acetylated pectins. $GalA_4MeAc$ was the only methylesterified and acetylated OG detected. It appears that VdPG2 has lower affinity for pectic population having acetyl and methyl groups. In particular, the distribution of methyl and acetyl groups on HGs was shown to have an impact on enzyme substrate interaction, as acetylation of HGs strongly change the association of enzyme on substrate (Ralet et al., 2003). Overall, following digestion by VdPG2, both genotypes, Évéa and Violin, produced similar diversity and relative abundance of OGs (**Figure 32**) except for $GalA_3Me$, which was specifically detected in Évéa, the *Verticillium*-partially resistant cultivar. This specific OG only produced from the roots of the resistant cultivar suggests that its cell wall structure differed to that of the susceptible cultivar. When *V. dahliae* infests flax roots, pectins digestion by PGs such as VdPG2 can lead to releasing OGs similar to the above-mentioned one. This could play a role in triggering distinct signalling events between resistant and susceptible cultivars. Indeed, previous reports show that small OGs, especially trimers could be involved in activation of genes involved in defence and phytohormone signalling, as well in the down-regulation of genes involved in growth regulation and development (Davidsson et al., 2017). In addition, this OG could act as

danger-associated molecular patterns (DAMPs) in flax which would lead to activation of defence-related pathways, thus reducing the susceptibility to pathogen infection (Pogorelko et al., 2013).

2.5. Conclusion

We characterized two novel enzymes from *V.dahliae:* VdPME1 and VdPG2. They show high activity on pectic substrates but also, for VdPG2, on cell wall pectins from flax roots. Biochemical characteristics were determined for both enzymes which showed, VdPG2 is an endo PG that can release methylesterified, non-methylesterified and acetylated OGs, with preference for unsubstituted and slightly substituted pectic populations. This, together with homology modelling suggests that small differences in the enzyme structure could be of importance to determine the substrate specificities. Model for VdPME1 shows similar structural features to that reported for fungal and plant PMEs, but a surprising processive behaviour commonly observed for plants PMEs. This processive behaviour could relate to the electrostatic potential of the protein. The processivemode of action of VdPME1 could enable release of pectins for which VdPG2 has a high affinity. This study shows that HP-SEC-MS can be used as a method of choice for the detection and quantification of OGs released by the action of VdPG2 and VdPME1 from commercial pectin and flax root cell wall pectins. Moreover, synergistic properties of these two enzymes suggest that VdPG2 and VdPME1 are important pectinolytic enzymes in *V.dahliae* arsenal. This study may lead to new approach for the protection of crops against pathogens.

Funding sources

This work was funded by the Conseil Regional Hauts-de-France and the FEDER (Fonds Européen de Développement Régional) through a PhD studentship awarded for to J.S.

CRediT authorship contribution statement

Josip Safran: Conceptualization, Data curation, Formal analysis, Investigation, Methodology, Writing - original draft. **Olivier Habrylo**: Formal analysis, Investigation, Methodology. **Mehdi Cherkaoui**: Methodology. **Sylvain Lecomte**: Methodology. **Aline Voxeur**: Methodology. **Serge Pilard**: Investigation, Methodology **Solène Bassard**: Methodology. **Corrine Pau-Roblot**: Conceptualization, Investigation, Methodology. **Davide Mercadante**: Conceptualization, Writing - review & editing **Jérôme Pelloux**: Funding acquisition, Conceptualization, Writing - review & editing. **Fabien Sénéchal**: Conceptualization, Writing - review & editing.

2.6. Supplemental data

Figure S13. Multiple sequences alignment of VdPME1
VdPME1 AA sequence was aligned with *Dickeya dadantii* (DdPME, P0C1A9), *Daucus carota* (DcPME, P83218) and *Aspergillus niger* (AnPME, G3YAL0*)*. The four highly conserved regions are blue-boxed and the AA of the active site AA are red-boxed. The alignment was performed using ClustalO.

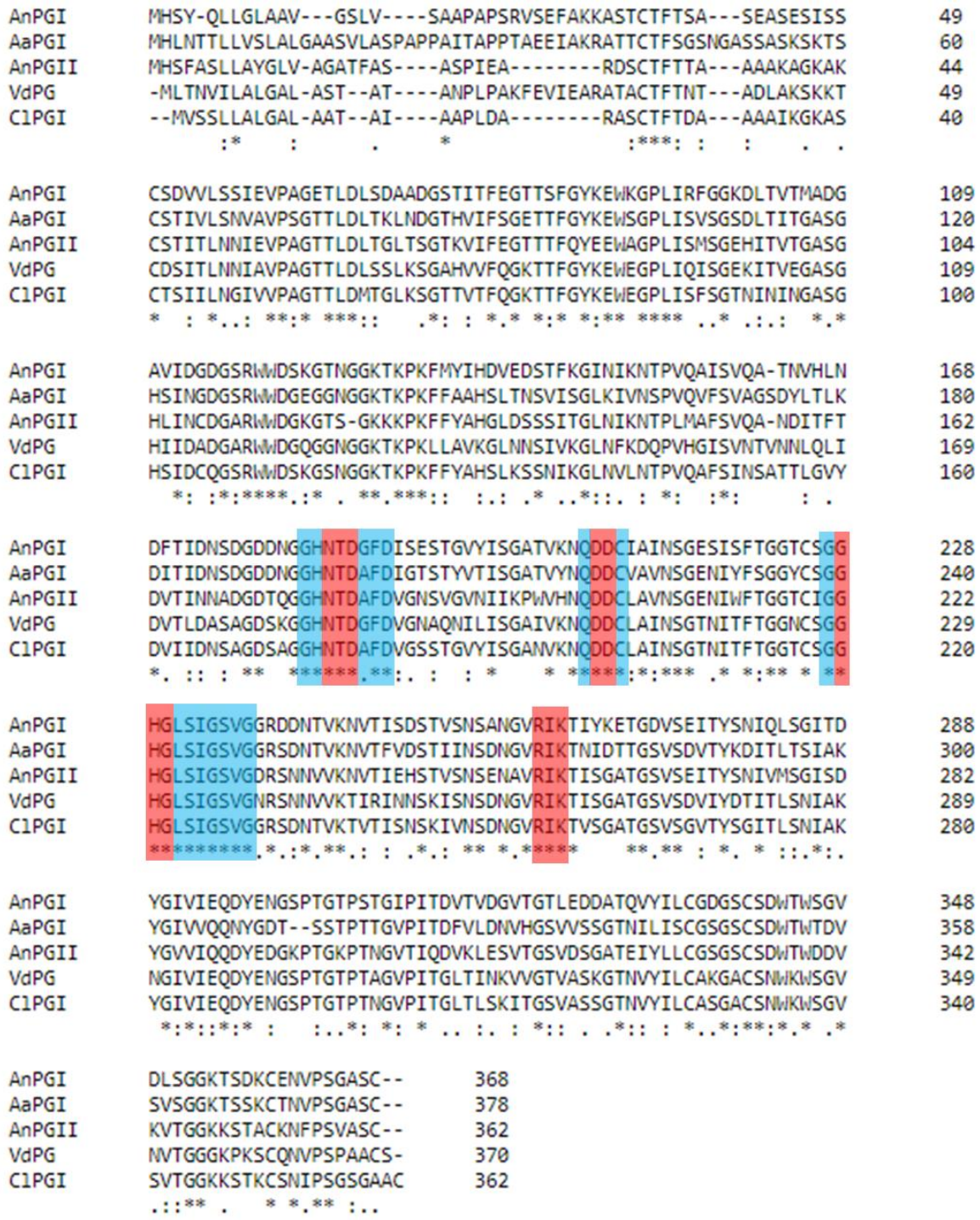

Figure S14. Multiple sequences alignment of VdPG2

VdPG2 AA sequence was aligned with *Aspergillus aculeatus* (AaPGI, O74213), *Aspergillus niger* (AnPGI, P26213), *Aspergillus niger* (AnPGII, P26214*)* and *Colletotrichum lupini var. setosum* (ClPG1, A1E266). The AA of the active site AA and the conserved AA are red and blue-boxed, respectively. The alignment was performed using ClustalO.

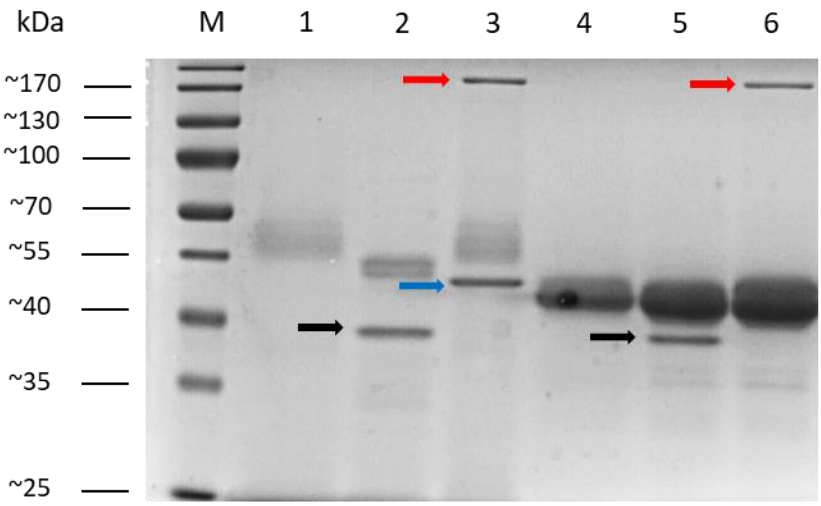

Figure S15. VdPG2 and VdPME1 are glycosylated
VdPG2 was incubated in the absence (**lane 1**) or presence of peptide – N – glycosidase F (PNGaseF, **lane 2**), of O-Glycosidase (O-glyc) and neuraminidase (Neur, **lane 3**). VdPME1 was incubated in the absence (lane 4) or presence of PNGase F (**lane 5**), or O – glyc and Neur (**lane 6**). Marker (M), PNGase F – black arrow, O-glyc – red arrow, Neur – blue arrow (not seen in lane 6).

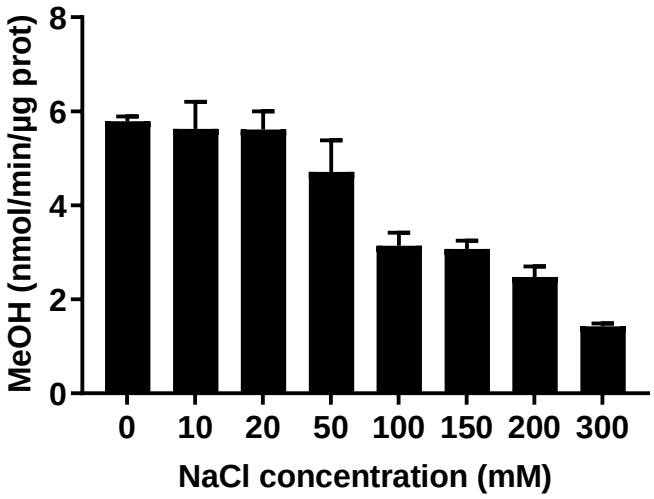

Figure S16. The VdPME1 salt optimum
Salt optimum was determined by incubating the enzymatic reaction with sodium chloride (NaCl) between 0- and 300-mM concentration using citrus pectin DM 55-70% as a substrate. Activity was measured at pH 7,5 using the alcohol oxidase assay. The values are calculated as a MeOH released in as nmol of MeOH.min^{-1}.µg^{-1} of proteins. Data represent mean ± SD, n = 3.

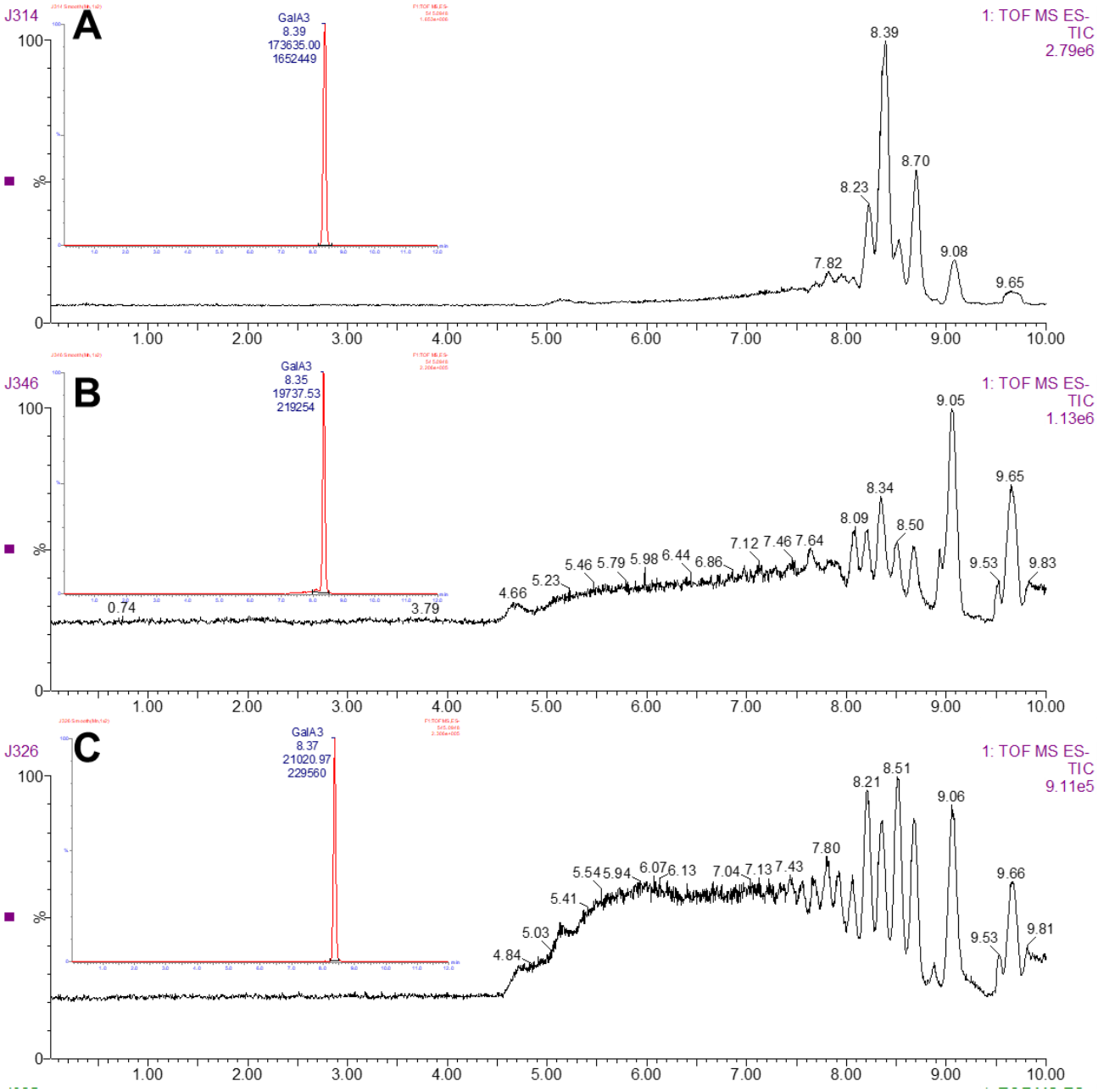

Figure S17. HP-SEC-MS analysis of OGs released by VdPG2 after over-night incubation with citrus pectins DM 24-30%, DM 55-70%, DM > 85%

Chromatograms of entire spectre (black) and mass spectre corresponding to $GalA_3$ (red) for pectins DM 24-30% (A), DM55-70% (B) and DM >85% (C) are shown.

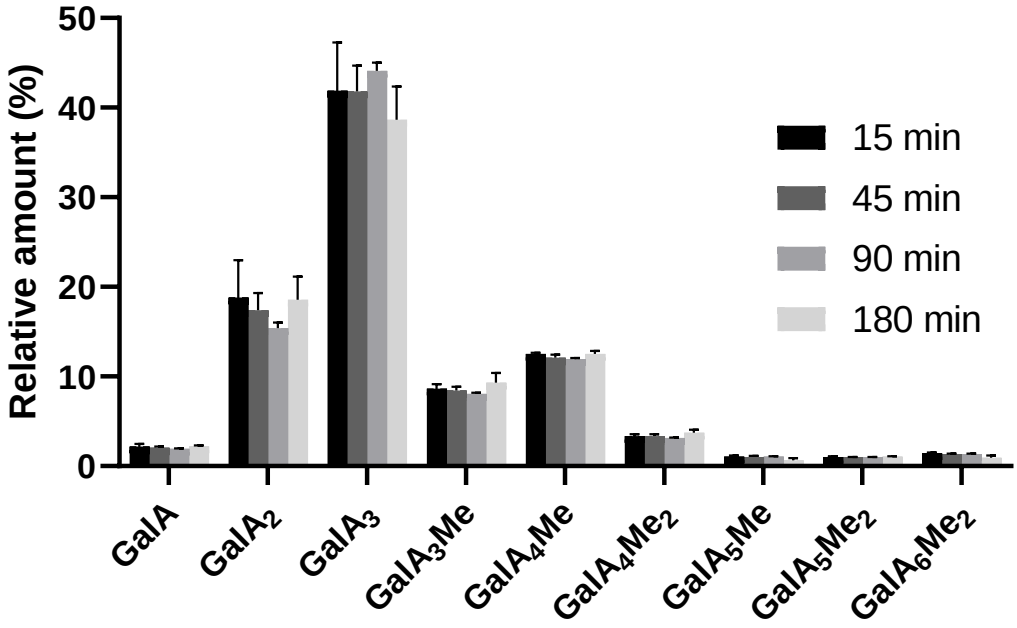

Figure S18. Time-dependence of OGs released by VdPG2
Analysis of the OGs released after digestion of pectin DM 24-30% by VdPG2 for 15, 45, 90 180 min. Data are means ± SD; n = 3. Subscript numbers indicate the DP and DM.

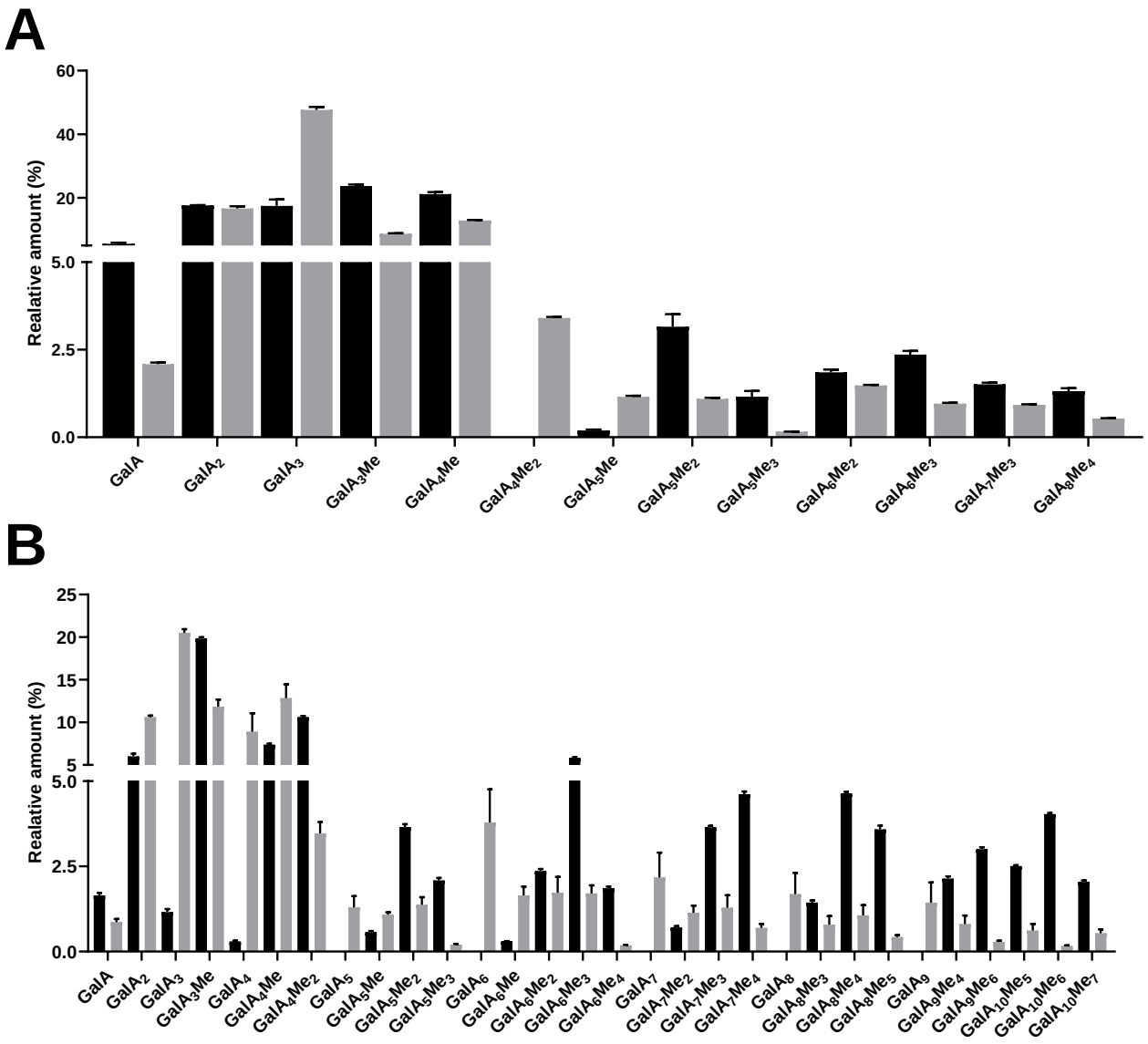

Figure S19. Analysis of OGs released by VdPG2 and AaPGM2
(A) Pectins DM 24-30% digested for 2h by VdPG2 (grey) and AaPGM2 (black). (B) Pectins DM 55-70% digested for 2h by VdPG2 (grey) and AaPGM2 (black) Data are means ± SD; n = 3. Subscript numbers indicate the DP and DM.

Table S3. Enzymatic characteristics of the purified recombinant *V. dahliae* PG2 and PME1

Characteristics	VdPG2	VdPME1
Classification	EC 3.2.1.171 - GH28	EC 3.1.1.11- CE8
Length (AA)	383	343
MW * (kDa)	39.7	36.5
pI *	8.59	8.64
pH optimum	5	6
Temperature optimum (°C)	50	40
Km ($mg.ml^{-1}$)	8.34 ± 0.74	3.27 ± 0.16
Vmax (nmol of (MeOH)(GalA).min^{-1}.μg^{-1})	40284.29 ± 1177.28	89.91 ± 1.39

* Theoretical values

2.7. Literature

Baker NA, Sept D, Joseph S, Holst MJ, McCammon JA (2001) Electrostatics of nanosystems: Application to microtubules and the ribosome. Proc Natl Acad Sci U S A **98**: 10037–10041

Benen JAE, Kester HCM, Visser J (1999) Kinetic characterization of Aspergillus niger N400 endopolygalacturonases I, II and C. Eur J Biochem **259**: 577–585

Blomberg N, Gabdoulline RR, Nilges M, Wade RC (1999) Classification of protein sequences by homology modeling and quantitative analysis of electrostatic similarity. Proteins Struct Funct Genet **37**: 379–387

Blum A, Bressan M, Zahid A, Trinsoutrot-Gattin I, Driouich A, Laval K (2018) Verticillium Wilt on Fiber Flax: Symptoms and Pathogen Development In Planta. Plant Dis **102**: 2421–2429

Bonivento D, Pontiggia D, Matteo A Di, Fernandez-Recio, Juan Salvi G, Tsernoglou D, Cervone F, Lorenzo G De, Federici4 L (2008) Crystal structure of the endopolygalacturonase from the phytopathogenic fungus Colletotrichum lupini and its interaction with polygalacturonase-inhibiting proteins. Proteins **70**: 311–319

Cameron RG, Savary BJ, Hotchkiss AT, Fishman L, Chau HK, Baker RA, Grohmann K (2003) Separation and Characterization of a Salt-Dependent Pectin Methylesterase from Citrus sinensis Var. Valencia Fruit Tissue. J Agric Food Chem **51**: 2070–2075

Carli S, Meleiro LP, Ward RJ (2019) Biochemical and kinetic characterization of the recombinant GH28 Stereum purpureum endopolygalacturonase and its biotechnological application. Int J Biol Macromol **137**: 469–474

Carpita NC, Gibeaut DM (1993) Structural models of primary cell walls in flowering plants: consistency of molecular structure with the physical properties of the walls during growth. Plant J **3**: 1–30

Castaldo D, Al. E (1989) Isolation and Characterization of Pectin Methylesterase from Apple Fruit. Enzyme **54**: 653–656

Cheng Z, Chen D, Wang Q, Xian L, Lu B, Wei Y, Tang H, Lu Z, Zhu Q, Chen Y, et al (2017) Identification of an acidic endo-polygalacturonase from Penicillium oxalicum CZ1028 and its broad use in major tropical and subtropical fruit juices production. J Biosci Bioeng **123**: 665–672

Cho SW, Lee S, Shin W (2001) The X-ray structure of Aspergillus aculeatus Polygalacturonase and a Modeled structure of the Polygalacturonase-Octagalacturonate Complex. J Mol Biol **311**: 863–878

Christensen TMIE, Nielsen JE, Kreiberg JD, Rasmussen P, Mikkelsen JD (1998) Pectin methyl esterase from orange fruit : characterization and localization by in-situ hybridization and immunohistochemistry. Planta **206**: 493–503

Christgau S, Kofod L V, Halkier T, Andersen LN, Hockauf M, Do K (1996) Pectin methyl

esterase from Aspergillus aculeatus : expression cloning in yeast and characterization of the recombinant enzyme. Biosystems **712**: 705–712

Davidsson P, Broberg M, Kariola T, Sipari N, Pirhonen M, Palva ET (2017) Short oligogalacturonides induce pathogen resistance-associated gene expression in Arabidopsis thaliana. BMC Plant Biol **17**: 1–17

Dheilly E, Gall S Le, Guillou MC, Renou JP, Bonnin E, Orsel M, Lahaye M (2016) Cell wall dynamics during apple development and storage involves hemicellulose modifications and related expressed genes. BMC Plant Biol. **16**: 1–20

Dolinsky TJ, Nielsen JE, McCammon JA, Baker NA (2004) PDB2PQR: An automated pipeline for the setup of Poisson-Boltzmann electrostatics calculations. Nucleic Acids Res **32**: 665–667

Fradin EF, Thomma BPHJ (2006) Physiology and molecular aspects of Verticillium wilt diseases caused by V. dahliae and V. albo-atrum. Mol Plant Pathol **7**: 71–86

Fries M, Ihrig J, Brocklehurst K, Shevchik VE, Pickersgill RW (2007) Molecular basis of the activity of the phytopathogen pectin methylesterase. EMBO J **26**: 3879–3887

Habrylo O, Evangelista DE, Castilho PV, Pelloux J, Henrique-Silva F (2018) The pectinases from Sphenophorus levis: Potential for biotechnological applications. Int J Biol Macromol **112**: 499–508

Ten Have A, Mulder W, Visser J, Van Kan JAL (1998) The endopolygalacturonase gene Bcpg1 is required to full virulence of Botrytis cinerea. Mol Plant-Microbe Interact **11**: 1009–1016

Hocq L, Guinand S, Habrylo O, Voxeur A, Tabi W, Safran J, Fournet F, Domon J-M, Mollet J-C, Pilard S, et al (2020) The exogenous application of At PGLR, an endo - polygalacturonase, triggers pollen tube burst and repair. Plant J 1–17

Jayani RS, Saxena S, Gupta R (2005) Microbial pectinolytic enzymes: A review. Process Biochem **40**: 2931–2944

Johansson K, El-Ahmad M, Friemann R, Jörnvall H, Markovič O, Eklund H (2002) Crystal structure of plant pectin methylesterase. FEBS Lett **514**: 243–249

Jolie RP, Duvetter T, Van Loey AM, Hendrickx ME (2010) Pectin methylesterase and its proteinaceous inhibitor: A review. Carbohydr Res **345**: 2583–2595

Kars I, Krooshof GH, Wagemakers L, Joosten R, Benen JAE, Van Kan JAL (2005a) Necrotizing activity of five Botrytis cinerea endopolygalacturonases produced in Pichia pastoris. Plant J **43**: 213–225

Kars I, McCalman M, Wagemakers L, Van Kan JAL (2005b) Functional analysis of Botrytis cinerea pectin methylesterase genes by PCR-based targeted mutagenesis: Bcpme1 and Bcpme2 are dispensable for virulence of strain B05.10. Mol Plant Pathol **6**: 641–652

Kent LM, Loo TS, Melton LD, Mercadante D, Williams MAK, Jameson GB (2016) Structure and properties of a non-processive, salt-requiring, and acidophilic pectin methylesterase from aspergillus Niger provide insights into the key determinants of processivity control. J Biol

Chem **291**: 1289–1306

Khanh NQ, Ruttkowski E, Leidinger K, Albrecht H, Gottschalk M (1991) Characterization and expression of a genomic pectin methyl esterase-encoding gene in Aspergillus niger. Gene **106**: 71–77

Klavons JA, Bennett RD (1986) Determination of Methanol Using Alcohol Oxidase and Its Application to Methyl Ester Content of Pectins. J Agric Food Chem **34**: 597–599

L'Enfant M, Kutudila P, Rayon C, Domon JM, Shin WH, Kihara D, Wadouachi A, Pelloux J, Pourceau G, Pau-Roblot C (2019) Lactose derivatives as potential inhibitors of pectin methylesterases. Int J Biol Macromol **132**: 1140–1146

Ladeira Ázar RIS, da Luz Morales M, Piccolo Maitan-Alfenas G, Falkoski DL, Ferreira Alfenas R, Guimarães VM (2019) Apple juice clarification by a purified polygalacturonase from Calonectria pteridis. Food Bioprod Process **9**: 238–245

Lee H, Rivner J, Urbauer JL, Garti N, Wicker L (2008) De-esterification pattern of Valencia orange pectinmethylesterases and characterization of modified pectins. J Sci ofFood Agric **88**: 2102–2110

Lemaire A, Duran Garzon C, Perrin A, Habrylo O, Trezel P, Bassard S, Lefebvre V, Van Wuytswinkel O, Guillaume A, Pau-Roblot C, et al (2020) Three novel rhamnogalacturonan I- pectins degrading enzymes from Aspergillus aculeatinus: Biochemical characterization and application potential. Carbohydr Polym **248**: 116752

Limberg G, Körner R, Buchholt HC, Christensen TMIE, Roepstorff P, Mikkelsen JD (2000) Analysis of different de-esterification mechanisms for pectin by enzymatic fingerprinting using endopectin lyase and endopolygalacturonase II from A. Niger. Carbohydr Res **327**: 293–307

Lionetti V, Fabri E, De Caroli M, Hansen AR, Willats WGT, Piro G, Bellincampi D (2017) Three pectin methylesterase inhibitors protect cell wall integrity for arabidopsis immunity to Botrytis. Plant Physiol **173**: 1844–1863

Liu N, Ma X, Sun Y, Hou Y, Zhang X, Li F (2017) Necrotizing activity of Verticillium dahliae and Fusarium oxysporum f. Sp. Vasinfectum endopolygalacturonases in cotton. Plant Dis **101**: 1128–1138

Mandelc S, Javornik B (2015) The secretome of vascular wilt pathogen Verticillium albo-atrum in simulated xylem fluid. Proteomics **15**: 787–797

Markovič O, Cederlund E, Griffiths WJ, Lipka T, Jörnvall H (2002) Characterization of carrot pectin methylesterase. Cell Mol Life Sci **59**: 513–518

Markovič O, Janeček Š (2001) Pectin degrading glycoside hydrolases of family 28: sequence-structural features, specificities and evolution. Protein Eng Des Sel **14**: 615–631

Markovič O, Jörnvall H (1992) Disulfide bridges in tomato pectinesterase: Variations from pectinesterases of other species; conservation of possible active site segments. Protein Sci **1**: 1288–1292

Mercadante D, Melton LD, Jameson GB, Williams MAK (2014) Processive pectin methylesterases: The role of electrostatic potential, breathing motions and bond cleavage in the rectification of brownian motions. PLoS One **9**: 1–11

Miller GL (1959) Use of Dinitrosalicylic Acid Reagent for Determination of Reducing Sugar. Anal Chem **31**: 426–428

Mitchell DB, Vogel K, Weimann BJ, Pasamontes L, Van Loon APGM (1997) The phytase subfamily of histidine acid phosphatases: Isolation of genes for two novel phytases from the fungi Aspergillus terreus and Myceliophthora thermophila. Microbiology **143**: 245–252

Mohnen D (2008) Pectin structure and biosynthesis. Curr Opin Plant Biol **11**: 266–277

Niture SK (2008) Comparative biochemical and structural characterizations of fungal polygalacturonases. Biologia (Bratisl) **63**: 1–19

Pagès S, Heijne WHM, Kester HCM, Visser J, Benen JAE (2000) Subsite mapping of Aspergillus niger endopolygalacturonase II by site-directed mutagenesis. J Biol Chem **275**: 29348–29353

Pan X, Tu T, Wang L, Luo H, Ma R, Shi P, Meng K, Yao B (2014) A novel low-temperature-active pectin methylesterase from Penicillium chrysogenum F46 with high efficiency in fruit firming. Food Chem **162**: 229–234

Park K-C, Kwon S-J, Kim P-H, Bureau T, Kim N-S (2008) Gene structure dynamics and divergence of the polygalacturonase gene family of plants and fungus. Genome **51**: 30–40

Pogorelko G, Lionetti V, Fursova O, Sundaram RM, Qi M, Whitham SA, Bogdanove AJ, Bellincampi D, Zabotina OA (2013) Arabidopsis and Brachypodium distachyon transgenic plants expressing Aspergillus nidulans acetylesterases have decreased degree of polysaccharide acetylation and increased resistance to pathogens. Plant Physiol **162**: 9–23

Van Pouderoyen G, Snijder HJ, Benen JAE, Dijkstra BW (2003) Structural insights into the processivity of endopolygalacturonase I from Aspergillus niger. FEBS Lett **554**: 462–466

Ralet MC, Crépeau MJ, Buchholt HC, Thibault JF (2003) Polyelectrolyte behaviour and calcium binding properties of sugar beet pectins differing in their degrees of methylation and acetylation. Biochem Eng J **16**: 191–201

Remoroza C, Wagenknecht M, Buchholt HC, Moerschbacher BM, Gruppen H, Schols HA (2015) Mode of action of Bacillus licheniformis pectin methylesterase on highly methylesterified and acetylated pectins. Carbohydr Polym **115**: 540–550

Rexova-Benkova L (1973) The Size of the Substrate-Binding Site of an Aspergillus niger Extracellular Endopolygalacturonase. Eur J Biochem **39**: 109–115

Ridley BL, O'Neill MA, Mohnen D (2001) Pectins: structure, biosynthesis, and oligogalacturonide-related signaling. Phytochemistry **57**: 929–967

Sassi AH, Tounsi H, Trigui-Lahiani H, Bouzouita R, Romdhane Z Ben, Gargouri A (2016) A low-temperature polygalacturonase from P. occitanis: Characterization and application in juice clarification. Int J Biol Macromol **91**: 158–164

Savary BJ, Hotchkiss AT, Cameron RG (2002) Characterization of a salt-independent pectin methylesterase purified from Valencia orange peel. J Agric Food Chem **50**: 3553–3558

Silva JDC, de França PRL, Converti A, Porto TS (2019) Pectin hydrolysis in cashew apple juice by Aspergillus aculeatus URM4953 polygalacturonase covalently-immobilized on calcium alginate beads: A kinetic and thermodynamic study. Int J Biol Macromol **126**: 820–827

Søndergaard CR, Olsson MHM, Rostkowski M, Jensen JH (2011) Improved treatment of ligands and coupling effects in empirical calculation and rationalization of p K a values. J Chem Theory Comput **7**: 2284–2295

Tan H, Yang G, Chen W, Liu Q, Li K, Yin H (2020) Identification and characterization of thermostable endo- polygalacturonase II B from Aspergillus luchuensis. J Food Biochem **e13133**: 1–11

Tanaka Y, Suzuki T, Nakamura L, Nakamura M, Ebihara S, Kurokura T, Iigo M, Dohra H, Habu N, Konno N (2019) A GH family 28 endo-polygalacturonase from the brown-rot fungus Fomitopsis palustris: Purification, gene cloning, enzymatic characterization and effects of oxalate. Int J Biol Macromol **123**: 108–116

Vicente CSL, Nemchinov LG, Mota M, Eisenback JD, Kamo K, Vieira P (2019) Identification and characterization of the first pectin methylesterase gene discovered in the root lesion nematode Pratylenchus penetrans. PLoS One **14**: 1–19

Voxeur A, Habrylo O, Guénin S, Miart F, Soulié MC, Rihouey C, Pau-Roblot C, Domon JM, Gutierrez L, Pelloux J, et al (2019) Oligogalacturonide production upon Arabidopsis thaliana-Botrytis cinerea interaction. Proc Natl Acad Sci U S A **116**: 19743–19752

de Vries JA, Rombouts FM, Voragen AGJ, Pilnik W (1984) Comparison of the structural features of apple and citrus pectic substances. Carbohydr Polym **4**: 89–101

Wade RC, Gabdoulline RR, De Rienzo F (2001) Protein interaction property similarity analysis. Int J Quantum Chem **83**: 122–127

Wang J, Cieplak P, Kollman PA (2000) How Well Does a Restrained Electrostatic Potential (RESP) Model Perform in Calculating Conformational Energies of Organic and Biological Molecules? J Comput Chem **21**: 1049–1074

Yang Y, Yu Y, Liang Y, Anderson CT, Cao J (2018) A Profusion of Molecular Scissors for Pectins: Classification, Expression, and Functions of Plant Polygalacturonases. **9**: 1–16

Zhang Z, Dong J, Zhang D, Wang J, Qin X, Liu B, Xu X, Zhang W, Zhang Y (2018) Expression and characterization of a pectin methylesterase from Aspergillus niger ZJ5 and its application in fruit processing. J Biosci Bioeng **126**: 690–696

3. Chapter – Structural and biochemical characterization of an unusual pectin/pectate lyase from *Verticillium dahliae*

As previously mentioned, HG is modified in the cell wall by a set of dedicated enzymes that control their degree of polymerization (PG and PLL), methylesterification (PME) and acetylation (PAE). Therefore, in addition to determining the biochemical specificities of plant and fungal PME/PGs there is a need in characterizing PLL. For this purpose, we have expressed a PLL from *V. dahliae* (VdPelB) in heterologous system, purified the protein and demonstrated that VdPelB possess unusual biochemical characteristics, acting both on pectate and on pectins of high degree of methylesterification. We used LC-MS/MS profiling of digestions products on commercially available pectins and flax root pectins to determine the mode of action of VdPelB. To understand the structural determinants of such peculiar activity, we solved the first 3D structure of VdPelB, shedding new light of amino-acids that might be responsible for the activity on both substrates;

Results are formatted as a manuscript for submission to *Journal of Biological Chemistry*.

Additional data are reported in **Annex 10** to **Annex 13**.

Authors list

Josip Safran[1], Olivier Habrylo[1], Julie Bouckaert[2], Roland Molinié[1], Jean-Xavier Fontaine[1], Serge Pilard[3], Aline Voxeur[4], Corinne Pau-Roblot[1], Fabien Sénéchal[1], Jérôme Pelloux[1]

[1]: UMRT INRAE 1158 BioEcoAgro – BIOPI Biologie des Plantes et Innovation, SFR Condorcet FR CNRS 3417, Université de Picardie, 33 Rue St Leu, 80039 Amiens, France. [2] : UMR 8576 Unité de Glycobiologie Structurale et Fonctionnelle (UGSF) IRI50, Avenue de Halley, 59658 Villeneuve d'Ascq, France. [3]: Plateforme Analytique, Université de Picardie, 33, Rue St Leu, 80039 Amiens, France. [4]: Institut Jean-Pierre Bourgin, INRAE, AgroParisTech, Université Paris-Saclay, 78000 Versailles, France.

Corresponding author: Jérôme Pelloux (jerome.pelloux@u-picardie.fr)

3.1. Abstract

Pectins, which are complex polysaccharides and major components of the primary cell wall, can be degraded by pectate lyase-like (PLLs). PLLs can cleave glycosidic bonds of homogalacturonans (HG), the main pectic domain, by β-elimination, releasing unsaturated oligogalacturonides (OGs). To understand the catalytic mechanism and substrate/function of these enzymes, we characterized one PLL (VdPelB) from *Verticillium dahliae*, a plant pathogen, after its expression in *Pichia pastoris*. We showed that VdPelB has a dual pectin-pectate lyase activity, being most active, on both non-methylesterified and highly methylesterified pectins, at alkaline pH in presence of Ca^{2+} ions. OGs released were distinct to that of Aspergillus pectate lyase. To understand the structural determinants of this peculiar specificity, we solved the 3D structure of VdPelB at 1.2Å resolution. VdPelB consists of 9 complete coils of right-handed parallel β-helix, which is formed by three parallel sheets extending along the longitudinal axis. Loop regions form a tunnel-like cleft on the outer part of the β-helix, flanking the active site. The amino acids involved in the active site were determined by comparing VdPelB structure with homologous structures of PLLs in complex with substrate. This first structure of *V. dahliae* pectin-pectate lyase undoubtedly provides explanation for its dual activity, and for the release of specific OGs. By comparing OGs released from *Verticillium*-partially tolerant and sensitive flax cultivars, our study provides new insights into the enzymatic arms race between plant and pathogens, and could facilitate the identification of novel elicitors of defence responses.

Keywords: *Verticillium dahliae*, pectins, homogalacturonan, pectin-pectate lyase, oligogalacturonides.

3.2. Introduction

Primary cell wall, a complex structure of proteins, cellulose and hemicellulose, is embedded in a pectin matrix. Pectins, are the most complex polysaccharides composing up to 30% of cell wall dry mass in dicotyledonous species (Ridley et al., 2001). Pectin is mainly constituted of homogalacturonan (HG), rhamnogalacturonan I (RG-I) and rhamnogalacturonan II (RG-II) domains, but its composition can differ between plant organs and species. The most abundant pectic domain is HG, a linear homopolymer of α-1,4-linked galacturonic acids (GalA), which represents up to 65% of pectins (Mohnen, 2008). During synthesis, HG can be O-acetylated at O-2 or O-3 and/or methylesterified at C-6 carboxyl, before being exported at the cell wall with a degree of methylesterification (DM) of 80% and a degree of acetylation (DA) of 5~10%, depending on species. At the wall, HG chains can be modified by different enzyme families, including pectin acetylesterase (PAEs; CE13, EC 3.1.1.6), pectin methylesterases (PMEs; CE8, EC 3.1.1.11), polygalacturonases (PGs; GH28, EC 3.2.1.15, EC 3.2.1.67, EC 3.2.1.82), and Pectate Lyase-Like (PLLs), which comprise pectate lyases (PLs; endo-PLs, EC 4.2.2.2 and exo-PLs, 4.2.2.9) and Pectin Lyases (PNLs; endo-PNL, EC 4.2.2.10). All of these enzymes are produced by plants to fine-tune pectins during development (Pelloux et al., 2007; Nocker and Sun, 2010; Xiao et al., 2014; Sénéchal et al., 2015; Rui et al., 2017), but they are also secreted by most of phytopathogenic bacteria and fungi during plant infection (Jayani et al., 2005; Kars et al., 2005; Jolie et al., 2010; Voxeur et al., 2019). PMEs and PAEs hydrolase the O6-ester and O2-acetylated linkages which can makes HG more susceptible for PG- and PLL-mediated degradation (Limberg et al., 2000). PLLs are pectolytic enzymes that cleave the HG by β-elimination mechanism leading to the formation of an unsaturated C4-C5 bond (Mayans et al., 1997) and they can be divided into two subfamilies depending on their biochemical specificities: i) PLs, that are mostly produced by bacteria, have a high affinity for non- or low-methylesterified pectins, and an optimal pH near 8.5. Their activity requires Ca^{2+} ions. ii) PNLs are most active on high DM pectins and at acidic pHs, Ca^{2+} being dispensable for their activity (Yadav et al., 2009). Both type of enzymes can degrade HG chains, thus releasing oligogalacturonides (OGs), but their mode of action can differ: For PL both endo and exo modes of action have been described, while only endo-PNL have been characterised so far (Sénéchal et al., 2014). For the latter, it was notably showed that endo-PNLs from Aspergillus sp., *B. fuckeliana* and *A. parasiticus* can first release OGs of degree of polymerisation (DP) 5–7 that are subsequently used as substrates to generate OGs of DP3 and DP4

as end-products (Voxeur et al., 2019; Yang et al., 2020; Zeuner et al., 2020). While having the same DP, depending on the enzymes' specificities, the final products can differ in their degrees and patterns of methylesterification (DM), implying potential differences in substrate recognition and binding, and therefore in PNL/PL structures. Several structures of bacterial and fungal PLLs have been reported (Yoder et al., 1993; Pickersgill et al., 1994; Lietzke et al., 1996b; Mayans et al., 1997; Vitali et al., 1998; Akita et al., 2001). PLL structures resemble to that of a published PME, PGs and rhamnogalacturonan lyases (Cho et al., 2001; Johansson et al., 2002; Luis et al., 2018) and are composed of three parallel β-sheets composing right handed parallel β-helix. Three β-sheets are called PB1, PB2 and PB3 and the turns connecting them T1, T2 and T3 (Petersen et al., 1997). The active site is formed by three Asp, situated on PB1 β-sheet and, in the case of PLs, it accommodates Ca^{2+} (Scavetta et al., 1999). In PNLs Ca^{2+} is replaced by Asp (Mayans et al., 1997). In addition, the PL binding site is dominated by charged acidic and basic residues (Glu, Lys, Arg) which can overall accommodate negatively-charged pectate substrates. In contrast, PNL binding site is dominated by aromatic residues (Mayans et al., 1997; Scavetta et al., 1999), which have less affinity for low-methylesterified pectins.

Verticillium dahliae Kleb. A soil-borne vascular fungus, is becoming widespread among fiber flax, causing Verticillium wilt disease (Blum et al., 2018). Up to now, there is no effective chemical control against the pathogen. *V. dahliae* infects plants by piercing the root surface using hyphae and, during this process, a number of pectinolytic enzymes are secreted, including thirty PLLs. Considering the role of PLLs in determining pathogenicity, it is of paramount importance to determine their biochemical and structural properties (Duressa et al., 2013; Blum et al., 2018; Yang et al., 2018). This could allow engineering novel strategies to control, or inhibit, the pathogen's pectinolytic enzymes. For this purpose, we characterized one *V. dahliae* PLL (VdPelB, VDAG_04718) after its heterologous expression in *Pichia pastoris*. We showed that it had a surprising pectin-pectate lyase activity and that it released specific OGs from either commercially-available pectins or flax roots cell walls. The obtention of the 3D structure of VdPelB after X-ray diffraction of crystals allowed determining the amino acids (AA) that are likely involved in generating the dual pectin-pectate lyase activity.

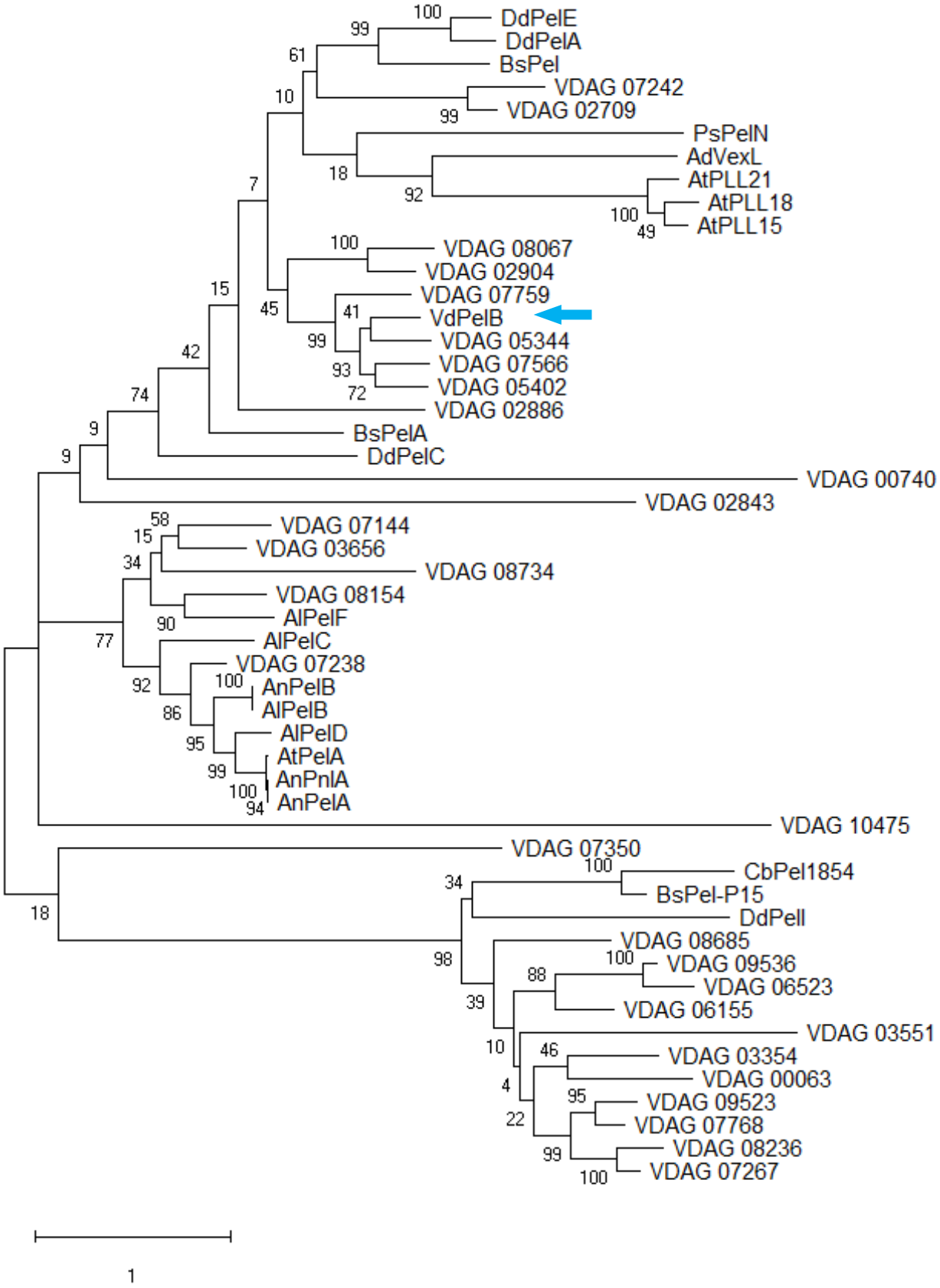
DdPelE
DdPelA
BsPel
VDAG 07242
VDAG 02709
PsPelN
AdVexL
AtPLL21
AtPLL18
AtPLL15
VDAG 08067
VDAG 02904
VDAG 07759
VdPelB
VDAG 05344
VDAG 07566
VDAG 05402
VDAG 02886
BsPelA
DdPelC
VDAG 00740
VDAG 02843
VDAG 07144
VDAG 03656
VDAG 08734
VDAG 08154
AlPelF
AlPelC
VDAG 07238
AnPelB
AlPelB
AlPelD
AtPelA
AnPnlA
AnPelA
VDAG 10475
VDAG 07350
CbPel1854
BsPel-P15
DdPell
VDAG 08685
VDAG 09536
VDAG 06523
VDAG 06155
VDAG 03551
VDAG 03354
VDAG 00063
VDAG 09523
VDAG 07768
VDAG 08236
VDAG 07267
1

Figure 33. Phylogenetic analysis of *V. dahliae* VdPelB with selected PLLs
V. dahliae VdPelB (VDAG_04718, G2X3Y1) was compared with PLLs from Verticillium [VDAG_00740 (G2WQU8), VDAG_02904 (G2WXC5), VDAG_05344 (G2X628), VDAG_07242 (G2XBA4), VDAG_07759 (G2XC77), VDAG_02709 (G2WWT0), VDAG_02843 (G2WX64), VDAG_02886 (G2WXA7), VDAG_03656 (G2X1P5), VDAG_05402 (G2X597), VDAG_07144 (G2X9U9), VDAG_07238 (G2XBA0), VDAG_07566 (G2XBY8), VDAG_08067 (G2XD35), VDAG_08154 (G2XDC2), VDAG_08734 (G2XF02), VDAG_10475 (G2XJZ3), VDAG_03354 (G2WZB2), VDAG_03551 (G2WZV9), VDAG_07267 (G2XBC9), VDAG_07768 (G2XC86), VDAG_08236 (G2XDK4), VDAG_06155 (G2X8L4), VDAG_06523 (G2X7R5), VDAG_08685 (G2XEV0), VDAG_09523 (G2XH91), VDAG_09536 (G2XHA4), VDAG_00063 (G2WR80), VDAG_07350 (G2XGG7)], *Arabidopsis thaliana* [AtPLL15 (At5g63180), AtPLL18 (At3g27400), AtPLL21 (At5g48900)], *Dickeya dadanti* [DdPelA (P0C1A2), DdPelC (P11073), DdPelE (P04960), DdPelI (O50325)], *Bacillus subtilis* [BsPel (P39116)], *Bacillus Sp*. KSM-P15 [BsPel-P15 (Q9RHW0)], *Bacillus sp*. N16-5 [BsPelA (D0VP31)], *Aspergillus niger* AnPelA [(Q01172), AnPelB (Q00205), AnPnlA (A2R3I1)], *Achromobacter denitrificans* [AdVexL (A0A160EBC2)], *Aspergillus tubingensis* [AtPelA (A0A100IK89)], *Aspergillus luchuensis* [AlPelB (G7Y0I4)], *Acidovorax citrulli* [AcPel343, (A1TSQ3)], *Paenibacillus sp.* 0602 [PsPelN (W8CR80)], *Caldicellulosiruptor bescii* [CbPel1854 (B9MKT4)]. Maximum likelihood tree was constructed with 1000 bootstrap replicates. Scale indicates 0.1 distance from the root of the tree. Uniprot and TAIR IDs were used.

3.3. Results and Discussion

3.3.1. Sequence and phylogeny analysis

In addition to 9 PGs (polygalacturonases) and 4 PMEs (pectin methylesterases), *V. dahliae* encodes 30 putative endo-pectate lyases (EC 4.2.2.2), exo-pectate lyases (EC 4.2.2.9), endo-pectin lyases (EC 4.2.2.10), belonging to PL1-PL3 and PL9 families, respectively (Klosterman et al., 2011). Fifty-five AA sequences encoding putative PLLs, belonging to bacteria, fungi and plants were analysed and a phylogenetic tree was built (**Figure 33,** Kumar et al., 2018). Several different clades can be distinguished. *V. dahliae* PelB (VdPelB, VDAG_04718) clustered with VDAG_05344 (59.68% sequence identity) with close relations to VDAG_05402 (57.19% sequence identity) and VDAG_07566 (56.95% sequence identity). VDAG_05402 and VDAG_05344, that are found in the protein secretome, have orthologues in *Verticillium alfalfa* (VDBG_07839 and VDBG_10041), which were shown to possess putative lyase activity (Duressa et al., 2013; Mandelc and Javornik, 2015). Plant PLLs from *Arabidopsis thaliana* (AtPLL21, AtPLL15 and AtPLL18) formed a separate clade with a close connection to *Achromobacter denitrificans* (AdVexL), a PLL homologue (Liston et al., 2018). *Dickeya dadanti* (DdPelI), Bacillus Sp. KSM-P15 (BsPel-P15)

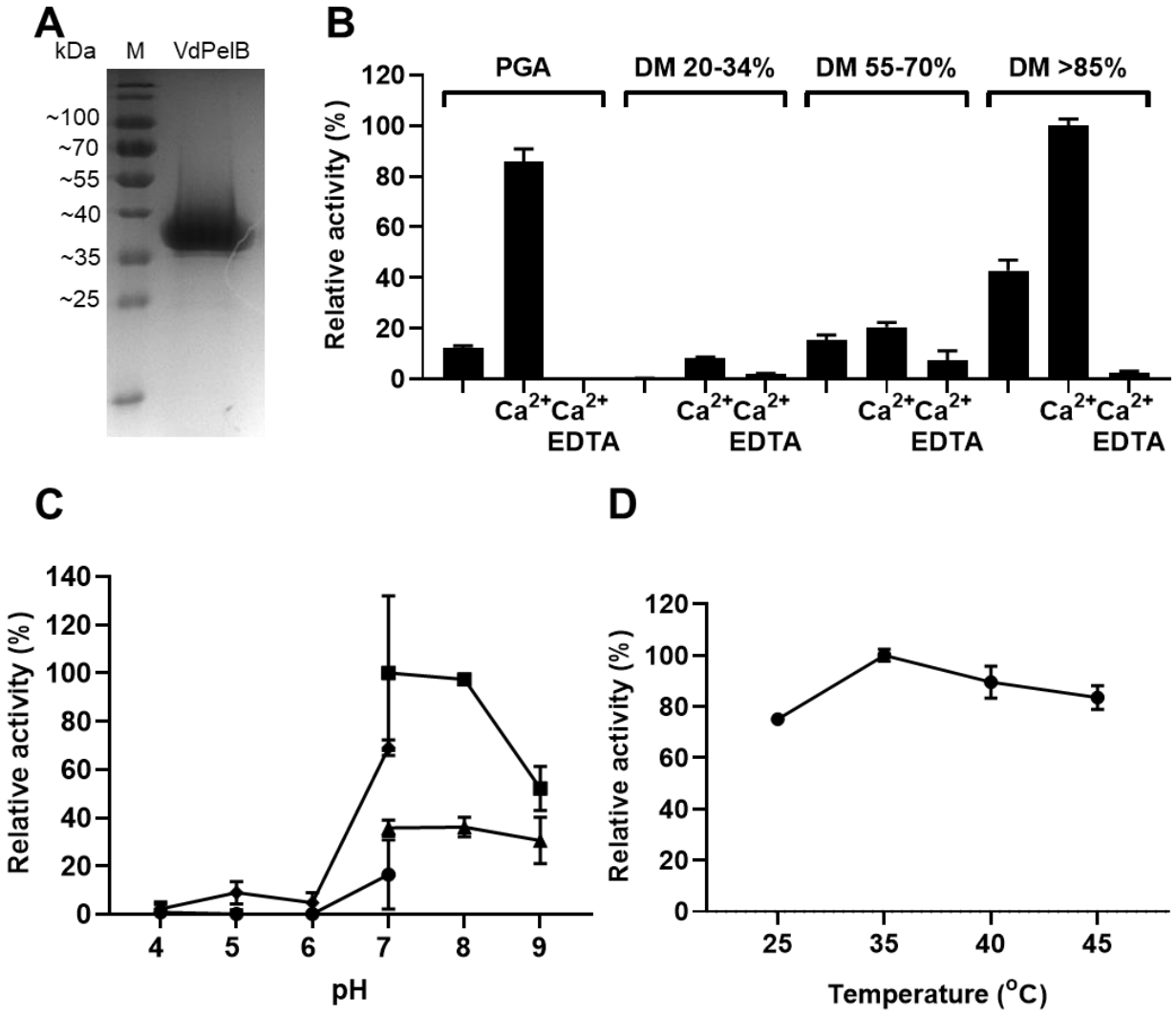

Figure 34. Purification and biochemical characterization of VdPelB
A) SDS-PAGE analysis of VdPelB B) Substrate-dependence of VdPelB activity. The activities were measured after 12 min of incubation with PGA, pectins DM 24-30%, DM 55-70%, DM>85% with/without addition of Ca^{2+}or Ca^{2+} and EDTA, at 40°C. C) pH-dependence of VdPelB activity. The activities were measured after 12 min of incubation with PGA (circles McIlvaine buffer, triangles Tris-Hcl buffer) and pectins of DM >85% (romboides McIlvaine buffer, squares Tris-Hcl buffer, at 40°C. D) Temperature-dependence of VdPelB activity. The activities were measured after 12 min of incubation with DM>85% at pH7. Values correspond to means and standard errors with n=3.

and *Caldicellulosiruptor bescii* (CbPel1854) formed separate clade with BsPel, DdPelA and DdPelC. The clade corresponding to PNLs consisted of *A. tubingensis* PelA (AtPelA), *Aspergillus niger* AnPelA, AnPnlA and AnPelB. *A. luchuensis* AlPelB was closely related to VDAG_07238 and VDAG_08154 which were indeed annotated as putative PNLs (Klosterman et al., 2011; Zeuner et al., 2020). VDAG_06155 was previously named VdPel1 and was previously characterized as a pectate lyase (Yang et al., 2018).

3.3.2. Cloning, expression and purification of VdPelB

The *VdPelB* (*VDAG_04718*) gene consists of 1 single exon of 1002 bp length. The coding sequence, minus the putative signal peptide was PCR-amplified using gene-specific primers, ligated in pPICZαB vector and expressed in *P. pastoris* heterologous expression system, allowing its secretion in the culture media. Secreted VdPelB consisted of 343 AA, including the poly-histidine tag at the C-terminus used for affinity chromatography purification. After purification, VdPelB had an apparent mass of ~38 kDa (**Figure 34A**), which is higher than what predicted on the basis of the AA sequence (33.8 kDa). However, this shift is likely to correspond to the tags (His and C-myc) and to the presence of 19 putative O-glycosylation sites predicted by the NetOGlyc 4.0 Server.

3.3.3. Biochemical characterization of VdPelB

We first determined VdPelB activity by the formation of 4,5-unsaturated OGs which can be detected at 235 nm using UV spectrophotometer. Four substrates with different DM were tested (**Figure 34B**). VdPelB was most active on citrus pectin of high DM (>85%) in the presence of 0.5 mM $CaCl_2$. Without Ca^{2+} ions the activity was 42% of the maximum while, with the addition of EDTA as a chelating agent, it was only 2.4% of the maximum, confirming the calcium-dependent activity of the enzyme (Mayans et al., 1997). Activity measured in absence of added $CaCl_2$ reflects the presence of calcium from the culture media that is bound to VdPelB during production. We tested the effects of increasing $CaCl_2$ concentrations and showed that the maximum activity was already reached when using as low as 0.125 µM (**Figure S20**). Surprisingly, the second-best substrate was polygalacturonic acid (PGA), for which the relative activity of VdPelB was 85% of the maximum in presence of Ca^{2+}ions. Without added $CaCl_2$, the activity was only 12% of the maximum, and in presence of EDTA no activity was detected. On pectins of moderate DM (55-70%) and low DM (20-34%), and in presence of $CaCl_2$, only 20% and 8% of the maximum activity

were detected, respectively. Thus, PGA and citrus pectin DM>85% were used as substrate to test the pH-dependence of the enzyme's activity in McIlvaine and Tris-HCl buffers (**Figure 34C)**. VdPelB was most active on DM>85% at pH 7, with only a slight decrease in activity at pH 8 (97%). In contrast, at pH 9, the relative activity was 52% of the maximum while at pH 4-6 it was close to null. At pH 7, using PGA, the relative activity was 69 % of the maximum. The pH optimum for VdPelB was close to that reported for *Dickeya dadantii* PelN (pH 7.4, Hassan et al., 2013), but was lower to that measured for *Bacillus clausii* Pel (pH 10.5, Zhou et al., 2017) and *Botryotinia fuckeliana* Pel (pH 8, Chilosi and Magro, 1997). In contrast, the pH optimum was higher compared to five PNL from Aspergillus sp. AaPelA (pH 6.1), AtPelA (pH 4.5), AtPelA (pH 6.4), AtPelD (pH 4.3, Zeuner et al., 2020) and *Aspergillus parasiticus* Pel (pH 4, Yang et al., 2020). We next tested the optimum temperature. We showed that the activity, measured on pectins DM>85% was rather stable, with a maximum relative activity at 30°C, and 75% and 89% of maximum activity at 20 and 40°C, respectively (**Figure 34D**). VdPelB appeared less heat-tolerant as compared to other thermophilic PLL reported from Bacillus sp. RN1 90°C (Sukhumsiirchart et al., 2009), *B. clausii* Pel, 70°C (Zhou et al., 2017), *B. subtilis* Pel168, 50°C (Zhang et al., 2013). However, its optimum temperature is in the range of that measured for *Xanthomonas campestris* Pel (Yuan et al., 2012) and cold-active Pel1 from *Massilia eurypsychrophila* (Tang et al., 2019).

PLLs can generally be divided into two groups, regarding their substrate and pH specificities: PNLs and PLs. PNL have optimal activity for acidic pH on moderate to high DM pectins, while PL have better activity for pectate, polygalacturonic acid, at alkaline pH with Ca^{2+}-dependency (PGA, Henrissat et al., 1995; Mayans et al., 1997; Dubey et al., 2016). VdPelB thus appears to have dual biochemical properties, in between PNL and PL. Recently, several reports described PNL/PL with dual biochemical properties: *D. dadanti* PelN is most active at pH 7.4 on PGA but have >50% residual activity on pectins DM 91% (Hassan et al., 2013). In addition, *Bacillus sp.* Pel-22, Pel-66, and Pel-90 have their maximum activities on pectins of DM 7% but had 40% to 70% residual activities on pectins DM 75% (Ouattara et al., 2010). *Humicola insolens* PLHY1 had a strong activity on PGA and on apple pectins DM 50-70 and 70-75% at pH 10 (Wang et al., 2020) which appeared similar to that described for *Bacillus sp.* (highest activity at pH 10 using PGA and citrus pectin DM 89%, Soriano et al., 2000). If, in the two latter cases, high pH could induce spontaneous demethylesterification that would create demethylesterified substrates favourable for the enzyme's activity, this is highly unlikely for VdPelB in our assay conditions at pH 7 (Brown et al., 2001).

Table 7. List of oligogalacturonides identified by LC-MS/MS analysis

For each OG, elemental composition, retention time (RT) and ion mass used for the analysis are highlighted. In the case of detection of mono and di-charged OGs, the *italicized* and **BOLD** mass, corresponding to the more intense ion, was used for the quantification. * indicate non-insaturated OGs.

Name	Elemental composition	RT (min)	$[M-2H]^-$	$[M-2H]^{2-}$
GalA1*	C6H10O7	9.3	193.0353763	
GalA1Ac2	C10H12O8	9.1	259.045941	
GalA2*	C12H18O13	8.88	369.0674644	
GalA2	C12H16O12	8.95	351.0568997	
GalA2Ac2	C16H20O14	8.67	435.0780291	
GalA2Me1*	C13H20O13	8.85	383.0831145	
GalA2Me1	C13H18O12	8.92	365.0725498	
GalA3*	C18H26O19	8.56	545.0995525	
GalA3	C18H24O18	8.61	527.0889878	
GalA3Ac1	C20H26O19	8.59	569.0995525	
GalA3Me1	C19H26O18	8.56	541.1046379	
GalA3Me2*	C20H30O19	8.62	573.1308527	
GalA4*	C24H34O25	8.27	721.1316406	
GalA4	C24H32O24	8.33	***703.1210759***	351.0568997
GalA4Ac1	C26H34O25	8.31	745.1316406	
GalA4Me1*	C25H36O25	8.37	735.1472907	
GalA4Me1	C25H34O24	8.32	***717.136726***	358.0647248
GalA4Me2	C26H36O24	8.3	731.1523761	
GalA5*	C30H42O31	8.04	897.1637287	
GalA5	C30H40O30	8.09	***879.153164***	439.0729438
GalA5Ac1	C32H42O31	8.09	921.1637287	
GalA5Me1*	C31H44O31	8.11	***911.1793788***	455.0860512
GalA5Me1	C31H42O30	8.13	***893.1688141***	446.0807688
GalA5Me2*	C32H46O31	8.13	925.1950289	
GalA5Me2	C32H44O30	8.03	907.1844642	***453.0885939***
GalA6*	C36H50O37	7.84		536.0942702
GalA6	C36H48O36	7.82	1055.185252	***527.0889878***
GalA6Me1	C37H50O36	7.92	1069.200902	***534.0968129***
GalA6Me2	C38H52O36	7.83	1083.216552	***541.1046379***
GalA7*	C42H58O43	7.65		624.1103142
GalA7	C42H56O42	7.62	1231.21734	***615.1050318***

Name	Elemental composition	RT (min)	$[M-2H]^-$	$[M-2H]^{2-}$
GalA7Me1	C43H58O42	7.72	1245.23299	***622.1128569***
GalA7Me2*	C44H62O43	7.75		638.1259643
GalA7Me2	C44H60O42	7.72	1259.24864	***629.1206819***
GalA8	C48H64O48	7.45		703.1210759
GalA8Me1*	C49H68O49	7.53		719.1341833
GalA8Me1	C49H66O48	7.52	1421.265078	***710.1289009***
GalA8Me2*	C50H70O49	7.55		726.1420083
GalA8Me2	C50H68O48	7.58	1435.280728	***717.136726***
GalA9*	C54H74O55	7.29		800.1424023
GalA9	C54H72O54	7.3		791.1371199
GalA9Me1	C55H74O54	7.34		798.144945
GalA9Me2	C56H76O54	7.37		805.15277
GalA9Me2	C56H76O54	7.41		805.15277
GalA9Me3	C57H78O54	7.45		812.1605951
GalA10	C60H80O60	7.15		879.153164
GalA10Ac1	C62H82O61	7.29		900.1584463
GalA10Me1	C61H82O60	7.19		886.160989
GalA10Me2*	C62H86O61	7.24		902.1740964
GalA10Me2	C62H84O60	7.24		893.1688141
GalA10Me3	C63H86O60	7.3		900.1766391
GalA11	C66H88O66	7.03		967.169208
GalA11Ac1	C68H90O67	7.14		988.1744904
GalA11Me1	C67H90O66	7.06		974.1770331
GalA11Me2	C68H92O66	7.09		981.1848581
GalA11Me3	C69H94O66	7.14		988.1926832
GalA12Me2	C74H100O72	6.96		1069.200902
GalA12Me3	C75H102O72	6.99		1076.208727
GalA12Me4	C76H104O72	7.0419		1083.216552
GalA13Me2	C80H108O78	6.82		1157.216946
GalA13Me3	C81H110O78	6.86		1164.224771
GalA13Me4	C82H112O78	6.9		1171.232596
GalA14Me3	C87H118O84	6.73		1252.240815
GalA14Me4	C88H120O84	6.77		1259.24864
GalA15Me5	C95H130O90	6.69		1354.272509

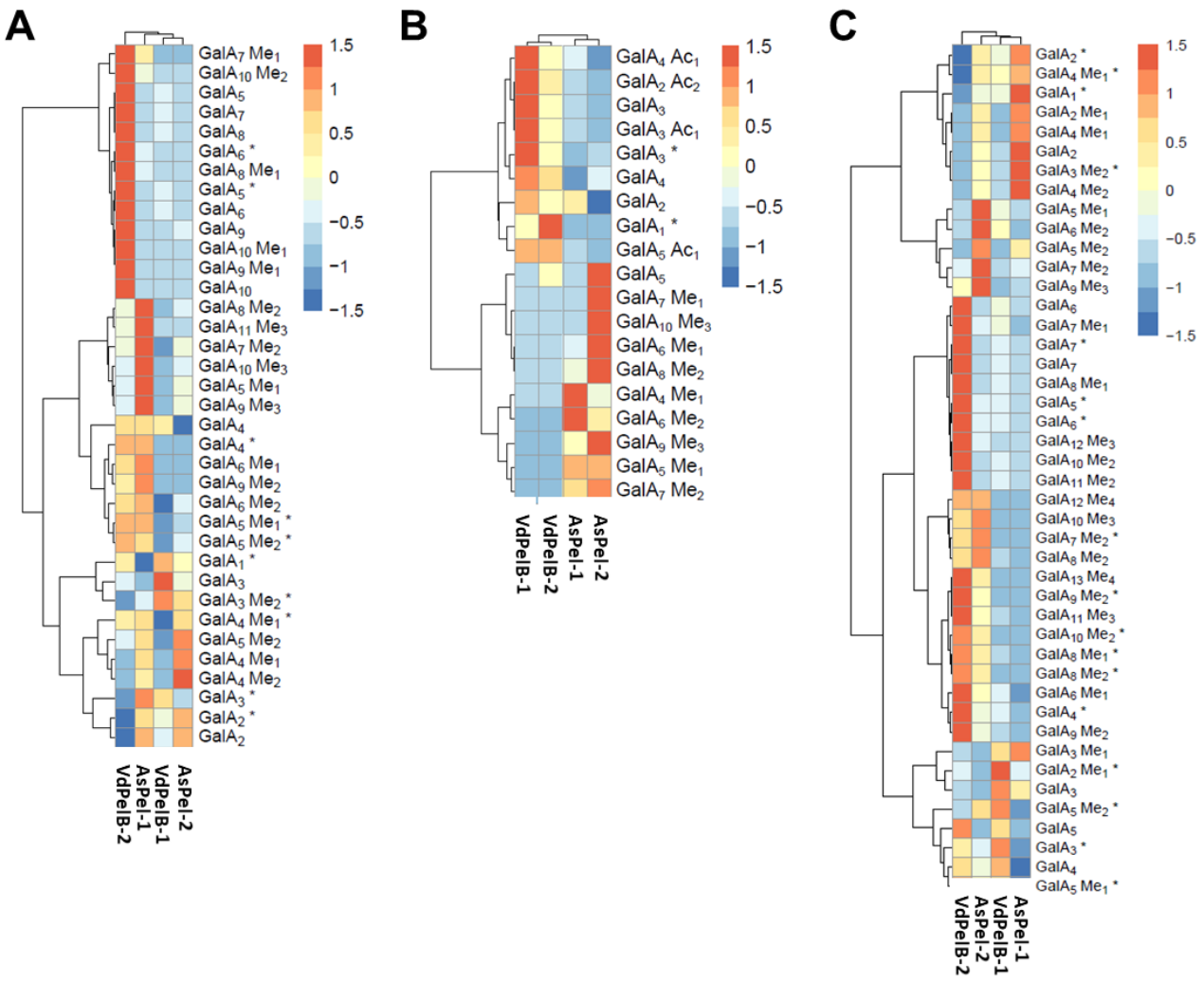

Figure 35. Analysis of OGs produced following action of VdPelB and AsPeI on pectins of various degrees of methylesterification and acetylation

OGs were separated by SEC and analysed by MS/MS. A) Pectins DM 24-30%. B) Sugar beet pectins (DM 42% DA 31%). C) Pectins DM>85%. Substrates were digested overnight at 40°C and pH 7 using iso-activities of VdPelB and AsPel. Enzyme concentrations are stated in Supplemental Table 1. Subscript numbers indicate the DP, DM and DA**.** * indicate non-unsaturated OGs.

VdPelB thus appears to have a dual activity, acting both as an PL and a PNL, suggesting specific structural determinants.

3.3.4. Identification of the OGs released by VdPelB from commercial and cell wall pectins

To further understand the specificity of VdPelB on different substrates, we performed LC-ESI-MS/MS to determine the profile of digestion products (OGs) and to compare with that of commercially available *Aspergillus sp.* Pel (AsPel). To be fully comparable, digestions were realized, for each substrate, at iso-activities for the two enzymes. On the basis of digestion profiles, we identified 48 OGs and created a dedicated library that was used for identification and integration of peaks (**Table 7**). MS^2 fragmentation allowed determining the specificity of the OGs (**Figure S21** and **Figure S22**). OGs released by the two enzymes mainly corresponded to 4,5-unsaturated OGs, which is in accordance with action of PLLs (**Figure 35**). When using pectins DM 20-34% and at low enzyme's concentration (VdPelB-2), VdPelB mainly released unmethylesterified OGs of high DP ($GalA_5$, $GalA_6$, $GalA_7$, $GalA_8$, $GalA_9$, $GalA_{10}$) that were subsequently hydrolysed when using more concentrated VdPelB (VdPelB-1, **Figure 35A**). These digestion products strikingly differed to that generated by AsPel, that are methylesterified OGs of higher DP ($GalA_4Me_1$, $GalA_4Me_2$, $GalA_5Me_1$, $GalA_6Me_2$, $GalA_{11}Me_3$…) showing distinct specificities. Altogether, these first results unequivocally show VdPelB act as an endo-PL (Voxeur et al., 2019), and that its processivity differ to that of AsPel, which act as well as an endo-PL. When using sugar beet pectins, that are known to be highly acetylated (DM 42%, DA 31%), VdPelB released acetylated OGs ($GalA_2Ac_2$, $GalA_3Ac_1$, $GalA_4Ac_1$, $GalA_5Ac_1$), while AsPel showed much lower activity and relative abundance of these OGs (**Figure 35B**). Previous reports have shown that differences exist between PNL, in particular with regards to acetyl substitutions (Zeuner et al., 2020). In contrast, AsPeI released mainly methylesterifed OGs ($GalA_6Me_1$, $GalA_8Me_1$, $GalA_{10}Me_3$…). Finally, the differences between VdPelB and AsPeI were striking following digestions of pectins of DM >85% (**Figure 35C**). At low concentrations, AsPel released more methylesterifed OGs of short DP ($GalA_2Me_1$, $GalA_3Me_1$, $GalA_4Me_1$, $GalA_4Me_2$, $GalA_5Me_2$) while VdPelB generated rather methylesterified OGs of higher DP ($GalA_9Me_2$, $GalA_{10}Me_2$, $GalA_{11}Me_2$, $GalA_{12}Me_2$). Almost all of these OGs were hydrolysed when using more concentrated VdPelB (VdPelB-1) suggesting that methylesterification status does not affect enzyme's activity (Voxeur et al., 2019; Zeuner et al., 2020).

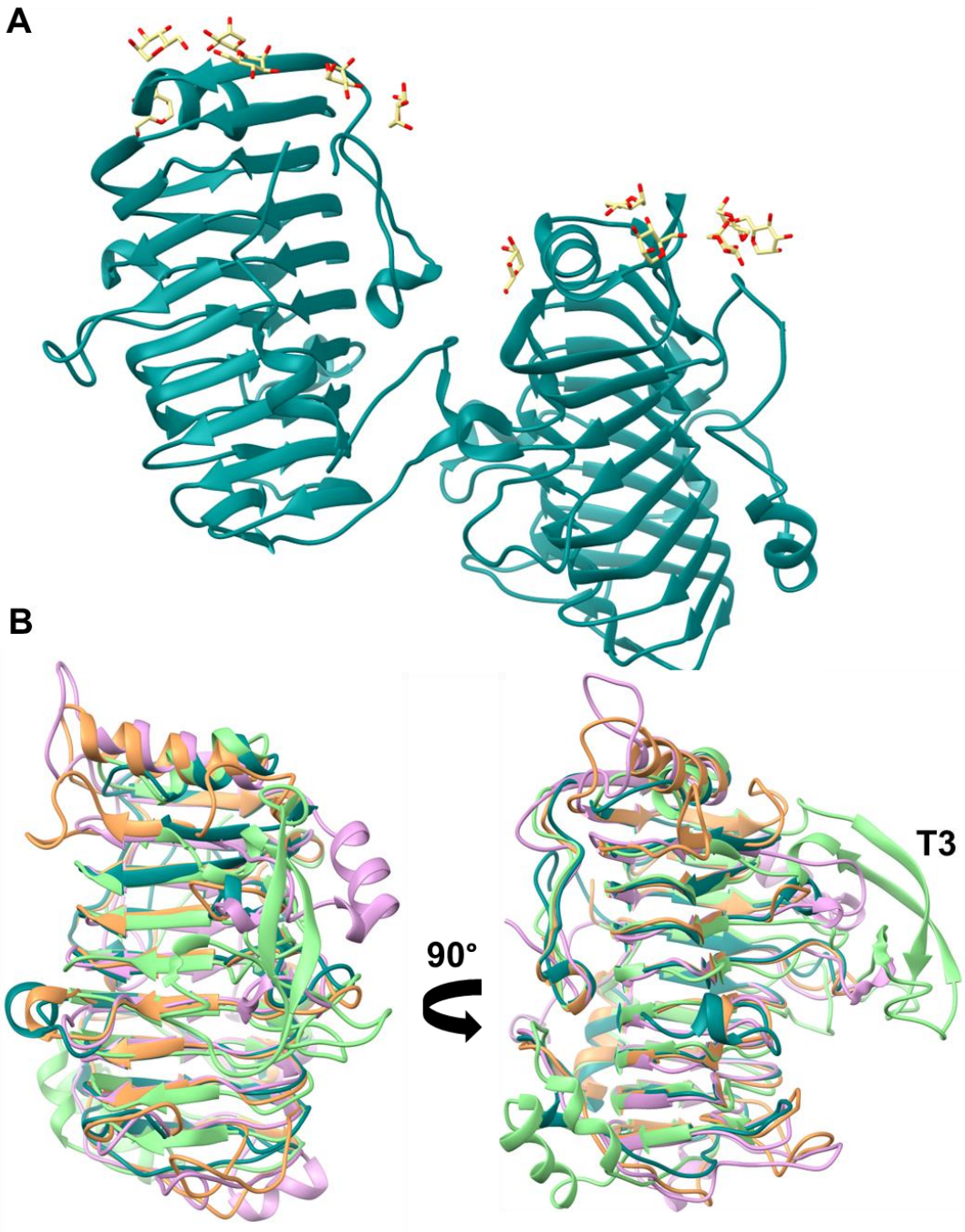

Figure 36. Structure determination of VdPelB and structural alignment
A) Surface and ribbon diagram of VdPelB crystalized in P1 21 1 space group. B) Structural alignement of VdPelB with BsPelA, DdPelC, AnPelA. VdPelB shares highest structural alignment with BsPelA (PDB: 3VMV, orange) with 30.06% sequence identity and rmsd of 1.202 Å. Second best alignment was with DdPelC (PDB: 1AIR, plum) with 24.20% identity and rmsd of 1.453 Å. Pectin lyase withT3 loop described in AnPelA (PDB: 1IDJ, green).

V. dahliae and closely related fungus from the same genus are a known flax pathogen, where they use their enzymatic arsenal, that includes pectin degrading enzymes, for penetrating the host cell leading to infection (Blum et al., 2018). To assess the potential role of VdPelB in flax pathogenicity we digested root cell walls from two flax cultivars, Évéa (Verticillium-partially resistant), and Violin (Verticillium-susceptible), and we compared the OGs released. On root cell walls, VdPelB released mainly unsaturated OGs up to DP5 (**Figure S23**). From similar starting root material, the OG total peak area detected was five times lower for Evéa (black bar) compared to Violin (grey bar), suggesting that it is less susceptible to digestion by VdPelB. OGs released by VdPelB were mainly un-methylesterified but could be acetylated ($GalA_2$, $GalA_3$, $GalA_3Ac_1$, $GalA_4$, $GalA_4Ac_1$ $GalA_5$, $GalA_5Ac_1$), and the abundance of $GalA_3$ and $GalA_4$ was five and fifteen times higher in Violin, respectively. These data together with that obtained from sugar beet pectins strongly suggests that VdPelB preference is for non-methylesterified and acetylated substrates. Our data suggest that cell wall structure differ between the two cultivars and that VdPelB could determine Verticillium pathogenicity thanks to a better degradation of the cell wall pectins of sensitive cultivars (Safran et al., 2021). Similarly, VdPel1 was previously identified as virulence factor, where the deletion of this gene decreased virulence in tobacco, as compared with the wild-type Verticillium (Yang et al., 2018).

3.3.5. Structure determination of VdPelB

To understand the biochemical specificities of VdPelB, we determined its 3D structure following crystallization of the protein. VdPelB crystallised in monoclinic P 1 2_1 1 space group. Four data sets were collected from the same crystal at 1.2 Å resolution and merged. There are two molecules in asymmetric units: chains A and B highly similar with a Cα root mean square deviation (rmsd) value of 0.227 Å (**Figure 36A**). VdPelB structure consists of 298 AAs with 18 AA at the N-terminus and 27 AA at the C-terminus that were not modelled because of poor electron densities. Overall electron densities were well defined. While no N-glycosylation sites could be revealed on VdPelB structure, six O-glycosylation sites carrying mannose are visible for each molecule: Thr22, Thr44, Thr45, Thr46, Ser48 and Thr54, in accordance with the shift in size previously observed. During data acquisition no heating of the crystal was observed, as shown by low B factors and good occupancies (**Figure S24A** and **B**). The final models' geometry, processing and refinement statistics are summarized (**Table S4**). VdPelB structure has been deposited in the Protein Data Bank as entry 7BBV.

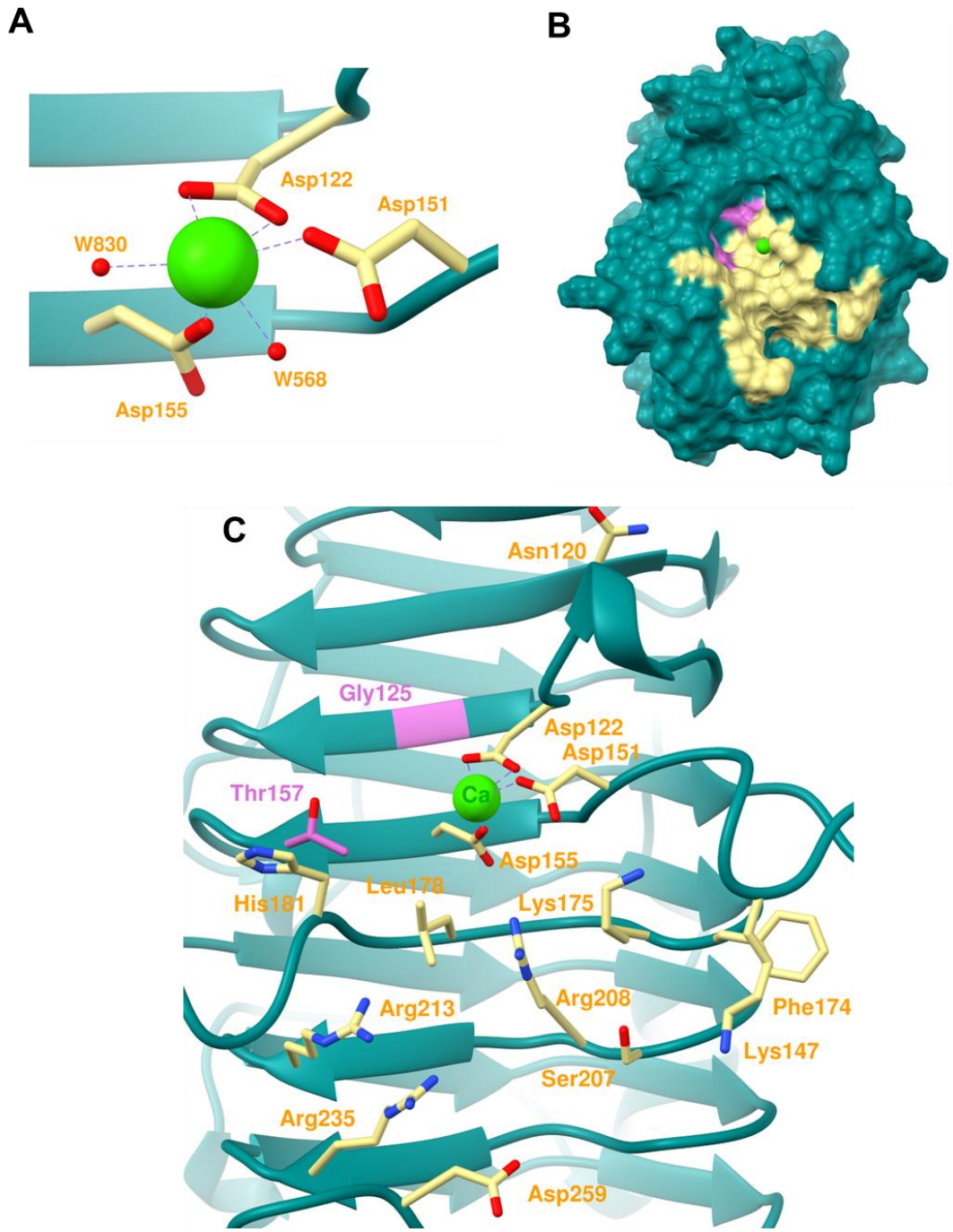

Figure 37. Structure determination of VdPelB

A) Ribbon diagram and licorice of the active site of VdPelB: AA (yellow) and water molecules involved in the binding of Ca^{2+}(green) are highlighted. B) Surface presentation of VdPelB chain A colored in dark cyan. Amino-acids of the binding site characteristics of pectate lyases are shown in yellow while those characteristics of pectin lyase structures are shown in pink. Ca^{2+} is highlighted in green. C) Structure of the active site. AA involved in catalysis and in the binding groove of pectate lyases are yellow-colored. Gly125 and Thr157 are characteristics of pectin lyases. W-water molecule.

3.3.6. Structure comparisons of VdPelB

VdPelB consist of right-handed parallel β-helix fold which is common to pectinases (Jenkins and Pickersgill, 2001). The β-helix is formed by three parallel β-sheets - PB1, PB2 and PB3 which contain 7, 8 and 5 β-strands. On total there are 4 double β-strands, 2 on N-terminus connecting PB3-PB1 and 2 on C-terminus connecting PB2-PB3 (**Figure S25A**). Turns connecting the PB1-PB2, PB2-PB3 and PB3-PB1 β-sheets are named T1-turns, T2-turns and T3-turns according to Yoder and Jurnak (**Figure S25B**, Yoder and Jurnak, 1995). T1 turns consist of 2 up to 14 AA and it builds the loop around the active site on the C-terminus. T2 turns mostly consist of 2 AA with Asn being one of the predominant one, forming an Asn ladder with an exception of an Asn245Thr mutation in VdPelB (Yoder et al., 1993; Mayans et al., 1997). T3 turns have between 2 and 13 AA, including N-terminus loop. VdPelB has a α-helix on N-terminus end that shields the hydrophobic core and is conserved in PLs and PGs (Mayans et al., 1997; van Santen et al., 1999) while the C–terminus end is also protected by tail-like structure carrying one α-helix. Interestingly N- and C-terminus tails pack against PB2. There are only two Cys (Cys25 and Cys137) that do not form a disulphide bridge. The lack of disulphide bridges could be responsible for the lower stability of the enzyme at high temperatures, in comparison with previously reported PNL (Yin et al., 2015). The putative active site is positioned between the T3 and T2 loops.

Sequence and structural alignments show that VdPelB belong to the PL1 family. VdPelB shares the highest structural alignment with BsPelA (PDB: 3VMV, Zheng et al., 2012) with 30.06% sequence identity and a rmsd of 1.202 Å. Second best structural alignment was with DdPelC (PDB: 1AIR, Lietzke et al., 1996) with 24.20% identity and a rmsd of 1.453 Å. Both of these structures lack the long T3 loop described in AnPelA (PDB: 1IDJ, **Figure 36B**, **Figure S26**, Mayans et al., 1997).

3.3.7. Structure of active site

Active site of PLs is well conserved, and it harbours strictly conserved acidic and basic AA required for binding Ca^{2+} (**Figure 37A**). Previously reported structure showed that two Asp, Asp122 and Asp155 and one Arg208 (VdPelB numbering), are absolutely conserved, while Asp151 can be mutated in Glu, or Arg in PNLs (Mayans et al., 1997). Other conserved AA include Lys175 and Arg213 (VdPelB numbering), Lys175 being responsible for binding the carboxyl oxygen while Arg213 hydrogen bonds to C-2 and C-3 of GalA (Henrissat et al., 1995; Scavetta et al., 1999). Mutating any of these AA leads to decrease in enzyme activity (Kita et al., 1996). Ca^{2+} ion is

directly coordinated by Asp122 (two carboxyl oxygen), Asp151, Asp155 and two water molecules (W568 and W830, VdPelB numbering). In DdPelC one more link exist between Asp129 and Ca^{2+}, and the mutation of Asp129 (DcPelC) into Asn121 (VdPelB) could decrease the number of ligand interactions with Ca^{2+} from seven to six (Scavetta et al., 1999). In addition, one mutation in BsPelA, Asp122Thr (VdPelB numbering) is responsible for reduced affinity for Ca^{2+} (**Figure 37A**, Zheng et al., 2012). In the catalytic mechanism, Ca^{2+} is directly involved in acidification of the proton absorption from C5 and elimination of group from C4, generating an unsaturated product. Arg208 act as a base, similarly to the hydrolysis in the reaction mechanism of the GH28 family (Creze et al., 2008; Ali et al., 2015). On position 181 in PLs and PNLs there is a small AA, Ser or Ala, which is replaced with His181/His183 in VdPelB/BsPelA (**Figure 37C**). This AA can act with Ca^{2+} in the active site by directly interacting with the substrate (Zheng et al., 2012).

3.3.8. Characterization of the binding sites

VdPelB binding groove comprises a number of basic and acidic AA Asp151, Lys175 Leu178, Arg213 and Arg235 (VdPelB numbering) that were shown to be characteristics of PLs (**Figure 37B** and **Figure 37C**). This could partly explain the activity of the enzyme on low DM pectins as AA positioned at the binding groove were indeed shown to differ between PNL and PL (Pickersgill et al., 1994; Mayans et al., 1997; Vitali et al., 1998; Scavetta et al., 1999). These AA are mutated in Arg, Trp, Tyr, Gln and Gly in PNLs, which, by reducing their charge, favours higher affinity for highly methylesterified pectins (Mayans et al., 1997; Scavetta et al., 1999). In VdPelB, as the T3 loop is missing, there are no equivalent to Trp66, Trp81, Tyr85, Trp151 (AnPelA numbering), but Tyr211, Trp212 and Tyr215 are replaced by Phe174, Lys175 and Leu178 (VdPelB numbering). In BsPelA and DdPelC, are Trp176/Lys189, Lys177/Lys190 and Leu180/Leu193, highlighting that VdPelB/BsPelA are slightly more hydrophobic than DdPelC. However, when a DP4 ligand from DdPelC is superimposed to VdPelB, similar interactions are observed (**Figure S27**, Mayans et al., 1997; Vitali et al., 1998; Scavetta et al., 1999; Zheng et al., 2012). If these substitutions can help distinguishing PNL and PL, it does not explain the activity of VdPelB on high DM pectins. This peculiar activity could arise from two substitutions specific for VdPelB, Gly125 and Thr157, that are not present in other PLs. Instead, at this position, *bona fide* PL harbour Arg/Gln and Lys. These AA being overall positively charged, it could explain the binding preference towards non-methylesterified, negatively charged, substrates in the vicinity of the active site. In contrast,

considering the size of Gly and Thr, this would sterically accommodate the increased size of methylesterified substrate. To confirm these hypothesis Gly125 and Thr157 would have to be mutated in Arg and Lys.

3.4. Conclusion

We have characterised a novel pectinolytic enzyme from *V.dahliae*, VdPelB, that belongs to the PNL/PL family. Surprisingly, this enzyme showed high activity on both non-methylesterified substrate and pectins with DM>85%, suggesting that it acts as a pectin-pectate lyase. The maximum activity was at pH 7 and 35°C. The analysis of the digestion products of VdPelB showed that the enzyme can release a wide range of OGs with a preference for non-methylesterified and acetylated products. The OGs generated by VdPelB on *Verticillium*-partially tolerant and *Verticillium*-sensitive flax cultivars showed that the enzyme could be a determinant of pathogenicity as a function of pectins' structure. In order to understand the peculiar dual activity of VdPelB, the protein was crystallised and its 3D structure determined. VdPelB showed a conserved structure, with typical topology for PL/PNL. The conserved active site harboured three Asp (Asp122, Asp151 and Asp155) and Arg208 involved in the β-elimination mechanism. Binding site of VdPelB showed conserved AA characteristics of PLs except for two AA, Gly125 and Thr157, that are found in PNL. This strongly suggests that the differences between PL and PNL, and the dual activity of VdPelB could rely on only on few AA. This hypothesis needs however to be further confirmed using site-directed mutagenesis.

3.5. Material and Methods

3.5.1. Bioinformatical analysis

Verticillium dahliae PLL sequence was recovered using available genome data (ftp.broadinstitute.org/). SignalP-5.0 Server (http://www.cbs.dtu.dk/services/ SignalP/) was used for identifying putative signal peptide. Glycosylation sites were predicted using NetNGlyc 1.0 Server (http://www.cbs.dtu.dk/services/NetNGlyc/) and NetOGlyc 4.0 Server (http://www.cbs.dtu.dk/services/NetOGlyc/). Sequences were aligned and phylogeny analysis was carried out using MEGA multiple sequence alignment program (https://www.megasoftware.net/). Homology models were created using I-TASSER structure prediction software (https://zhanglab.ccmb.med.umich.edu/I-TASSER/) and UCSF Chimera (http://www.cgl.ucsf.edu/chimera/) was used for creation of graphics.

3.1.1. Fungal strain and growth

V.dahliae was isolated from CALIRA company flax test fields (Martainneville, France) and was kindly provided by Linéa-Semences company (Grandvilliers, France). Fungus was grown as described in (Safran et al., 2021). Briefly, fungus was grown on polygalacturonic acid sodium salt (PGA, P3850, Sigma) at 10 g. L^{-1} and in pectin methylesterified potassium salt from citrus fruit (55–70% DM, P9436, Sigma) to induce PLL expression. After 15 days of growth in dark conditions at 25°C, 80 rpm agitation mycelium was collected and filtered under vacuum filtration using Buchner flask. Collected mycelium was frozen in liquid nitrogen, lyophilized and ground. Isolation of RNA and cDNA synthesis was done as previously described in Lemaire et al., 2020.

3.1.2. Cloning, heterologous expression and purification of VdPelB

V. dahliae PLL coding sequence (VdPelB, Uniprot: G2X3Y1, GenBank: EGY23280.1), minus the signal peptide was amplified using cDNA and gene-specific primers: forward *TCTAA*CTGCAG*GA*ACGCCCACTCCCACC and reverse *TGCAC*GCGGCCGCGAAGCCAAG GGTCTGGC. Restriction enzymes sites for *Pst*I and *Not*I are underlined, and added bases are written in *italics*. Cloning, heterologous expression in *Pichia pastoris* and purification of VdPelB was done as previously described in Safran et al., 2021.

3.1.3. VdPelB biochemical assays

Pierce BCA Protein Assay Kit (Thermo Fisher Scientific, Waltham, Massachusetts, United States) was used to determine the protein concentration, with Bovine Serum Albumin (A7906, Sigma) as a standard. Deglycosylation was performed using Peptide-N-Glycosidase F (PNGase F) at 37°C for one hour according to the supplier's protocol (New England Biolabs, Hitchin, UK). Enzyme purity and molecular weight were estimated by 12% SDS-PAGE using mini-PROTEAN 3 system (BioRad, Hercules, California, United States) Gels were stained using PageBlue Protein Staining Solution (Thermo Fisher Scientific) according to the manufacturer's protocol.

3.1.4. VdPelB biochemical characterization

The substrate specificity of VdPelB was determined using PGA (81325, Sigma) and citrus pectin of various DM: 20–34% (P9311, Sigma), 55–70% (P9436, Sigma) and >85% (P9561, Sigma), with 0.5 µM $CaCl_2$ or 5 µM EDTA (Sigma) final concentrations. Enzyme activity was

measured by monitoring the increase in optical density at 235 nm due to formation of unsaturated uronide product using UV/VIS Spectrophotometer (PowerWave Xs2, BioTek, France) during 60 min. The optimum temperature was determined by incubating the enzymatic reaction between 25 and 45°C for 12 min using pectin of DM >85% (0.4%, w/v). The optimum pH was determined between pH 4 and 9 using McIlvaine buffer (pH 3 to 7) and Tris-HCl buffer (pH 7 to 9) and 0.4% (w/v) pectin DM>85% as a substrate. All experiments were realized in triplicate.

3.1.5. Digestion of commercial pectins and released OGs profiling

OGs released after digestions by recombinant VdPelB or commercially available Aspergillus PL (named AsPel) were identified as described in Voxeur et al., 2019, using a novel in-house OGs library. All OG masses and retention times are stated in **Table 7**. Briefly, DM 20–34% (P9311, Sigma), DM 55–70% (P9436, Sigma), DM >85% (P9561, Sigma) and sugar beet pectin with DM 42% and degree of acetylation (DA) 31% (CP Kelco, Atlanta, United States) were prepared at 0.4 % (w/v) final concentration diluted in 50 mM Tris-HCl buffer (pH 7) and incubated with either VdPelB or AsPel (E-PCLYAN, Megazyme) 50 mM Tris-HCl buffer (pH 8). For each substrate, enzyme concentrations were adjusted to have enzymes at iso-activities (**Table S5**). For each substrate two dilutions were used for analysing OGs released in early and late phase of digestion. Digestion was performed overnight. Non-digested pectins were pelleted by centrifugation and the supernatant dried in a speed vacuum concentrator (Concentrator plus, Eppendorf, Hamburg, Germany). Separation of OGs was done as described previously (Hocq et al., 2020) using an ACQUITY UPLC Protein BEH SEC column (125Å, 1.7 μm, 4.6 mm x 300 mm). The intensities were defined as the area under the curve, for each OG. Peak areas were clustered by hierarchical clustering with complete linkage on the euclidian distance matrix and visualized in the heatmap-package using R version 3.6.0.

3.1.6. Crystallization of VdPelB

VdPelB was concentrated at 10 mg.mL^{-1}. Crystallization was performed using the sitting-drop vapour-diffusion method. Crystallisation conditions were screened using a Mosquito robot (TTP Labtech) and the PACT premier plate (Molecular Dimensions, Sheffield, UK). VdPelB (100 nL) was mixed with an equal volume of precipitant (1:1). The crystals that resulted in best diffraction data were obtained with 0.1 M MIB 8.0 25 % w/v PEG 1500 (B5 condition PACT premier plate). Crystals for VdPelB formed after 1 month. Scale-up of the best condition was realized by mixing

1 µL of the best precipitant condition with 1 µL of the enzyme in the vapor-diffusion hanging drop method. Crystals were mixed with precipitation solution and PEG 1500 (35%, w/v) before mounting in a loop and flash cooling in liquid nitrogen.

3.1.7. VdPelB X-ray data collection and processing

The diffraction data were collected at PROXIMA-2a beamline (Synchrotron Soleil, Saint Aubin, France), at a temperature of -173°C using an EIGER 9M detector (Dectris). Data were collected using X-rays with wavelength 0.980 Å. For VdPelB four data sets were collected from the same crystal at 1.2 Å resolution. Data were merged, scaled and processed using XDS (Kabsch, 2010a) and XSCALE (Kabsch, 2010b). VePelB crystal belonged to monoclinic space group P1 2_1 1 with two molecules in asymmetric unit.

3.1.8. Structure solution and refinement

The structure of VdPelB was solved by molecular replacement using *Phaser* (McCoy et al., 2007). The data were phased using pectate lyase BsPelA (PDB: 3VMV, Uniprot D0VP31, Zheng et al., 2012) as a search model. Model was build using *Autobuild* and refined using *Refine* from PHENIX suite (Liebschner et al., 2019). The model was iteratively improved with *Coot* (Emsley et al., 2010) and *Refine.* The final refinement statistics are summarized (**Table S4**)**.** The final structure for VdPelB has been deposited in the Protein Data Bank as entries 7BBV.

Funding sources

This work was supported by the Conseil Regional Hauts-de-France and the FEDER (Fonds Européen de Développement Régional) through a PhD studentship awarded to J.S.

Acknowledgements

We wish to thank Sylvain Lecomte and Mehdi Cherkaoui for providing the *V. dahliae* DNA and Martin Savko and the staff at Proxima 2a beamline (Synchrotron SOLEIL, Gif sur Yvette, France) for X-ray diffraction and data collection.

Author's contribution

Josip Safran: Conceptualization, Data curation, Formal analysis, Investigation, Methodology, Writing - original draft. **Olivier Habrylo**: Formal analysis, Investigation, Methodology. **Julie Bouckaert**: Investigation, Methodology. **Roland Molinié**: Data curation, Formal analysis,

Investigation, Methodology. **Jean-Xavier Fontaine**: Data curation, Formal analysis, Investigation, Methodology. **Serge Pilard**: Investigation, Methodology. **Corrine Pau-Roblot:** Conceptualization, Methodology. **Fabien Sénéchal**: Conceptualization, Writing - review & editing. **Jérôme Pelloux**: Funding acquisition, Conceptualization, Writing - review & editing.

Conflicts of interest

There are no conflicts of interest.

3.2. Supplemental data

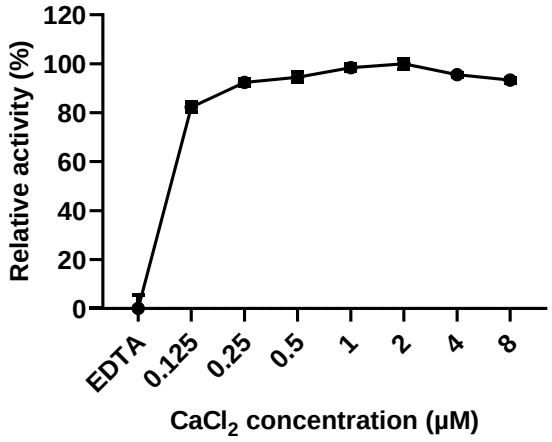

Figure S20. Effects on increasing concentrations of Ca2+ on VdPelB activity
Pectins DM>85% were digested using VdPelB for 12 min at 40°C and pH 7 with increasing concentrations of Ca^{2+}or Ca^{2+} and EDTA.

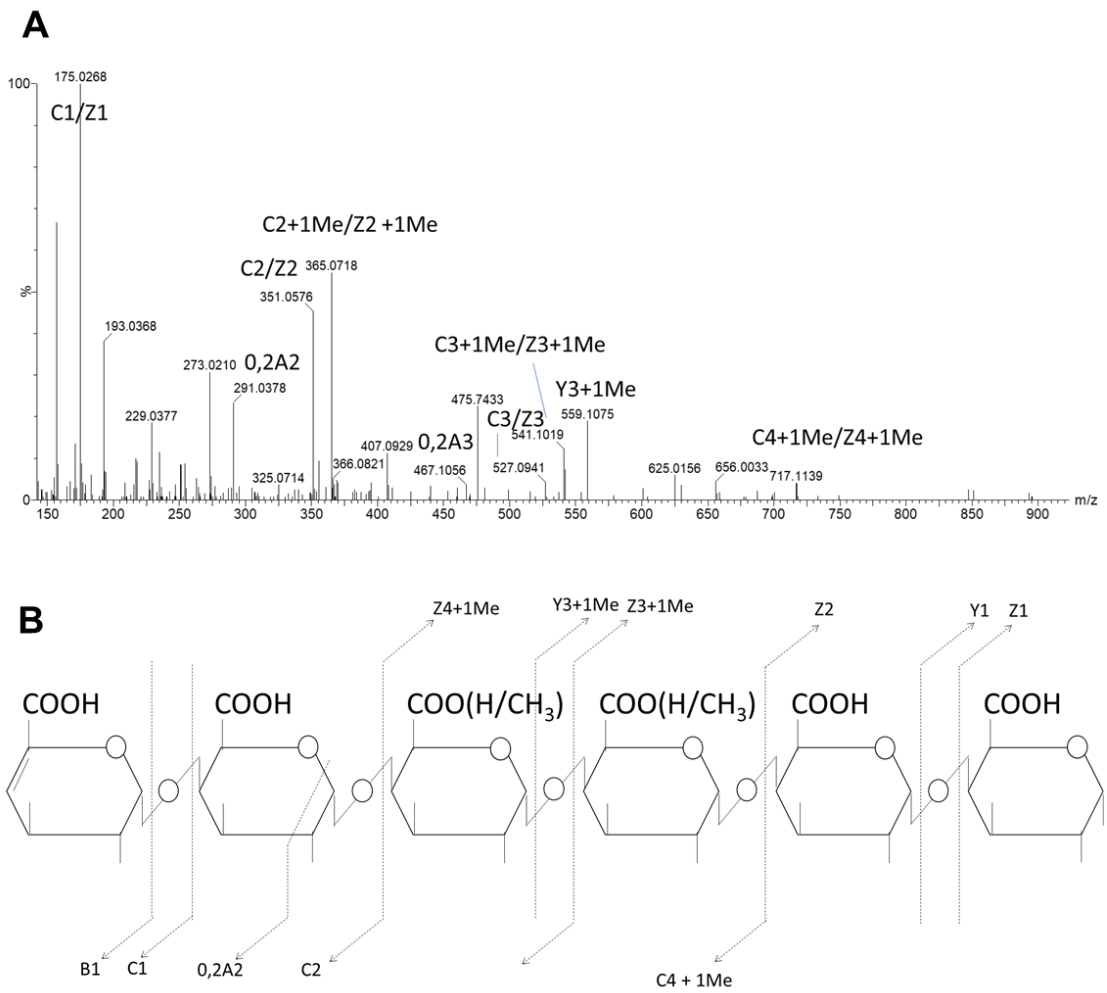

Figure S21. Example of MS2 fragmentation pattern of $GalA_6Me1\text{-}H_2O$
MS^2 fragmentation pattern of $GalA_6Me_1\text{-}H_2O$ oligomer (m/z 1055,185252, *527,0889878*) produced by VdPelB from pectin DM >85%. Subscript numbers indicate the degree of polymerization

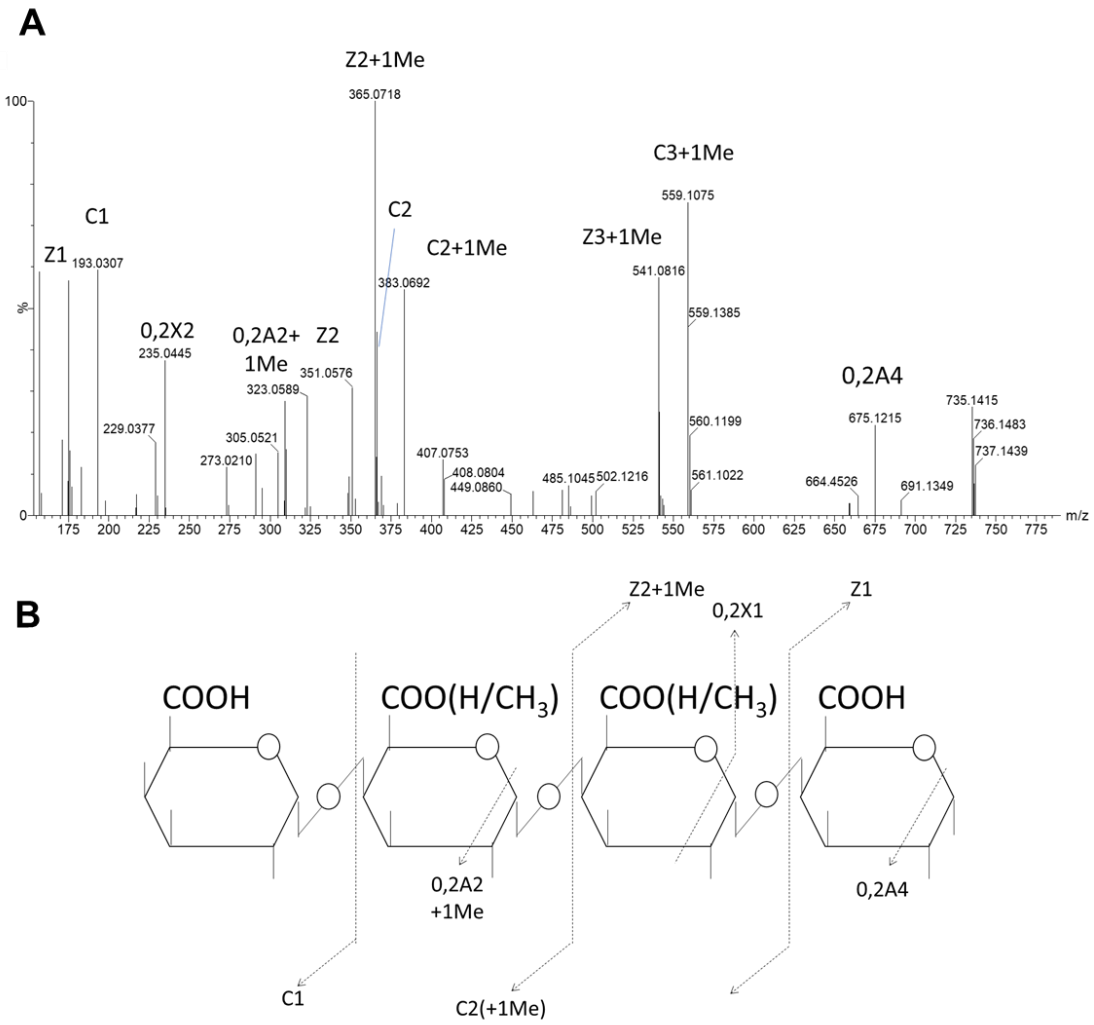

Figure S22. Example of MS_2 fragmentation pattern of $GalA_4Me_1$
MS^2 fragmentation pattern of $GalA_4Me_1$ oligomer (m/z 735,1472907) produced by VdPelB from pectin DM >85%. Subscript numbers indicate the degree of polymerization

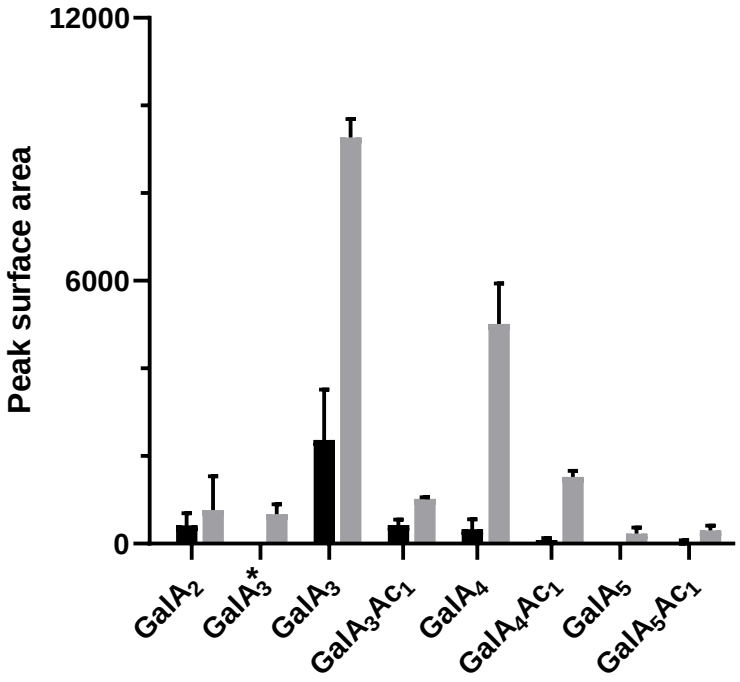

Figure S23. Analysis of OGs released by VdPelB from flax roots.
VdPelB was incubated overnight with roots from Évéa (spring flax, partially resistant to Verticillium wilt, black) and Violin (winter flax, more susceptible to Verticillium wilt, grey). Data are means ± SD; n = 3. Subscript numbers indicate the DP, DM and DA while * indicates non-unsaturated OGs**.**

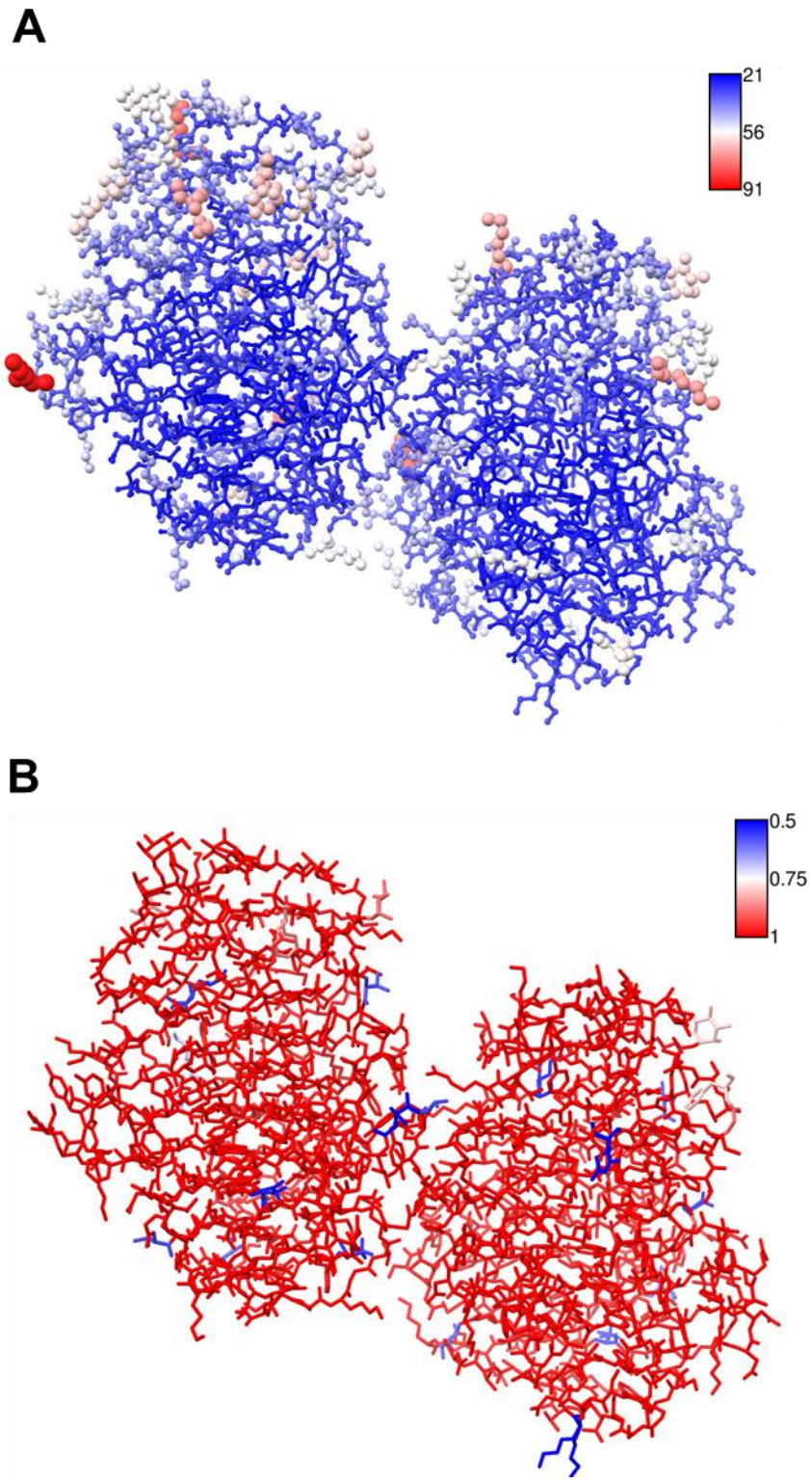

Figure S24. Average B-factors and occupancies of VdPelB
A) VdPelB chain A and B colored by B-factors. **B)** VdPelB chain A and B colored by occupancies.

Table S4. Data collection, processing and refinement for VdPelB

Characteristics	VdPelB
Data collection	
Diffraction source	PROXIMA2
Wavelength (Å)	0.980
Temperature (°C)	100.15
Detector	DECTRIS EIGER X 9M
Crystal-to-detector distance (mm)	115.02
Rotation range per image (°)	0.1
Total rotation range (°)	360
Crystal data	
Space group	P1 21 1
a, b, c (Å)	60.89, 59.69, 93.87
α, β, γ, (°)	90.00, 96.35, 90.00
Subunits per asymmetric unit	2
Data statistics	
Resolution range (Å)	60.52-1.2
Total No. of reflection	413550
No. of unique reflection	207382
No. of reflections, test set	10378
R_{merge} (%)	1.4 (222)
Completeness (%)	99.1 (93.8)
$(I/\sigma(I))$	18.3 (0.2)
Multiplicity	2.0 (2.0)
$CC_{1/2}$ (%)	1 (13.6)
Refinement	
R_{crys} /R_{free} (%)	17.2/19.6
Average B-factor (Å^2)	33.19
No. of non-H atoms	
Protein	9097
Ion	2
Ligand	234
Water	1052
Total	10385
R.m.s. deviations	
Bonds (Å)	0.013
Angles (°)	1.400
Ramachandran plot	
Most favoured (%)	95
Allowed (%)	5
Outlier (%)	-

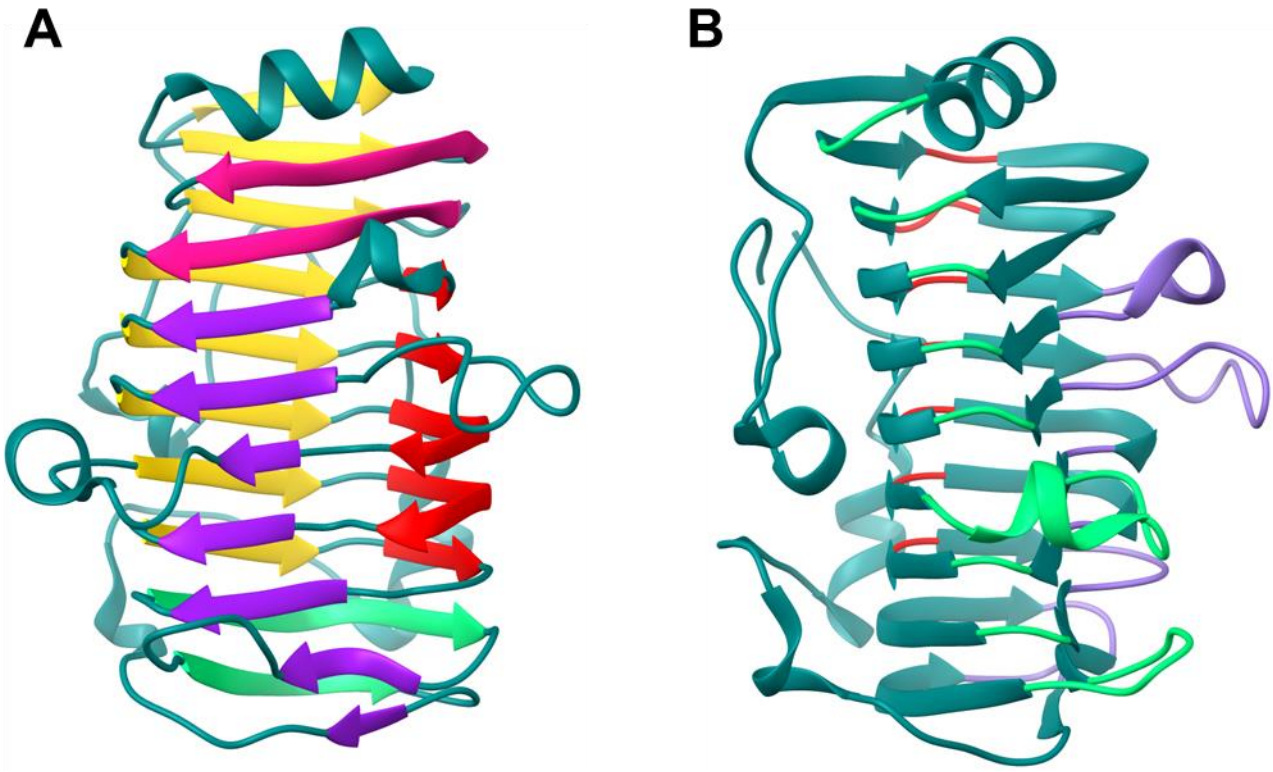

Figure S25. β-sheets and T-turns structures of VdPelB
A) Ribbon structure representing β-sheets (PB1-purple, PB2-yellow and PB3-red) and two β-sheets consisting of PB3-PB1-pink and PB2-PB3-lime green. **B)** Ribbon structure representing T-turns for VdPelB (T1-lime green, T2- orange red, T3 medium purple. β-strands and T-turns are named accordingly to Petersen et al. 1997

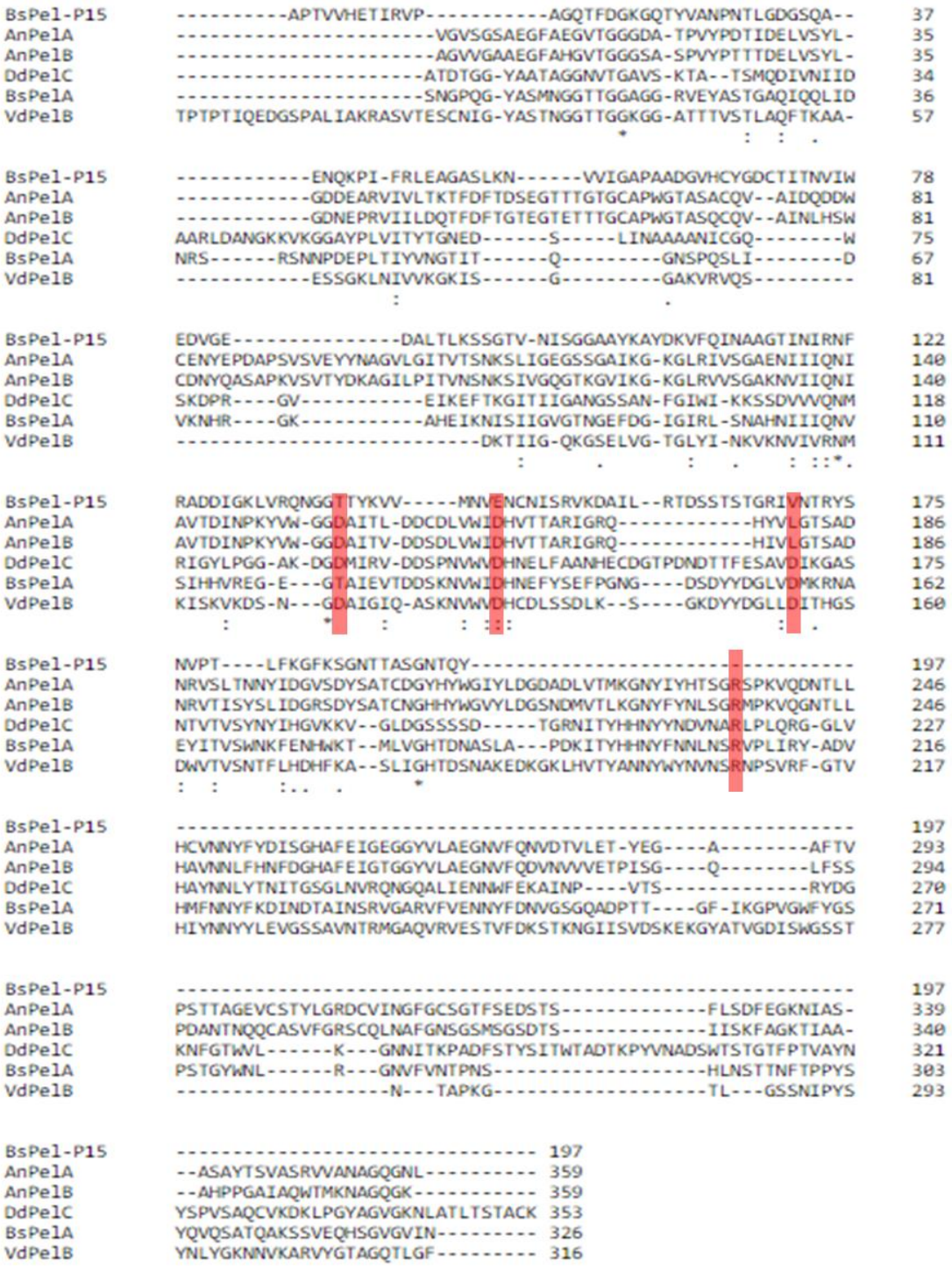

Figure S26. Primary sequence alignement of VdPelB with BsPelA, BsPelA-P15, DdPelC, AnPelA, AnPelB

VdPelB primary sequence alignment with Dickeya *dadanti* DdPelC (P11073), Bacillus Sp. KSM-P15 BsPel-P15 (Q9RHW0), Bacillus sp. N16-5 BsPelA (D0VP31), *Aspergillus niger* AnPelA (Q01172), AnPelB (Q00205). Conserved AA are red boxed.

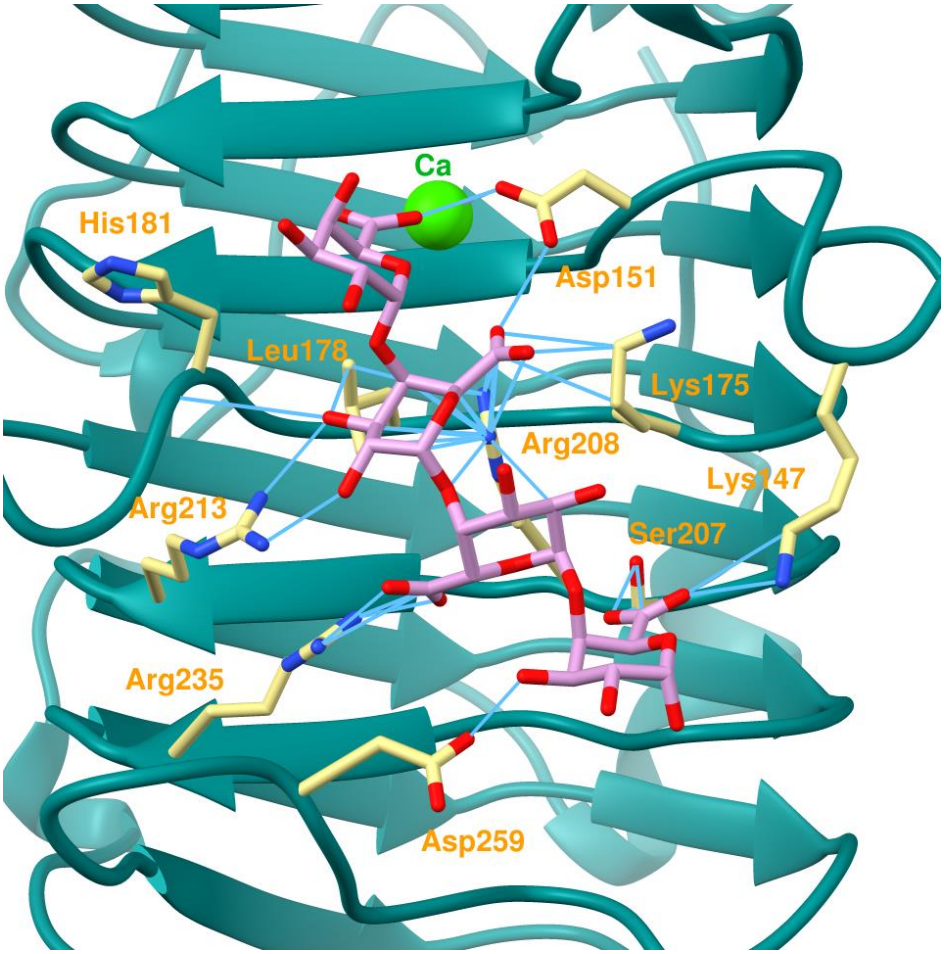

Figure S27. Superimposed tetramer ligand from DdPelC onto VdPelB structure
Tetramer ligand from DdPelC (PDB: 2EWE, plum) superimposed to VdPelB structure. AA involved in interaction are yellow-colored. Van der Waals contacts are coloured blue.

Table S5. VdPelB and AsPel concentration used for pectin degradation and OGs analysis.
The different enzymes concentrations were used to have enzymes at iso-activities.

Name	**VdPelB***		**AsPel****	
	1	**2**	**1**	**2**
Sugar beet pectin DM 42% DA 31%	0.077	0.00385	0.7	0.0875
Citrus pectin DM 24-30%.	0.077	0.0385	0.7	0.35
Citrus pectin DM>85%	0.0385	0.01925	1.4	0.35

* µg/µL, ** U/mL final concentration

3.3. Literature

Akita M, Suzuki A, Kobayashi T, Ito S, Yamane T (2001) The first structure of pectate lyase belonging to polysaccharide lyase family 3. Acta Crystallogr Sect D Biol Crystallogr **57**: 1786–1792

Ali S, Søndergaard CR, Teixeira S, Pickersgill RW (2015) Structural insights into the loss of catalytic competence in pectate lyase activity at low pH. FEBS Lett **589**: 3242–3246

Blum A, Bressan M, Zahid A, Trinsoutrot-Gattin I, Driouich A, Laval K (2018) Verticillium Wilt on Fiber Flax: Symptoms and Pathogen Development In Planta. Plant Dis **102**: 2421–2429

Brown IE, Mallen MH, Charnock SJ, Davies GJ, Black GW (2001) Pectate lyase 10A from Pseudomonas cellulosa is a modular enzyme containing a family 2a carbohydrate-binding module. Biochem J **355**: 155

Chilosi G, Magro P (1997) Pectin lyase and polygalacturonase isoenzyme production by Botrytis cinerea during the early stages of infection on different host plants. J Plant Pathol **79**: 61–69

Cho SW, Lee S, Shin W (2001) The X-ray structure of Aspergillus aculeatus Polygalacturonase and a Modeled structure of the Polygalacturonase-Octagalacturonate Complex. J Mol Biol **311**: 863–878

Creze C, Castang S, Derivery E, Haser R, Hugouvieux-Cotte-Pattat N, Shevchik VE, Gouet P (2008) The Crystal Structure of Pectate Lyase PelI from Soft Rot Pathogen *Erwinia chrysanthemi* in Complex with Its Substrate. J Biol Chem **283**: 18260–18268

Dubey A, Yadav S, Kumar M, Anand G, Yadav D (2016) Molecular Biology of Microbial Pectate Lyase: A Review. Br Biotechnol J **13**: 1–26

Duressa D, Anchieta A, Chen D, Klimes A, Garcia-Pedrajas MD, Dobinson KF, Klosterman SJ (2013) RNA-seq analyses of gene expression in the microsclerotia of Verticillium dahliae. BMC Genomics **14**: 5–18

Emsley P, Lohkamp B, Scott WG, Cowtan K (2010) Features and development of Coot. Acta Crystallogr Sect D Biol Crystallogr **66**: 486–501

Hassan S, Shevchik VE, Robert X, Hugouvieux-Cotte-Pattat N (2013) PelN is a new pectate lyase of dickeya dadantii with unusual characteristics. J Bacteriol **195**: 2197–2206

Henrissat B, Heffron SE, Yoder MD, Lietzke SE, Jurnak F (1995) Functional implications of structure-based sequence alignment of proteins in the extracellular pectate lyase superfamily. Plant Physiol **107**: 963–76

Hocq L, Guinand S, Habrylo O, Voxeur A, Tabi W, Safran J, Fournet F, Domon J-M, Mollet J-C, Pilard S, et al (2020) The exogenous application of AtPGLR, an endo - polygalacturonase, triggers pollen tube burst and repair. Plant J **103**: 617–633

Jayani RS, Saxena S, Gupta R (2005) Microbial pectinolytic enzymes: A review. Process Biochem **40**: 2931–2944

Jenkins J, Pickersgill R (2001) The architecture of parallel β-helices and related folds. Prog Biophys Mol Biol **77**: 111–175

Johansson K, El-Ahmad M, Friemann R, Jörnvall H, Markovič O, Eklund H (2002) Crystal structure of plant pectin methylesterase. FEBS Lett **514**: 243–249

Jolie RP, Duvetter T, Van Loey AM, Hendrickx ME (2010) Pectin methylesterase and its proteinaceous inhibitor: A review. Carbohydr Res **345**: 2583–2595

Kabsch W (2010a) Integration, scaling, space-group assignment and post-refinement. Acta Crystallogr Sect D Biol Crystallogr **66**: 133–144

Kabsch W (2010b) Xds. Acta Crystallogr D Biol Crystallogr **66**: 125–32

Kars I, Krooshof GH, Wagemakers L, Joosten R, Benen JAE, Van Kan JAL (2005) Necrotizing activity of five Botrytis cinerea endopolygalacturonases produced in Pichia pastoris. Plant J **43**: 213–225

Kita N, Boyd CM, Garrett MR, Jurnak F, Keen NT (1996) Differential Effect of Site-directed Mutations in pelC on Pectate Lyase Activity, Plant Tissue Maceration, and Elicitor Activity. J Biol Chem **271**: 26529–26535

Klosterman SJ, Subbarao K V., Kang S, Veronese P, Gold SE, Thomma BPHJ, Chen Z, Henrissat B, Lee Y-H, Park J, et al (2011) Comparative Genomics Yields Insights into Niche Adaptation of Plant Vascular Wilt Pathogens. PLoS Pathog **7**: e1002137

Kumar S, Stecher G, Li M, Knyaz C, Tamura K (2018) MEGA X: Molecular Evolutionary Genetics Analysis across Computing Platforms. Mol Biol Evol **35**: 1547–1549

Lemaire A, Duran Garzon C, Perrin A, Habrylo O, Trezel P, Bassard S, Lefebvre V, Van Wuytswinkel O, Guillaume A, Pau-Roblot C, et al (2020) Three novel rhamnogalacturonan I- pectins degrading enzymes from Aspergillus aculeatinus: Biochemical characterization and application potential. Carbohydr Polym **248**: 116752

Liebschner D, Afonine P V., Baker ML, Bunkoczi G, Chen VB, Croll TI, Hintze B, Hung LW, Jain S, McCoy AJ, et al (2019) Macromolecular structure determination using X-rays, neutrons and electrons: Recent developments in Phenix. Acta Crystallogr Sect D Struct Biol **75**: 861–877

Lietzke SE, Scavetta RD, Yoder MD (1996a) The Refined Three-Dimensional Structure of Pectate Lyase E from. Plant Physiol **111**: 73–92

Lietzke SE, Scavetta RD, Yoder MD, Jurnak F (1996b) The Refined Three-Dimensional Structure of Pectate Lyase E from Erwinia chrysanthemi at 2.2 A Resolution. Plant Physiol **111**: 73–92

Limberg G, Körner R, Buchholt HC, Christensen TMIE, Roepstorff P, Mikkelsen JD (2000) Analysis of different de-esterification mechanisms for pectin by enzymatic fingerprinting using endopectin lyase and endopolygalacturonase II from A. Niger. Carbohydr Res **327**: 293–307

Liston SD, McMahon SA, Le Bas A, Suits MDL, Naismith JH, Whitfield C (2018) Periplasmic

depolymerase provides insight into ABC transporter-dependent secretion of bacterial capsular polysaccharides. Proc Natl Acad Sci U S A **115**: E4870–E4879

Luis AS, Briggs J, Zhang X, Farnell B, Ndeh D, Labourel A, Baslé A, Cartmell A, Terrapon N, Stott K, et al (2018) Dietary pectic glycans are degraded by coordinated enzyme pathways in human colonic Bacteroides. Nat Microbiol **3**: 210–219

Mandelc S, Javornik B (2015) The secretome of vascular wilt pathogen Verticillium albo-atrum in simulated xylem fluid. Proteomics **15**: 787–797

Mayans O, Scott M, Connerton I, Gravesen T, Benen J, Visser J, Pickersgill R, Jenkins J (1997) Two crystal structures of pectin lyase A from Aspergillus reveal a pH driven conformational change and striking divergence in the substrate-binding clefts of pectin and pectate lyases. Structure **5**: 677–689

McCoy AJ, Grosse-Kunstleve RW, Adams PD, Winn MD, Storoni LC, Read RJ (2007) Phaser crystallographic software. J Appl Crystallogr **40**: 658–674

Mohnen D (2008) Pectin structure and biosynthesis. Curr Opin Plant Biol **11**: 266–277

Nocker VS, Sun L (2010) Analysis of promoter activity of members of the Pectate lyase-like(PLL) gene family in cell separation in Arabidopsis. BMC Plant Biol **10**: 152

Ouattara HG, Reverchon S, Niamke SL, Nasser W (2010) Biochemical Properties of Pectate Lyases Produced by Three Different Bacillus Strains Isolated from Fermenting Cocoa Beans and Characterization of Their Cloned Genes. Appl Environ Microbiol **76**: 5214–5220

Pelloux J, Rustérucci C, Mellerowicz EJ (2007) New insights into pectin methylesterase structure and function. Trends Plant Sci **12**: 267–277

Petersen TN, Kauppinen S, Larsen S (1997) The crystal structure of rhamnogalacturonase a from Aspergillus aculeatus: A right-handed parallel β helix. Structure **5**: 533–544

Pickersgill R, Jenkins J, Harris G, Nasser W, Robert Baudouy J (1994) The structure of Bacillus subtil is pectate lyase in complex with calcium. Nat Struct Biol **1**: 717–723

Ridley BL, O'Neill MA, Mohnen D (2001) Pectins: structure, biosynthesis, and oligogalacturonide-related signaling. Phytochemistry **57**: 929–967

Rui Y, Xiao C, Yi H, Kandemir B, Wang JZ, Puri VM, Anderson CT (2017) POLYGALACTURONASE INVOLVED IN EXPANSION3 functions in seedling development, rosette growth, and stomatal dynamics in Arabidopsis thaliana. Plant Cell **29**: 2413–2432

Safran J, Habrylo O, Cherkaoui M, Lecomte S, Voxeur A, Pilard S, Bassard S, Pau-Roblot C, Mercadante D, Pelloux J, et al (2021) New insights into the specificity and processivity of two novel pectinases from Verticillium dahliae. Int J Biol Macromol **176**: 165–176

van Santen Y, Benen JAE, Schroter KH, Kalk KH, Armand S, Visser J, Dijkstra BW (1999) 1.68-angstrom crystal structure of endopolygalacturonase II from Aspergillus niger and identification of active site residues by site-directed mutagenesis. J Biol Chem **274**: 30474–30480

Scavetta RD, Herron SR, Hotchkiss AT, Kita N, Keen NT, Benen JAE, Kester HCM, Visser J, Jurnak F (1999) Structure of a plant cell wall fragment complexed to pectate lyase C. Plant Cell **11**: 1081–1092

Sénéchal F, Mareck A, Marcelo P, Lerouge P, Pelloux J (2015) Arabidopsis PME17 Activity can be Controlled by Pectin Methylesterase Inhibitor4. Plant Signal Behav **10**: e983351

Sénéchal F, Wattier C, Rustérucci C, Pelloux J (2014) Homogalacturonan-modifying enzymes: Structure, expression, and roles in plants. J Exp Bot **65**: 5125–5160

Soriano M, Blanco A, Díaz P, Pastor FIJ (2000) An unusual pectate lyase from a Bacillus sp. with high activity on pectin: Cloning and characterization. Microbiology **146**: 89–95

Sukhumsiirchart W, Kawanishi S, Deesukon W, Chansiri K, Kawasaki H, Sakamoto T (2009) Purification, Characterization, and Overexpression of Thermophilic Pectate Lyase of Bacillus sp. RN1 Isolated from a Hot Spring in Thailand. Biosci Biotechnol Biochem **73**: 268–273

Tang Y, Wu P, Jiang S, Selvaraj JN, Yang S, Zhang G (2019) A new cold-active and alkaline pectate lyase from Antarctic bacterium with high catalytic efficiency. Appl Microbiol Biotechnol **103**: 5231–5241

Vitali J, Schick B, Kester HCM, Visser J, Jurnak F (1998) The Three-Dimensional Structure of Aspergillus niger Pectin Lyase B at 1.7-Å Resolution. Plant Physiol **116**: 69–80

Voxeur A, Habrylo O, Guénin S, Miart F, Soulié MC, Rihouey C, Pau-Roblot C, Domon JM, Gutierrez L, Pelloux J, et al (2019) Oligogalacturonide production upon Arabidopsis thaliana-Botrytis cinerea interaction. Proc Natl Acad Sci U S A **116**: 19743–19752

Wang Z, Xu B, Luo H, Meng K, Wang Y, Liu M, Bai Y, Yao B, Tu T (2020) Production pectin oligosaccharides using Humicola insolens Y1-derived unusual pectate lyase. J Biosci Bioeng **129**: 16–22

Xiao C, Somerville C, Anderson CT (2014) POLYGALACTURONASE INVOLVED IN EXPANSION1 functions in cell elongation and flower development in Arabidopsis. Plant Cell **26**: 1018–1035

Yadav S, Yadav PK, Yadav D, Yadav KDS (2009) Pectin lyase: A review. Process Biochem **44**: 1–10

Yang G, Chen W, Tan H, Li K, Li J, Yin H (2020) Biochemical characterization and evolutionary analysis of a novel pectate lyase from Aspergillus parasiticus. Int J Biol Macromol **152**: 180–188

Yang Y, Zhang Y, Li B, Yang X, Dong Y, Qiu D (2018) A Verticillium dahliae Pectate Lyase Induces Plant Immune Responses and Contributes to Virulence. Front Plant Sci **9**: 1–15

Yin X, Hu D, Li J-F, He Y, Zhu T-D, Wu M-C (2015) Contribution of Disulfide Bridges to the Thermostability of a Type A Feruloyl Esterase from Aspergillus usamii. PLoS One **10**: e0126864

Yoder MD, Jurnak F (1995) The Refined Three-Dimensional Structure of Pectate Lyase C lmplications for an Enzymatic Mechanism. Plant Physiol **107**: 349–364

Yoder MD, Lietzke SE, Jurnak F (1993) Unusual structural features in the parallel β-helix in pectate lyases. Structure **1**: 241–251

Yuan P, Meng K, Wang Y, Luo H, Shi P, Huang H, Tu T, Yang P, Yao B (2012) A Low-Temperature-Active Alkaline Pectate Lyase from Xanthomonas campestris ACCC 10048 with High Activity over a Wide pH Range. Appl Biochem Biotechnol **168**: 1489–1500

Zeuner B, Thomsen TB, Stringer MA, Krogh KBRM, Meyer AS, Holck J, Meyer AS (2020) Comparative Characterization of Aspergillus Pectin Lyases by Discriminative Substrate Degradation Profiling. Front Bioeng Biotechnol. **8**: 873

Zhang C, Yao J, Zhou C, Mao L, Zhang G, Ma Y (2013) The alkaline pectate lyase PEL168 of Bacillus subtilis heterologously expressed in Pichia pastorisis more stable and efficient for degumming ramie fiber. BMC Biotechnol **13**: 26

Zheng Y, Huang CH, Liu W, Ko TP, Xue Y, Zhou C, Guo RT, Ma Y (2012) Crystal structure and substrate-binding mode of a novel pectate lyase from alkaliphilic Bacillus sp. N16-5. Biochem Biophys Res Commun **420**: 269–274

Zhou C, Xue Y, Ma Y (2017) Cloning, evaluation, and high-level expression of a thermo-alkaline pectate lyase from alkaliphilic Bacillus clausii with potential in ramie degumming. Appl Microbiol Biotechnol **101**: 3663–3676

GENERAL DISCUSSION

The pectic network, and in particular HG, plays a central role in the control of plant development and is degraded during pathogens' attack (Klosterman et al., 2009; Ogawa et al., 2009; Rui et al., 2017; Blum et al., 2018). In Arabidopsis there are 66 PME, 12 PAE, 68 PG and 26 PLL putative genes that are expressed during different developmental processes, which questions the biochemical characteristics, and the role, of the various isoforms in the fine-tuning of HG. On the other hand, *V. dahliae*, secretes 4 PMEs, 2 PAEs, 9 PGs and 30 PLLs, which are likely to be determinant of pathogenicity towards a wide range of plant species. In this work, we report on the characterization of five enzymes: Two plant PGs, PGLR and ADPG2, that have overlapping expression patterns in Arabidopsis during lateral root emergence, as well as three fungal enzymes, VdPME1, VdPG2, and VdPelB, that are expressed by *V.dahliae* during infection of the root system (González-Carranza et al., 2007; Ogawa et al., 2009; Blum et al., 2018; Hocq et al., 2020). These enzymes appear particularly suited to: i) sample the biochemical diversity among plant enzymes (PGLR vs ADPG2). ii) compare plant and fungal enzymes (VdPG2 and PGLR/ADPG2), iii) understand the differences between PG and PLL. We indeed showed that, if all five enzymes share a common β-helix fold and target HG-type pectins, they differ in their biochemical properties.

All of the above-mentioned enzymes share the same β-helix fold, even if PGs have four β-sheets compared to PLLs and PMEs which have three (Jenkins and Pickersgill, 2001). In average each β-sheet comprises about 10 β-strands. Major differences in the structure of the proteins come from the loop regions on the N- and C- terminus. The T3 and T1 loop are composed from different AA, and these loops are important for substrate recognition and, for instance for PG, determine the interaction with PGIP. Active site in PGs, revealed from PGLR/ADPG2 structures and VdPG2 model, is well conserved consisting of three Asp (Cho et al., 2001) while in PLLs the active site architecture differs between PLs and PNLs (Mayans et al., 1997; Scavetta et al., 1999). The PLs' active site, as shown from VdPelB structure, has three conserved Asp, with same position compared to that of PGs, but they coordinate one Ca^{2+} ion. In contrast, in PNLs, Ca^{2+} is replaced by an Asp that plays a similar role. In VdPelB we further showed that Arg208 is the second AA involved in

catalysis together with Ca^{2+}. Based on homology modelling, VdPME1 active site harbours conserved AA characteristic of PMEs: Asp144, Gln143 Asp165 and Arg229. The presence of conserved AA in the active site of PME, PG and PLL suggests similar roles in the catalysis of HG, either consisting in the demethylesterification or the hydrolysis/β-elimination of the glycosidic bond.

Our results further showed that, while having conserved active sites, binding sites strikingly differed between the three PGs. In particular, in the -5 subsite VdPG2 has Ala118, which corresponds to Ala108 of AaPG1, but which differed from PGLR/ADPG2 AA (Arg146/Thr172). In subsites -4, -3 and -2 the positively charged patch formed by Gln198, Gln220 and Lys246 in PGLR differs that of VdPG2 where Gly174 and Asn196 are present while Lys246 (PGLR) does not have a counterpart. In contrast, in VdPG2, Gly200 is the closest structurally positioned AA. These three AA (Gly174, Asn196 and Gly200) correspond to AaPG1 AA (Cho et al., 2001). At subsite -1 Ser269 in ADPG2 correspond to Ser218 in VdPG2. Lastly, at subsite +2 Asp293 corresponds to Asp241 and at +3 Ala270 corresponds to Ala296, respectively in ADPG2 and PGLR. Thus, the structure of subsites is likely to explain the substrate specificity and processivity of the three PGs.

VdPelB was most active at pH 7 which is rather similar to pH 6 of VdPME1. VdPG2 is most active at pH 5 and a temperature of 50°C, which appears similar to PGLR (pH 4, 40°C) and ADPG2 (pH5, 50°C). Furthermore, VdPG2 activity was negatively correlated with increased DM of pectins while PGLR and ADPG2 had residual activity on pectins DM >85%, showing peculiar substrate specificity. These activities, measured *in vitro*, could be of importance in the context of the cell wall where PGLR and ADPG2 could finely modulate pectin structure to control development. In contrast VdPG2 is secreted with other pectinases, including VdPelB and VdPME1, during *V. dahliae* infection which contributes to the degradation of cell wall and promote fungal infections. The biochemical characterization of the three enzymes shed new light on their possible sequential action leading to pectin degradation. VdPME1 can create demethylesterified HG that could be substrates for VdPG2 and VePelB. We indeed showed that *V.dahliae* VdPME1, contrary to numerous fungal PMEs, has a processive mode of action on commercial pectins leading to highly demethylesterified HG chain (**Figure 31**). This processivity, unusual for fungal PMEs, is normally found in bacterial and plant PMEs (Kent et al., 2016). However, the processivity appears to be

highly dependent of the enzyme's microenvironment as, for instance Arabidopsis PME2's processivity was shown to be pH-dependent, switching from high processivity at pH 8 to low processivity at pH 5 (Hocq et al., 2021, BioRxiv). The processivity of VdPME1, and the pH-dependent switch of the processivity of PME2 appears to be directly related with the electrostatic potential of the protein, where overall negative potentials facilitate the dissociations from the demethylesterified, negatively charged, substrate (Kent et al., 2016; Safran et al., 2021).

In addition, the processivity of VdPME1 could play a role in generating substrates for VdPelB. The subsite of VdPelB comprises a number of basic and acidic AA (Mayans et al., 1997; Scavetta et al., 1999) that are characteristic of PL. This structure in part determines the substrate specificity of VdPelB on PGA. However, the structure and the biochemical specificities of VdPelB show that it has an activity on pectins of DM >85%. Although this peculiar behaviour was seen before for distinct enzymes, it appears related to the structure of VdPelB, with the identification of two AA characteristics of PNL (Soriano et al., 2000; Wang et al., 2020).

The use of LC-MS/MS oligoprofiling approach allowed the identifying the OGs that are produced by VdPG2, PGLR, ADPG2 and VdPelB. We showed that the four pectinases are endo-enzymes that can release OGs that differ in their DPs, DMs and DAs. However, consistent with the structure of the enzymes, VdPelB preferentially released unsaturated OGs created by its β-elimination reaction mechanism, while PG released non-unsaturated OGs. From pectins DM 24-30% VdPelB, VdPG2 and ADPG2 released OGs of short DPs (non-methylesterified OGs of DP2 to DP4, as well as GalA4Me), while PGLR released mostly OGs of DP5 to DP9 as well as specific methylesterified forms. This suggest distinct processivity of the enzymes on a given substrate, that could be related to the above-mentioned structures. We further showed that OGs of DP2 and DP3 are considered the end product of the reaction and cannot be further recut (Rexova-Benkova, 1973). On pectin DM >85% all of the four enzymes released higher levels of methylesterified OGs, in accordance with the higher DM of the substrate. The high DA of sugar beet pectin appeared to inhibit the activities of the enzymes although a number of acetylated OGs were released by VdPelB. However, when testing the enzymes on either flax or Arabidopsis roots. PGLR released predominately acetylated OGs from DP3 to DP7, while ADPG2 and VdPG2 mainly released DP3 and DP4. Similar trend was observed for VdPelB except that the predominant OGs were unsaturated. This data suggests that the acetylation of root cell wall pectins, lower than sugar beet,

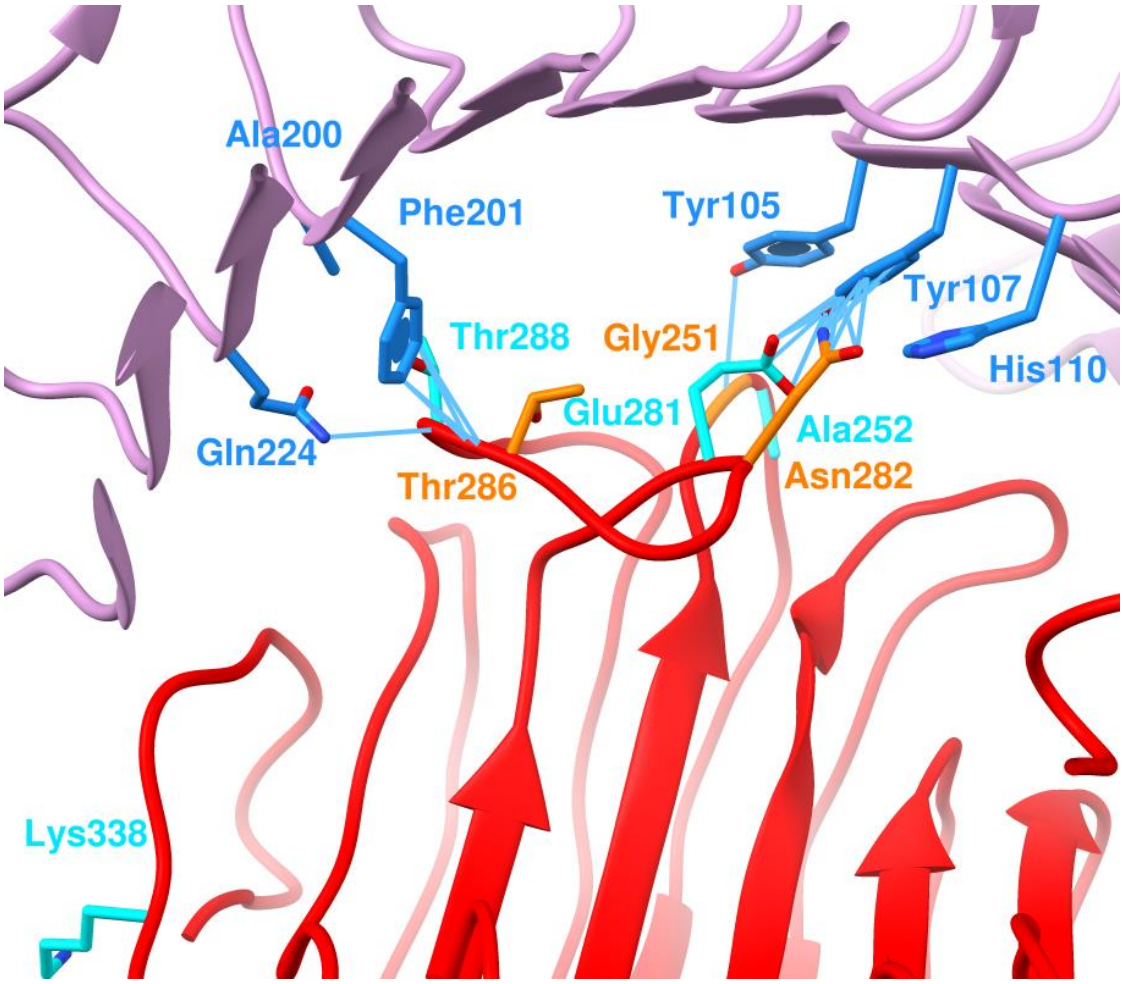

Figure 38. Structural determinant for VdPG2-PvPGIP2 interaction
Ribbon representation of *Phaseolus vulgaris* PGIP2 (PvPGIP2, plum) and VdPG2 (red), interactions. PvPGIP2 AA involved in interaction with FpPG1 are coloured blue. VdPG2 AA detected to be involved in interaction with PvPGIP2 are coloured orange while conserved AA homologues from FpPG1 and CluPG1 are cyan coloured. Glu281 is the only conserved AA that showed interaction. Blue lines represent van der Waals contacts.

does not impair the PGs expressed endogenously nor the pectinases from Verticillium, a root piercing fungus. Moreover, this suggests similarities in the cell wall between Arabidopsis and flax.

One important aspect of PGs is their regulation. While plant PMEs are inhibited by plant PMEIs (Hocq et al., 2017b; Sénéchal et al., 2017) there are no such evidence, for plant PG-plant PGIP interactions. PGLR was indeed not inhibited by *P. vulgaris* PvPGIP2 (Hocq et al., 2020). Our study brings new insights into the structural determinant of the absence of inhibition of plant PGs by endogenous PGIPs. In comparison with fungal enzymes, PGLR and ADPG2 harbour distinct AA in specific parts of the structure, which impair their recognition by PGIP. In particular, on the N-terminus, the T3 loop does not harbour the required Asn121 while on C-terminus Gly is positioned at the position of Ala274 in FpPG1 (Benedetti et al., 2011). The mutation of these two AA appears sufficient for explaining the absence of regulation of plant PGs by plant PGIPs. This therefore suggests that, in plants, the fine-tuning of the degree of methylesterification of pectins by PMEs is the main control point of pectin degradation, since only PMEs are regulated by protein inhibitors.

VdPG2 shared only 22.16% and 24.72% sequence identity with PGLR and ADPG2, respectively. In contrast, VdPG2 shares 41.55% and 67.73% sequence identity with FpPG1 and CluPG1, two PGs that show distinct PG-PGIP interactions. FpPG1 interact with PGIP competitively on both sides of active site, while CluPG1 is inhibited only through interaction at the C-terminus, causing non-competitive inhibition (Benedetti et al., 2011; Benedetti et al., 2013). The structure superimposition of the three enzymes and analysis of the possible interactions with PvPGIP2 indicates that an interaction is likely on C-terminus loop between VdPG2 and PvPGIP2. VdPG2 indeed harbours the conserved Glu281, Thr288 and Lys338 equivalents of Glu290, Thr297 and Lys350 in CluPG1 (**Figure 38**) suggesting potential inhibition with PvPGIP2 (Benedetti et al., 2011; Benedetti et al., 2013).

GENERAL CONCLUSION AND PERSPECTIVES

The objectives of this thesis were first to understand the differences between plant PGs and to determine, for the first time, the 3D structure of plant PG. This aimed at explaining the rationale for having 68 putative isoforms in Arabidopsis as well as the differences between plant and fungal enzymes, in particular the non-interaction of plant PGs with PGIPs. Furthermore, we were interested in understanding the mode of action and structure of fungal PME1, PG2 and PelB from plant pathogen *V. dahliae* to understand their contribution in pathogenicity. Altogether, these results obtained in this thesis contribute to a better understanding the structure-function relations of pectin remodelling enzymes.

Two plant PGs, PGLR and ADPG2, with overlapping expression in Arabidopsis' roots, were shown to have overall similar biochemical specificities (substrate, pH, temperature) but the digestions products (OGs) of either of the enzymes strikingly differed, as PGLR released OGs of higher DP and DA, compared to ADPG2. This suggests structural differences and substrate specificity *in muro*. PGLR and ADPG2 showed similar structural features to that reported from fungal PGs with regards to β-helix fold and conserved AA in the active site. However, structural differences exist, since ADPG2 subsites harbour more polar AA compared to PGLR, which suggests that it can tolerate more methylesterified substrates. This work shows that all PGs are not equal with regards to their processivity. As the charges of the binding site governs the substrate specificities it would be of interest to test what are consequences of the mutations of some PGLR's AA into the ones from ADPG2. In particular, suitable candidates could be: i) Thr267 and Ala296 in PGLR could be mutated into Asp293 and Lys322 in order to confirm that these AA are responsible for PGLR lack of activity on short DPs, ii) Polar AA on subsites -3, -4 and -5 in ADPG2, comprising Ser195, Thr172 and Asp129 could be mutated into Arg146, Lys169 and Gln198, corresponding to that of PGLR. Changing them could reduce the ability of ADPG2 for hydrolysing methylesterified substrates and releasing methylesterified OGs, iii) The processive mode of action proposed for PGLR differs of the single attack suspected for ADPG2. A way of testing this hypothesis would be to mutate Asp133, Thr176 and Ser199 in ADPG2 with positively-charged AA, Lys108, Arg146, Lys169 from PGLR. This could be done in conjunction with changing the entire loops of ADPG2 around the active site with the loops of PGLR that better

enclose the substrate. These mutated forms of PGs, while time-consuming to prepare could be easily tested using the LC-MS/MS oligoprofiling approach. Furthermore, concerning the potential structural determinants of the absence of inhibition of PGLR by PvPGIP2, the AA located at the crucial positions in the structures of fungal PGs could be introduced in place of existing AA in PGLR, through a gain of function approach, to see how this can affect the inhibition of the plant PGs by PGIPs. However, the true test would be to express the two Arabidopsis PGIPs and observe their inhibitory capacities against the two plant PGs.

As we have defined the differences in the subsites of PGLR and ADPG2 and in order to confirm if, and how, the different substrates can bind, more effort should be done on co-crystallisation studies. We have in hand a number of OGs that could be used as potential substrates, but the mutations required for having binding without hydrolysis can be time consuming to prepare. Thus, the use, beforehand of computational methods such MD simulations and docking studies, could be of importance for designing the most useful mutations.

VdPME1 and VdPG2 are a part of *V. dahliae* enzymatic arsenal to degrade plant cell wall. If these enzymes showed similar biochemical properties compared to previously reported fungal enzymes, their mode of action differed. For instance, VdPME1 showed, at pH 7, a processive behaviour that was previously reported only for bacterial and plant PMEs. This processive behaviour appears to be related to surface electrostatic charges of the enzyme. In order to further characterize the processivity of VdPME1, its mode of action could be tested at different pH values. Again, the use of computational approaches is of prime importance to determine key AA that could fine-tune the pH-dependence of the processivity of PMEs.

VdPelB, together with VdPME1 and VdPG2, is likely to be a key element for *V. dahliae*'s infection. VdPelB showed biochemical characteristics of PLs, including requirement for Ca^{2+}, slightly alkaline pH and high activity on pectate. However, as high activity was observed on pectin DM >85%, characteristic for PNLs, this highlights that VdPelB has a dual activity. While this unusual behaviour was previously reported for some other enzymes, it was not further investigated. Furthermore, VdPelB can release unsaturated OGs with low DM and high DA, suggesting a preference for non-methylesterified and acetylated substrates. Structurally, VdPelB showed conserve structure, common for pectinases. While harbouring Ca^{2+} and conserved AA at the active site, characteristic of PLs, two AA (Gly125 and Thr157), are not commonly found in PLs but in

VdPelB. To formally demonstrate the role of these AA in determining the dual PL/PNL activity, they should be mutated in Arg and Lys that are characteristics of PLs. As *Verticillium* secretes VdPelB together with VdPME1 and VdPG2 during the infection process, it would be interesting to test their cumulative effects on flax cell wall. Additionally, these enzymes have the potential to be used for the production of OG pools of specific DP, DM and DA. These OGs could have the potential to be used as elicitor of plant defences.

COMPLEMENTARY MATERIALS & METHODS

This chapter will concern only the Materials and Methods that were not fully described in each of the chapters.

1. Part: Molecular biology methods

1.1. RNA extraction

RNA extraction was realized as described in RNeasy Plant Mini Kit (Qiagen, Germany). 100 mg of fungal mycelium was ground with mortar and pestle and transferred to 2 mL microcentrifuge tube, followed by the addition of 450 µL RLC buffer. The mixture was stirred and lysate was transferred to QIA shredder spin column, which was placed in a 2 mL collection tube. After 2 min centrifugation at full speed, the supernatant was transferred to a new tube and 225 µL of 96% ethanol (EtOH) was added. Sample was transferred to RNeasy spin column placed in a 2 mL collection tube, followed by centrifugation at 8000 g for 15 sec. The flow-through was discarded and 700 µL of RW1 buffer was added to the RNeasy spin column followed by centrifugation at 8000 g for 15 sec. The flow-through was discarded and 500 µL RPE buffer was added onto the RNeasy spin column to wash the column. After centrifugation at 8000 g for 2 min, the RNeasy spin column was transferred to a new 2 mL column and centrifugated at 8000 g for 1 min to discard all the remaining RPE buffer. RNeasy spin column was placed in a new 1.5 mL collection tube and 30 µL of RNAse-free water was added. After centrifugation at 8000 g for 1 min, the total RNA was recovered. This step was repeated twice. Total RNA was quantified using Nanodrop 1000 (Thermo Fisher Scientific, United States).

1.2. DNase Treatment

Genomic DNA was removed using TURBO DNA-free ™ Kit (Invitrogen, United States). 0.1 volume (6 µL) of 10X TURBO DNase Buffer and 1 µL TURBO DNase was added to the extracted RNA. After incubation at 37°C for 20–30 min, 7 µL of DNase Inactivation Reagent was added, the sample was mixed and incubated at RT for 5 min. Sample was centrifugated at 10000 g for 1.5 min and supernatant was transferred to a new tube.

Table 8. First step in the cDNA synthesis

Components	Volume	Final concentration
RNA	Variable	1 ng - up to 4 µg*
Anchored-oligo(dT) 18 Primer, 50 pmol/ µL	1 µL	2.5 µM
dH_2O	Variable	
Final volume	11.4 µL	

Table 9. Second step in the cDNA synthesis

Components	Volume	Final concentration
Reverse Transcriptase Reaction Buffer, 5X	4 µL	1X
Protector RNase Inhibitor, 40 U/L	0.5 µL	20 U/L
Deoxynucleotide Mix, 10 mM	2 µL	1 mM
DTT	1 µL	5 mM
Transcriptor High Fidelity Reverse Transcriptase	1.1 µL	10 U
Final volume	20 µL	

Table 10. Dream Taq and Phusion ® polymerase reaction composition and volumes

Dream Taq polymerase		Phusion ® polymerase	
Dream Taq Buffer, 10X	2 µL	Phusion Buffer, 5X	4 µL
dNTP, 10 mM	0.4 µL	dNTP, 10 mM	0.4 µL
Primer forward, 10 µM	1 µL	Primer forward, 10 µM	1 µL
Primer reverse, 10 µM	1 µL	Primer reverse, 10 µM	1 µL
DNA	1 µL	DNA	1 µL
dH_2O	14.5 µL	dH_2O	12.5 µL
Dream Taq polymerase	0.1 µL	Phusion ® polymerase	0.1 µL
Final volume	20 µL	Final volume	2 µL

1.3. cDNA Synthesis

The protocol from Transcriptor High Fidelity cDNA Synthesis Kit (Roche, Switzerland) was followed. Sample was prepared in 1.5 mL as described in **Table 8**. After heating for 10 min at 65°C, the tube was cooled down, and reagents from **Table 9** were added. Reaction was incubated for 30 min at 45°C, before addition of High-Fidelity Reverse Transcriptase inactivation at 85°C for 5 min.

1.4. cDNA polymer chain reaction (PCR) amplification

PCR reaction was used to amplify the cDNA for subsequent cloning steps. Two PCR Taq-Polymerases, Dream Taq (Thermo Fisher Scientific, Unites States) and Phusion ® Hot-Start High Fidelity (Finnzymes, Finland) were used. Reagents and volumes for the PCR reaction are summarized in **Table 10**. PCR reaction, depending on the polymerase type and length of the target cDNA uses specific conditions summarized in **Table 11**. Specific primer pairs for cDNA amplification are indicated in each Result and Discussion chapter.

1.5. DNA visualisation on the agarose gels

DNA was visualized on 1% (w/v) agarose gels. Gel was prepared by mixing appropriate amount of agarose (4905009, Dutscher, France) and 1X TAE buffer with ethidium bromide. Stock solution of 50X TAE buffer contains 50 mM EDTA, 2M Trizma base, 1M acetic acid. After migration DNA was visualised using UV camera (Quantum Vilbern Lourmat, France) set at 590 nm.

1.6. Gel and PCR clean up system protocol

Bands of appropriate size were cut from the agarose gel and purified using Gel Extraction / PCR and DNA Fragment Purification Kit (NB-03-0177, Neo Biotech, France). First, agarose cut from the gel was weighted, and 10 µL of Gel Solubilization Buffer solution per 10 mg of agarose was added. Mixture was heated at 60°C for 10 min until the gel was completely dissolved. Mixture was transferred to the Quick Gel Extraction Columns assembly and incubated for 2 min at RT, followed by 1 min centrifugation at 14000 g. Flow-through was discarded. 500 µL of Wash Buffer was added before 1 min centrifugation at 14000 g. This step was repeated twice. DNA was eluted by adding 50 µL dH_2O, 2 min incubation at RT followed by 1 min centrifugation at 14000 g centrifugation. This step was repeated twice and DNA was concentrated using Speed-Vac concentrator plus (Eppendorf, Germany).

Table 11. Dream Taq and Phusion ® polymerase conditions used during PCR reaction

	Dream Taq polymerase		**Phusion ® polymerase**		**Cycles**
	Temperature	Duration	Temperature	Duration	
Initial DNA denaturation	95°C	5 min	98°C	3 min	1
Denaturation	95°C	1 min	98°C	30 min	
Annealing	Variable*	30 sec	Variable*	15 sec	35
Elongation	72°C	1min/kb	72°C	15-30 sec/kb	
Final elongation	72°C	10 min	72°C	10 min	
Storage	18°C	∞	18°C	∞	1

*Depending on the primer pair.

Table 12. T4 DNA ligase ligation mixture

Components	**Reaction**
T4 DNA Ligase Buffer, 10X	2 µL
Vector DNA	50 ng, 0.020 pmol
Insert DNA	37.5 ng, 0.060 pmol
T4 DNA Ligase	1 µL
dH_2O	Up to 20 µL

1.7. DNA digestion with NEB restriction enzymes

Each primer pair was designed by including specific sites for restriction enzyme (RE) to allow cloning into specific vectors. Reaction was performed in 60 µL by adding 1 µL of each RE, 6 µL of appropriate 10X NEB buffer and 52 µL of amplified DNA dissolved in dH2O. RE used PstI, NotI use 1X NEBuffer™ r3.1 (100 mM NaCl, 50 mM Tris-HCl, 10 mM MgCl2, 100 µg/ml Recombinant Albumin, pH 7.9), while for EcoRI, 1X NEBuffer™ EcoRI/SspI (100 mM Tris-HCl, 50 mM NaCl, 10 mM MgCl2, 0.025% Triton® X-100, pH 7.5) was used. Samples were incubated in a water-bath at 37°C for 90 min. DNA was purified by Gel and PCR clean up system protocol as described.

1.8. Ligation Protocol with T4 DNA Ligase

Purified DNA was ligated into pPICZαB vector previously digested with specific REs. For this purpose, the T4 DNA Ligase (M0202, NEB) in T4 DNA Ligase Reaction Buffer (50 mM Tris-HCl, 10 mM MgCl, 1 mM ATP, 10 mM DTT, pH 7.5) was used (**Table 12)**. Ligation was preformed overnight at 4°C. At the end of the reaction, the T4 ligase was inactivated at 65°C for 10 min.

1.9. Preparation of the competent *E.coli* using $CaCl_2$ technique

E.coli TOP10 starter culture was grown overnight in 10 mL LB (1% (w/v) tryptone, 0.5% (w/v) yeast extract, 0.5% (w/v) NaCl) at 37°C with 200 rpm shaking. The next day 200 mL of LB was inoculated with 1 mL of overnight culture at 37°C under 200 rpm shaking (from an initial optical density (OD) of 0.04) to reach an OD of 0.3. Culture was cooled down on ice in four 50 mL tubes during 10 min and centrifuged for 10 min, 4000 rpm at 4°C. Supernatant was removed and 20 mL of ice-cold 0.1M $CaCl_2$ was gently added. Content of two falcons was pulled and left 30 min on ice ice; After centrifugation for 10 min, 4000 rpm at 4°C, the supernatant was discarded and pellets were resuspended in 4 mL of 0.1M $CaCl_2$ with 15% (v/w) glycerol. Aliquot of 100 µL were prepared and stored at -80°C until transformation.

1.10. *E.coli* TOP10 Transformation

Forty five µL of competent *E.coli* TOP10 was mixed with 2 µL of vector. The mixture was incubated on ice during 20 min, before heat shock at 42°C during 40 sec. *E.coli* was incubated on ice for 5 min. 250 µL of SOC (2% (w/v) tryptone, 0.5% (w/v) yeast extract, 0.48% (w/v) $MgSO_4$, 0.186% (w/v) KCl, 0.3603% (w/v) Dextrose) medium was added before incubation at 37°C, 200

rpm for 90 min. The entire volume was spread on two LB agar (4% (w/v) plates with Zeocin (25 µg/mL). The colonies appeared after 24h incubation at 37°C.

1.11. Colony PCR

To identify colonies that carry the gene of interest, each colony was picked using a 10 µL tip and placed into 50 µL sterile water. Tubes were incubated for 8 min at 95°C. Heat-desaturated DNA was used in a PCR reaction with pPICZαB specific primers 5´AOX (5´-GACTGGTTCCAATTGACAAGC-3´) / 3´AOX (5´-GCAAATGGCATTCTGACATCC-3´) and Dream Taq. Amplified DNA was visualised on agarose gel and positives clones were sent for sequencing (Eurofins, Germany). Positive clones after sequencing were used for *Pichia pastoris* transformation.

1.12. DNA extraction with High Purity Plasmid Miniprep Kit

In this step we are performing plasmid DNA extraction from *E.coli* using the High Purity Plasmid Miniprep Kit (Neo Biotech, France) to obtain sufficient amounts for *Pichia pastoris* transformation. One colony was inoculated in 5 mL of LB with Zeocin and grown overnight at 37°C under200 rpm shaking. The next day the overnight culture was pelleted by centrifugation at 8000 g for 7 min. Supernatant was removed and 250 µL of the Resuspension Solution was added. The solution was transferred to a microcentrifuge tube and Lysis Solution was added. After 5 min incubation, 350 µL of the Neutralization Solution was added and the tube was vigorously mixed. The tube was centrifuged for 10 min at 14 000 g to pellet the cell debris and chromosomal DNA. Supernatant was transferred to the supplied spin column and was centrifuged for 1 min at 14 000 g. After two washes with Wash PB Buffer, the plasmid was recovered in 50 µL by centrifugation at 14 000 g. The DNA was concentrated using Speed-Vac concentrator plus (Eppendorf, Germany).

1.13. *P. pastoris* X33 transformation

1.13.1. Preparing *P. pastoris* for electroporation

Before transformation of P. pastoris X33, vectors were linearized with *Pme*I, that cuts once in the 5´ AOX1 region of pPICZαB. The incubation was at 37°C for 2h, followed by DNA purification as previously described. *P. pastoris* was grown overnight in 5 mL of YPD (1% (w/v) yeast extract 2% (w/v) peptone, 2% (w/v) dextrose) in a 50 mL tube at 30°C. On the second day two 1 liter baffled flasks containing 225 mL of YPD were inoculated with 10 and 20 µL of the overnight culture respectively. The culture was grown overnight to an OD_{600} of 1.3–1.5. One flask was

divided in six 50 mL tubes and cells were pelleted at 1,500 g for 5 min at 6°C. Pellets were resuspended in 500 mL of ice-cold, sterile water. Centrifugation was repeated and pellets were resuspended in 250 ml of ice-cold, sterile water. After a third centrifugation, the pellets were resuspended in 20 ml of ice-cold 1 M sorbitol. On the fourth centrifugation, the pellets were resuspended with 900 µL of ice-cold 1 M sorbitol for a final volume of approximately 1 mL.

1.13.2. Transformation by electroporation

80 µL of the electrocompetent *P. pastoris* cells were mixed with 10 µL (equivalent of 10 µg) of linearized DNA in 2 mL tubes and incubated for 5 min on ice. The whole content was transferred to electroporation cuvette and cells were pulse with 1500 V electric shock in Eporator (Eppendorf, Germany). Immediately, 1 mL of ice-cold 1 M sorbitol was added and the whole content was transferred to a sterile 15 mL tube and incubated at 30°C without shaking for 2 h. 200 µL of the mix was spread on YPD plates containing 100 $\mu g.mL^{-1}$Zeocin while the rest was pelleted by centrifugation at 1500 g for 5 min at 4°C. Supernatant was discarded and cells were resuspended in 100 µL of YPD and spread on YPD plates containing 100 $\mu g.mL^{-1}$ Zeocin. Plates were incubated for 2 days at 30°C. 30 colonies were picked and transferred on new YPD plates.

2. Part: Biochemical methods

2.1. Enzyme expression

Five colonies of each construct were checked for enzyme expression. Starter cultures containing 1.5 mL BMGY (1% (w/v) yeast extract 2% (w/v) peptone, 1.34% (w/v) yeast nitrogen base, 4×10^{-5}% (w/v) biotin, 1% (v/v) glycerol, 100 mM potassium phosphate, pH 6) were inoculated with one colony and grown overnight at 30°C, 250 rpm. The next day OD_{600} was measured and cells at OD_{600} of 1 were transferred to 5 mL BMMY, which has similar composition to BMGY except that 1% (v/v) glycerol is replaced by 0.5% (v/v) MeOH. Enzymes were expressed for 3 days with daily addition of 0.5% (v/v) of 100 % MeOH. Culture was stopped on the fifth day by centrifugation at 1500 g during 7 min. Supernatant was recovered as proteins are secreted by *P. pastoris* thanks to the signal peptide present in the pPICZαB vector. Colonies that showed highest expression and active enzymes were subsequently produced in 200 mL BMMY.

Table 13. Composition and volumes used for preparation of SDS-page

Resolving gel		Stacking gel	
Components	**Volume**	**Component**	**Volume**
dH_2O	2.05 mL	dH_2O	3.125 mL
30% Acrylamide/Bis-acrylamide	4 mL	30% Acrylamide/Bis-acrylamide	625 μL
1M Tris-HCl pH 8.8	3.75 mL	1M Tris pH 6.8	625 μL
10% SDS[1]	100 μL	10% SDS[1]	50 μL
10% APS[2]	100 μL	10% APS[2]	50 μL
TEMED[3]	8 μL	TEMED[3]	5 μL
Final volume	10 mL	Final volume	5 mL

[1]Sodium Dodecyl Sulfate, [2]Ammonium persulfate, [3] N,N,N′,N′-Tetramethylethylenediamine

2.2. Enzymes purification and concentration and buffer change

For enzyme purification we have used affinity chromatography (IMAC) as the pPICZαB vector harbours C-myc and poly-His tag in frame with our coding sequences. Supernatants recovered after culture centrifugation were filtered with GD/X 0.45 µm PES filter Media (Whatman, United Kingdom) and HisTrap excel columns (GE Healthcare, Unites States) were used for purification. 100 mL supernatant was loaded onto the column at a 1 $mL.min^{-1}$ flow rate. His-trap column was washed with 10 column volumes of equilibration buffer (25 mM imidazole, 250 mM NaCl, 50 mM NaP pH 7,5). Proteins were recovered with 15 mL of elution buffer (250 mM imidazole, 250 mM NaCl, 50 mM NaP pH 7.5). Proteins were concentrated with Amicon Ultra Centrifugal filter with a 10 kDa cut-off (Merck Millipore). Concentration was performed multiple times at 8°C, 6000 g for 7 min until a final volume of 140 µL.

As the buffer contains high amount of imidazole and NaCl we performed buffer exchange using PD SpinTrap G-25 (28-9180-04, GE Healthcare). Column was equilibrated by adding 400 µL of equilibration buffer (in the case of VdPME1 and VdPelB; 50 mM Tris-HCl pH 7, VdPG2, ADP2; 50 mM sodium acetate pH 5, PGLR; 50 mM sodium acetate pH 4) followed by 1 min 800 g centrifugation. This step was repeated eight times. 140 µL of appropriate buffer was then applied to the column and final centrifugation of 2 min at 800 g was performed.

2.3. Enzyme detection

2.3.1. Polyacrylamide gel electrophoresis

For enzyme detection we have used polyacrylamide gel electrophoresis under denaturing conditions (SDS-PAGE) followed by Western blotting as the pPICZαB vector carries C-myc and poly-His tags for immunodetection. SDS-PAGE was prepared as stated in **Table 13**. Enzymes were denatured by mixing proteins with gel loading dye (#B7025, NEB) and heating at 95°C for 10 min. Electrophoresis was run on mini-PROTEAN 3 system (BioRad, France). Gels were stained using PageBlue Protein Staining Solution (Thermo Fisher Scientific, United States) during 1h followed by overnight destaining.

2.3.2. Western blot

SDS-PAGE was prepared as mentioned above. Gels was placed in cathode buffer (25mM Tris pH 9.4, 40 mM glycine, 10% (v/v) EtOH) for 15 min. Polyvinylidene difluoride (PVDF) membrane was soaked 15 sec in 100% EtOH, 2 min in dH_2O and 5 min in anode II buffer (25mM Tris pH

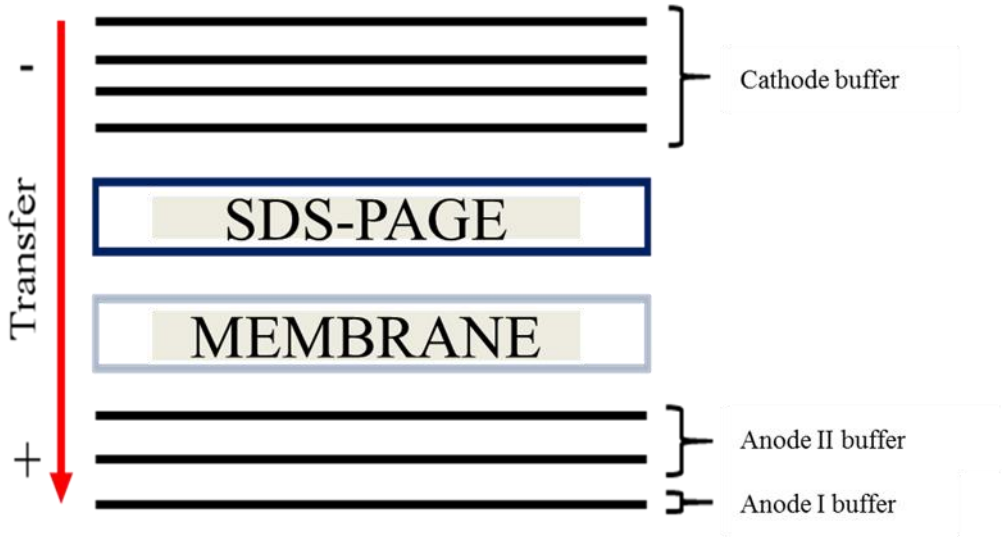

Figure 39. Schematic representation of protein transfer on PVDF membrane

Table 14. DNS composition used for determining the amount of PG-products

DNS	
Components	**Reaction**
dH_2O	70 mL
3,5 dinitrosalicylic acid (D-0550, Sigma)	1 g
NaOH (S-5881, Sigma)	1 g
Sodium sulfite Na_2SO_3 (S4672, Sigma)	0.05 g
Sodium potassium tartarate (S2377, Sigma)	30 g
3,5 dinitrosalicylic acid (D-0550, Sigma)	1 g
Final volume	100 mL

10.4, 10% (v/v) EtOH). We used semi dry system Trans-blot Turbo (Bio-Rad). The membrane and the gel are arranged according to the set-up in **Figure 39** and packed with layers of Whatman 3M paper (Sigma, France) soaked in Anode I buffer (300 mM Tris pH 10.4, 10% (v/v) EtOH). Transfer was conducted at 60 mA for 40 min. After the transfer PVDF membrane was placed in 96% EtOH for 1min and dried.

2.3.3. Immunodetection with anti-His antibody

Monoclonal anti-His antibodies from goat coupled with horse radish peroxidase (Sigma, France) were used for the detection of proteins bound on the PVDF membrane. PVDF membrane was incubated in 25 mL 4% milk solution for 30 min followed by 1h 30 min of immunostaining in 20 mL anti-His antibodies (diluted 4000 times) solution. The washes are done in 1X TBS Tween 20 (20 mL TBS 10X (50 mM Tris, 150 mM NaCl, pH 7.6), 0.5 (v/v) Tween 20) for 15 min, 15 min and 5 min. Revelation of the protein was by adding the 3 mL of 1X DAB substrate (10% (v/v) 10X DAB substrate (#1855920, Thermo Fisher) in 1X Peroxidase substrate buffer (#1855910, Thermo Fisher).

2.4. Enzyme activity tests

2.4.1. PG activity test

VdPG2, PGLR and ADPG2 activity assays were performed using dinitrosalicylic acid (DNS) protocol for the detection of non-reducing sugars (Miller, 1959). All substrates were prepared at 8% (w/v) in buffers specified in the Result and Discussion chapters. Reaction was prepared in 24 µL by mixing 12 µL of the specific enzyme buffer with 12 µL of dissolved pectins. Reaction was stopped by adding 150 µL of DNS (**Table 14**). 100 µL of the reaction was transferred in 98 wells plate and the absorbance was read spectrophotometrically at 550 nm.

2.4.2. PME activity test

VdPME1 activity was measured according to Anthon and Barrett, 2004.A standard curve of MeOH (0–20 $\mu g.ml^{-1}$) was used. Incubation was performed at 40°C for 30 min with 5 µL of purified VdPME1 protein ($2.3.10^{-3}$ $\mu g.\mu L^{-1}$), 5 µL of substrate (0.8% (w/v) and 85 µL of 50 mM sodium acetate buffer (pH 3 to 5) or Tris-HCl buffer (pH 6 to 9). Enzyme was inactivated by heating the solution 10 min at 85°C. The volume was divided into two equal volumes and lyophilized. 40 µL of cold water and 40 µL of 0.2 M NaOH was added to one of the lyophilized tubes and incubated

for 1 h at 4°C. 40 µL of 0.2 M HCl was then added to stop saponification. In parallel the second tube, corresponding to non-saponified samples, contained 40 µL of cold dH_2O, 40 µL of 0.2 M NaOH and 40 µL of 0.2 M HCl. In two new tubes, 100 µL of 200 mM Tris–HCl (pH 7.5), 40 µL of 3-Methyl-2-benzothiazolinone hydrazine (MBTH, 3% (w/v)), and 20 µL of 0.02 U $µl^{-1}$ alcohol oxidase were added to 50 µL of saponified or non-saponified solutions, respectively. These tubes were incubated at 30°C for 20 min. 200 µL of solution containing 0.5% ($FeNH_4(SO_4)2$) $12H_2O$, 0.5% sulfamic acid was added and cooled to room temperature. 590 µL of dH_2O was added to stop the reaction. The absorbance was determined at 620 nm on an Uvikon spectrophotometer. PME activity was calculated as the difference in absorbance between saponified and non-saponified samples.

2.4.3. PL/PNL activity test

VdPelB activity was measured by monitoring the increase in optical density at 235 nm due to formation of unsaturated uronide product using UV/VIS Spectrophotometer (PowerWave Xs2, BioTek, France) during 60 min. All substrates were prepared at 8% (w/v) in buffers specified in the Result and Discussion chapter. 50 µL of pectins were mixed with 40 µL of buffer and 10 µL of enzymes with 0.5 µM $CaCl_2$ or 5 µM EDTA (Sigma) final concentrations.

3. Part: Mass spectrometry analysis

3.1. Digestion of commercial pectin for LC-MS/MS oligoprofiling

Pectin substrates were dissolved in 50 mM ammonium acetate pH 5 buffer at 0.4% (w/v) final concertation. PGs (PGLR, ADPG2, VdPG2) were prepared in the same buffer. VdPelB and pectin substrates were prepared in 50 mM Tris-HCl pH 7buffer. 50 µL of pectins were mixed with 40 µL of buffer and 10 µL of enzymes. Samples were incubated at 50°C for various incubation times. Reactions were stopped by boiling the samples at 100°C for 15 min and by adding 100 µL of 100% EtOH. Undigested pectins were pelleted by centrifugation for 5 min at 5000 g. 100 µL of supernatant was transferred in a new tube and evaporated for minimum 2 h at 45°C. OGs were dissolved in dH_2O before analysis.

3.2. Digestion of plant CW for LC-MS/MS oligoprofiling

Flax seeds from two different varieties, Evea (spring fiber, partially tolerant to Verticillium wilt disease) and Violin (autumn fiber, susceptible to Verticillium wilt disease) were kindly provided

by Linea semences (Grandvilliers, France). Seeds were sterilized using Triton 0.01 % (v/v, T8787, Sigma) diluted in ethanol 70 % (w/v) during 15 min followed by 15 min incubation in ethanol 95% (v/v). Seeds were dried overnight. Seeds were during three days on wet towel tissue at 21°C, 16 h/8 h light/dark. Similarly, Arabidopsis seeds (Col-0 ecotype) were grown during 7 days at 21°C, 16 h/8 h light/dark. Roots were cut and placed into ethanol 100% (v/v) for 24 h. They were then washed two times during 5 min with acetone 100 % (v/v) and left to dry for 24 h. Forty roots for flax and 30 roots for Arabidopsis per replica were rehydrated in 140 µL 50 mM ammonium acetate pH 5 during 2 h on room temperature and digested with VdPG2, PGLR, ADPG2 or VdPelB using the above-mentioned protocol.

3.3. Ultra-performance size-exclusion chromatography (UP-SEC)

Samples were prepared in water at a concentration of 8 $mg.ml^{-1}$. Chromatographic separations were performed on an ACQUITY UPLC H-Class system (Waters Corporation, Milford, MA, USA) using an ACQUITY UPLC Protein BEH SEC column (125Å, 1.7 µm, 4.6 mm x 300 mm). Elution was in 50 mM ammonium formate, formic acid 0.1% at a flow rate of 400 µL/min and a column oven temperature of 40°C. The injection volume was set to 2 µL.

3.4. Electrospray ionization high-resolution mass spectrometry (ESI-HRMS)

MS-detection was performed with the SYNAPT G2-Si instrument hyphenated with the ACQUITY UPLC H-Class system. The ESI source was operating in the negative ionization mode using a capillary voltage of -2.5 kV and the following conditions: cone voltage, 120 V; source offset, 20 V; source temperature, 120°C; desolvation gas temperature, 450°C; desolvation gas flow, 800 $L.h^{-1}$, and cone gas flow, 50 $L.h^{-1}$. Nitrogen (> 99.5%) was employed as the desolvation gas. Mass calibration was carried out using a sodium formate solution (10mM NaOH in isopropanol/water/formic acid 49.9:49.9:0.2, v/v/v) and a lock mass correction was applied for accurate mass measurements using the $[M-H]^-$ ion (m/z 554.2615) obtained from a Leu-enkephalin solution (1 ng. μL^{-1} in H_2O/CH_3CN/formic acid 50:49.9:0.1, v/v/v). The scan range was m/z 50-2500 at 0.25 s/scan. The TOF was operated in the sensitivity mode, providing an average resolving power of 20,000 (FWHM). All spectra were recorded in the centroid mode. Data acquisition was performed with MassLynx software (V4.1, Waters).

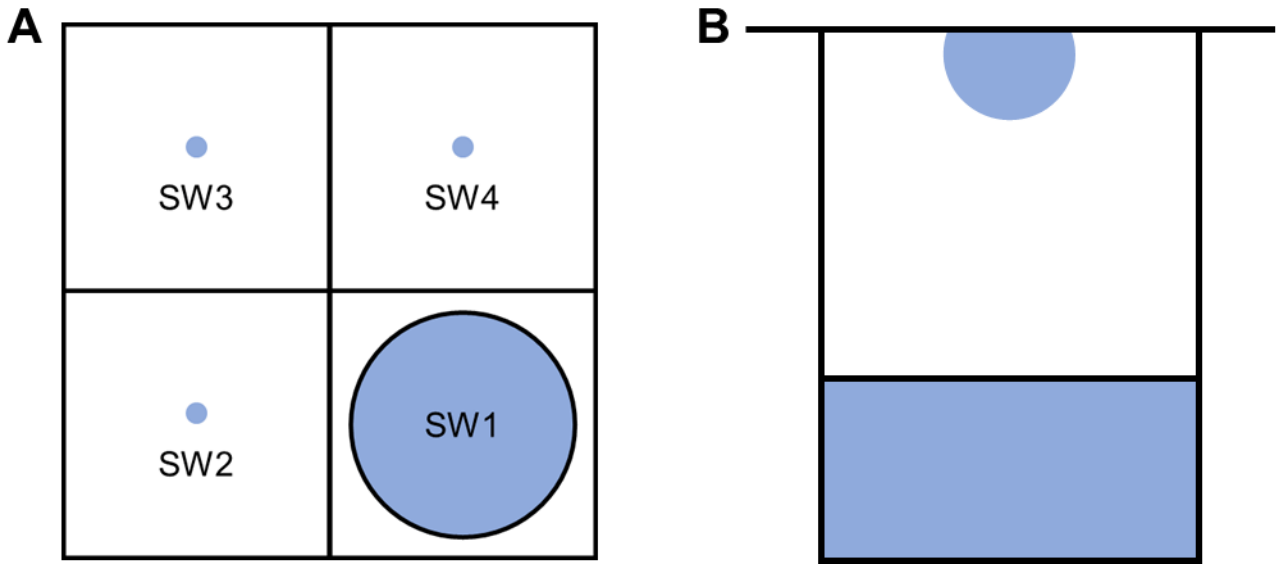

Figure 40. Schematic representation sitting and hanging drop vapour diffusion methods
A) Sitting drop, 96 wells plate in each well containing 4 SW (SubWells). In the SW1 is filled with 50 µL of precipitation solution while the three different protein concentrations in SW2, SW3, and SW4 are 20 mg ml^{-1}, 10 mg ml^{-1} and 5 mg ml^{-1}, respectively B) Scale up well is filled with 200 µL of precipitation solution while 1 µL of the precipitant condition with 1 µL of protein is mixed in hanging drop vapour diffusion method.

4. Part: Crystallisation of enzymes

PGLR, ADPG2 and VdPelB were concentrated at 20 mg ml^{-1}. Crystallization was performed using the sitting-drop vapour-diffusion method. Crystallisation conditions were screened using a Mosquito robot (TTP Labtech) and the following kits: PACT premier plate, JCSG crystallization screen, MemGold, MIDAS, ProPlex PGA Screen (Molecular Dimensions, United Kingdom). On each plate 50 µL of precipitant was added into the sub well (SW) 1. Enzyme concentration were 20 mg ml^{-1} in SW2, 10 mg ml^{-1} in SW3 and 5 mg ml^{-1} in SW4 (**Figure 40A**). PGLR, ADPG2 and VdPelB (100 nL) were mixed with an equal volume of precipitant (1:1). Crystals for PGLR, ADPG2 and VdPelB formed after 6, 2 and 1month, respectively. Scale-up of the best condition was realized by mixing 1 µL of the best precipitant condition with 1 µL of the enzyme in the hanging drop vapor-diffusion method (**Figure 40B**).

REFERENCES

In this part, only the references corresponding to General Introduction are included. In Results and Discussion corresponding references can be found at the end of each chapter.

Abbott DW, Boraston AB (2007) The Structural Basis for Exopolygalacturonase Activity in a Family 28 Glycoside Hydrolase. J Mol Biol **368**: 1215–1222

Agüero CB, Uratsu SL, Greve C, Powell ALT, Labavitch JM, Meredith CP, Dandekar AM (2005) Evaluation of tolerance to Pierce's disease and Botrytis in transgenic plants of Vitis vinifera L. expressing the pear PGIP gene. Mol Plant Pathol **6**: 43–51

Akita M, Suzuki A, Kobayashi T, Ito S, Yamane T (2001) The first structure of pectate lyase belonging to polysaccharide lyase family 3. Acta Crystallogr Sect D Biol Crystallogr **57**: 1786–1792

Alahuhta M, Chandrayan P, Kataeva I, Adams MWW, Himmel ME, Lunin V V. (2011) A 1.5 Å resolution X-ray structure of the catalytic module of Caldicellulosiruptor bescii family 3 pectate lyase. Acta Crystallogr Sect F Struct Biol Cryst Commun **67**: 1498–1500

Van Alebeek GJWM, Christensen TMIE, Schols HA, Mikkelsen JD, Voragen AGJ (2002) Mode of action of pectin lyase A of Aspergillus niger on differently C6-substituted oligogalacturonides. J Biol Chem **277**: 25929–25936

Alexandersson E, Becker JVW, Jacobson D, Nguema-Ona E, Steyn C, Denby KJ, Vivier MA (2011) Constitutive expression of a grapevine polygalacturonase-inhibiting protein affects gene expression and cell wall properties in uninfected tobacco. BMC Res Notes **4**: 493

Ali S, Søndergaard CR, Teixeira S, Pickersgill RW (2015) Structural insights into the loss of catalytic competence in pectate lyase activity at low pH. FEBS Lett **589**: 3242–3246

Altartouri B, Bidhendi AJ, Tani T, Suzuki J, Conrad C, Chebli Y, Liu N, Karunakaran C, Scarcelli G, Geitmann A (2019) Pectin Chemistry and Cellulose Crystallinity Govern Pavement Cell Morphogenesis in a Multi-Step Mechanism. Plant Physiol **181**: 127–141

Altartouri B, Geitmann A (2015) Understanding plant cell morphogenesis requires real-time monitoring of cell wall polymers. Curr Opin Plant Biol **23**: 76–82

Amos RA, Pattathil S, Yang J-Y, Atmodjo MA, Urbanowicz BR, Moremen KW, Mohnen D (2018) A two-phase model for the non-processive biosynthesis of homogalacturonan polysaccharides by the GAUT1:GAUT7 complex. J Biol Chem **293**: 19047–19063

Amsbury S, Hunt L, Elhaddad N, Baillie A, Lundgren M, Verhertbruggen Y, Scheller H V., Knox JP, Fleming AJ, Gray JE (2016) Stomatal Function Requires Pectin De-methyl-esterification of the Guard Cell Wall. Curr Biol **26**: 2899–2906

Anand G, Yadav S, Yadav D (2017) Production, purification and biochemical characterization of an exo-polygalacturonase from Aspergillus niger MTCC 478 suitable for clarification of

orange juice. 3 Biotech **7**: 122

Anderson CT (2016) We be jammin': An update on pectin biosynthesis, trafficking and dynamics. J Exp Bot **67**: 495–502

André-Leroux G, Tessier D, Bonnin E (2005) Action pattern of Fusarium moniliforme endopolygalacturonase towards pectin fragments: Comprehension and prediction. Biochim Biophys Acta - Proteins Proteomics **1749**: 53–64

André-Leroux G, Tessier D, Bonnin E (2009) Endopolygalacturonases reveal molecular features for processivity pattern and tolerance towards acetylated pectin. Biochim Biophys Acta - Proteins Proteomics **1794**: 5–13

Anthon GE, Barrett DM (2004) Comparison of three colorimetric reagents in the determination of methanol with alcohol oxidase. Application to the assay of pectin methylesterase. J Agric Food Chem **52**: 3749–3753

Armand S, Wagemaker MJM, Sánchez-Torres P, Kester HCM, Van Santen Y, Dijkstra BW, Visser J, Benen JAE (2000) The active site topology of Aspergillus niger endopolygalacturonase II as studied by site-directed mutagenesis. J Biol Chem **275**: 691–696

Ashworth LJ (1974) Free and Bound Microsclerotia of Verticillium albo-atrum in Soils. Phytopathology **64**: 563

Atmodjo MA, Hao Z, Mohnen D (2013) Evolving views of pectin biosynthesis. Annu Rev Plant Biol **64**: 747–779

Atmodjo MA, Sakuragi Y, Zhu X, Burrell AJ, Mohanty SS, Atwood JA, Orlando R, Scheller H V., Mohnen D (2011) Galacturonosyltransferase (GAUT)1 and GAUT7 are the core of a plant cell wall pectin biosynthetic homogalacturonan:galacturonosyltransferase complex. Proc Natl Acad Sci **108**: 20225–20230

Babu Y, Bayer M (2014) Plant polygalacturonases involved in cell elongation and separation—the same but different? Plants **3**: 613–623

Bacete L, Mélida H, López G, Dabos P, Tremousaygue D, Denancé N, Miedes E, Bulone V, Goffner D, Molina A (2020) Arabidopsis response reGUlator 6 (ARR6) modulates plant cell-wall composition and disease resistance. Mol Plant-Microbe Interact **33**: 767–780

Bashi ZD, Rimmer SR, Khachatourians GG, Hegedus DD (2013) Brassica napus polygalacturonase inhibitor proteins inhibit Sclerotinia sclerotiorum polygalacturonase enzymatic and necrotizing activities and delay symptoms in transgenic plants. Can J Microbiol **59**: 79–86

Benedetti M, Andreani F, Leggio C, Galantini L, Di Matteo A, Pavel NV, De Lorenzo G, Cervone F, Federici L, Sicilia F (2013) A single amino-acid substitution allows endo-polygalacturonase of Fusarium verticillioides to acquire recognition by PGIP2 from Phaseolus vulgaris. PLoS One **8**: 1–11

Benedetti M, Leggio C, Federici L, de Lorenzo G, Pavel NV, Cervone F (2011) Structural resolution of the complex between a fungal polygalacturonase and a plant polygalacturonase-inhibiting protein by small-angle x-ray scattering. Plant Physiol **157**: 599–607

Benedetti M, Pontiggia D, Raggi S, Cheng Z, Scaloni F, Ferrari S, Ausubel FM, Cervone F, De Lorenzo G (2015) Plant immunity triggered by engineered in vivo release of oligogalacturonides, damage-associated molecular patterns. Proc Natl Acad Sci **112**: 5533–5538

Benen JAE, Kester HCM, Visser J (1999) Kinetic characterization of Aspergillus niger N400 endopolygalacturonases I, II and C. Eur J Biochem **259**: 577–585

Bennett MD, Leitch IJ, Price HJ, Johnston JS (2003) Comparisons with Caenorhabditis (∼100 Mb) and Drosophila (∼175 Mb) using flow cytometry show genome size in Arabidopsis to be ∼157 Mb and thus ∼25% larger than the Arabidopsis genome initiative estimate of ∼125 Mb. Ann Bot **91**: 547–557

Blanco P, Sieiro C, Diaz A, Villa TG (1994) Production and partial characterization of an endopolygalacturonase from Saccharomyces cerevisiae. Can J Microbiol **40**: 974–977

Blum A, Bressan M, Zahid A, Trinsoutrot-Gattin I, Driouich A, Laval K (2018) Verticillium Wilt on Fiber Flax: Symptoms and Pathogen Development In Planta. Plant Dis **102**: 2421–2429

Bonivento D, Pontiggia D, Matteo A Di, Fernandez-Recio, Juan Salvi G, Tsernoglou D, Cervone F, Lorenzo G De, Federici4 L (2008) Crystal structure of the endopolygalacturonase from the phytopathogenic fungus Colletotrichum lupini and its interaction with polygalacturonase-inhibiting proteins. Proteins **70**: 311–319

Bonnin E, Garnier C, Ralet M (2014) Pectin-modifying enzymes and pectin-derived materials : applications and impacts. Appl Microbiol Biotechnol **98**: 519–532

Bonnin E, Le Goff A, Körner R, Van Alebeek GJWM, Christensen TMIE, Voragen AGJ, Roepstorff P, Caprari C, Thibault JF (2001) Study of the mode of action of endopolygalacturonase from Fusarium moniliforme. Biochim Biophys Acta- Gen Subj **1526**: 301–309

Bonnin E, Le Goff A, Körner R, Vigouroux J, Roepstorff P, Thibault JF (2002) Hydrolysis of pectins with different degrees and patterns of methylation by the endopolygalacturonase of Fusarium moniliforme. Biochim Biophys Acta - Protein Struct Mol Enzymol **1596**: 83–94

Boraston AB, Abbott DW (2012) Structure of a pectin methylesterase from Yersinia enterocolitica. Acta Crystallogr Sect F Struct Biol Cryst Commun **68**: 129–133

Braybrook SA, Peaucelle A (2013) Mechano-Chemical Aspects of Organ Formation in Arabidopsis thaliana: The Relationship between Auxin and Pectin. PLoS One **8**: e57813

Brutus A, Sicilia F, Macone A, Cervone F, De Lorenzo G (2010) A domain swap approach reveals a role of the plant wall-associated kinase 1 (WAK1) as a receptor of oligogalacturonides. Proc Natl Acad Sci **107**: 9452–9457

Bussink HJD, Brouwer KB, de Graaff LH, Kester HCM, Visser J (1991) Identification and characterization of a second polygalacturonase gene of Aspergillus niger. Curr Genet **20**: 301–307

Bussink HJD, Kester HCM, Visser J (1990) Molecular cloning, nucleotide sequence and

expression of the gene encoding prepro-polygalacturonasell of Aspergillus niger. FEBS Lett **273**: 127–130

Cabanne C, Donèche B (2002) Purification and characterization of two isozymes of polygalacturonase from Botrytis cinerea. Effect of calcium ions on polygalacturonase activity. Microbiol Res **157**: 183–189

Cabrera JC, Boland A, Messiaen J, Cambier P, Van Cutsem P (2008) Egg box conformation of oligogalacturonides: The time-dependent stabilization of the elicitor-active conformation increases its biological activity. Glycobiology **18**: 473–482

Caffall KH, Mohnen D (2009) The structure, function, and biosynthesis of plant cell wall pectic polysaccharides. Carbohydr Res **344**: 1879–1900

Camardella L, Carratore V, Ciardiello MA, Servillo L, Balestrieri C, Giovane A (2000) Kiwi protein inhibitor of pectin methylesterase. Eur J Biochem **267**: 4561–4565

Cantu D, Vicente AR, Labavitch JM, Bennett AB, Powell ALT (2008) Strangers in the matrix: plant cell walls and pathogen susceptibility. Trends Plant Sci **13**: 610–617

Cao J (2012) The Pectin Lyases in Arabidopsis thaliana: Evolution, Selection and Expression Profiles. PLoS One **7**: e46944

Caprari C, Richter A, Bergmann C, Lo Cicero S, Salvi G, Cervone F, De Lorenzo G (1993) Cloning and characterization of a gene encoding the endopolygalacturonase of Fusarium moniliforme. Mycol Res **97**: 497–505

Carpita NC (1996) Structure and biogenesis of the cell walls of grasses. Annu Rev Plant Physiol Plant Mol Biol **47**: 445–476

Carpita NC, Gibeaut DM (1993) Structural models of primary cell walls in flowering plants: consistency of molecular structure with the physical properties of the walls during growth. Plant J **3**: 1–30

Chen JY, Xiao HL, Gui YJ, Zhang DD, Li L, Bao YM, Dai XF (2016) Characterization of the Verticillium dahliae exoproteome involves in pathogenicity from cotton-containing medium. Front Microbiol **7**: 1–15

Chen Y, Sun D, Zhou Y, Liu L, Han W, Zheng B, Wang Z, Zhang Z (2014) Cloning, Expression and Characterization of a Novel Thermophilic Polygalacturonase from Caldicellulosiruptor bescii DSM 6725. Int J Mol Sci **15**: 5717–5729

Cho SW, Lee S, Shin W (2001) The X-ray structure of Aspergillus aculeatus Polygalacturonase and a Modeled structure of the Polygalacturonase-Octagalacturonate Complex. J Mol Biol **311**: 863–878

Chotigeat W, Duangchu S, Wititsuwannakun R, Phongdara A (2009) Cloning and characterization of pectate lyase from Hevea brasiliensis. Plant Physiol Biochem **47**: 243–247

Chourasia A, Sane VA, Nath P (2006) Differential expression of pectate lyase during ethylene-induced postharvest softening of mango (Mangifera indica var. Dashehari). Physiol Plant **128**: 546–555

Christgau S, Kofod L V, Halkier T, Andersen LN, Hockauf M, Do K (1996) Pectin methyl esterase from Aspergillus aculeatus : expression cloning in yeast and characterization of the recombinant enzyme. Biosystems **712**: 705–712

Chun J-P, Huber DJ (1998) Polygalacturonase-Mediated Solubilization and Depolymerization of Pectic Polymers in Tomato Fruit Cell Walls. Plant Physiol **117**: 1293–1299

Del Corpo D, Fullone MR, Miele R, Lafond M, Pontiggia D, Grisel S, Kieffer-Jaquinod S, Giardina T, Bellincampi D, Lionetti V (2020) AtPME17 is a functional Arabidopsis thaliana pectin methylesterase regulated by its PRO region that triggers PME activity in the resistance to Botrytis cinerea. Mol Plant Pathol **21**: 1620–1633

Cosgrove DJ (1997) Assembly and enlargement of the primary cell wall in plants. Annu Rev Cell Dev Biol **13**: 171–201

Cosgrove DJ (2016a) Plant cell wall extensibility: Connecting plant cell growth with cell wall structure, mechanics, and the action of wall-modifying enzymes. J Exp Bot **67**: 463–476

Cosgrove DJ (2016b) Catalysts of plant cell wall loosening. F1000Research **5**: 1–13

Cosgrove DJ (2005) Growth of the plant cell wall. Nat Rev Mol Cell Biol **6**: 850–861

Creze C, Castang S, Derivery E, Haser R, Hugouvieux-Cotte-Pattat N, Shevchik VE, Gouet P (2008) The Crystal Structure of Pectate Lyase PelI from Soft Rot Pathogen *Erwinia chrysanthemi* in Complex with Its Substrate. J Biol Chem **283**: 18260–18268

Czerwinski EW, Midoro-Horiuti T, White MA, Brooks EG, Goldblum RM (2005) Crystal structure of jun a 1, the major cedar pollen allergen from Juniperus ashei, reveals a parallel β-helical core. J Biol Chem **280**: 3740–3746

D'Ovidio R, Roberti S, Di Giovanni M, Capodicasa C, Melaragni M, Sella L, Tosi P, Favaron F (2006) The characterization of the soybean polygalacturonase-inhibiting proteins (Pgip) gene family reveals that a single member is responsible for the activity detected in soybean tissues. Planta **224**: 633–645

Davidsson P, Broberg M, Kariola T, Sipari N, Pirhonen M, Palva ET (2017) Short oligogalacturonides induce pathogen resistance-associated gene expression in Arabidopsis thaliana. BMC Plant Biol **17**: 1–17

Davies G, Henrissat B (1995) Structures and mechanisms of glycosyl hydrolases. Structure **3**: 853–859

Dehors J, Mareck A, Kiefer-Meyer MC, Menu-Bouaouiche L, Lehner A, Mollet JC (2019) Evolution of cell wall polymers in tip-growing land plant gametophytes: Composition, distribution, functional aspects and their remodeling. Front Plant Sci **10**: 1–28

Denoux C, Galletti R, Mammarella N, Gopalan S, Werck D, De Lorenzo G, Ferrari S, Ausubel FM, Dewdney J (2008) Activation of defense response pathways by OGs and Flg22 elicitors in Arabidopsis seedlings. Mol Plant **1**: 423–445

Derbyshire P, McCann MC, Roberts K (2007) Restricted cell elongation in Arabidopsis hypocotyls is associated with a reduced average pectin esterification level. BMC Plant Biol **7**:

Deshpande AB, Anamika K, Jha V, Chidley HG, Oak PS, Kadoo NY, Pujari KH, Giri AP, Gupta VS (2017) Transcriptional transitions in Alphonso mango (Mangifera indica L.) during fruit development and ripening explain its distinct aroma and shelf life characteristics. Sci Rep **7**: 8711

DeVay JE, Forreste LL, Garber RH, Butterfield EJ (1974) Characteristics and Concentration of Propagules of Verticillium dahliae in Air-Dried Field Soils in Relation to the Prevalence of Verticillium Wilt in Cotton. Phytopathology **64**: 22–29

Doblin MS, Pettolino F, Bacic A (2010) Evans Review: Plant cell walls: The skeleton of the plant world. Funct Plant Biol **37**: 357–381

Domingo C, Roberts K, Stacey NJ, Connerton I, Ruíz-Teran F, McCann MC (1998) A pectate lyase from Zinnia elegans is auxin inducible. Plant J **13**: 17–28

Dominguez-Puigjaner E, Llop I, Vendrell M, Prat S (1997) A cDNA Clone Highly Expressed in Ripe Banana Fruit Shows Homology to Pectate Lyases. Plant Physiol **114**: 1071–1076

Doyle EA, Lambert KN (2002) Cloning and Characterization of an Esophageal-Gland-Specific Pectate Lyase from the Root-Knot Nematode Meloidogyne javanica. Mol Plant-Microbe Interact **15**: 549–556

Dranca F, Oroian M (2018) Extraction, purification and characterization of pectin from alternative sources with potential technological applications. Food Res Int **113**: 327–350

Duressa D, Anchieta A, Chen D, Klimes A, Garcia-Pedrajas MD, Dobinson KF, Klosterman SJ (2013) RNA-seq analyses of gene expression in the microsclerotia of Verticillium dahliae. BMC Genomics **14**: 5–18

Ehwald R, Woehlecke H, Titel C (1992) Cell wall microcapsules with different porosity from suspension cultured Chenopodium album. Phytochemistry **31**: 3033–3038

Eklöf JM, Tan TC, Divne C, Brumer H (2009) The crystal structure of the outer membrane lipoprotein YbhC from Escherichia coli sheds new light on the phylogeny of carbohydrate esterase family 8. Proteins Struct Funct Bioinforma **76**: 1029–1036

Federici L, Caprari C, Mattei B, Savino C, Di Matteo A, De Lorenzo G, Cervone F, Tsernoglou D (2001) Structural requirements of endopolygalacturonase for the interaction with PGIP (polygalacturonase-inhibiting protein). Proc Natl Acad Sci U S A **98**: 13425–13430

Ferrari S, Galletti R, Denoux C, De Lorenzo G, Ausubel FM, Dewdney J (2007) Resistance to Botrytis cinerea Induced in Arabidopsis by Elicitors Is Independent of Salicylic Acid, Ethylene, or Jasmonate Signaling But Requires PHYTOALEXIN DEFICIENT3. Plant Physiol **144**: 367–379

Ferrari S, Galletti R, Vairo D, Cervone F, De Lorenzo G (2006) Antisense expression of the Arabidopsis thaliana AtPGIP1 gene reduces polygalacturonase-inhibiting protein accumulation and enhances susceptibility to Botrytis cinerea. Mol Plant-Microbe Interact **19**: 931–936

Ferrari S, Savatin D V, Sicilia F, Gramegna G, Cervone F, Lorenzo G de (2013) Oligogalacturonides: plant damage-associated molecular patterns and regulators of growth and development. Front Plant Sci **4**: 1–9

Ferrari S, Sella L, Janni M, De Lorenzo G, Favaron F, D'Ovidio R (2012) Transgenic expression of polygalacturonase-inhibiting proteins in Arabidopsis and wheat increases resistance to the flower pathogen Fusarium graminearum. Plant Biol **14**: 31–38

Ferrari S, Vairo D, Ausubel FM, Cervone F, De Lorenzo G (2003) Tandemly duplicated Arabidopsis genes that encode polygalacturonase-inhibiting proteins are regulated coordinately by different signal transduction pathways in response to fungal infection. Plant Cell **15**: 93–106

Fitzell R, Evans G, Fahy PC (1980) Studies on the colonization of plant roots by Verticillium dahliae klebahn with use of immunofluorescent staining. Aust J Bot **28**: 357–368

Fradin EF, Thomma BPHJ (2006) Physiology and molecular aspects of Verticillium wilt diseases caused by V. dahliae and V. albo-atrum. Mol Plant Pathol **7**: 71–86

Francis KE, Lam SY, Copenhaver GP (2006) Separation of Arabidopsis Pollen Tetrads Is Regulated by QUARTET1 , a Pectin Methylesterase Gene. Plant Physiol **142**: 1004–1013

Fries M, Ihrig J, Brocklehurst K, Shevchik VE, Pickersgill RW (2007) Molecular basis of the activity of the phytopathogen pectin methylesterase. EMBO J **26**: 3879–3887

Fry SC (2004) Primary cell wall metabolism: Tracking the careers of wall polymers in living plant cells. New Phytol **161**: 641–675

Le Gall H, Philippe F, Domon JM, Gillet F, Pelloux J, Rayon C (2015) Cell wall metabolism in response to abiotic stress. Plants **4**: 112–166

Gao S, Shain L (1995) Activity of polygalacturonase produced by Cryphonectria parasitica in chestnut bark and its inhibition by extracts from American and Chinese chestnut. Physiol Mol Plant Pathol **46**: 199–213

Di Giovanni M, Cenci A, Janni M, D'Ovidio R (2008) A LTR copia retrotransposon and Mutator transposons interrupt Pgip genes in cultivated and wild wheats. Theor Appl Genet **116**: 859–867

González-Carranza ZH, Elliott KA, Roberts JA (2007) Expression of polygalacturonases and evidence to support their role during cell separation processes in Arabidopsis thaliana. J Exp Bot **58**: 3719–3730

Gou JY, Miller LM, Hou G, Yu XH, Chen XY, Liu CJ (2012) Acetylesterase-mediated deacetylation of pectin impairs cell elongation, pollen germination, and plant reproduction. Plant Cell **24**: 50–65

Haas KT, Wightman R, Meyerowitz EM, Peaucelle A (2020) Pectin homogalacturonan nanofilament expansion drives morphogenesis in plant epidermal cells. Science (80-) **367**: 1003–1007

Habrylo O, Evangelista DE, Castilho PV, Pelloux J, Henrique-Silva F (2018) The pectinases

from Sphenophorus levis: Potential for biotechnological applications. Int J Biol Macromol **112**: 499–508

Haltiwanger RS, Lowe JB (2004) Role of Glycosylation in Development. Annu Rev Biochem **73**: 491–537

Hassan S, Shevchik VE, Robert X, Hugouvieux-Cotte-Pattat N (2013) PelN is a new pectate lyase of dickeya dadantii with unusual characteristics. J Bacteriol **195**: 2197–2206

Ten Have A, Mulder W, Visser J, Van Kan JAL (1998) The endopolygalacturonase gene Bcpg1 is required to full virulence of Botrytis cinerea. Mol Plant-Microbe Interact **11**: 1009–1016

Hegedus DD, Li R, Buchwaldt L, Parkin I, Whitwill S, Coutu C, Bekkaoui D, Roger Rimmer S (2008) Brassica napus possesses an expanded set of polygalacturonase inhibitor protein genes that are differentially regulated in response to Sclerotinia sclerotiorum infection, wounding and defense hormone treatment. Planta **228**: 241–253

Held MA, Be E, Zemelis S, Withers S, Wilkerson C, Brandizzi F (2011) CGR3: A Golgi-Localized Protein Influencing Homogalacturonan Methylesterification. Mol Plant **4**: 832–844

Henrissat B (1991) A classification of glycosyl hydrolases based on amino acid sequence similarities. Biochem J **280**: 309–316

Hewezi T, Howe P, Maier TR, Hussey RS, Mitchum MG, Davis EL, Baum TJ (2008) Cellulose binding protein from the parasitic nematode heterodera Schachtii interacts with arabidopsis pectin methylesterase: Cooperative cell wall modification during parasitism. Plant Cell **20**: 3080–3093

Hocq L, Guinand S, Habrylo O, Voxeur A, Tabi W, Safran J, Fournet F, Domon J-M, Mollet J-C, Pilard S, et al (2020) The exogenous application of AtPGLR, an endo - polygalacturonase, triggers pollen tube burst and repair. Plant J **103**: 617–633

Hocq L, Habrylo O, Voxeur A, Pau-Roblot C, Safran J, Sénéchal F, Fournet F, Bassard S, Battu V, Demailly H, et al (2021) The pH-dependent processivity of Arabidopsis AtPME2 can control cell wall mechanical properties. bioRxiv https://doi.org/10.1101/2021.03.03.433777

Hocq L, Pelloux J, Lefebvre V (2017a) Connecting Homogalacturonan-Type Pectin Remodeling to Acid Growth. Trends Plant Sci **22**: 20–29

Hocq L, Sénéchal F, Lefebvre V, Lehner A, Domon JM, Mollet JC, Dehors J, Pageau K, Marcelo P, Guérineau F, et al (2017b) Combined experimental and computational approaches reveal distinct pH dependence of pectin Methylesterase Inhibitors. Plant Physiol **173**: 1075–1093

Hongo S, Sato K, Yokoyama R, Nishitani K (2012) Demethylesterification of the Primary Wall by PECTIN METHYLESTERASE35 Provides Mechanical Support to the Arabidopsis Stem. Plant Cell **24**: 2624–2634

Hou W, Singh RK, Zhao P, Martins V, Aguilar E, Canto T, Tenllado F, Franklin G, Dias ACP (2020) Overexpression of polygalacturonase-inhibiting protein (PGIP) gene from Hypericum perforatum alters expression of multiple defense-related genes and modulates

recalcitrance to Agrobacterium tumefaciens in tobacco. J Plant Physiol **253**: 153268

Huang Y-C, Wu H-C, Wang Y-D, Liu C-H, Lin C-C, Luo D-L, Jinn T-L (2017) PECTIN METHYLESTERASE34 Contributes to Heat Tolerance through Its Role in Promoting Stomatal Movement. Plant Physiol **174**: 748–763

Inderbitzin P, Bostock RM, Davis RM, Usami T, Platt HW, Subbarao K V. (2011) Phylogenetics and Taxonomy of the Fungal Vascular Wilt Pathogen Verticillium, with the Descriptions of Five New Species. PLoS One **6**: e28341

Jayani RS, Saxena S, Gupta R (2005) Microbial pectinolytic enzymes: A review. Process Biochem **40**: 2931–2944

Jenkins J, Mayans O, Pickersgill R (1998) Structure and evolution of parallel beta-helix proteins. J Struct Biol **122**: 236–246

Jenkins J, Mayans O, Smith D, Worboys K, Pickersgill RW (2001) Three-dimensional structure of Erwinia chrysanthemi pectin methylesterase reveals a novel esterase active site. J Mol Biol **305**: 951–960

Jenkins J, Pickersgill R (2001) The architecture of parallel β-helices and related folds. Prog Biophys Mol Biol **77**: 111–175

Jiang L, Yang S-L, Xie L-F, Puah CS, Zhang X-Q, Yang W-C, Sundaresan V, Ye D (2005) VANGUARD1 Encodes a Pectin Methylesterase That Enhances Pollen Tube Growth in the Arabidopsis Style and Transmitting Tract. Plant Cell **17**: 584–596

Jiménez-Bermúdez S, Redondo-Nevado J, Muñoz-Blanco J, Caballero JL, López-Aranda JM, Valpuesta V, Pliego-Alfaro F, Quesada MA, Mercado JA (2002) Manipulation of Strawberry Fruit Softening by Antisense Expression of a Pectate Lyase Gene. Plant Physiol **128**: 751–759

Johansson K, El-Ahmad M, Friemann R, Jörnvall H, Markovič O, Eklund H (2002) Crystal structure of plant pectin methylesterase. FEBS Lett **514**: 243–249

Jolie RP, Duvetter T, Van Loey AM, Hendrickx ME (2010) Pectin methylesterase and its proteinaceous inhibitor: A review. Carbohydr Res **345**: 2583–2595

Joubert DA, Slaughter AR, Kemp G, Becker JVW, Krooshof GH, Bergmann C, Benen J, Pretorius IS, Vivier MA (2006) The grapevine polygalacturonase-inhibiting protein (VvPGIP1) reduces Botrytis cinerea susceptibility in transgenic tobacco and differentially inhibits fungal polygalacturonases. Transgenic Res **15**: 687–702

Kalunke RM, Tundo S, Benedetti M, Cervone F, De Lorenzo G, D'Ovidio R (2015) An update on polygalacturonase-inhibiting protein (PGIP), aleucine-rich repeat protein that protects crop plants against pathogens. Front Plant Sci **6**: 1–17

Kamiya M, Higashio S-Y, Isomoto A, Kim J-M, Seki M, Miyashima S, Nakajima K (2016) Control of root cap maturation and cell detachment by BEARSKIN transcription factors in Arabidopsis. Development **143**: 4063–4072

Kars I, Krooshof GH, Wagemakers L, Joosten R, Benen JAE, Van Kan JAL (2005a)

Necrotizing activity of five Botrytis cinerea endopolygalacturonases produced in Pichia pastoris. Plant J **43**: 213–225

Kars I, McCalman M, Wagemakers L, Van Kan JAL (2005b) Functional analysis of Botrytis cinerea pectin methylesterase genes by PCR-based targeted mutagenesis: Bcpme1 and Bcpme2 are dispensable for virulence of strain B05.10. Mol Plant Pathol **6**: 641–652

Kataoka Y, Kondo T (1999) Quantitative analysis for the cellulose Iα crystalline phase in developing wood cell walls. Int J Biol Macromol **24**: 37–41

Kaul S, Koo HL, Jenkins J, Rizzo M, Rooney T, Tallon LJ, Feldblyum T, Nierman W, Benito MI, Lin X, et al (2000) Analysis of the genome sequence of the flowering plant Arabidopsis thaliana. Nature **408**: 796–815

Kent LM, Loo TS, Melton LD, Mercadante D, Williams MAK, Jameson GB (2016) Structure and properties of a non-processive, salt-requiring, and acidophilic pectin methylesterase from aspergillus Niger provide insights into the key determinants of processivity control. J Biol Chem **291**: 1289–1306

Kester HCM, Someren MAK-V, Muller Y, Visser J (1996) Primary Structure and Characterization of an Exopolygalacturonase from Aspergillus Tubingensis. Eur J Biochem **240**: 738–746

Kim S-J, Held MA, Zemelis S, Wilkerson C, Brandizzi F (2015) CGR2 and CGR3 have critical overlapping roles in pectin methylesterification and plant growth in Arabidopsis thaliana. Plant J **82**: 208–220

Kim W-C, Kim J-Y, Ko J-H, Kang H, Kim J, Han K-H (2014) AtC3H14, a plant-specific tandem CCCH zinc-finger protein, binds to its target mRNAs in a sequence-specific manner and affects cell elongation in Arabidopsis thaliana. Plant J **80**: 772–784

Klemm D, Heublein B, Fink HP, Bohn A (2005) Cellulose: Fascinating biopolymer and sustainable raw material. Angew Chemie - Int Ed **44**: 3358–3393

Klosterman SJ, Atallah ZK, Vallad GE, Subbarao K V. (2009) Diversity, Pathogenicity, and Management of Verticillium Species. Annu Rev Phytopathol **47**: 39–62

Klosterman SJ, Subbarao K V., Kang S, Veronese P, Gold SE, Thomma BPHJ, Chen Z, Henrissat B, Lee Y-H, Park J, et al (2011) Comparative Genomics Yields Insights into Niche Adaptation of Plant Vascular Wilt Pathogens. PLoS Pathog **7**: e1002137

Kluskens LD, Van Alebeek GJWM, Walther J, Voragen AGJ, De Vos WM, Van Der Oost J (2005) Characterization and mode of action of an exopolygalacturonase from the hyperthermophilic bacterium Thermotoga maritima. FEBS J **272**: 5464–5473

Kohli P, Gupta R (2019) Application of calcium alginate immobilized and crude pectin lyase from Bacillus cereus in degumming of plant fibres. Biocatal Biotransformation **37**: 341–348

Kohorn BD, Kohorn SL (2012) The cell wall-associated kinases, WAKs, as pectin receptors. Front Plant Sci **3**: 1–5

Kotnala B, Shashirekha M. N, Vasu P (2018) Purification and Characterization of a Salt-

Dependent Pectin Methylesterase from Carica papaya Fruit Mesocarp-Exocarp Tissue. J Food Sci **83**: 2062–2070

Krämer U (2015) Planting molecular functions in an ecological context with Arabidopsis thaliana. Elife **4**: 1–13

Kumpf RP, Shi CL, Larrieu A, Stø IM, Butenko MA, Péret B, Riiser ES, Bennett MJ, Aalen RB (2013) Floral organ abscission peptide IDA and its HAE/HSL2 receptors control cell separation during lateral root emergence. Proc Natl Acad Sci U S A **110**: 5235–5240

Kusters-van Someren M, Flipphi M, de Graaff L, van den Broeck H, Kester H, Hinnen A, Visser J (1992) Characterization of the Aspergillus niger pelB gene: structure and regulation of expression. Mol Gen Genet MGG **234**: 113–120

Kusters-van Someren MA, Harmsen JAM, Kester HCM, Visser J (1991) Structure of the Aspergillus niger pelA gene and its expression in Aspergillus niger and Aspergillus nidulans. Curr Genet **20**: 293–299

Lee H, Rivner J, Urbauer JL, Garti N, Wicker L (2008) De-esterification pattern of Valencia orange pectinmethylesterases and characterization of modified pectins. J Sci ofFood Agric **88**: 2102–2110

Lee HW, Cho C, Kim J (2015) Lateral organ boundaries domain16 and 18 act downstream of the AUXIN1 and LIKE-AUXIN3 auxin influx carriers to control lateral root development in arabidopsis. Plant Physiol **168**: 1792–1806

Leng Y, Yang Y, Ren D, Huang L, Dai L, Wang Y, Chen L, Tu Z, Gao Y, Li X, et al (2017) A Rice PECTATE LYASE-LIKE Gene Is Required for Plant Growth and Leaf Senescence. Plant Physiol **174**: 1151–1166

Leroux C, Bouton S, Kiefer-Meyer MC, Fabrice TN, Mareck A, Guénin S, Fournet F, Ringli C, Pelloux J, Driouich A, et al (2015) PECTIN METHYLESTERASE48 is involved in arabidopsis pollen grain germination. Plant Physiol **167**: 367–380

Levesque-Tremblay G, Müller K, Mansfield SD, Haughn GW (2015) HIGHLY METHYL ESTERIFIED SEEDS Is a Pectin Methyl Esterase Involved in Embryo Development. Plant Physiol **167**: 725–737

Liao CH, Revear L, Hotchkiss A, Savary B (1999) Genetic and biochemical characterization of an exopolygalacturonase and a pectate lyase from Yersinia enterocolitica. Can J Microbiol **45**: 396–403

Liepman AH, Wightman R, Geshi N, Turner SR, Scheller HV (2010) Arabidopsis - A powerful model system for plant cell wall research. Plant J **61**: 1107–1121

Lietzke SE, Scavetta RD, Yoder MD, Jurnak F (1996) The Refined Three-Dimensional Structure of Pectate Lyase E from Erwinia chrysanthemi at 2.2 A Resolution. Plant Physiol **111**: 73–92

Liston SD, McMahon SA, Le Bas A, Suits MDL, Naismith JH, Whitfield C (2018) Periplasmic depolymerase provides insight into ABC transporter-dependent secretion of bacterial capsular polysaccharides. Proc Natl Acad Sci U S A **115**: E4870–E4879

Lombard V, Bernard T, Rancurel C, Brumer H, Coutinho PM, Henrissat B (2010) A hierarchical classification of polysaccharide lyases for glycogenomics. Biochem J **432**: 437–444

Luis AS, Briggs J, Zhang X, Farnell B, Ndeh D, Labourel A, Baslé A, Cartmell A, Terrapon N, Stott K, et al (2018) Dietary pectic glycans are degraded by coordinated enzyme pathways in human colonic Bacteroides. Nat Microbiol **3**: 210–219

Lund CH, Stenbæk A, Atmodjo MA, Rasmussen RE, Moller IE, Erstad SM, Biswal AK, Mohnen D, Mravec J, Sakuragi Y (2020) Pectin Synthesis and Pollen Tube Growth in Arabidopsis Involves Three GAUT1 Golgi-Anchoring Proteins: GAUT5, GAUT6, and GAUT7. Front Plant Sci **11**: 1–15

Ma L, van der Does HC, Borkovich KA, Coleman JJ, Daboussi M, Di Pietro A, Dufresne M, Freitag M, Grabherr M, Henrissat B, et al (2010) Comparative genomics reveals mobile pathogenicity chromosomes in Fusarium. Nature **464**: 367–373

Mahmood U, Fan Y, Wei S, Niu Y, Li Y, Huang H, Chen Y, Tang Z, Liu L, Qu C, et al (2021) Comprehensive analysis of polygalacturonase genes offers new insights into their origin and functional evolution in land plants. Genomics **113**: 1096–1108

Malamy JE, Benfey PN (1997) Organization and cell differentiation in lateral roots of Arabidopsis thaliana. Development **124**: 33–44

Mandaokar A, Thines B, Shin B, Markus Lange B, Choi G, Koo YJ, Yoo YJ, Choi YD, Choi G, Browse J (2006) Transcriptional regulators of stamen development in Arabidopsis identified by transcriptional profiling. Plant J **46**: 984–1008

Manfredini C, Sicilia F, Ferrari S, Pontiggia D, Salvi G, Caprari C, Lorito M, Lorenzo G De (2005) Polygalacturonase-inhibiting protein 2 of Phaseolus vulgaris inhibits BcPG1, a polygalacturonase of Botrytis cinerea important for pathogenicity, and protects transgenic plants from infection. Physiol Mol Plant Pathol **67**: 108–115

Marin-Rodriguez MC (2002) Pectate lyases, cell wall degradation and fruit softening. J Exp Bot **53**: 2115–2119

Marín-Rodríguez MC, Smith DL, Manning K, Orchard J, Seymour GB (2003) Pectate lyase gene expression and enzyme activity in ripening banana fruit. Plant Mol Biol **51**: 851–857

Mariotti L, Casasoli M, Caprari C, De Lorenzo G (2009) A divergent polygalacturonase of Fusarium phyllophilum shows sequence and functional similarity to the enzyme of F. Verticillioides. J Plant Pathol **91**: 129–139

Markovič O, Janeček Š (2004) Pectin methylesterases: sequence-structural features and phylogenetic relationships. Carbohydr Res **339**: 2281–2295

Markovič O, Janeček Š (2001) Pectin degrading glycoside hydrolases of family 28: sequence-structural features, specificities and evolution. Protein Eng Des Sel **14**: 615–631

Martins ES, Silva D, Leite RSR, Gomes E (2007) Purification and characterization of polygalacturonase produced by thermophilic Thermoascus aurantiacus CBMAI-756 in submerged fermentation. Antonie van Leeuwenhoek, Int J Gen Mol Microbiol **91**: 291–299

Mattei B, Bernalda MS, Federici L, Roepstorff P, Cervone F, Boffi A (2001) Secondary Structure and Post-Translational Modifications of the Leucine-Rich Repeat Protein PGIP (Polygalacturonase-Inhibiting Protein) from Phaseolus vulgaris †. Biochemistry **40**: 569–576

Di Matteo A, Bonivento D, Tsernoglou D, Federici L, Cervone F (2006) Polygalacturonase-inhibiting protein (PGIP) in plant defence: A structural view. Phytochemistry **67**: 528–533

Matteo A Di, Giovane A, Raiola A, Camardella L, Bonivento D, Lorenzo G De, Cervone F, Bellincampi D, Tsernoglou D (2005) Structural Basis for the Interaction between Pectin Methylesterase and a Specific Inhibitor Protein. **17**: 849–858

Mayans O, Scott M, Connerton I, Gravesen T, Benen J, Visser J, Pickersgill R, Jenkins J (1997) Two crystal structures of pectin lyase A from Aspergillus reveal a pH driven conformational change and striking divergence in the substrate-binding clefts of pectin and pectate lyases. Structure **5**: 677–689

McCann M, Carpita N (2008) Designing the deconstruction of plant cell walls. Curr Opin Plant Biol **11**: 314–320

McCarthy TW, Der JP, Honaas LA, dePamphilis CW, Anderson CT (2014) Phylogenetic analysis of pectin-related gene families in Physcomitrella patens and nine other plant species yields evolutionary insights into cell walls. BMC Plant Biol **14**: 1–13

McNeil M, Darvill AG, Fry SC, Albersheim P (1984) Structure and Function of the Primary Cell Walls of Plants. Annu Rev Biochem **53**: 625–663

Mercadante D, Melton LD, Jameson GB, Williams MAK (2014) Processive pectin methylesterases: The role of electrostatic potential, breathing motions and bond cleavage in the rectification of brownian motions. PLoS One **9**: 1–11

Miao Y, Li H-Y, Shen J, Wang J, Jiang L (2011) QUASIMODO 3 (QUA3) is a putative homogalacturonan methyltransferase regulating cell wall biosynthesis in Arabidopsis suspension-cultured cells. J Exp Bot **62**: 5063–5078

Micheli F (2001) Pectin methylesterases: Cell wall enzymes with important roles in plant physiology. Trends Plant Sci **6**: 414–419

Miller GL (1959) Use of Dinitrosalicylic Acid Reagent for Determination of Reducing Sugar. Anal Chem **31**: 426–428

Miyairi K, Senda M, Watanabe M, Hasui Y, Okuno T (1997) Cloning and Sequence Analysis of cDNA Encoding Endopolygalacturonase I from Stereum purpureum. Biosci Biotechnol Biochem **61**: 655–659

Mohamed SA, Farid NM, Hossiny EN, Bassuiny RI (2006) Biochemical characterization of an extracellular polygalacturonase from Trichoderma harzianum. J Biotechnol **127**: 54–64

Mohamed Zakriya G, Ramakrishnan G (2020) Natural Fibre Composites, 1st Editio. Kinds Nat Fibres Its Spec Charact. doi: 10.1201/9780429326738

Mohnen D (2008) Pectin structure and biosynthesis. Curr Opin Plant Biol **11**: 266–277

Mollet J-C, Leroux C, Dardelle F, Lehner A (2013) Cell Wall Composition, Biosynthesis and

Remodeling during Pollen Tube Growth. Plants **2**: 107–147

Mouille G, Ralet MC, Cavelier C, Eland C, Effroy D, Hématy K, McCartney L, Truong HN, Gaudon V, Thibault JF, et al (2007) Homogalacturonan synthesis in Arabidopsis thaliana requires a Golgi-localized protein with a putative methyltransferase domain. Plant J **50**: 605–614

Nakamura A, Furuta H, Maeda H, Takao T, Nagamatsu Y (2002) Structural Studies by Stepwise Enzymatic Degradation of the Main Backbone of Soybean Soluble Polysaccharides Consisting of Galacturonan and Rhamnogalacturonan. Biosci Biotechnol Biochem **66**: 1301–1313

Nguema-Ona E, Moore JP, Fagerström AD, Fangel JU, Willats WGT, Hugo A, Vivier MA (2013) Overexpression of the grapevine PGIP1 in tobacco results in compositional changes in the leaf arabinoxyloglucan network in the absence of fungal infection. BMC Plant Biol **13**: 46

Nighojkar A, Patidar MK, Nighojkar S (2019) Pectinases: Production and Applications for Fruit Juice Beverages. Process. Sustain. Beverages. Elsevier, pp 235–273

Niture SK (2008) Comparative biochemical and structural characterizations of fungal polygalacturonases. Biologia (Bratisl) **63**: 1–19

Nocker VS, Sun L (2010) Analysis of promoter activity of members of the Pectate lyase-like(PLL) gene family in cell separation in Arabidopsis. BMC Plant Biol **10**: 152

Norman C, Vidal S, Palva ET (1999) Oligogalacturonide-mediated induction of a gene involved in jasmonic acid synthesis in response to the cell-wall-degrading enzymes of the plant pathogen Erwinia carotovora. Mol Plant-Microbe Interact **12**: 640–644

Nunan KJ, Davies C, Robinson SP, Fincher GB (2001) Expression patterns of cell wall-modifying enzymes during grape berry development. Planta **214**: 257–264

O'Neill MA, Ishii T, Albersheim P, Darvill AG (2004) RHAMNOGALACTURONAN II: Structure and Function of a Borate Cross-Linked Cell Wall Pectic Polysaccharide. Annu Rev Plant Biol **55**: 109–139

O'Neill MA, York WS (2003) The Composition and Structure of Plant Primary Cell Walls. Annu. Plant Rev. online. John Wiley & Sons, Ltd, Chichester, UK, pp 1–54

Ogawa M, Kay P, Wilson S, Swain SM (2009) Arabidopsis Dehiscence Zone Polygalacturonase1 (ADPG1), ADPG2, and Quartet2 are polygalacturonases required for cell separation during reproductive development in Arabidopsis. Plant Cell **21**: 216–233

Ouattara HG, Reverchon S, Niamke SL, Nasser W (2010) Biochemical Properties of Pectate Lyases Produced by Three Different Bacillus Strains Isolated from Fermenting Cocoa Beans and Characterization of Their Cloned Genes. Appl Environ Microbiol **76**: 5214–5220

Pagès S, Heijne WHM, Kester HCM, Visser J, Benen JAE (2000) Subsite mapping of Aspergillus niger endopolygalacturonase II by site-directed mutagenesis. J Biol Chem **275**: 29348–29353

Pagès S, Kester HCM, Visser J, Benen JAE (2001) Changing a Single Amino Acid Residue

Switches Processive and Non-processive Behavior of Aspergillus niger Endopolygalacturonase I and II. J Biol Chem **276**: 33652–33656

Palusa SG, Golovkin M, Shin S, Richardson DN, Reddy ASN (2007) Organ-specific, developmental, hormonal and stress regulation of expression of putative pectate lyase genes in Arabidopsis. New Phytol **174**: 537–550

Pan X, Tu T, Wang L, Luo H, Ma R, Shi P, Meng K, Yao B (2014) A novel low-temperature-active pectin methylesterase from Penicillium chrysogenum F46 with high efficiency in fruit firming. Food Chem **162**: 229–234

Park K-C, Kwon S-J, Kim P-H, Bureau T, Kim N-S (2008) Gene structure dynamics and divergence of the polygalacturonase gene family of plants and fungus. Genome **51**: 30–40

Pathak N, Mishra S, Sanwal GG (2000) Purification and characterization of polygalacturonase from banana fruit. Phytochemistry **54**: 147–152

Patil SS, Dimond AE (1967) Inhibition of Verticillium polygalacturonase by oxidation products of polyphenols. Phytopathology **57**: 492–6

Paumier D, Bammé B, Penaud A, Valade R, Suffert F (2021) First report of the sexual stage of the flax pathogen Mycosphaerella linicola in France and its impact on pasmo epidemiology. Plant Pathol **70**: 475–483

Peaucelle A, Braybrook S, Höfte H (2012) Cell wall mechanics and growth control in plants: the role of pectins revisited. Front Plant Sci **3**: 1–6

Peaucelle A, Louvet R, Johansen JN, Salsac F, Morin H, Fournet F, Belcram K, Gillet F, Hofte H, Laufs P, et al (2011) The transcription factor BELLRINGER modulates phyllotaxis by regulating the expression of a pectin methylesterase in Arabidopsis. Development **138**: 4733–4741

Pel HJ, De Winde JH, Archer DB, Dyer PS, Hofmann G, Schaap PJ, Turner G, De Vries RP, Albang R, Albermann K, et al (2007) Genome sequencing and analysis of the versatile cell factory Aspergillus niger CBS 513.88. Nat Biotechnol **25**: 221–231

Pelloux J, Rustérucci C, Mellerowicz EJ (2007) New insights into pectin methylesterase structure and function. Trends Plant Sci **12**: 267–277

Pérez-Fuentes C, Cristina Ravanal M, Eyzaguirre J (2014) Heterologous expression of a Penicillium purpurogenum pectin lyase in Pichia pastoris and its characterization. Fungal Biol **118**: 507–515

Petersen TN, Kauppinen S, Larsen S (1997) The crystal structure of rhamnogalacturonase a from Aspergillus aculeatus: A right-handed parallel β helix. Structure **5**: 533–544

Philippe F, Pelloux J, Rayon C (2017) Plant pectin acetylesterase structure and function: new insights from bioinformatic analysis. BMC Genomics **18**: 456

Pickersgill R, Jenkins J, Harris G, Nasser W, Robert Baudouy J (1994) The structure of Bacillus subtil is pectate lyase in complex with calcium. Nat Struct Biol **1**: 717–723

Pickersgill R, Smith D, Worboys K, Jenkins J (1998) Crystal Structure of Polygalacturonase

from Erwinia carotovora ssp. carotovora. J Biol Chem **273**: 24660–24664

Di Pietro A (1996) Purification and characterization of an exo-polygalacturonase from the tomato vascular wilt pathogen Fusarium oxysporum f.sp. lycopersici. FEMS Microbiol Lett **145**: 295–299

Pijning T, van Pouderoyen G, Kluskens L, van der Oost J, Dijkstra BW (2009) The crystal structure of a hyperthermoactive exopolygalacturonase from Thermotoga maritima reveals a unique tetramer. FEBS Lett **583**: 3665–3670

Pina C, Pinto F, Feijó JA, Becker JD (2005) Gene Family Analysis of the Arabidopsis Pollen Transcriptome Reveals Biological Implications for Cell Growth, Division Control, and Gene Expression Regulation. Plant Physiol **138**: 744–756

Van Pouderoyen G, Snijder HJ, Benen JAE, Dijkstra BW (2003) Structural insights into the processivity of endopolygalacturonase I from Aspergillus niger. FEBS Lett **554**: 462–466

Powell ALT, van Kan J, ten Have A, Visser J, Greve LC, Bennett AB, Labavitch JM (2000) Transgenic Expression of Pear PGIP in Tomato Limits Fungal Colonization. Mol Plant-Microbe Interact **13**: 942–950

Protsenko MA, Buza NL, Krinitsyna AA, Bulantseva EA, Korableva NP (2008) Polygalacturonase-inhibiting protein is a structural component of plant cell wall. Biochem Biokhimiia **73**: 1053–62

Qu T, Liu R, Wang W, An L, Chen T, Liu G, Zhao Z (2011) Brassinosteroids regulate pectin methylesterase activity and AtPME41 expression in Arabidopsis under chilling stress. Cryobiology **63**: 111–117

Rahman MS, Choi YS, Kim YK, Park C, Yoo JC (2019) Production of novel polygalacturonase from Bacillus paralicheniformis CBS32 and application to depolymerization of ramie fiber. Polymers (Basel) **11(9)**: 1–11

Ralet MC, Crépeau MJ, Bonnin E (2008) Evidence for a blockwise distribution of acetyl groups onto homogalacturonans from a commercial sugar beet (Beta vulgaris) pectin. Phytochemistry **69**: 1903–1909

Rep M (2005) Small proteins of plant-pathogenic fungi secreted during host colonization. FEMS Microbiol Lett **253**: 19–27

Rexova-Benkova L (1973) The Size of the Substrate-Binding Site of an Aspergillus niger Extracellular Endopolygalacturonase. Eur J Biochem **39**: 109–115

Rhee SY, Osborne E, Poindexter PD, Somerville CR (2003) Microspore Separation in the quartet 3 Mutants of Arabidopsis Is Impaired by a Defect in a Developmentally Regulated Polygalacturonase Required for Pollen Mother Cell Wall Degradation. Plant Physiol **133**: 1170–1180

Ribeiro DM, Araújo WL, Fernie AR, Schippers JHM, Mueller-Roeber B (2012) Translatome and metabolome effects triggered by gibberellins during rosette growth in Arabidopsis. J Exp Bot **63**: 2769–2786

Ridley BL, O'Neill MA, Mohnen D (2001) Pectins: structure, biosynthesis, and oligogalacturonide-related signaling. Phytochemistry **57**: 929–967

Rui Y, Xiao C, Yi H, Kandemir B, Wang JZ, Puri VM, Anderson CT (2017) POLYGALACTURONASE INVOLVED IN EXPANSION3 functions in seedling development, rosette growth, and stomatal dynamics in Arabidopsis thaliana. Plant Cell **29**: 2413–2432

Safran J, Habrylo O, Cherkaoui M, Lecomte S, Voxeur A, Pilard S, Bassard S, Pau-Roblot C, Mercadante D, Pelloux J, et al (2021) New insights into the specificity and processivity of two novel pectinases from Verticillium dahliae. Int J Biol Macromol **176**: 165–176

Salama A (2019) Cellulose/calcium phosphate hybrids: New materials for biomedical and environmental applications. Int J Biol Macromol **127**: 606–617

van Santen Y, Benen JAE, Schroter KH, Kalk KH, Armand S, Visser J, Dijkstra BW (1999) 1.68-angstrom crystal structure of endopolygalacturonase II from Aspergillus niger and identification of active site residues by site-directed mutagenesis. J Biol Chem **274**: 30474–30480

Santiago-Domenech N, Jimenez-Bemudez S, Matas AJ, Rose JKC, Munoz-Blanco J, Mercado JA, Quesada MA (2008) Antisense inhibition of a pectate lyase gene supports a role for pectin depolymerization in strawberry fruit softening. J Exp Bot **59**: 2769–2779

Savary BJ, Hotchkiss AT, Cameron RG (2002) Characterization of a salt-independent pectin methylesterase purified from Valencia orange peel. J Agric Food Chem **50**: 3553–3558

Scavetta RD, Herron SR, Hotchkiss AT, Kita N, Keen NT, Benen JAE, Kester HCM, Visser J, Jurnak F (1999) Structure of a plant cell wall fragment complexed to pectate lyase C. Plant Cell **11**: 1081–1092

Scheller HV, Jensen JK, Sørensen SO, Harholt J, Geshi N (2007) Biosynthesis of pectin. Physiol Plant **129**: 283–295

Scheller HV, Ulvskov P (2010) Hemicelluloses. Annu Rev Plant Biol **61**: 263–289

Schuster-Böckler B, Schultz J, Rahmann S (2004) HMM Logos for visualization of protein families. BMC Bioinformatics **5**: 7

Sénéchal F, Habrylo O, Hocq L, Domon JM, Marcelo P, Lefebvre V, Pelloux J, Mercadante D (2017) Structural and dynamical characterization of the pH-dependence of the pectin methylesterase-pectin methylesterase inhibitor complex. J Biol Chem **292**: 21538–21547

Sénéchal F, Mareck A, Marcelo P, Lerouge P, Pelloux J (2015) Arabidopsis PME17 Activity can be Controlled by Pectin Methylesterase Inhibitor4. Plant Signal Behav **10**: e983351

Sénéchal F, Wattier C, Rustérucci C, Pelloux J (2014) Homogalacturonan-modifying enzymes: Structure, expression, and roles in plants. J Exp Bot **65**: 5125–5160

Shen Z, Denton M, Mutti N, Pappan K, Michael R. K, Reese JC, R. Reeck G (2003) Polygalacturonase from Sitophilus oryzae: Possible horizontal transfer of a pectinase gene from fungi to weevils. J Insect Sci **3**: 1–9

Shental-Bechor D, Levy Y (2008) Effect of glycosylation on protein folding: A close look at thermodynamic stabilization. Proc Natl Acad Sci **105**: 8256–8261

Shimizu T, Nakatsu T, Miyairi K, Okuno T, Kato H (2002) Active-site architecture of endopolygalacturonase I from Stereum purpureum revealed by crystal structures in native and ligand-bound forms at atomic resolution. Biochemistry **41**: 6651–6659

Sinclair SA, Larue C, Bonk L, Khan A, Castillo-Michel H, Stein RJ, Grolimund D, Begerow D, Neumann U, Haydon MJ, et al (2017) Etiolated Seedling Development Requires Repression of Photomorphogenesis by a Small Cell-Wall-Derived Dark Signal. Curr Biol **27**: 3403–3418

Singh SA, Appu Rao AG (2002) A simple fractionation protocol for, and a comprehensive study of the molecular properties of, two major endopolygalacturonases from Aspergillus niger. Biotechnol Appl Biochem **35**: 115

Sinitsyna OA, Fedorova EA, Semenova M V, Gusakov A V, Sokolova LM, Bubnova TM, Okunev ON, Chulkin AM, Vavilova EA, Vinetsky YP, et al (2007) Isolation and characterization of extracellular pectin lyase from Penicillium canescens. Biochem **72**: 565–571

Somerville C (2004) Toward a Systems Approach to Understanding Plant Cell Walls. Science (80-) **306**: 2206–2211

Soriano M, Blanco A, Díaz P, Pastor FIJ (2000) An unusual pectate lyase from a Bacillus sp. with high activity on pectin: Cloning and characterization. Microbiology **146**: 89–95

de Souza A, Hull PA, Gille S, Pauly M (2014) Identification and functional characterization of the distinct plant pectin esterases PAE8 and PAE9 and their deletion mutants. Planta **240**: 1123–1138

Sterling JD, Atmodjo MA, Inwood SE, Kumar Kolli VS, Quigley HF, Hahn MG, Mohnen D (2006) Functional identification of an Arabidopsis pectin biosynthetic homogalacturonan galacturonosyltransferase. Proc Natl Acad Sci **103**: 5236–5241

Sterling JD, Quigley HF, Orellana A, Mohnen D (2001) The Catalytic Site of the Pectin Biosynthetic Enzyme α-1,4-Galacturonosyltransferase Is Located in the Lumen of the Golgi. Plant Physiol **127**: 360–371

Stratilová E, Dzúrová M, Markovič O, Jörnvall H (1996) An essential tyrosine residue of Aspergillus polygalacturonase. FEBS Lett **382**: 164–166

Stratilová E, Mislovicová D, Kacuráková M, Machová E, Kolarová N, Markovic O, Jörnvall H (1998) The glycoprotein character of multiple forms of Aspergillus polygalacturonase. J Protein Chem **17**: 173–9

Sukhumsiirchart W, Kawanishi S, Deesukon W, Chansiri K, Kawasaki H, Sakamoto T (2009) Purification, Characterization, and Overexpression of Thermophilic Pectate Lyase of Bacillus sp. RN1 Isolated from a Hot Spring in Thailand. Biosci Biotechnol Biochem **73**: 268–273

Sun Y, Fan X-Y, Cao D-M, Tang W, He K, Zhu J-Y, He J-X, Bai M-Y, Zhu S, Oh E, et al (2010) Integration of Brassinosteroid Signal Transduction with the Transcription Network for

Plant Growth Regulation in Arabidopsis. Dev Cell **19**: 765–777

Swarup K, Benková E, Swarup R, Casimiro I, Péret B, Yang Y, Parry G, Nielsen E, De Smet I, Vanneste S, et al (2008) The auxin influx carrier LAX3 promotes lateral root emergence. Nat Cell Biol **10**: 946–954

Takao M, Nakaniwa T, Yoshikawa K, Terashita T, Sakai T (2000) Purification and characterization of thermostable pectate lyase with protopectinase activity from thermophilic bacillus sp. TS 47. Biosci Biotechnol Biochem **64**: 2360–2367

Tang Q, Liu YP, Ren ZG, Yan XX, Zhang LQ (2013) 1.37 Å Crystal structure of pathogenic factor pectate lyase from Acidovorax citrulli. Proteins Struct Funct Bioinforma **81**: 1485–1490

Tang Y, Wu P, Jiang S, Selvaraj JN, Yang S, Zhang G (2019) A new cold-active and alkaline pectate lyase from Antarctic bacterium with high catalytic efficiency. Appl Microbiol Biotechnol **103**: 5231–5241

Teller DC, Craig A, Pappan K, Shen Z, Reese JC, Reeck GR, Ronald E (2014) The structure of rice weevil pectin methylesterase. 1480–1484

Thibault J-F, Renard CMGC, Axelos MAV, Roger P, Crépeau M-J (1993) Studies of the length of homogalacturonic regions in pectins by acid hydrolysis. Carbohydr Res **238**: 271–286

Thomas LM, Doan CN, Oliver RL, Yoder MD (2002) Structure of pectate lyase a: Comparison to other isoforms. Acta Crystallogr Sect D Biol Crystallogr **58**: 1008–1015

Tian G-W, Chen M-H, Zaltsman A, Citovsky V (2006) Pollen-specific pectin methylesterase involved in pollen tube growth. Dev Biol **294**: 83–91

Turbant A, Fournet F, Lequart M, Zabijak L, Pageau K, Bouton S, Van Wuytswinkel O (2016) PME58 plays a role in pectin distribution during seed coat mucilage extrusion through homogalacturonan modification. J Exp Bot **67**: 2177–2190

Uluisik S, Seymour GB (2020) Pectate lyases: Their role in plants and importance in fruit ripening. Food Chem **309**: 125559

Underwood W (2012) The Plant Cell Wall: A Dynamic Barrier Against Pathogen Invasion. Front Plant Sci **3**: 1–6

Verlent I, Van Loey A, Smout C, Duvetter T, Hendrickx ME (2004) Purified tomato polygalacturonase activity during thermal and high-pressure treatment. Biotechnol Bioeng **86**: 63–71

Verlent I, Smout C, Duvetter T, Hendrickx ME, Van Loey A (2005) Effect of temperature and pressure on the activity of purified tomato polygalacturonase in the presence of pectins with different patterns of methyl esterification. Innov Food Sci Emerg Technol **6**: 293–303

Vitali J, Schick B, Kester HCM, Visser J, Jurnak F (1998) The Three-Dimensional Structure of Aspergillus niger Pectin Lyase B at 1.7-Å Resolution. Plant Physiol **116**: 69–80

Vogel J (2008) Unique aspects of the grass cell wall. Curr Opin Plant Biol **11**: 301–307

Voxeur A, Habrylo O, Guénin S, Miart F, Soulié MC, Rihouey C, Pau-Roblot C, Domon JM,

Gutierrez L, Pelloux J, et al (2019) Oligogalacturonide production upon Arabidopsis thaliana-Botrytis cinerea interaction. Proc Natl Acad Sci U S A **116**: 19743–19752

de Vries RP, Riley R, Wiebenga A, Aguilar-Osorio G, Amillis S, Uchima CA, Anderluh G, Asadollahi M, Askin M, Barry K, et al (2017) Comparative genomics reveals high biological diversity and specific adaptations in the industrially and medically important fungal genus Aspergillus. Genome Biol **18**: 28

Wallace AC, Laskowski RA, Thornton JM (1995) LIGPLOT: a program to generate schematic diagrams of protein-ligand interactions. "Protein Eng Des Sel **8**: 127–134

Wang H, Guo Y, Lv F, Zhu H, Wu S, Jiang Y, Li F, Zhou B, Guo W, Zhang T (2010) The essential role of GhPEL gene, encoding a pectate lyase, in cell wall loosening by depolymerization of the de-esterified pectin during fiber elongation in cotton. Plant Mol Biol **72**: 397–406

Wang L, Wang W, Wang Y-Q, Liu Y-Y, Wang J-X, Zhang X-Q, Ye D, Chen L-Q (2013) Arabidopsis Galacturonosyltransferase (GAUT) 13 and GAUT14 Have Redundant Functions in Pollen Tube Growth. Mol Plant **6**: 1131–1148

Wang Z, Xu B, Luo H, Meng K, Wang Y, Liu M, Bai Y, Yao B, Tu T (2020) Production pectin oligosaccharides using Humicola insolens Y1-derived unusual pectate lyase. J Biosci Bioeng **129**: 16–22

Wei P-C, Tan F, Gao X-Q, Zhang X-Q, Wang G-Q, Xu H, Li L-J, Chen J, Wang X-C (2010) Overexpression of AtDOF4.7, an Arabidopsis DOF Family Transcription Factor, Induces Floral Organ Abscission Deficiency in Arabidopsis. Plant Physiol **153**: 1031–1045

Weiller F, Gerber L, Trygg J, Fangel JU, Willats WGT, Driouich A, Vivier MA, Moore JP (2020) Overexpression of VviPGIP1 and NtCAD14 in Tobacco Screened Using Glycan Microarrays Reveals Cell Wall Reorganisation in the Absence of Fungal Infection. Vaccines **8**: 388

Willats WGT, Orfila C, Limberg G, Buchholt HC, Van Alebeek GJWM, Voragen AGJ, Marcus SE, Christensen TMIE, Mikkelsen JD, Murray BS, et al (2001) Modulation of the degree and pattern of methyl-esterification of pectic homogalacturonan in plant cell walls: Implications for pectin methyl esterase action, matrix properties, and cell adhesion. J Biol Chem **276**: 19404–19413

Wojtasik W, Kulma A, Dymińska L, Hanuza J, Czemplik M, Szopa J (2016) Evaluation of the significance of cell wall polymers in flax infected with a pathogenic strain of Fusarium oxysporum. BMC Plant Biol **16**: 1–16

Wolf S, Hématy K, Höfte H (2012) Growth control and cell wall signaling in plants. Annu Rev Plant Biol **63**: 381–407

Wolf S, Mouille G, Pelloux J (2009) Homogalacturonan methyl-esterification and plant development. Mol Plant **2**: 851–860

Wu H, Bulgakov VP, Jinn T, Mortimer JC (2018) Pectin Methylesterases : Cell Wall Remodeling Proteins Are Required for Plant Response to Heat Stress. Front Plant Sci **9**: 1–21

Wu P, Yang S, Zhan Z, Zhang G (2020) Origins and features of pectate lyases and their applications in industry. Appl Microbiol Biotechnol **104**: 7247–7260

Xiao C, Barnes WJ, Zamil MS, Yi H, Puri VM, Anderson CT (2017) Activation tagging of Arabidopsis POLYGALACTURONASE INVOLVED IN EXPANSION2 promotes hypocotyl elongation, leaf expansion, stem lignification, mechanical stiffening, and lodging. Plant J **89**: 1159–1173

Xiao C, Somerville C, Anderson CT (2014) POLYGALACTURONASE INVOLVED IN EXPANSION1 functions in cell elongation and flower development in Arabidopsis. Plant Cell **26**: 1018–1035

Xu P, Lu B, Liu J, Chao J, Donkersley P, Holdbrook R, Lu Y (2019) Duplication and expression of horizontally transferred polygalacturonase genes is associated with host range expansion of mirid bugs 06 Biological Sciences 0604 Genetics. BMC Evol Biol **19**: 1–9

Yadav S, Maurya SK, Anand G, Dwivedi R, Yadav D (2017) Purification and characterization of a highly alkaline pectin lyase from Fusarium lateritum MTCC 8794. Biol **72**: 245–251

Yadav S, Yadav PK, Yadav D, Yadav KDS (2009) Pectin lyase: A review. Process Biochem **44**: 1–10

Yan J, He H, Fang L, Zhang A (2018) Pectin methylesterase31 positively regulates salt stress tolerance in Arabidopsis. Biochem Biophys Res Commun **496**: 497–501

Yan L, Chouw N, Jayaraman K (2014) Flax fibre and its composites - A review. Compos Part B Eng **56**: 296–317

Yan L, Chouw N, Yuan X (2012) Improving the mechanical properties of natural fibre fabric reinforced epoxy composites by alkali treatment. J Reinf Plast Compos **31**: 425–437

Yang G, Chen W, Tan H, Li K, Li J, Yin H (2020) Biochemical characterization and evolutionary analysis of a novel pectate lyase from Aspergillus parasiticus. Int J Biol Macromol **152**: 180–188

Yang L, Huang W, Xiong F, Xian Z, Su D, Ren M, Li Z (2017) Silencing of SlPL , which encodes a pectate lyase in tomato, confers enhanced fruit firmness, prolonged shelf-life and reduced susceptibility to grey mould. Plant Biotechnol J **15**: 1544–1555

Yang Y, Yu Y, Liang Y, Anderson CT, Cao J (2018) A Profusion of Molecular Scissors for Pectins: Classification, Expression, and Functions of Plant Polygalacturonases. **9**: 1–16

Yoder M, Keen N, Jurnak F (1993a) New domain motif: the structure of pectate lyase C, a secreted plant virulence factor. Science (80-) **260**: 1503–1507

Yoder MD, Jurnak F (1995) The Refined Three-Dimensional Structure of Pectate Lyase C lmplications for an Enzymatic Mechanism. Plant Physiol **107**: 349–364

Yoder MD, Lietzke SE, Jurnak F (1993b) Unusual structural features in the parallel β-helix in pectate lyases. Structure **1**: 241–251

Yuan P, Meng K, Wang Y, Luo H, Shi P, Huang H, Tu T, Yang P, Yao B (2012) A Low-Temperature-Active Alkaline Pectate Lyase from Xanthomonas campestris ACCC 10048

with High Activity over a Wide pH Range. Appl Biochem Biotechnol **168**: 1489–1500

Zeuner B, Thomsen TB, Stringer MA, Krogh KBRM, Meyer AS, Holck J (2020) Comparative Characterization of Aspergillus Pectin Lyases by Discriminative Substrate Degradation Profiling. Front Bioeng Biotechnol. doi: 10.3389/fbioe.2020.00873

Zhang C, Yao J, Zhou C, Mao L, Zhang G, Ma Y (2013) The alkaline pectate lyase PEL168 of Bacillus subtilis heterologously expressed in Pichia pastorisis more stable and efficient for degumming ramie fiber. BMC Biotechnol **13**: 26

Zhang Y, Yu J, Wang X, Durachko DM, Zhang S, Cosgrove DJ (2021) Molecular insights into the complex mechanics of plant epidermal cell walls. Science (80-) **372**: 706–711

Zheng Y, Huang CH, Liu W, Ko TP, Xue Y, Zhou C, Guo RT, Ma Y (2012) Crystal structure and substrate-binding mode of a novel pectate lyase from alkaliphilic Bacillus sp. N16-5. Biochem Biophys Res Commun **420**: 269–274

Zhou C, Xue Y, Ma Y (2017a) Cloning, evaluation, and high-level expression of a thermo-alkaline pectate lyase from alkaliphilic Bacillus clausii with potential in ramie degumming. Appl Microbiol Biotechnol **101**: 3663–3676

Zhou Z, Liu Y, Chang Z, Wang H, Leier A, Marquez-Lago TT, Ma Y, Li J, Song J (2017b) Structure-based engineering of a pectate lyase with improved specific activity for ramie degumming. Appl Microbiol Biotechnol **101**: 2919–2929

ANNEXES

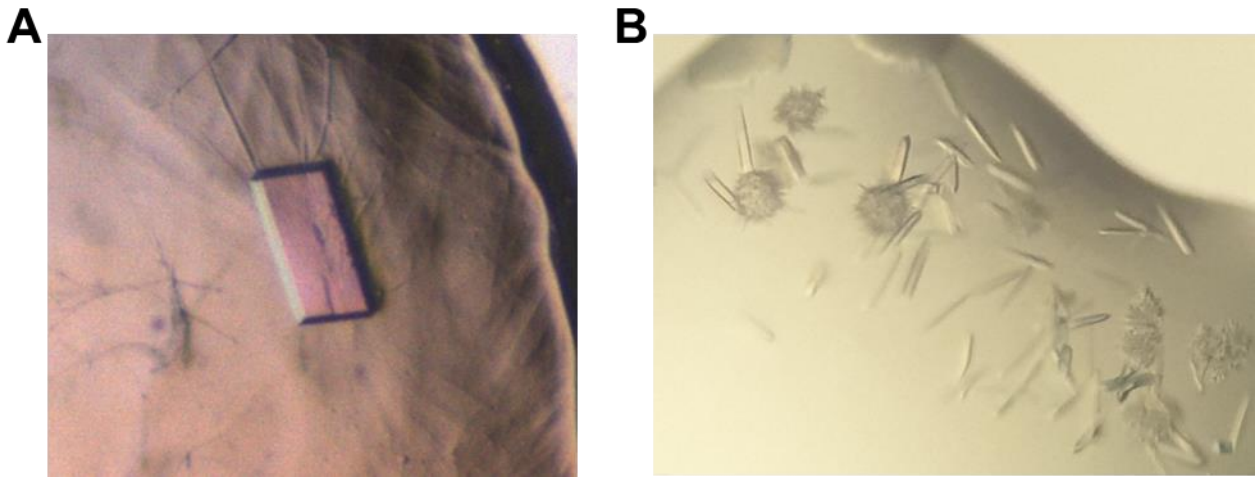

Annex 1. Pictures of the PGLR and ADPG2 crystals grown on the PACT premier plate
A) Only one crystal was obtained for PGLR on PACT premier plate in H1 condition. B) Multiple crystals were observed for ADPG2 on PACT Premier E12 condition.

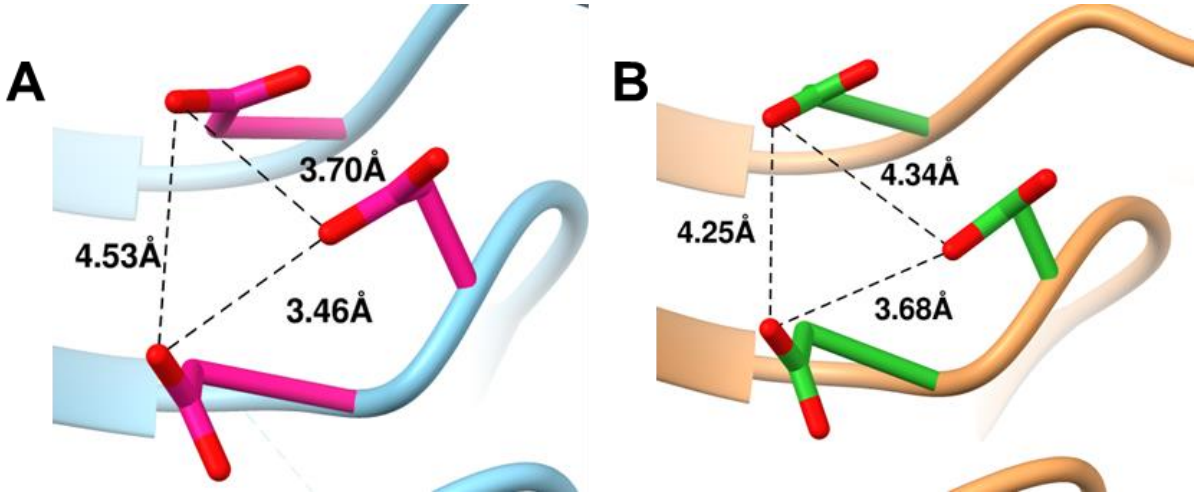

Annex 2. Distances between the Asp inside the PGLR and ADPG2 active site
A) PGLR, B) ADPG2. PGs active site characterised by the non-standard inverting mechanism in which the distance between the side chains of the acidic residues are all less than 5.7 Å apart. Distances are coloured in black.

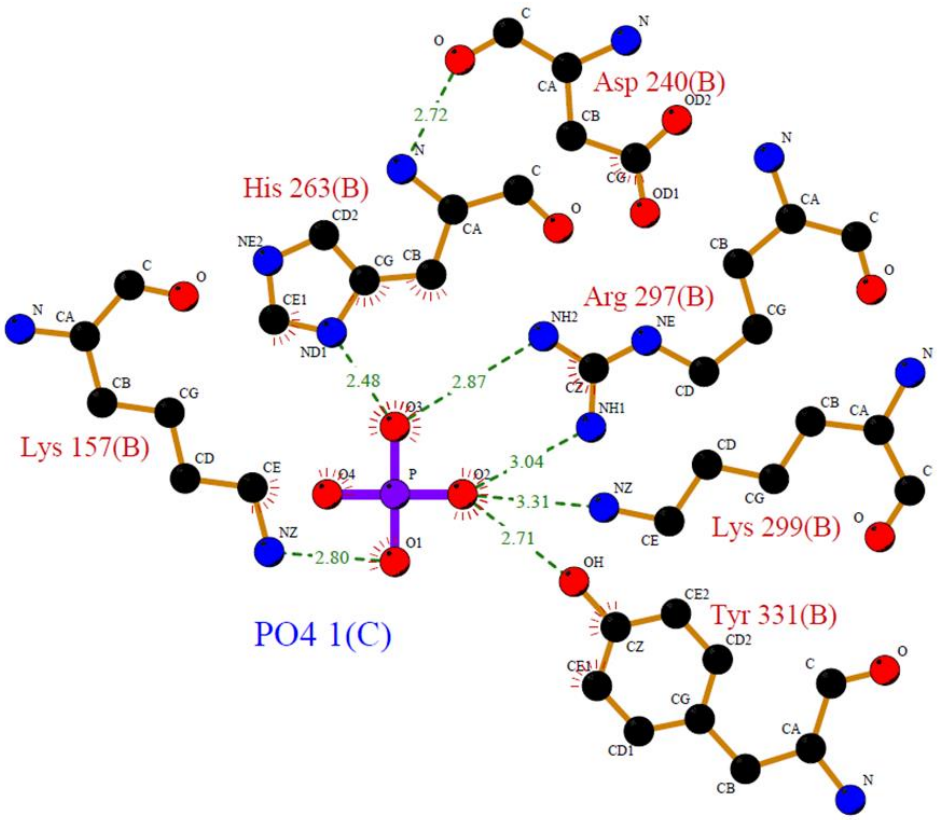

Annex 3. Schematic diagrams of distances and interaction of the PO_4^- crystallised in chain B of ADPG2

Active site of ADPG2 with PO_4^- molecule. Hydrogen bonds are represented in green while hydrophobic contacts are represented by an arc with spokes radiating towards the ligand atoms they contact. Figure was created using LIGPLOT v.4.5.3. (Wallace et al., 1995).

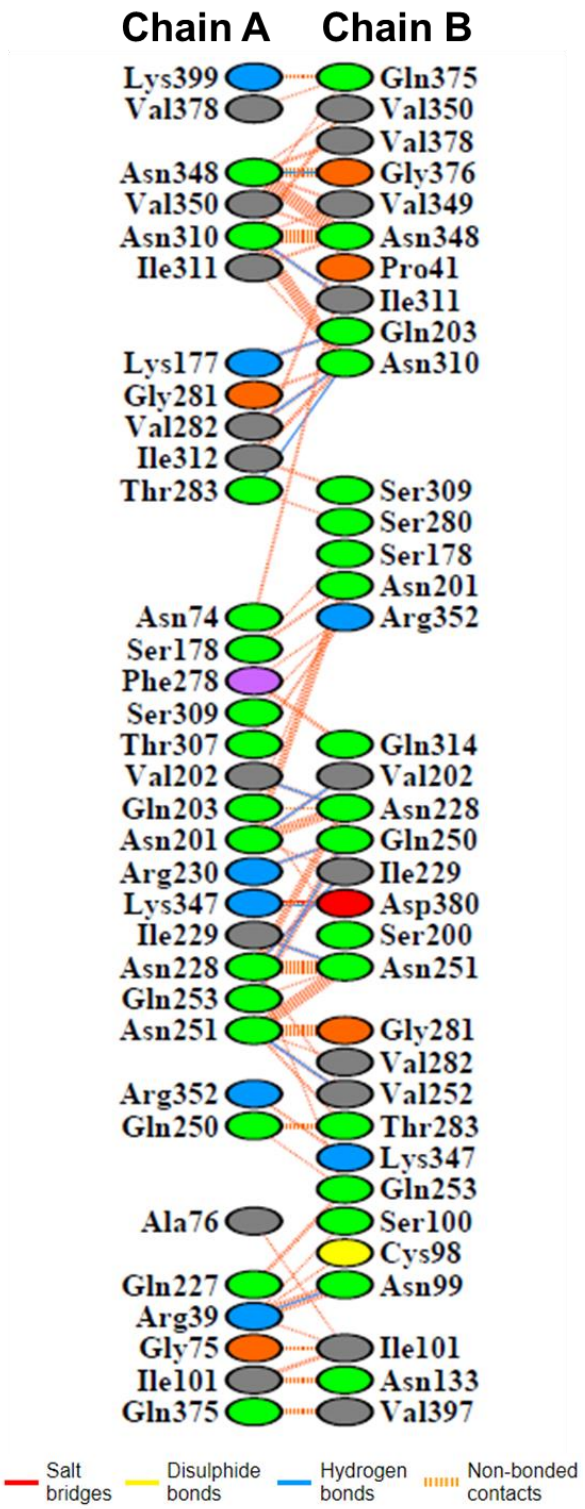

Annex 4. Schematic diagram of interactions between protein chains A and B of ADPG2
Interacting chains are joined by coloured lines, each representing a different type of interaction. Figure was created using PDBSum (http://www.ebi.ac.uk/thornton-srv/databases/cgi-bin/pdbsum/GetPage.pl?pdbcode=index.html)

WORLDWIDE PDB PROTEIN DATA BANK

Full wwPDB X-ray Structure Validation Report (i)

Mar 31, 2021 – 10:19 pm BST

PDB ID	:	7B7A
Title	:	ENDO-POLYGALACTURONASE FROM ARABIDOPSIS THALIANA
Deposited on	:	2020-12-10
Resolution	:	1.30 Å(reported)

This is a Full wwPDB X-ray Structure Validation Report.

This report is produced by the wwPDB biocuration pipeline after annotation of the structure.

We welcome your comments at *validation@mail.wwpdb.org*
A user guide is available at
https://www.wwpdb.org/validation/2017/XrayValidationReportHelp
with specific help available everywhere you see the (i) symbol.

The following versions of software and data (see references (i)) were used in the production of this report:

MolProbity	:	4.02b-467
Mogul	:	1.8.5 (274361), CSD as541be (2020)
Xtriage (Phenix)	:	1.13
EDS	:	2.18
Percentile statistics	:	20191225.v01 (using entries in the PDB archive December 25th 2019)
Refmac	:	5.8.0158
CCP4	:	7.0.044 (Gargrove)
Ideal geometry (proteins)	:	Engh & Huber (2001)
Ideal geometry (DNA, RNA)	:	Parkinson et al. (1996)
Validation Pipeline (wwPDB-VP)	:	2.18

1 Overall quality at a glance

The following experimental techniques were used to determine the structure:
X-RAY DIFFRACTION

The reported resolution of this entry is 1.30 Å.

Percentile scores (ranging between 0-100) for global validation metrics of the entry are shown in the following graphic. The table shows the number of entries on which the scores are based.

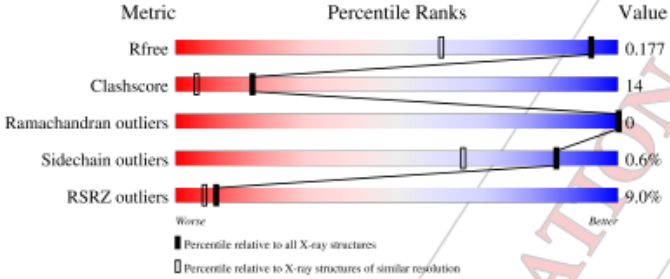

Metric	Whole archive (#Entries)	Similar resolution (#Entries, resolution range(Å))
R_{free}	130704	1058 (1.30-1.30)
Clashscore	141614	1101 (1.30-1.30)
Ramachandran outliers	138981	1058 (1.30-1.30)
Sidechain outliers	138945	1058 (1.30-1.30)
RSRZ outliers	127900	1029 (1.30-1.30)

The table below summarises the geometric issues observed across the polymeric chains and their fit to the electron density. The red, orange, yellow and green segments of the lower bar indicate the fraction of residues that contain outliers for >=3, 2, 1 and 0 types of geometric quality criteria respectively. A grey segment represents the fraction of residues that are not modelled. The numeric value for each fraction is indicated below the corresponding segment, with a dot representing fractions <=5% The upper red bar (where present) indicates the fraction of residues that have poor fit to the electron density. The numeric value is given above the bar.

Mol	Chain	Length	Quality of chain
1	A	429	8% 73% 17% 9%
2	C	2	100%
3	B	6	100%

Annex 5. Full wwPDB X-ray Structure Validation Report for PGLR
First two pages of VdPelB validation report received after depositing the structure to PDB. Full validation report contains 19 pages and can be downloaded on the following link: PGLR_7B7A_Validation_ report

WORLDWIDE PDB
PROTEIN DATA BANK

Full wwPDB X-ray Structure Validation Report (i)

Feb 21, 2021 – 04:30 pm GMT

PDB ID	:	7B8B
Title	:	ADPG2 - ENDOPOLYGALACTURONASE FROM ARABIDOPSIS THALIANA
Deposited on	:	2020-12-12
Resolution	:	2.03 Å(reported)

This is a Full wwPDB X-ray Structure Validation Report.

This report is produced by the wwPDB biocuration pipeline after annotation of the structure.

We welcome your comments at *validation@mail.wwpdb.org*
A user guide is available at
https://www.wwpdb.org/validation/2017/XrayValidationReportHelp
with specific help available everywhere you see the (i) symbol.

The following versions of software and data (see references (i)) were used in the production of this report:

MolProbity	:	4.02b-467
Mogul	:	1.8.5 (274361), CSD as541be (2020)
Xtriage (Phenix)	:	1.13
EDS	:	2.17.1.dev1
Percentile statistics	:	20191225.v01 (using entries in the PDB archive December 25th 2019)
Refmac	:	5.8.0158
CCP4	:	7.0.044 (Gargrove)
Ideal geometry (proteins)	:	Engh & Huber (2001)
Ideal geometry (DNA, RNA)	:	Parkinson et al. (1996)
Validation Pipeline (wwPDB-VP)	:	2.17.1.dev1

1 Overall quality at a glance

The following experimental techniques were used to determine the structure:
X-RAY DIFFRACTION

The reported resolution of this entry is 2.03 Å.

Percentile scores (ranging between 0-100) for global validation metrics of the entry are shown in the following graphic. The table shows the number of entries on which the scores are based.

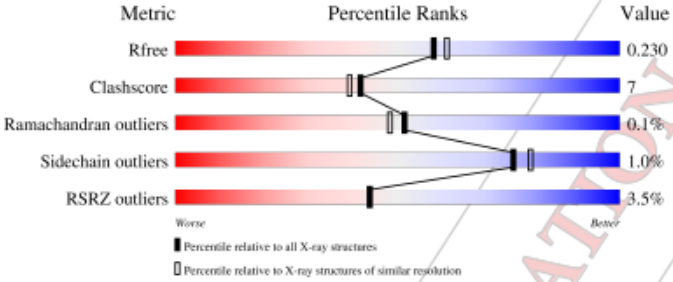

Metric	Whole archive (#Entries)	Similar resolution (#Entries, resolution range(Å))
R_{free}	130704	10434 (2.04-2.00)
Clashscore	141614	11643 (2.04-2.00)
Ramachandran outliers	138981	11493 (2.04-2.00)
Sidechain outliers	138945	11492 (2.04-2.00)
RSRZ outliers	127900	10220 (2.04-2.00)

The table below summarises the geometric issues observed across the polymeric chains and their fit to the electron density. The red, orange, yellow and green segments of the lower bar indicate the fraction of residues that contain outliers for >=3, 2, 1 and 0 types of geometric quality criteria respectively. A grey segment represents the fraction of residues that are not modelled. The numeric value for each fraction is indicated below the corresponding segment, with a dot representing fractions <=5% The upper red bar (where present) indicates the fraction of residues that have poor fit to the electron density. The numeric value is given above the bar.

Mol	Chain	Length	Quality of chain
1	A	420	2% 78% 10% 12%
1	B	420	5% 73% 14% 13%

Annex 6. Full wwPDB X-ray Structure Validation Report for ADPG2
First two pages of VdPelB validation report received after depositing the structure to PDB. Full validation report contains 19 pages and can be downloaded on the following link: ADPG2_7B8B_Validation_ report

Annex 7. HPAEC-PAD analysis of commercial pectin

The pectin monosaccharide composition was determined by high-performance anion-exchange chromatography (HPAEC) with a pulsed amperometric detector (Dionex ICS 3000 system). Standard of fucose, arabinose, rhamnose, glucose, galactose, xylose, mannose, galacturonic acid and glucuronic acid from.5.00 x 10^{-4} to 2.5 x 10^{-1} $mg.ml^{-1}$ concentration were used for quantification.

	Citrus pectin			**Apple pectin**	**Beet pectin**
	DM 20-34%	**DM 55-70%**	**DM >85%**	**DM 70-75%**	**DM 42%, DA 31%**
Fucose	0.75	0.80	0.59	0.88	1.40
Rhamnose	15.61	14.65	12.53	12.69	10.82
Arabinose	12.72	10.52	5.97	15.40	18.24
Galactose	31.32	32.35	24.44	21.03	23.65
Glucose	3.25	3.02	6.33	6.45	4.01
GalA	34.49	37.00	44.78	37.97	38.88
GlcA	0.23	0.16	0.19	0.18	1.60
Man/Xyl	1.64	1.50	5.15	5.40	1.40
DM (%)	-	68	85	70	42
DA (%)	-	2	0	4	31

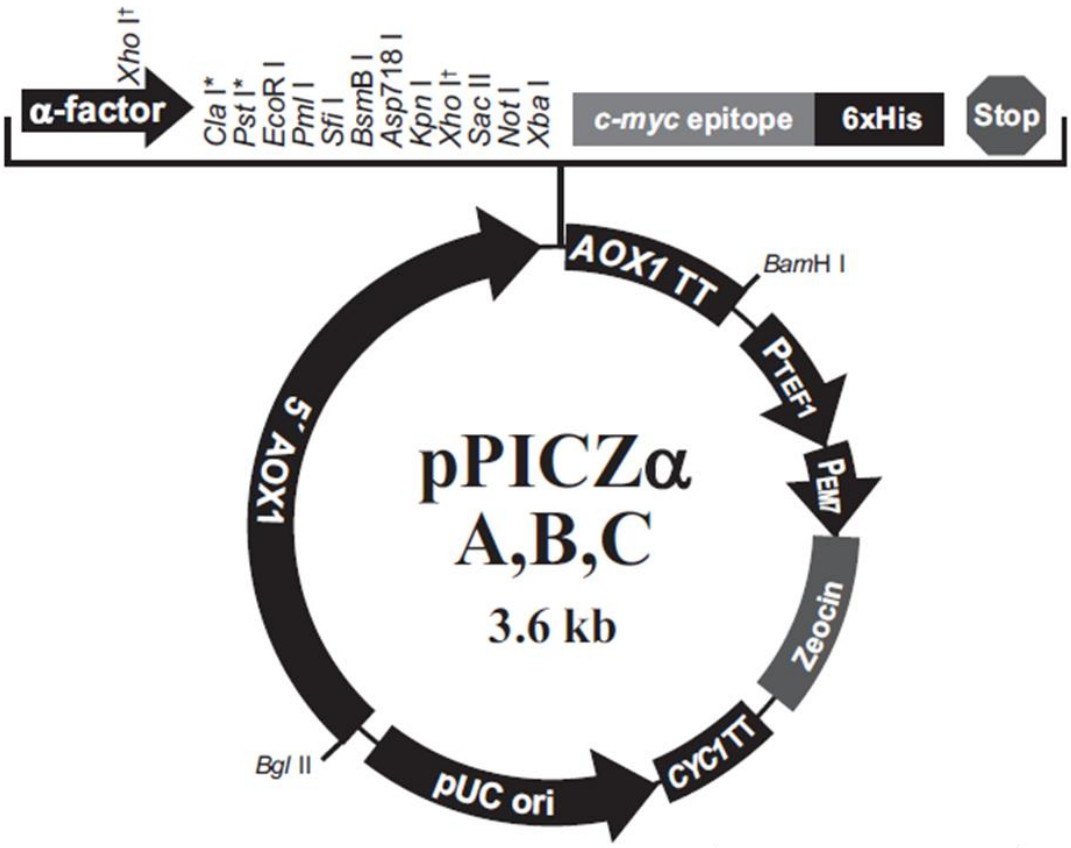

Annex 8. Map of pPICZαB vector used for *P. pastoris* transformation.

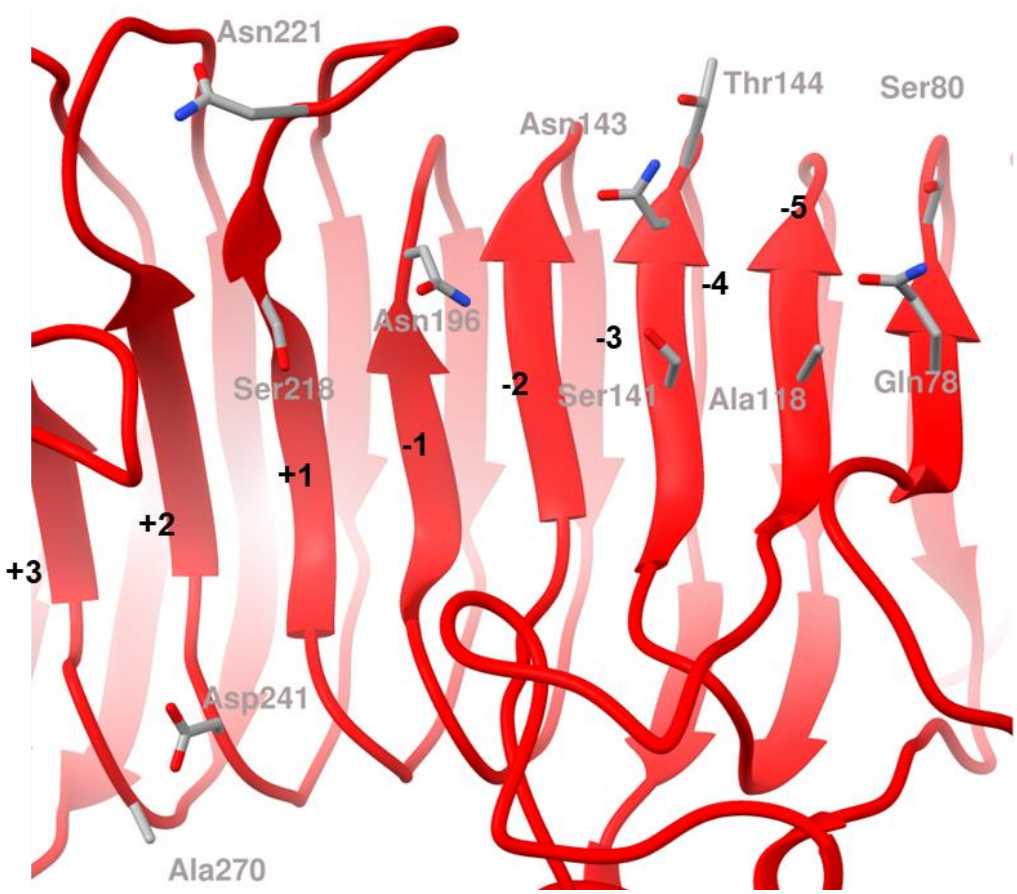

Annex 9. Structure of VdPG2 subsites
Ribbon structure of VdPG2 subsites (red) with AA coloured grey. Black numbers indicate the subsites.

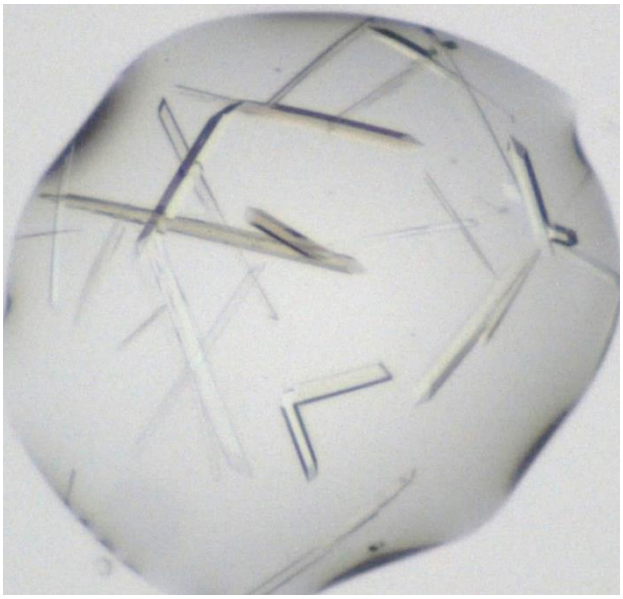

Annex 10. Pictures of the VdPelB crystals grown on the PACT premier plate B5 condition

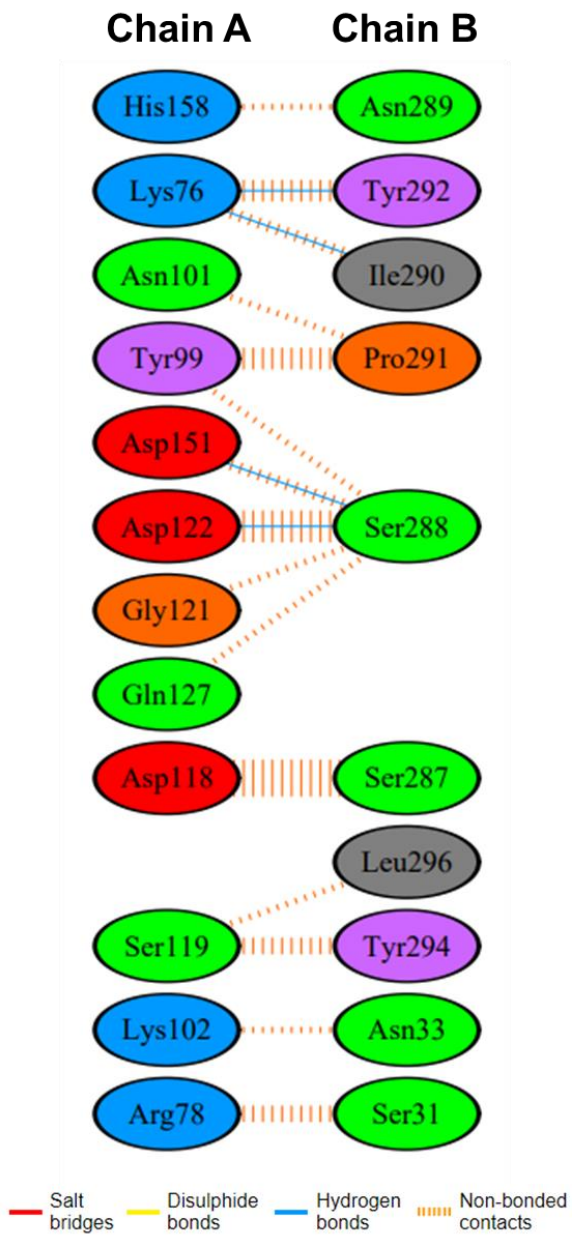

Annex 11. Schematic diagram of interactions between protein chains A and B of VdPelB
Interacting chains are joined by coloured lines, each representing a different type of interaction. Figure was created using PDBSum (http://www.ebi.ac.uk/thornton-srv/databases/cgi-bin/pdbsum/GetPage.pl?pdbcode=index.html)

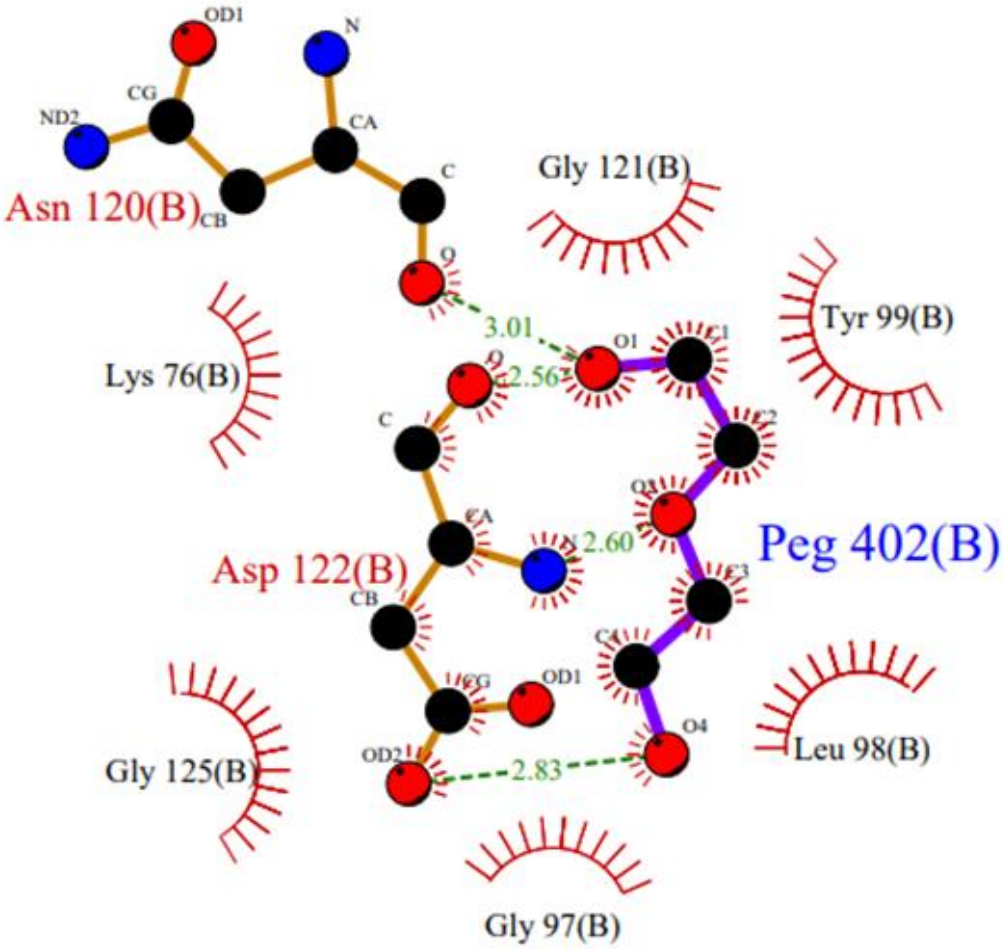

Annex 12. Schematic diagrams of distances and interaction of the PEG crystallised in the chain B of VdPelB

Active site of VdPelB 2 with PEG molecule. Hydrogen bonds are represented in green while hydrophobic contacts are represented by an arc with spokes radiating towards the ligand atoms they contact. Figure was created using LIGPLOT v.4.5.3. (Wallace et al., 1995).

WORLDWIDE PDB PROTEIN DATA BANK

Full wwPDB X-ray Structure Validation Report (i)

Feb 26, 2021 – 08:03 am GMT

PDB ID	:	7BBV
Title	:	Pectae lyase B from Verticillium dahliae
Deposited on	:	2020-12-18
Resolution	:	1.20 Å(reported)

This is a Full wwPDB X-ray Structure Validation Report.

This report is produced by the wwPDB biocuration pipeline after annotation of the structure.

We welcome your comments at *validation@mail.wwpdb.org*
A user guide is available at
https://www.wwpdb.org/validation/2017/XrayValidationReportHelp
with specific help available everywhere you see the (i) symbol.

The following versions of software and data (see references (i)) were used in the production of this report:

MolProbity	:	4.02b-467
Mogul	:	1.8.5 (274361), CSD as541be (2020)
Xtriage (Phenix)	:	1.13
EDS	:	2.17.1.dev1
Percentile statistics	:	20191225.v01 (using entries in the PDB archive December 25th 2019)
Refmac	:	5.8.0158
CCP4	:	7.0.044 (Gargrove)
Ideal geometry (proteins)	:	Engh & Huber (2001)
Ideal geometry (DNA, RNA)	:	Parkinson et al. (1996)
Validation Pipeline (wwPDB-VP)	:	2.17.1.dev1

1 Overall quality at a glance

The following experimental techniques were used to determine the structure:
X-RAY DIFFRACTION

The reported resolution of this entry is 1.20 Å.

Percentile scores (ranging between 0-100) for global validation metrics of the entry are shown in the following graphic. The table shows the number of entries on which the scores are based.

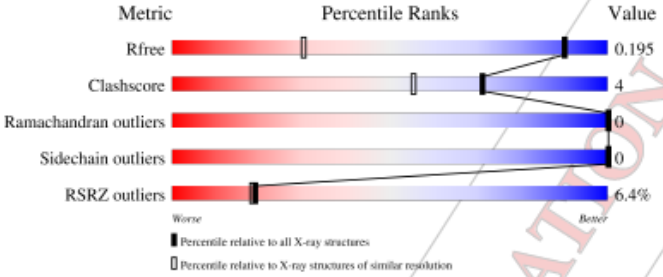

Metric	Whole archive (#Entries)	Similar resolution (#Entries, resolution range(Å))
R_{free}	130704	1223 (1.22-1.18)
Clashscore	141614	1286 (1.22-1.18)
Ramachandran outliers	138981	1240 (1.22-1.18)
Sidechain outliers	138945	1239 (1.22-1.18)
RSRZ outliers	127900	1200 (1.22-1.18)

The table below summarises the geometric issues observed across the polymeric chains and their fit to the electron density. The red, orange, yellow and green segments of the lower bar indicate the fraction of residues that contain outliers for >=3, 2, 1 and 0 types of geometric quality criteria respectively. A grey segment represents the fraction of residues that are not modelled. The numeric value for each fraction is indicated below the corresponding segment, with a dot representing fractions <=5% The upper red bar (where present) indicates the fraction of residues that have poor fit to the electron density. The numeric value is given above the bar.

Mol	Chain	Length	Quality of chain
1	A	343	4% 83% 13%
1	B	343	7% 79% 8% 13%

The following table lists non-polymeric compounds, carbohydrate monomers and non-standard residues in protein, DNA, RNA chains that are outliers for geometric or electron-density-fit criteria:

Annex 13. Full wwPDB X-ray Structure Validation Report for VdPelB

First two pages of VdPelB validation report received after depositing the structure to PDB. Full validation report contains 19 pages and can be downloaded on the following link: VdPelB_7BBV_Validation_ report

Abstract

Plant cell wall plays a key role in the control of cell elongation and differentiation as well as in defence against pathogens. Homogalacturonan (HG)-type pectin, one of the major components of the primary cell wall in dicotyledonous plants, comprises 1,4 linked α-D galacturonic acids (GalA) that can be methylesterified. HG is modified by homogalacturonan modifying enzymes (HGME), such as pectin methylesterase (PME), polygalacturonases (PG) and pectin/pectate lyases like (PLLs), that control their degree of methylesterification (DM) and polymerization (DP), respectively. Plant enzymes fine-tune the cell wall pectins during development, while pathogens' enzymes degrade the pectin matrix to facilitate infection. These enzymes are encoded, in plants and pathogens, by large multigenic families, which questions the rationale for such abundance. Thus, to understand the biochemistry, catalytic mechanisms and structure/function relationships of these enzymes, we expressed and characterized isoforms from *Verticillium dahliae* (VdPME1, VdPG2 and VdPelB) and *Arabidopsis thaliana* (PGLR, ADPG2). VdPME1 had processive mode of action at pH 7 for demethylesterification, that could be related to the surface electrostatic properties of the protein, and which creates a substrate for VdPG2. VdPG2, act as an endo-enzyme and was most active at pH 5 and temperature of 50°C. VdPelB had surprising PNL-PL biochemical characteristics, being most active at alkaline pH in presence of Ca^{2+} ions and on high DM pectins. Using X-ray diffraction, we resolved the VdPelB structure at 1.2 Å and showed that it indeed differed from previously reported fungal enzymes. We further characterized Arabidopsis PGLR and ADPG2, whose expression overlaps in roots. LC-MS/MS analyses of digested pectins showed that the oligogalacturonides (OGs) released by both enzymes differed. To understand these differences in processivity, we resolved the structures of PGLR and ADPG2 at 1.3 and 2.03 Å, respectively. The two enzymes had right-handed parallel β-helix fold, characteristic for pectinases with the tunnel-like active site allowing the release of OGs of distinct DP. If the amino acids at the active site were conserved, those in subsites differed, partly explaining substrate specificities. These first structures of plant PGs shed new light on the functional diversity of enzymes in plants and the differences with that of pathogens.
Keywords: *Arabidopsis thaliana* – *Verticillium dahliae* – Pectin – Pectin methylesterases - Polygalacturonases – Pectin Lyases

Resumé

La paroi cellulaire des plantes joue un rôle clé dans le contrôle de l'élongation et de la différenciation, ainsi que dans la défense des plantes face aux pathogènes. Les pectines de type homogalacturonanes (HG), un des composants majeurs de la paroi primaire des plantes dicotylédones, sont constituées d'acides galacturoniques (α-D GalA) liés en 1,4, qui peuvent être méthylestérifiés. Les HG sont modifiés par des enzymes telles que les pectine-méthylestérases (PME), les polygalacturonases (PG) et pectine-pectate lyases (PLL), qui contrôlent respectivement leur degré de méthylestérification (DM) et de polymérisation (DP). Alors que les enzymes de plantes permettent une régulation fine de la structure des pectines de la paroi lors du développement, celles de pathogènes sont impliquées dans la dégradation de celle-ci lors de l'infection. Elles sont par ailleurs codées par des familles multigéniques, ce qui questionne les raisons d'une telle abondance. Ainsi, pour comprendre leurs spécificités biochimiques, des isoformes de *Verticillium dahliae* (VdPME1, VdPG2 et VdPelB) et d'*Arabidopsis thaliana* (PGLR, ADPG2) ont été exprimées et caractérisées. VdPME1 déméthylestérifie les pectines de façon processive à pH 7, ce qui peut être relié au potentiel électrostatique de surface de la protéine, et créé des substrats préférentiels pour VdPG2, une endo-polygalacturonase. VdPelB présente des caractéristiques biochimiques intermédiaires entre une PNL et une PL : elle est plus active à pH alcalin et agit préférentiellement sur des pectines de fort DM en présence de calcium. La structure 3D de la protéine, résolue à 1,2 Å par diffraction au rayon X, permet de confirmer les particularités structurales de VdPelB en regard d'enzymes fongiques. PGLR et ADPG2, qui présentent un patron d'expression similaire dans les racines d'Arabidopsis, produisent des oligogalacturonides (OGs) distincts. Afin de comprendre ces différences de mode d'action, les structures 3D des protéines ont été déterminées à 1.3 (PGLR) et 2.03Å (ADPG2). Si les deux enzymes présentent une structure caractéristique des pectinases et un site actif conservé, la séquence particulière de leurs sous-sites, peut expliquer leurs différences de processivité. Ces structures de PG, les premières obtenues chez les plantes, permettent de comprendre leur diversité fonctionnelle ainsi que les différences majeures avec les enzymes de phytopathogènes.
Mots clés : *Arabidopsis thaliana* – *Verticillium dahliae* – Pectines – Pectine méthylestérases – Polygalacturonases – Pectine Lyases